Cristallisation d'hydrates de cyclopentane en présence de l'eau salée et de dioxyde de carbone pour le traitement et le dessalement de l'eau

Son Ho Van

N°d'ordre NNT : 2019LYSEM019

THESE de DOCTORAT DE L'UNIVERSITE DE LYON
opérée au sein de
l'Ecole des Mines de Saint-Etienne

Ecole Doctorale N° 488
Sciences, Ingénierie, Santé

Spécialité de doctorat : Génie des Procédés
Discipline : DS8 Sciences pour l'ingénieur

Soutenue publiquement le 19/07/2019, par :
Son Ho-Van

Cristallisation d'hydrates de cyclopentane en présence de l'eau salée et de dioxyde de carbone pour le traitement et le dessalement de l'eau

Crystallization of cyclopentane hydrates in presence of brine and carbon dioxide for water treatment and desalination

Devant le jury composé de :

Christelle GOUTAUDIER	Professeure, Université Lyon, Université Claude Bernard Lyon 1, France	Présidente
Beatrice BISCANS	Directrice de Recherche CNRS, Laboratoire de Génie Chimique, Toulouse, France	Rapporteure
Praveen LINGA	Associate professor, National University of Singapore, Singapour	Rapporteur
Jean-Michel HERRI	Professeur, École Nationale Supérieure des Mines de Saint-Étienne, Saint-Étienne, France	Directeur de thèse
Baptiste BOUILLOT	Maître de conférences, École Nationale Supérieure des Mines de Saint-Étienne, Saint-Étienne, France	Co-Directeur de thèse

List of contents

List of contents 1
List of figures 3
List of tables 4
Acknowledgements 5
Résumé 7
Abstract 8
General Introduction 9
Chapter I. State of the art 13
1.1. Clathrate hydrates 13
1.1.1. Definition and structure 13
1.1.2. Phase equilibria of clathrate hydrates 16
1.1.3. Issues and potential applications of clathrate hydrates 19
1.2. Cyclopentane hydrates 21
1.2.1. Introduction to cyclopentane hydrates 22
1.2.2. Thermodynamics of Cyclopentane hydrates 23
1.2.3. Mixed CO_2+cyclopentane hydrates 23
1.3. Clathrate hydrates for desalination 25
1.4. Case of Cyclopentane hydrates-based desalination 27
Chapter II. Experimental system for thermodynamics 31
2.1. Materials 31
2.2. Experimental apparatus 31
2.2.1. Experimental apparatus for Cyclopentane hydrates thermodynamics study 31
2.2.2. Experimental apparatus for CP+CO_2 hydrates thermodynamics study 33
Chapter III. Modeling clathrate hydrates equilibrium 35
3.1. Standard freezing point depression (SFPD) approach 35
3.2. Hu-Lee-Sum (HLS) correlation 36
3.3. Kihara approach 37
3.4. Activity-Based Occupancy Correlation (ABOC) approach 39
Chapter IV. Thermodynamics results 41
4.1. CPH equilibrium results 41
4.2. CP/CO_2 hydrates equilibrium results 43
Chapter V. Cydopentane hydrates crystallization and morphology study 45
5.1. Apparatus description 45

5.2. Experimental procedure 46
5.3. Results 47
References 50
Chapter VI. Introduction to the papers 59
6.1. Paper I: Cyclopentane hydrates – a candidate for desalination? 60
6.2. Paper II: Experimental Measurement and Thermodynamic Modeling of Cyclopentane Hydrates with NaCl, KCl, $CaCl_2$, or NaCl-KCl Present 121
6.3. Paper III: Implementing Cyclopentane Hydrates Phase Equilibrium Data and Simulations in Brine Solutions 135
6.4. Paper IV: Crystallization mechanisms and rates of Cyclopentane Hydrates formation in Brine 147
6.5. Paper V: Morphology of Cyclopentane Hydrates in Saline Water 161
6.6. Paper VI: Phase equilibrium investigations of mixed cyclopentane and carbon dioxide hydrates in presence of different salt solutions 167
Chapter VII. General conclusion and perspectives 193
Scientific production (2015-2019) 197

List of figures

Figure 1: Three main hydrate structures and their constitutive cavities (taken from Sloan and Koh [7]) 14
Figure 2: Hydrate phase diagrams. (a) CH_4+H_2O or N_2+H_2O, (b) Hydrocarbon + H_2O with upper quadruple points, (c) Multicomponent natural gas + H_2O, (d) Hydrocarbon + H_2O with upper quadruple points and inhibitors (taken from [1]) 17
Figure 3: Solid hydrates obtained from the slugcatcher [2] 19
Figure 4: Occupation of the large cages ($5^{12}6^4$) of hydrates sII by CP molecules [30] 22
Figure 5: A simplified schematic of clathrate hydrates based desalination 25
Figure 6: Progression in desalination via hydrate formation [53,54,58–63] (adapted from Babu et al [24]) 26
Figure 7: Simplified schematic of the apparatus for CPH thermodynamic study [28] 32
Figure 8: Diagram of experimental set-up for mixed CP+CO_2 hydrates thermodynamic study 34
Figure 9: Equilibrium temperature of CPH in the presence of NaCl, KCl, NaCl-KCl, or $CaCl_2$ from experiments 41
Figure 10: Equilibrium temperature of CPH in the presence of $MgCl_2$, $MgCl_2$-NaCl, $MgCl_2$-NaCl-KCl, or Na_2SO_4 from experiments 42
Figure 11: V-L_W-L_{HC}-H equilibrium data of CP/CO_2 hydrates in pure water and in brine 43
Figure 12: Schematic illustration of the experimental set-up for CPH crystallization mechanism and morphology study [106] 46
Figure 13: Simplified scheme of the CPH crystallization mechanism near the interface in the reactor cell 47
Figure 14: The mass transfer mechanism of CP, water, and salt during CPH crystallization 48
Figure 15. An example of CPH crystals morphology in pure water and in brine 49

List of tables

Table 1. Summary of three principle hydrate structures [7]..... 14
Table 2. A list of guest molecules and their hydrate structures [1]..... 15
Table 3: A summary on equilibrium data of mixed CP+CO_2 hydrates..... 24
Table 4: Purity of initial material used 31
Table 5: Thermodynamic data used for Kihara parameters optimization in binary CP/CO_2 hydrates.. 38
Table 6: Optimized Kihara parameters for CP in two different hydrates systems..... 39
Table 7: Average deviation (°C) of different approaches for simulating CPH equilibrium 43
Table 8: Average deviation between simulations and measurements of CP/CO_2 hydrates equilibrium. 44

Acknowledgements

First of all, I would like to thank my supervisor Professor Jean-Michel HERRI and my co-supervisor Dr. Baptiste BOUILLOT for the constant support during my four-year PhD course, for their patience, gentleness, inspiration, and immense knowledge. This was my great honor to work with them since I have gained so much from them in the hydrate field. They both have been very supportive sine the very first days when I and my family arrived in France and started working on the PhD project in 2015.

My thanks also goes to Professor Daniel GARCIA and Professor Ana CAMEIRAO for their discussions and valuable ideas in the experiments and in the manuscripts, and for being co-authors in my some publications.

I am grateful to Dr. Jérôme DOUZET and Dr. Saheb MAGHSOODLOO BABAKHANI for their help and support in almost experiments on thermodynamic and crystallization in the laboratory in Spin center. They are always available and willing to share and discuss with me to solve problems.

I sincerely thank Dr. BISCANS and Dr. Praveen LINGA who have accepted the difficult task of being referees of this work. I also thank Professor Christelle GOUTAUDIER for giving me the pleasure and honor of chairing my defense.

In addition, I would like to thank to my colleagues, technicians and personnel in SPIN center: Trung-Kien PHAM, Thang LE, Du LE-QUANG, Vinicius RODRIGUES DE ALMEIDA VENICIUS, Carlos LANGE-BASSANI, Fabien CHAUVY, Jacques MOUTTE, Frédéric GALLICE, Hubert FAURE, Jean-Pierre POYET, Marc ROUVIERE, Jérôme MANCUSO, Andrée-Aimée TOUCAS, Marie-Claude BARTHOLIN, Céline BACHEKOUR, Joëlle VERNEY, Florence DUJARDIN for their help in science, informatics, and administrations.

I would like to sincerely acknowledge the Vietnam International Education Development, Ministry of Education and Training, for the financial support through the PhD (scholarship program 911). I would like to thank also Hanoi University of Mining and Geology for allowing and supporting me to study PhD in France.

Lastly, I would like to thank my beloved family: my mother Thi-Lieu NGUYEN, my father Dai HO, my wife Thi-Duc TRAN, my sons Minh-An HO, Anh-Minh HO, and my sisters Thi-Luong HO, Thi-Huong HO, my brother Duc-Cuong HO for all their love, and encouragement.

Résumé

Ces travaux de thèse ont pour but de compléter les connaissances actuelles sur la cristallisation des hydrates de cyclopentane dans les domaines de la désalinisation et du traitement de l'eau. Ils débutent donc par une étude bibliographique la plus exhaustive possible incluant les aspects thermodynamiques, cinétiques et morphologiques des hydrates de cyclopentane dans les nouveaux procédés de désalinisation par cristallisation. Les principaux verrous à lever sont mis en lumière, tout en apportant quelques suggestions pour le développement à long terme de ce type de technologie. Une conclusion montre que les hydrates de cyclopentane pourraient être de bons candidats, en plus d'autres additifs, pour des applications dans le domaine de la désalinisation.

Ensuite, d'importantes nouvelles données d'équilibre des hydrates de cyclopentane dans de l'eau en présence de sels ont été obtenues (NaCl, KCl, NaCl-KCl, $CaCl_2$, $MgCl_2$, $MgCl_2$-NaCl, $MgCl_2$-NaCl-KCl, ou Na_2SO_4). Les résultats ont été modélisés selon quatre approches. La première est basée selon l'équation SFPD (standard freezing point depression). La seconde sur la nouvelle corrélation Hu-Lee-Sum (HLS). Les deux autres sur le modèles de van der Waals et de Platteeuw, soit en utilisant le potentiel d'interaction de Kihara, soit avec une simple corrélation entre le coefficient d'activité de l'eau et la stœchiométrie de l'hydrate. Cette dernière simule des résultats avec une précision de 0,2°C. Lors de ces expériences, en plus de la cristallisation des hydrates, la précipitation des sels a été observée, ce qui offre la possibilité de récupérer ces derniers sous forme cristallisée, en plus du traitement de l'eau.

En parallèle, un travail plus fondamental a été mené sur les mécanismes de cristallisation, les vitesses de croissance des cristaux et la morphologie des hydrates de cyclopentane dans l'eau pure et en présence de sels. Une petite cellule refroidie et non agitée, placée sous un microscope a été utilisée à différentes conditions expérimentales (sous-refroidissements et concentrations en sels).

Pour terminer, un additif gazeux a été ajouté à l'étude : le dioxide de carbone. Des points d'équilibre d'hydrates mixtes de cyclopentane+CO_2 ont donc été obtenus expérimentalement, notamment en présence de sels (KCl, NaCl, et NaCl-KCl). Ces résultats sont nécessaires pour le développement de procédés pouvant combiner la désalinisation au captage du CO_2. Pour cela, une méthode isochore a été appliquée dans un réacteur de type batch. Un outil de modélisation thermodynamique basé sur l'approche de van der Waals a été utilisé pour simuler ces équilibres.

Abstract

This thesis is an effort to fulfill the gap in the literature on cyclopentane (CP) hydrates for desalination and water treatment applications. Accordingly, it begins with a comprehensive review on Cyclopentane hydrates for hydrate-based treatment processes. This literature work covers all aspects of thermodynamics, kinetics, morphology, hydrate phase properties, and the recent use of Cyclopentane hydrates in desalting process that require to develop an advanced and sustainable technique *via* hydrate crystallization. Some challenges to overcome in the long term, and critical perspective suggestions are also addressed. A short conclusion is that cyclopentane hydrates, with additives, could be a candidate for desalination.

Then, new thermodynamic equilibrium of cyclopentane hydrates are provided, in pure water and in presence of different electrolyte systems including NaCl, KCl, NaCl-KCl, $CaCl_2$, $MgCl_2$, $MgCl_2$-NaCl, $MgCl_2$-NaCl-KCl, or Na_2SO_4. Results have been modelled with four approaches. The first is based on the standard freezing point depression (SFPD) equation. The second is based on Hu-Lee-Sum (HLS) correlation. The two others are based on van de Waals and Platteeuw model: either with the use of Kihara potential, or a simple correlation between water activity and the hydrate stoichiometry. The last one simulates the experimental results within 0.2°C uncertainty. Moreover, salt crystallization has been achieved, opening the possibility for product recovery with hydrate crystallization.

Besides, the crystallization mechanisms, crystals growth rates, and morphology of cyclopentane hydrates crystals in pure water and in the presence of various salts (NaCl, NaCl-$MgCl_2$, NaCl-KCl-$MgCl_2$, or Na_2SO_4) have also been studied. A non-agitated reactor cell, connected to a microscope, has been employed, as well as different experimental conditions (subcooling and salinity).

Finally, equilibrium data of binary CP+CO_2 hydrates in pure water and in the presence of three electrolyte solutions (KCl, NaCl, and NaCl-KCl) are provided. Such results are interesting in the development of combined hydrate-based desalination and CO_2 capture. Accordingly, an isochoric method is applied in a batch-mode reactor. A thermodynamic simulation tool based on van der Waals and Platteeuw approach and Kihara potential approach is utilized to reproduce equilibrium.

Keywords: Cyclopentane hydrates, Binary Cyclopentane and Carbon dioxide hydrates, thermodynamics, crystallization, water treatment, desalination.

General Introduction

This thesis takes the form of an articles collection, after having properly introduced the state of the art, the experimental apparatus and procedures, and the main results. The articles are listed as follows:

1. *Paper I: Cyclopentane hydrates – a candidate for desalination?* This article presents a systematic review of cyclopentane hydrate for desalination applications
2. *Paper II: Experimental Measurement and Thermodynamic Modeling of Cyclopentane Hydrates with NaCl, KCl, $CaCl_2$, or NaCl-KCl Present*. This first article of the thermodynamic study provides equilibrium data in presence of salts, and suggests the use of three thermodynamic approaches to model the results.
3. *Paper III: Implementing Cyclopentane Hydrates Phase Equilibrium Data and Simulations in Brine Solutions.* This second article of the thermodynamic study expands the system to other salts, and introduces the use of another approach: the Hu-Lee-Sum correlation.
4. *Paper IV: Crystallization mechanisms and rates of Cyclopentane Hydrates formation in Brine.* This article present the layer growth phenomenology and calculate the growth rates of cyclopentane hydrate in pure water and in the presence of salts
5. *Paper V: Morphology of Cyclopentane Hydrates in Saline Water.* This next article focuses on the morphology of cyclopentane hydrates. The effects of salt and subcooling on the geometric shape and the size of individual hydrate crystals are explored.
6. *Paper VI: Phase equilibrium measurements and modelling of mixed cyclopentane and carbon dioxide hydrates in presence of different salt solutions.* This final article on thermodynamics introduces another guest molecule: carbon dioxide. This new guest is interesting to couple water treatment to carbon capture process.

More details on these articles are provided in the following:

Our first effort is to perform a comprehensive review on CPH for salt removal application. All published studies available in the literature related to the thermodynamic, kinetic, hydrate phase properties, morphology, and the advancements of CPH in desalination are considered. In this work, we compare the desalting process via CPH crystallization to other traditional methods like distillation, freezing, and reverse osmosis. Our findings suggest that beside some challenges yet to overcome, CPH is a potential applicant for desalination.

After, the thermodynamic of CPH formation in the presence of salts (NaCl, KCl, $CaCl_2$, or NaCl-KCl) is investigated. Two procedures are applied to determine equilibrium. The first is at high dissociation rate, for approximation. The second is at a much lower dissociation rate, for more reliable data. Our measurements show that the equilibrium temperatures dropped considerably with increasing of salinity for all tested electrolytes. In addition, three thermodynamic models are developed to reproduce the equilibrium data. The first is based on the standard freezing point depression (SFPD) equation; the two others are based on van de Waals and Platteuw model. While one approach used optimized Kihara parameters, the last introduced a novel correlation between the occupancy factor and water activity. Modelling results indicate that all models have good capacities of predicting equilibrium. The last method, the activity-based occupancy correlation (ABOC), is the most recommended method to achieve accurate equilibrium.

Our next effort extends CPH equilibrium to four more common electrolyte solutions: Na_2SO_4, $MgCl_2$, $MgCl_2$-NaCl, or $MgCl_2$-NaCl-KCl at various salt concentrations. Of course, the two procedures (quick and slow) were again applied as before. Then, four thermodynamic approaches SFPD, Hu-Lee-Sum (HLS) correlation from Hu *et al* (2017,2018), and the two van der Waals and Platteuw-based (Kihara and ABOC methods) are compared to this new data. Again, simulation results illustrate that all four approaches reproduce adequately the CPH equilibrium temperature. Nonetheless, the ABOC method is confirmed to be the best method to achieve rapid and reliable equilibrium data of CPH in brine, whatever the salts involved.

Apart from thermodynamics, crystallization mechanism has been also investigated, such as hydrate layer growth rates, and morphology of CPH, hydrate layer growth rates, and morphology of CPH from pure water and brine. Different brine solutions of Na_2SO_4, NaCl, NaCl-$MgCl_2$, or NaCl-KCl-$MgCl_2$ at different concentrations (3.5% and 5% mass) were considered. Three different driving forces (subcooling of 2.5°C, 3.5°C, and 4.3°C) were considered. For that purpose, a small non-mixing batch-type vessel (inner volume ≈ 1.23 ml) connected to a microscopy was employed. We detected the primary formation of some individual crystals at the liquid-liquid interface vicinity. The hydrate layer crystallization began with a rapid nucleation at this interface. Then, the layer propagated mostly into the CP phase. Hence, we suggested that the water phase transports advectively through the presumably porous water-wet hydrate layer. Moreover, the hydrate layer growth rates

augmented with increasing of subcooling, with all salts considered. The growth rates also dropped with time due to the increased thickness of the hydrate layer.

In addition, our observations indicates that the CPH crystals morphology is approximately comparable at the same subcooling, while the size of the individual crystals drops significantly with increasing of subcooling, regardless the type of salts and their concentrations. Accordingly, subcooling might be served as a criterion to classification the morphology and the size of individual hydrate crystals.

Our last effort is to investigate thermodynamics of Cyclopentane (CP) + CO_2 binary hydrates in the presence of salt. That is crucial addition for hydrate-based desalination, especially when CO_2 capture process is involved. In this effort, new four-phase equilibrium measurements (V-L_W-L_{HC}-H) for CP/CO_2 binary hydrates in the presence of NaCl, KCl and a mixture of NaCl-KCl was obtained. An isochoric procedure was applied in a batch-type reactor. Then, the van de Waals model was utilized to model equilibrium. Expectedly, our results illustrate that the mixed CP/CO_2 hydrates are formed under milder conditions compared to the pure CO_2 hydrate. The presence of electrolytes in solution, unsurprisingly strongly inhibits the CP/CO_2 hydrates formation. Moreover, NaCl present a stronger influence than KCl, for the same salt concentrations. In addition, two different dissociation rates have been observed, showing a probable co-existence of single CO_2 SI hydrate and mixed CP/CO_2 SII hydrates. Then, the van de Waals approach is applied to describe the equilibrium. Simulation results indicate that this approach is capable of regenerating CP/CO_2 dissociation conditions with an average deviation than 0.4K for all tested brine systems.

In conclusion, this study helps at providing a reliable reference, or extensive data set, for the development of hydrate-based promising techniques, such as water treatment via CPH crystallization. Valuable thermodynamics, as well as kinetics, data are furnished. Hopefully, this work will provide an index for the research in this field.

Chapter I. State of the art

1.1. Clathrate hydrates

1.1.1. Definition and structure

Clathrate hydrates, are ice-like crystalline solids composed of water and guest molecules [1]. Water molecules are connected through hydrogen bonding system and form cages that enclose different guest molecules. Guest compounds can be small gas molecules like H_2, CO_2, N_2, CH_4, C_2H_6 C_3H_8 or larger molecules like Cyclopentane, Tetrahydrofuran (THF), or Tetra-n-butyl ammonium bromide (TBAB) etc. Note that, when gaseous molecules are guest in the structure, Clathrate hydrates are also called ''Gas Hydrates''. Because all cages are not occupied by guest molecules, clathrate hydrates are "nonstoichiometric" compounds [1]. Hydrate formation is not a chemical reaction, but only a physical phase-change reaction. Low temperatures and high pressures are usually favorable conditions for their formation.

Three principal polymorphs of clathrate hydrates are well-known: structure I (sI), structure II (sII), and structure H (sH). Each one contains of a certain quantity of different cavities formed by water molecules through a hydrogen bonding system.

Figure 1 and Table 1 illustrate the three main hydrate structures. In structure I (sI), each unit cell has 8 cavities including of two pentagonal dodecahedron (5^{12}) cavities and six tetrakaidecahedron ($5^{12}6^2$) cavities. The sI unit crystal fits a cubic 12 Å on a side [2]. Small guest molecules having diameters from 4.2 to 6 Å such as CH_4, C_2H_6, CO_2, or H_2S can form this hydrate sI. Indeed, hydrate sI can be found mostly in nature because CH_4 is the main constituent of natural gas. Potential reserves of natural gas hydrated located offshore and on land was reported to be over 1.5×10^{16} m^3 [3].

Structure II and H hydrates can accommodate larger guest molecules, such as C_3H_8 or iso-butane (6Å <diameters <7 Å) for sII or mixtures of CH_4 and Neohexane or Cycloheptane (7Å <diameters <9 Å) for sH. Interestingly, smaller molecules with diameters inferior to 4.2 Å, such as Nitrogen or Hydrogen, can also form structure II as single and multiple guests [1]. In sII hydrates, each unit cell contains sixteen small pentagonal dodecahedron (5^{12}) cavities and eight large hexakaidecahedron ($5^{12}6^4$) cavities. Structure II hydrates are usually found in oil and gas operations and processes.

In the case of sH, each unit cell presents three small pentagonal dodecahedron ($5^{12}6^2$) cavities, two medium dodecahedron ($4^35^66^3$) cavities, and one large icosahedron ($5^{12}6^8$) cavity. Structure H hydrates are rarely found in non-natural (gas storage [4]), or in natural processes (Gulf of Mexico continental slop [5]) [2,6].

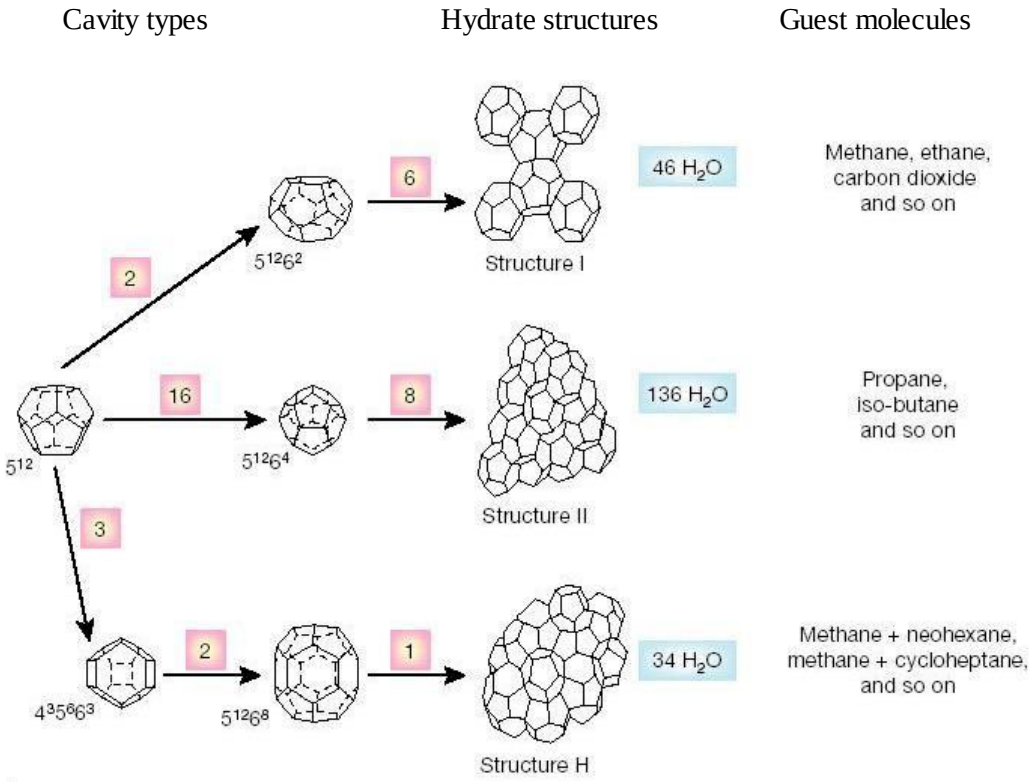

Figure 1: Three main hydrate structures and their constitutive cavities (taken from Sloan and Koh [7])

Table 1. Summary of three principle hydrate structures [7]

Hydrate structures	sI		sII		sH		
Cavity	Small	Large	Small	Large	Small	Medium	Large
Description	5^{12}	$5^{12}6^2$	5^{12}	$5^{12}6^4$	5^{12}	$4^35^66^3$	$5^{12}6^8$
Number of cavities per unit cell	2	6	16	8	3	2	1
Average cavity radius (Å)	3.95	4.33	3.91	4.73	3.91[b]	4.06[b]	5.71[b]
Coordination number [a]	20	24	20	28	20	20	36
Number of waters per unit cell	46		136		34		

[a]The number of oxygen atom per cavity; [b]Estimates of sH cavities from geometric model

Typically, in all three hydrate structures, each cage hosts only one guest molecule. Nevertheless, under very high pressure, the clathrate cages can be multiply occupied with several abnormally small guests, like hydrogen, or inert gases such as nitrogen. For instance, Mao et al [8] indicated that, at pressures from 180 to 200 MPa, the clathrate cavities can be multiply occupied, with a cluster of two hydrogen molecules in the small cavities and four in the large cavities.

Note that, when all cavities are fully occupied by guest molecules, the hydration number (number of water molecule/number of guest molecules) for Structure I, Structure II, and H hydrates is ideally 24/3, 17/3, and 17/3, respectively [1] .

Several examples of hydrate formers with their hydrate structures can be found in Table 2. Of course, the kind of hydrate structure depends on the type and the size of guest molecules. In addition, some help gases like Xe, CH_4 are utilized to stabilized hydrate structure since they occupy the small empty cages.

Table 2. A list of guest molecules and their hydrate structures [1].

Guest molecules	Hydrate structures
Ar	II
H_2	II
N_2	II
CO_2	I
CH_4	I
C_2H_6	I
C_3H_8	II
Cyclopentane	II
Benzene with help gases Xe	II
CH_2ClCH_2Cl with help gases air	II
2-Methylbutane with help gases Xe	H
Cycloheptane with help gases CH_4	H
Methylcyclopentane with help gases Xe, CH_4	H

1.1.2. Phase equilibria of clathrate hydrates

Usually, Clathrate hydrates phase equilibria are determined in terms of the following variables: (1) pressure, (2) temperature, and (3) phases' compositions. Other variables like volume or density, phase amount may be mathematically calculated by phase equilibria and validated by some measurements that are challenging to achieve and hence not common [1].

Let us remind the Gibbs' Phase rule, providing the number of degree of freedom, in terms of intensive parameters, for a system:

$$F=2+C-P' \quad (1)$$

Where F is the number of intensive variables needed to specify the system, C is the number of components in the system and P' is the number of phases in the system.

Temperature (T), pressure (P), and phase mole fractions (hydrate, liquid, or vapor phases) are intensive variables, measurable, and hence independent of the phase amount. However, masses or volumes are extensive variables, and cannot be considered in the Gibbs' Phase rule.

In the case of Clathrate hydrates, there are at least two compounds: water, and a guest molecule. An addition of guest molecules increases the number of degree of freedom. The number of phases depends on the kind of molecules, and the operating conditions. Let us take an example: methane hydrates, or nitrogen hydrates. Phase diagrams of these, at conditions inside and outside the hydrate region, are illustrated in Figure 2a. Note that Pressure and Temperature are the usual two variables considered, over composition. In the figure, I, L_W, H, V, and L_{HC} correspond to ice, water liquid, hydrate, vapor, and hydrocarbon liquid, respectively. Q_1 is the quadruple point, defining as the starting point for four three-phase lines. More details on all these three-phase lines are described as follows:

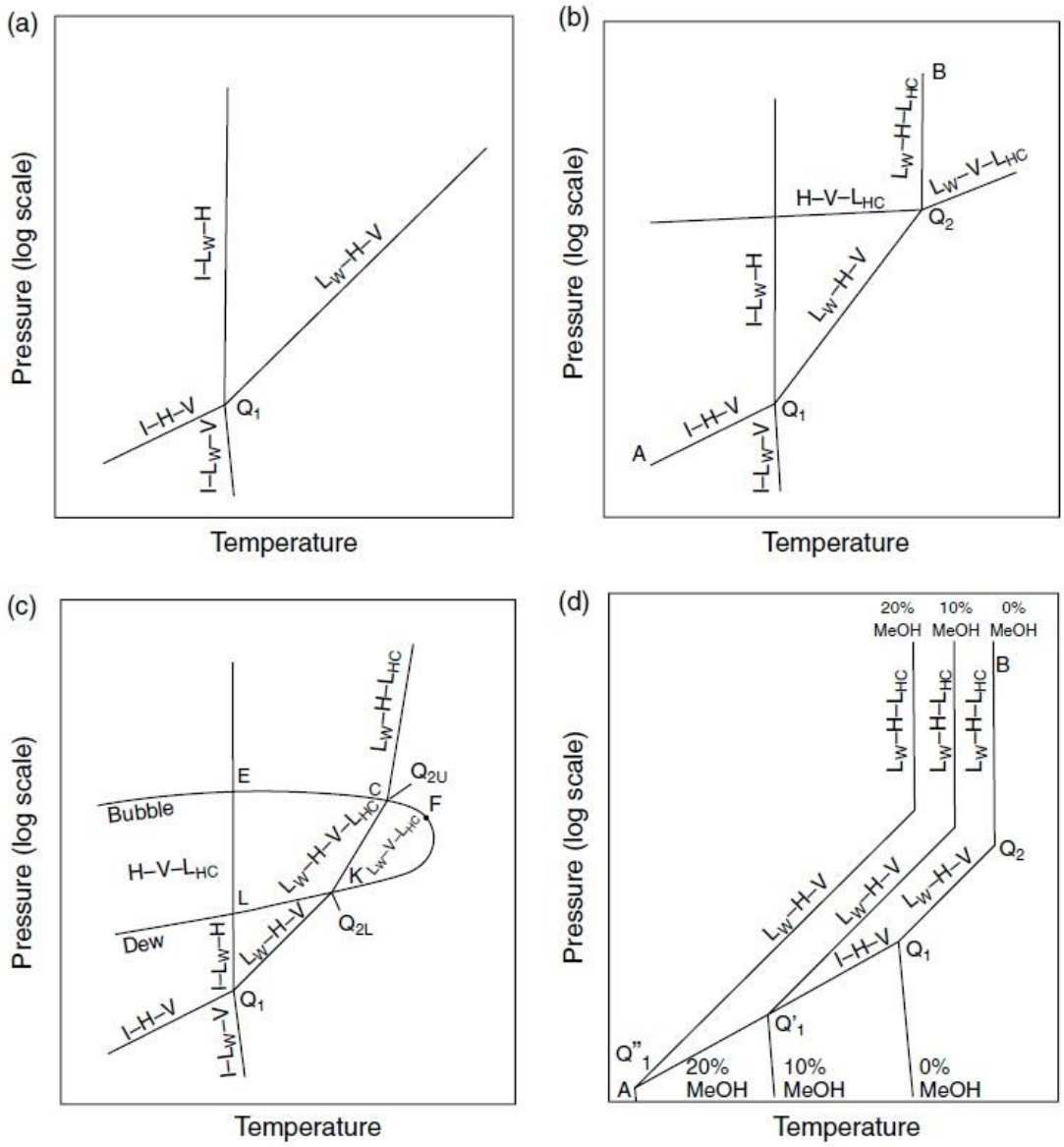

Figure 2: Hydrate phase diagrams. (a) CH_4+H_2O or N_2+H_2O, (b) Hydrocarbon + H_2O with upper quadruple points, (c) Multicomponent natural gas + H_2O, (d) Hydrocarbon + H_2O with upper quadruple points and inhibitors (taken from [1])

- The L_W-H-V line includes thermodynamic conditions of P-T that are crucial in natural gas systems.
- The I-H-V line has a lower P-T slope than the L_W-H-V line. Data in the region below 273 K are limited because of ice formation issues.
- The I-L_W-H line goes up vertically from the Q_1 point. Because phases are incompressible in this region, a huge pressure change is hence required for a minor temperature change.

- The I-L_W-V line links the quadruple point to the water triple point (I-L_W-V_W) (273.16 K, 0.62 kPa). This outlines the transition between water and ice without hydrate crystallization. The I-L_W-V line is nearly vertical below Q_1 to 0.62kPa because Q_1 is about 273 K for all natural gas systems.

Figure 2b illustrates a second quadruple point (Q_2=L_W-H-V-L_{HC}) formed at the intersection of L_W-V-L_{HC} line with the L_W-H-V line. In this system, the hydrate area is bounded by three lines: I-H-V below Q_1, L_W-H-V between Q_1 and Q_2, L_W-H-L_{HC} above Q_2. This means no hydrate can form at conditions (T, P) to the right of the area bounded by these three lines. Since the L_W-H-L_{HC} line rises vertically, the upper point Q_2 is close to the maximum temperature of hydrate crystallization.

Indeed, the lower quadruple point Q_1 represents the transition of liquid water to ice and hydrate crystallization from ice and vapor. The upper quadruple point Q_2 signifies the upper temperature limit for hydrate crystallization. Methane and nitrogen are known as hydrate formers with no upper quadruple point because of their low vapor pressure at the critical temperature, meaning no temperature limit for hydrate formation.

Multicomponent natural gas hydrate phase diagram is detailed in Figure 2c. Note that, the L_W-H-V line is applied for a hydrocarbon mixture, not for pure CH_4. The quadruple point Q_2 is at the intersection of the L_W-H-V line at 273 K at a pressure lower than that for CH_4.

Interestingly, the L_W-V-L_{HC} line becomes a region, labeled CFK in the figure. The reason is that no single hydrocarbon is present and that a combination of hydrocarbon + water vapor pressure generates a phase equilibrium envelope. Accordingly, the upper quadruple point Q_2 changes into a line (KC). The lower point K is created by the intersection of the phase envelope ECFKL with the L_W-H-V line. Whilst the upper point C is determined via a vapor-liquid equilibrium calculation.

The effects of inhibitors such as salts, alcohols, or glycols on thermodynamic equilibrium of hydrocarbon + water system are presented in Figure 2d. Simply, the hydrate bounding area (to the left of AQ_1Q_2B line) is illustrated. As seen in the figure, the line Q_1Q_2B is shifted approximately parallel to the left with inhibitor present. The ice formation temperature is also decreased. Accordingly, the intersection point between the L_W-H-V line and the I-H-V line is at lower location (labeled Q_1' and Q_2' for 10 % and 20 % mass methanol).

Obviously, each inhibitor has a different effect on the hydrate equilibrium. Numerous inhibitors have been also thermodynamically tested in the hydrate formation like glycol (EG or MEG) and salts. However, ethanol is considered to be the most economical inhibitor on a mass basis.

When hydrate formers are liquid such as Tetra-n-butyl ammonium bromide (TBAB), Tetrahydrofuran, Cyclopentene, or cyclopentane, no pressure is usually needed to form clathrates. The hydrate phase diagram is hence expected to be simpler compared to that with gas hydrates system. This fact brings potential opportunities for several hydrate-based applications in water treatment, air-conditioning, or cold thermal energy because no high pressure devices are required. Cyclopentane is one of these hydrate guests which have gained increasing attention in water treatment, or water decontamination applications in the last decades. Note that thermodynamic modelling will be presented later in the chapter III.

1.1.3. Issues and potential applications of clathrate hydrates

Clathrate hydrates have been extensively investigated in the last decades. In fact, hydrate formation is a common issue in the oil and gas industry. Clathrate hydrates are solid and non-flowing crystalline structure. Furthermore, oil and gas wells normally generate water along with gases or hydrocarbon. When they are in the hydrate zone, water and gases or hydrocarbon can form solid hydrates and plug pipelines, causing equipment and environment damages (see Figure 3) [7]. Therefore, safety is probably a key reason for understanding hydrate blockages [2].

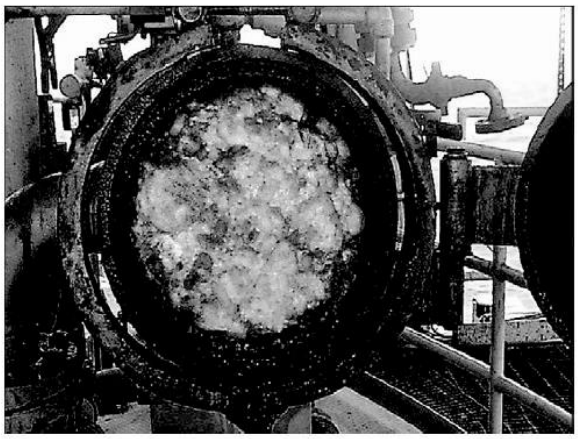

Figure 3: Solid hydrates obtained from the slugcatcher [2]

Hydrate formation issue in the pipeline can be prevented by both physical method (controlling pressure, temperature, and water removal) and chemical method (Thermodynamic Hydrate Inhibitor – THIs; Low Dosage Hydrate Inhibitors (LDHIs); Kinetic Inhibitor or Anti-Agglomerants – AAs [1]. Indeed, chemical methods are more widely utilized than physical methods as their low cost. Among the chemical techniques, LDHIs are recently considered to be an advanced and sustainable technology in flow assurance.

Besides, clathrate hydrates have also many potential applications in both industry and environment because of their several key physical and chemical properties [7]. Gas hydrates can be used for gas storage [9–11], hydrogen storage [12], carbon dioxide capture [13–15], gas separation [16,17], air-conditioning and cold thermal energy [18–20], and desalination [21–24]. Of course, more experimental studies are still required to optimize the innovative and sustainable hydrate-based applications. More details of these applications are provided in the following:

It was found that approximate 70% of the gas reserve is too far from a current pipeline system or too insignificant to justify a liquefaction system [7]. Thus, transport of natural gas by pipeline system or LNG is very costly. In addition, this technique is dangerous due to natural gas is super inflammable and explosive at high pressures. Transport gas in hydrate form technology could be cheaper and safer than traditional methods. Indeed, one cubic meter of clathrate hydrates can accommodate approximate 180 Nm^3 of CH_4 [4]. In addition, because no very low temperatures are required (0.1 MPa and 193 K without promotor, 0.1 MPa and 277.2 K with promotor [25]), natural gas storage in hydrate form is cheaper than in LNG form (0.20 MPa and 113.2 K [25]).

Furthermore, as hydrogen is considered as a next generation clean energy, investigations on hydrogen storage have been performed intensively in the last decades. Hydrate-based storage technology is safer and probably more economically feasible than other traditional methods [7,26]. An up-to-date systematic review and upcoming instructions for hydrogen storage in gas hydrate form can be found in the work of Veluswamy et al [12].

Carbon dioxide capture and gas separation are promising applications of clathrate hydrates. The concept of using clathrates for these applications is based on the fact that gas molecules are absorbed selectively in hydrate cavities depending on their shape and size during hydrate crystallization. Accordingly, this property of clathrates could be applied to separate [16,17] or storage [13–15] the desired guest molecules from their mixtures. The advantages of these

hydrate-based technologies are milder operating conditions and hence lower energy requirements are required.

Currently, numerous techniques for thermal energy storage have been developed for air-conditioning. Thermal energy storage systems via the liquid-solid phase change of water are now usually employed for both industrial and domestic air-conditioning [27]. However, this technique requires the coiled tubes on which the ice layers grow to be reserved at low temperatures from -4 to -10^{o}C, limiting factor of the coefficient or performance (COP) of the refrigerator. Accordingly, a new thermal energy storing material that undergoes a phase change at a temperature close to the desired temperature (7 to 12^{o}C) for air cooling is required. For instance, TBAB (tetra-n-butylammonium bromide) can form hydrates at temperatures between 5 and 12^{o}C [27,28]. This new cooling storage material is hence well-suited to air-conditioning. Consequently, the use of hydrate (TBAB) for air conditioning has been investigated [18,19] and commercialized [20]. This hydrate-based technique is considered to be a sustainable energy-saving technology.

Lastly, desalting seawater is also another promising application of clathrate hydrates [7,29]. The concept of this technique is simply based on the fact that, during hydrate crystallization, salts are excluded and remain in the liquid solution. Eventuelly, they can even precipitate in the concentrated solution. Afterward, salts can be removed by a physical separation technique. Finally, pure water can be achieved after dissociation of the hydrates. Note that this approach can also be used to treat wastewater, or recover dissolved value added products.

In order to optimize these hydrate based technology, more studies are still necessary including thermodynamics, kinetics, crystallization mechanisms, morphology, hydrate physical and chemical properties, hydrate composition, volume and storage capacity, consistent simulation tools to predict hydrate equilibrium.

1.2. Cyclopentane hydrates

This section presents a brief presentation about cyclopentane hydrates including hydrate structure, thermodynamic of pure cyclopentane hydrates and mixed CP-CO_2 hydrates which are crucial in hydrate-based applications via cyclopentane hydrate crystallization.

1.2.1. Introduction to cyclopentane hydrates

Cyclopentane forms hydrates sII with water at a temperature less than approximately 7.1°C [27] without a help of a high pressure equipment, according the following equation:

$$C_5H_{10} + 17\ H_2O = C_5H_{10}.17H_2O\ (CPH) \quad (2)$$

In this pure sII hydrates, due to its size, cyclopentane only occupies the large 51264 cages, while leaving the small 512 cages empty, as illustrated in Figure 4.

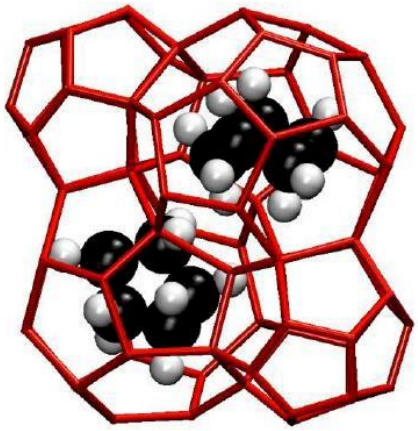

Figure 4: Occupation of the large cages ($5^{12}6^4$) of hydrates sII by CP molecules [30]

In the presence of a gas or several gases, a mixed hydrate of CP+H_2O+gas can be formed. In this mixed hydrates, large cages ($5^{12}6^4$) of the structure are occupied by the CP, while small cages (5^{12}) are occupied by small "gas'' molecules, like CH_4, CO_2, or N_2.

Unique structural features and physical and chemical properties of CPH have gained much attention of scientists. Indeed, their work focused on four distinct areas: the use of CPH as a thermodynamic promoter to lower the pressure of formation of mixed hydrates including gas [31,32]; the use of CPH as a "kinetic" promoter to improve the kinetics of capture gases, the use of CPH in hydrate slurries, and the use of CPH in water treatment.

In order to develop the use of CPH, phase equilibrium data of CPH are crucial. Thus, in the next subsection, the thermodynamic of CPH is presented.

1.2.2. Thermodynamics of Cyclopentane hydrates

At normal atmospheric conditions, according to literature, the equilibrium temperature of CPH in pure water rage from 6.3°C to 7.7°C. Several techniques were applied to determine the equilibrium temperatures of CPH like Differential Scanning Calorimetry (DSC) [27,33–36], or polythermal method [37–41]. Among these techniques, the polythermal method (at low heating rate) and DSC methods provide consistent and reliable equilibrium data for CPH (around 7.1°C). However, polythermal method is sometimes used with a high heating rate (room temperature) [40–42]. In this case, the induced quick dissociation usually misses the right equilibrium temperature, because of the high melting rate. Accordingly, the value of equilibrium temperature obtained by the quick technique (approximately 7.8°C) is usually higher than the supposed genuine value. Moreover, in the presence of surfactants, the equilibrium temperature can be reduced [35,36,43,44]. This is because surfactants modify the interfacial tension force between cyclopentane and water. The hydrate formation is hence affected.

Under vacuum conditions, Fan et al. [90] reported the CPH equilibrium data with the range of temperature of 0.21-7.07°C and the pressure of 6.9-19.8 kPa. Moreover, at high pressure (2.55-12.55 Mpa), Trueba et al. [94] reported hydrate (H) – aqueous liquid (L_W) – cyclopentane-rich liquid (L_a) phase equilibrium data. Their results show that the CPH equilibrium temperatures (range from 6.75°C to 6.88°C) are nearly constant with the increase of pressure.

In presence of common electrolytes, CPH equilibria have not been comprehensively investigated in the last past [35–37,39,40,45]. In these studies only NaCl at various salt concentrations is considered. Two main experimental procedures were applied to determine the hydrate dissociation temperatures: polythermal method [37,39,40,45], and DSC [35–37]. Again, the polythermal method at low heating rate and DSC are capable of providing the accurate equilibrium data

1.2.3. Mixed CO_2+cyclopentane hydrates

Mixed CP+CO_2 hydrates form structure II. As explained before, CP molecules occupy large cavities while CO_2 molecules occupy small cavities. However, although CP usually fill most of the larges cages, note that CO_2 molecules do not necessary fill all small cages. This will be supported later in thermodynamic modelling part of the experiments (section 6.6). CP-CO_2

binary could be a potential candidate for both desalination [46] and carbon capture [15] applications. Of course, in order to develop this combined application, equilibrium data of mixed CP+ CO_2 are needed.

A summary of all studies in the open literature on equilibria of mixed CP+CO_2 is presented in Table 3. In these mentioned studies, an isochoric procedure was applied to determine the equilibria. In pure water, numerous hydrate formation conditions ranging from 275.5 K to 292.60 K and from 0.08 Mpa to 4.88 Mpa were reported [15,32,47–50].

Obviously, equilibrium data in brine are required when attempting to apply mixed CP+CO_2 hydrates for desalination. Cha and Seol [51] investigated upper temperature limit of CO_2 hydrate formation in the presence of CP and simulated produced water (8.95 wt% salinity) at isobaric condition (3.1 MPa). They witnessed that the upper temperature limit for CO_2 hydrate is -2C, while for mixed CP-CO_2 hydrate is 16°C. Zheng et al. [46] measured equilibrium data of CP-CO_2 hydrates in the presence of 3 wt% NaCl. Their experiments were carried out with different molar ratios of CP/water. Results indicate that the increase in CP quantity led to a significant drop in equilibrium pressure. In addition, they reported the optimal molar ratio of CP is 0.01 for CO_2 hydrate-based desalination. Zhang et al. [52] studied on the phase equilibrium of CO_2-CP in the presence of NaCl under a wide range of salt concentrations (0, 3.5, 7.0, 10.0, 15, 25% mass). Interestingly, their results show that CP reduces the equilibrium pressure and improves the salt removal efficiency.

Table 3: A summary on equilibrium data of mixed CP+CO_2 hydrates

Aqueous solution	Temperature range (K)	Pressure range (Mpa)	Citation
Pure water	280.16 – 292.60	0.08 – 4.88	[47]
Pure water	284.6 – 291.6	0.49 – 2.58	[48]
Pure water	275.5 – 285.2	0.42 – 0.59	[15]
Pure water	284.3 – 291.8	0.35 – 2.52	[50]
Pure water	281.55 – 290.25	0.15 – 1.92	[49]
Pure water	283.5– 287.5	0.761– 1.130	[32]
Simulated produced water: 8.95 % mass	280.15 – 289.15	3.1 (isobaric)	[51]
NaCl: 3.0% mass	271.89 – 292.21	0.55 – 3.59	[46]
NaCl: 0, 3.5, 7.0, 10.0, 15, 25% mass	269.8 – 292.4	1.18 – 3.33	[52]

1.3. Clathrate hydrates for desalination

The use of clathrate hydrates for desalting is an inspiring potential hydrate application, since salts are left out from clathrate hydrates crystallization. The concept of desalination via clathrate hydrate is illustrated in Figure 5.

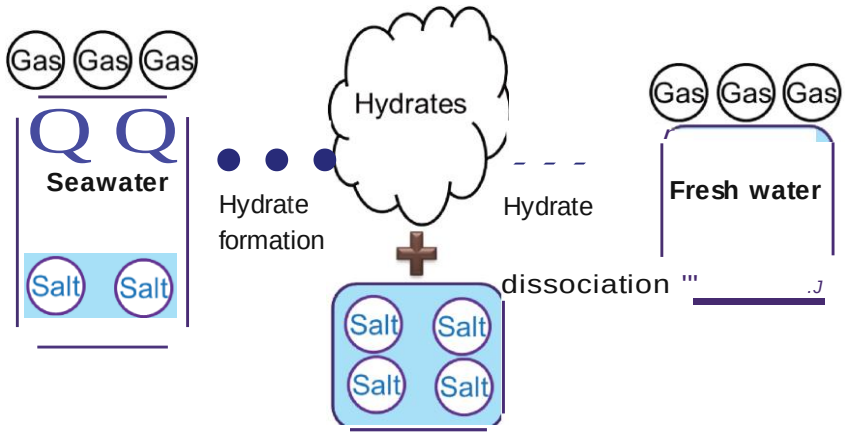

Figure 5: A simplified schematic of clathrate hydrates based desalination

This process increases the sait concentration in the aqueous solution. Moreover, hydrate phase can be removed by a physical separation process and then can be dissociated at normal room conditions. Upon dissociation process, fresh water and guest molecules can be released from clathrate crystals. Guest molecules can then be recycled (CP) or stored ($C0_2$).

Indeed, the utilization of clathrate hydrate for sait removing process was first explored in 1940s [53]. After, in the 1960s and 1970s, major researches and irnprovements on this process were performed [54-57]. A summary on the progress of desalination via hydrate formation is schematically demonstrated in Figure 6.

As shown in Figure 6, a remarkable progression on clathrate hydrate-based desalination was made. However, this technique is still not commercial ready since some challenges conceming the cost and the purification level of produced fresh water have not been overcome yet. Varied guest molecules were tested for this technique such as propane [58,59,63,64], carbon dioxide [22,62,64-69], refrigerant [23,59,60,70,71], or methane [72,73]. lndeed, methane and $C0_2$ are identified as greenhouse gases, thus these gases can bring risks into our environment when they are accidentally released. Refrigerants are ozone depletion compounds. They are hence restricted by current environmental regulations and are no longer practical candidates for a hydrate desalination process, despite their ease of use [61].

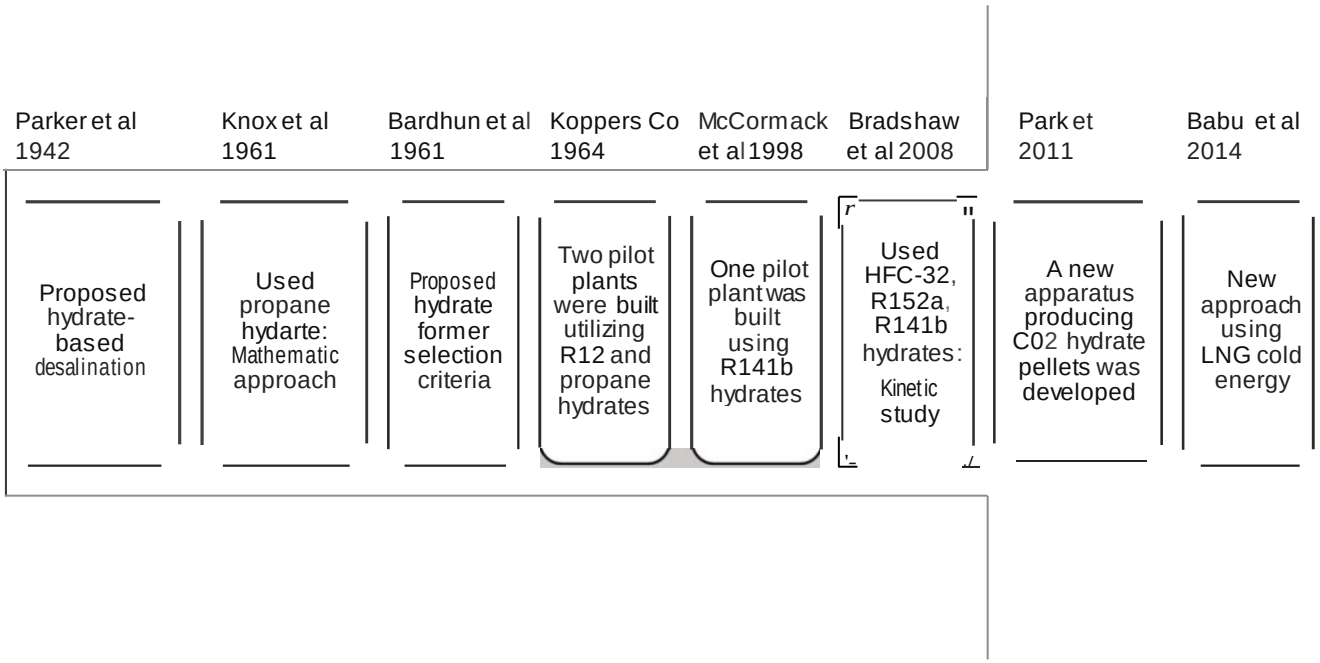

Figure 6: Progression in desalination via hydrate formation [53,54,58-63] (adapted from Babu et al [24])

Recently, more than 20 key inventions made over the world to desalination by using clathrate hydrates were detailed according the review work of Babu et al [24]. These efforts focused mainly on the improving the hydrate crystallization kinetics, as well as separating sait entrapped between hydrate particles . In order to reduce the induction time, some techniques were proposed such as the use of ultrasonic energy, or micro-bubbles, or localized super-cooling by depressurizing liquid propane. Furthermore, secondary purification treatments such as washing were also employed to remove sait entrapped on the hydrate crystals surface. Unfortunately, this step leads a decrease in the overall water recovery of the desalination. Another effort was the use refrigerants such as CFC in order to reduce the total operating cost due to it can form hydrate with water at atmospheric pressure. However, as aforementioned, CFC is considered as a toxic and damageable to the environment. The use of CFC for desalination application is hence not encouraged.

Lately, He *et al.[29]* suggested a new hydrate based desalination system using Liquefied Natural Gas (LNG) cold energy. Compared to multi-stage flash distillation (MSF), reverse osmosis (RO), and freezing desalination processes, this technology can be attractive since LNG cold energy replaces the external refrigeration cycle, and hence reduces the specific energy consumption.[29] Evident1y, this nove] techno1ogy sti11 requires a large and steady

source of LNG cold energy. High-pressure reactor is also needed because propane is utilized to form hydrate.

Obviously, before hydrate desalination becomes a practical commercial technology, the vital issues of controlled hydrate nucleation, formation rate, phase properties, as well as the amount of entrapped salt, and its removal efficiency must be thoroughly understood and optimized [61].

1.4. Case of Cyclopentane hydrates-based desalination

Gas hydrate-based desalination is costly when a gas is employed as a hydrate former. Cyclopentane is considered to be a promising replacement, or additive, of the gas molecules. Because CPH crystallization can take place at atmospheric pressure, the energy requirement for desalination process via CPH is hence expected to be lower than that when using gas hydrates. Plus, cyclopentane present a low, although not negligeable, solubility in water (0.156 g/l at 25 °C [74]). Therefore, it can be recycled easily after dissociation.

In term of latent heat of phase change, CPH has a lower phase change enthalpy [40,75,76] compared to that of CHFC 141b hydrate [77], CO_2 hydrate[78], propane hydrate [79]. In addition, the CPH dissociation heat is also lower than the heat of vaporization of water, and the heat of freezing of water [40]. The energy required for CPH-based desalination is hence likely less than that for desalination using CHFC 141b hydrate, CO_2 hydrate, propane hydrate, and for desalination via thermal distillation, the freezing processes.

Recently, several remarkable investigations on CPH based desalination were conducted [28,40,80–86]. Corak et al [82] investigated the effects of subcooling and quantity of cyclopentane desalination via CPH. They indicated that the effect of cyclopentane quantity is not considerable, while subcooling affects significantly on the hydrate formation and hence desalination. At subcooling of 5.6K, the desalination is more effective than that at a subcooling of 3.6K. They suspected that the adhesion force between hydrate crystals at 3.6K than that at higher subcooling. Consequently, the hydrate particles conserve more salt entrapped, resulting a difficulty in removing salt from hydrate crystals formed. Indeed, their observations remain still speculations, thus more experimental data of the effect of subcooling on desalination via CPH should be added.

Cai et al [84] studied a binary hydrate of cyclopentane + methane mixture in both thermodynamic and kinetics for desalination application. After, a new displacement washing technology was proposed to remove salts from CPH particles. Their results show that this technique can achieve a very high hydrate recovery rate (100%). Thus, a high water efficiency can be expected.

Han et al [40] tested several secondary treatment methods including washing, centrifuge, and sweating for the purification steps. They indicated that centrifuging provides the highest salt removal efficiency (approximately 96%). However, this method requires much energy compared to others. Sweating produced salt removal efficiency around 95%. Unfortunately this technique reduced the water produced quantity, whilst washing shows a salt removal efficiency about 93% without difficulties as two other methods are suffering. Washing is hence considered as a promising post-treatment technique for desalination via CPH. The authors [83] then tried to optimize several conditions such as operation temperature, or amount of washing water when utilizing the washing treatment method. Their results are hopefully useful for the CPH based desalination design.

Xu et al [81] examined the effect of some factors such as agitation speed, operation temperature, and cyclopentane injection method on water conversion to hydrate in order to improve desalination using CPH in a bubble column. Three-step separation technique, including gravitational separation, filtration, and washing was proposed to remove brine entrapped between hydrate crystals. Their results illustrate that this separation technique can reduce considerably salinity in the solid hydrates (salt removal efficiency approximately 81%).

Recently, Ho-Van et al [28,80,86] reported a numerous equilibrium data of CPH in the presence of diverse salts and four developed thermodynamic tools for simulations equilibrium in order to fill some of the gaps in the promising technique of sea-water separation via CPH crystallization. The authors also tried to explore the CPH crystallization mechanism, hydrate growth rate, as well as hydrate morphology in brine. Hopefully, the authors' results can be utilized to improve this desalting technique. See papers II and III of this thesis.

In term of water purification level, Mottet [87] indicated in his invention that the water produced via CPH crystallization has a salinity of 1000 ppm (mg/l of water). Cai et al [84] reported the salinity is less than 10 ppm when using a displacement washing technique. In

addition, while Han et al. [40,83], and Lv et al. [85] show the salinity is in the range of 1400-2000 ppm, Xu et al [81] and Li et al [88] indicate this level is 6700 and 5250 ppm, respectively.

Note that, the palatability of water with a total dissolved solids (TDS) level of less than about 600 mg/l is acceptable. The salinity of treated water via CPH crystallization is usually high since salts are entrapped in hydrate particles. Thus, post-treatment methods like washing or centrifuging are needed to eliminate salt in order to obtain fresh water with salinity in the range suggested by WHO.

As aforementioned, cyclopentane act as a hydrate crystallization promoter (both thermodynamic and kinetic) for other hydrate-based applications, such as carbon capture [14,46]. Indeed, the mixed hydrates of CP+ N_2 [89–92], CP+ CO_2 [47,48,89,90,93], CP+CH_4 [90,91,94,95], or CP+ H_2S [95] form at milder conditions compared to the pure gas hydrates without CP. Thus, CPH could be applicable for combined gas capture and desalination.

To sum up, although efforts on investigation of CPH based desalination technique have been made, but more effort on experimental studies regarding thermodynamic, kinetics, hydrate crystallization mechanism, hydrate crystal morphology, post-purification steps are still required in order to make this technique a reality.

Chapter II. Experimental system for thermodynamics

This section provides the experimental methodology to investigate the thermodynamic of pure CPH and mixed CP+CO_2 hydrates. Materials used, apparatus, and experimental protocols for each clathrate system study are presented in details. A summary of the results is also presented.

2.1. Materials

In this study, cyclopentane (CP, or C_5H_{10}), NaCl, KCl, $CaCl_2$, $MgCl_2$, Na_2SO_4 were all provided by Sigma-Aldrich Company. CO_2 was provided by Air Products. A water purification system was utilized to produce high-purity water with a conductivity $\sigma \leq 0.055$ $\mu S.cm^{-1}$ and TOC (total organic carbon content) less than 5 ppm. Details of chemicals are listed in Table 4.

Table 4: Purity of initial material used

Material	Chemical formula	Mol.weight (g. mol^{-1})	Solubility in water (g/l)	Purity %mol
Cyclopentane	C_5H_{10}	70.1	0.156 (25 °C)[74]	98.0%
Sodium chloride	NaCl	58.4	360 (20 °C)[96]	99.5%
Potassium chloride	KCl	74.55	344 (20 °C)[96]	99.0%
Magnesium chloride	$MgCl_2$	95.21	54.6 (20 °C)[96]	99.5%
Sodium sulfate	Na_2SO_4	142.04	19.5 (20 °C)[96]	99.5%
Calcium chloride	$CaCl_2$	110.978	745 (20 °C)[96]	99.0%
Carbon dioxide	CO_2	44,01	0.1688 (20°C)[96]	99.999%

2.2. Experimental apparatus

In this section, we present all experimental apparatus for CPH and binary CP+CO_2 hydrate thermodynamics study. Besides, for each apparatus system, a brief explanation of the experimental procedure is also offered.

2.2.1. Experimental apparatus for Cyclopentane hydrates thermodynamics study

Apparatus description

The experimental apparatus for CPH thermodynamic investigation is illustrated in Figure 7.

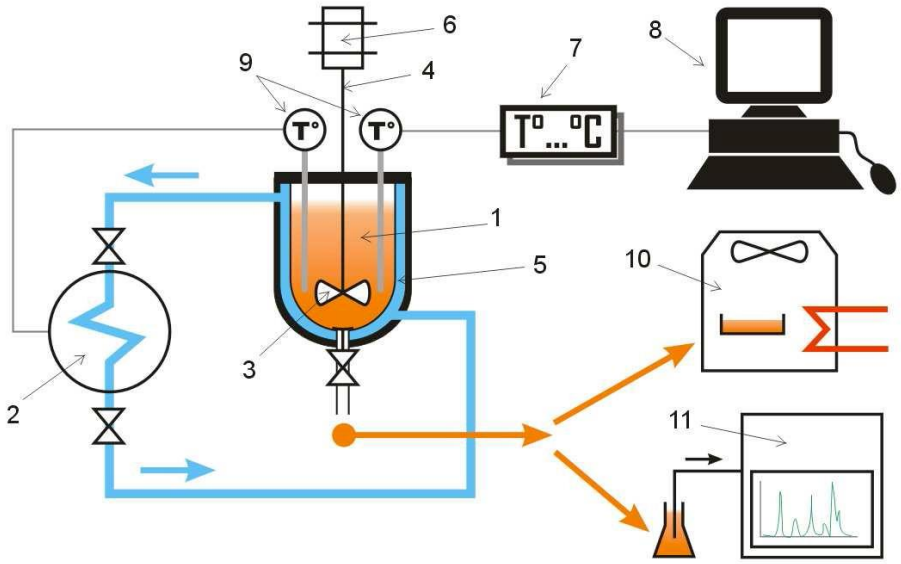

Figure 7: Simplified schematic of the apparatus for CPH thermodynamic study [28]

1-Vessel, 2-Chiller, 3-Impeller, 4-Agitator, 5-Cooling jacket, 6-Motor, 7-Temp transmitter, 8-Computer, 9-Temperature probe, 10-Drying oven, 11-Ion chromatography

A batch-type one-liter reactor (1) is equipped with a double jacket (5). Chiller (2) controls temperature of the solution inside the reactor. The impeller (3) is driven by a motor (6) to agitate the solution. Two temperature sensors (9) are employed to monitor the temperature inside the reactor which is then transferred to a computer (8) thanks to a transmitter (7). A drying oven (10) and an ion chromatography system (11) are also employed to measure salt concentration of the solution.

Experimental procedure.

In this study, two procedures are developed to determine the equilibrium temperatures of CPH: Quick and Slow dissociation, as presented by Ho-Van et al [28,80,86]. A brief description of these two procedures is offered as follows:

Quick dissociation procedure: This procedure provides a first and valuable estimation of equilibrium. At first, CP + brine solution are introduced into the reactor. Chiller is then employed to decrease temperature (1-2^{o}C above the freezing-point of the salt solution) to form clathrates. Sometimes, a small amount of ice is introduced to start the crystallization. When a remarkable CPH amount has been formed inside the reactor, the chiller is stopped. CPH then melts due to environment heat-transfer. When the dissociation has completely, a significant increase in temperature is observed. This point furnishes the equilibrium temperature

estimation of CPH at the initial salt concentration. Then, 1 ml and 5 ml of the brine are taken at the bottom of the reactor to measure salt concentration by both ion chromatography and drying oven. The objective of this step is to validate the accuracy of the equilibrium temperature. If two salt concentrations before the experiment and at the end of the hydrate dissociation process are identical, then this indicates that all CPH have completely dissociated. Hence, the recorded temperature either corresponds to the equilibrium or is slightly above the equilibrium value.

***Slow dissociation procedure*:** This procedure offers more accurate data, based on the approximation achieved from the previous experiment. After an adequate amount of CPH has been formed, the temperature inside the reactor is augmented at an increment of 0.1°C instead of using ambient temperature. The temperature is then maintained steady for at least 1 hour. If a noteworthy quantity of CPH is still observed after 1 hour, the temperature is augmented. Mixing is kept at 300-400 rpm. This process is iterated until a few CPH remains in the reactor. Then, temperature is augmented of 0.1 °C, and is kept for days to ensure that equilibrium is reached. If crystals are still witnessed, one more step is repeated. The equilibrium is supposed to be observed during penultimate step just before the final one as all three phases (CP, CPH and brine) exist, and its value is the equilibrium temperature of CPH. Images of brine are also taken at every step. The images are then compared in order to determine the final step in which only two aqueous transparent phases of brine and CP can be observed as seen in the initial condition.

2.2.2. Experimental apparatus for CP+CO_2 hydrates thermodynamics study

Apparatus description

Diagram of experimental set-up for mixed CP+CO_2 hydrates thermodynamic study is provided in Figure 8. The main devices are two jacketed batch-type reactors (2) with almost the same shape and configuration. The inner temperature is controlled by a cooling bath (1). Two sapphire windows (3) permit direct surveillance. The agitator (5) has two sets of blades; the top is in the gas phase and the bottom in liquid. Two temperature sensors (6) at the top and bottom of the reactor are employed to monitor the temperature in gas and liquid phases, respectively. A pressure probe is also utilized to record the pressure. A HPLC pump (8) at high pressure is used to introduce water and CP into the reactor. A mechanical valve is connected to a capillary tube in the liquid phase is employed to take liquid samples. Data is controlled on a personal computer (10) running Labview.

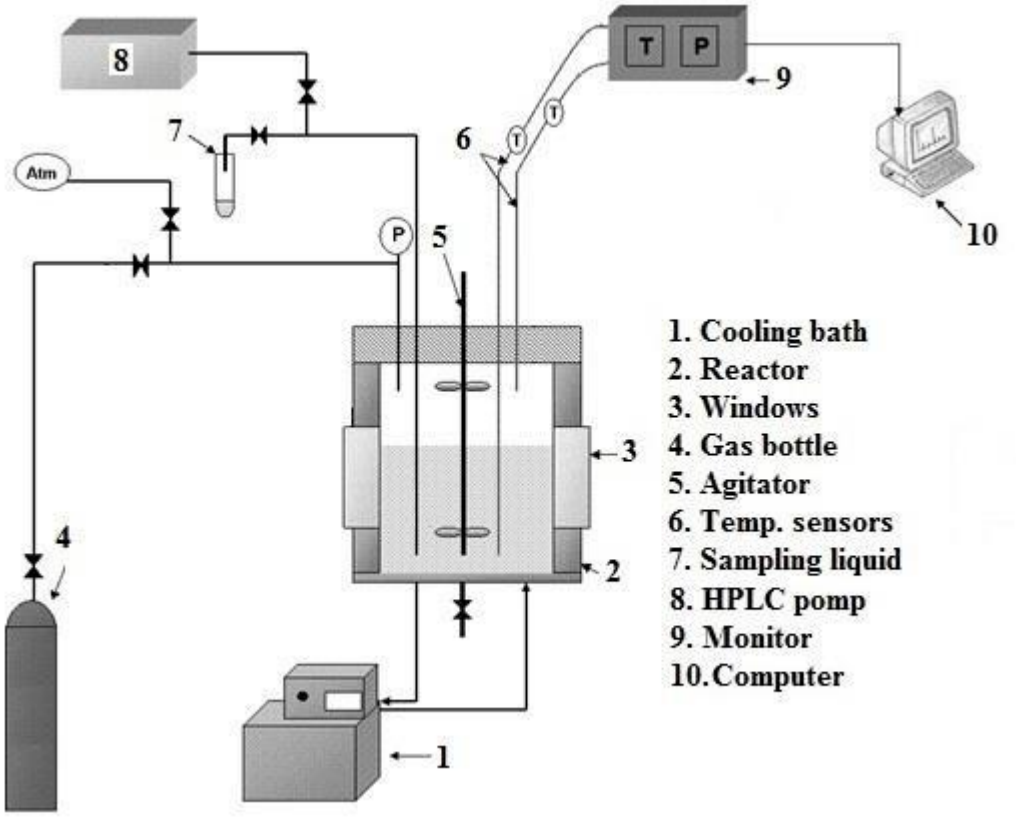

Figure 8: Diagram of experimental set-up for mixed CP+CO_2 hydrates thermodynamic study

Experimental procedure

The reactor is firstly washed by pure water. The reactor is then filled with N_2 at approximately 60 bars to test the leakage. The autoclave is then emptied by the vacuum pump. CO_2 a then introduced into the reactor at a desired pressure under mixing at 400 rpm. Approximately 800 mL of water and 66mL CP are injected into the reactor. The temperature is then reduced to 1-2^oC and is kept for hours or days to form hydrates. Then, we wait 1-3 days to reach completely equilibrium. Plus, 1-2 mL of aqueous solution is taken to measure salinity by ionic chromatography. The dissociation is then commenced. The temperature is augmented 1 K/h and we wait for stability of pressure and temperature. We take samples at second equilibrium point. When we are close to the equilibrium, the temperature is augmented 0.5 K/h to reach the final equilibrium. Then, one last sample is taken. The temperature is increased until the initial condition. The procedure is repeated to obtain more equilibrium points.

Chapter III. Modeling clathrate hydrates equilibrium

Four approaches have been considered to simulate the CPH equilibrium. The first is based on the standard freezing point depression equation (or standard Solid-Liquid equilibrium equation). The second is based on novel Hu-Lee-Sum (HLS) correlation explored by Hu *et al.* The two others are based on van der Waals and Platteuw model [97]. While an interaction potential can be used, a new correlatioin has also been introduced.

Finally, note that, the van der Waals-Platteeuw model with Kihara potential has been employed to describe the equilibrium of mixed CP+CO_2 hydrates.

In all models, the average absolute deviation (*AAD*) between measurements and simulations is described as follows:

$$AAD = \frac{1}{N}\sum_{i=1}^{N} |T_{i,pred} - T_{i,exp}| \quad (3)$$

where N is the number of experimental data points, $T_{i,pred}$ (K) the predicted-equilibrium temperature, and $T_{i,exp}$ (K) the experimental equilibrium temperature.

All experimental data in the presence of NaCl have been considered to optimize the models.

3.1. Standard freezing point depression (SFPD) approach

This first approach is based on the Hildebrand and Scott's equation [98,99], expressed as follows:

$$\ln a_w = \frac{\Delta H_{fm}}{R}\frac{(T_f - T)}{T_f T} + \frac{\Delta C_{fm}}{R}\left[\frac{(T_f - T)}{T} - \ln\left(\frac{T_f}{T}\right)\right] \quad (4)$$

where T_f is the dissociation temperature in K [27], ΔH_{fm} the molar heat of dissociation in J/mol [27], ΔC_{fm} the change of molar heat capacity between the subcooled liquid and the crystals in J/mol/K, and a_w the water activity. The geochemical model PHREEQC [100] was utilized to calculate water activity in brine. Indeed, the term ΔC_{mf} has not been explored for CPH. Thus, a new correlation for ΔC_{mf} was developped utilizing the experimental data when NaCl is present. This correlation can be expressed as follows:

$$\Delta C_{fm} = F(T) = a \times \exp(b \times T) \quad (5)$$

where *a*, and *b* are the empirical constants [28]. While many authors in the literature consider that this term can be neglected, it was found in this effort that it is necessary.

Afterward, equilibrium temperatures in the presence of others salts have been predicted by utilizing both equations (4) and (5).

The optimization coefficients *a*, and *b* have been found to be -10^{-19}, and 0.1813, respectively [28].

3.2. Hu-Lee-Sum (HLS) correlation

This approach is based on an innovative correlation explored by Hu *et al* between the suppression temperature ($\Delta T = T_o - T$) and the effective mole fraction, as described as follows [101–103]:

$$\frac{\Delta T}{T_0 T} = -\frac{nR}{\Delta H_{diss}} \ln a_w = C_1 X + C_2 X^2 + C_3 X^3 \quad (6)$$

where T_o and T are the hydrate formation temperatures in pure water and in brine, respectively. ΔH_{diss} is the heat of hydrate dissociation, n is the hydration number, and a_w the water activity. C_1, C_2, and C_3 are fitted coefficients, X the effective mole fraction. X can be expressed as follows [103]:

$$X = \sum_{j=salts} \sum_{i=ions} |z_{j,i}| x_{j,i} \quad (7)$$

where *i* and *j* denote the ion and salt, respectively. *z* is the ion charge number, *x* is the mole fraction. Lastly, the hydrate equilibrium temperatures can be calculated as follows:

$$T = T_0 \left[1 + \left(\frac{\Delta T}{T_0 T}\right) T_0\right]^{-1} \quad (8)$$

Equation (6) was initially explored for structure sI hydrates. After, for sII hydrates calculations, Hu et al [103] proposed a new constant α:

$$\alpha = \frac{\left(\frac{\Delta T}{T_0 T}\right)_{SII}}{\left(\frac{\Delta T}{T_0 T}\right)_{SI}} \quad (9)$$

Therefore, the SII hydrates formation temperatures are now expressed as follows:

$$T = T_0 \left[1 + \alpha \left(\frac{\Delta T}{T_0 T_I} T_0\right)\right]^{-1} \quad (10)$$

In our present work, because cyclopentane is considered instead of a gas molecule, hence the studied system is different. The pressure dependency of CPH can be ignored. Consequently, assumptions from Hu *et al* are firstly checked with four salts present: NaCl, KCl, $CaCl_2$, $MgCl_2$. Because the parameters explored by Hu *et al.*[102] provided inconsistent estimations for CPH equilibrium, experimental data in the presence NaCl, KCl, $CaCl_2$, $MgCl_2$ are utilized to calculate C_1, C_2, and C_3 coefficients for CPH. After, $\frac{\Delta T}{T_0 T}$ can be rewritten as a fitted function of X as follows:

$$\frac{\Delta T}{T_0 T} = 0.000956623X + 0.00059779X^2 + 0.01897593X^3 \quad (11)$$

The equation (11) is then employed to calculate the hydrate equilibrium when other salts are included.

3.3. Kihara approach

van der Waals and Platteeuw model [97] is a standard model for clathrate equilibrium modeling. This model is employed to describe the equilibrium of CPH and also mixed CP+CO_2 hydrates. A detailed explanation of this model has been described by Herri et al.[104], Le-Quang et al. [105], and Ho-Van et al [28]. Here is a brief description of this approach:

Equilibrium is computed by searching identical chemical potentials of water in both liquid and hydrate phase. A reference state (β) is employed: the empty clathrate. Hence, it can be written as follow:

$$\Delta\mu_w^{\beta-H} = \Delta\mu_w^{\beta-L} \quad (12)$$

$\Delta\mu_w^{\beta-L}$, the difference between chemical activity of water in β state and liquid phase, can be calculated from the Gibbs-Duhem equation [104], while $\Delta\mu_w^{\beta-H}$, the difference between β state and hydrate phase, can be computed using van der Waals and Platteeuw model [97]:

$$\Delta\mu_w^{\beta-H} = -RT\sum_i v_i \ln(1-\sum_j \theta_j^i) \quad (13)$$

where R is the universal gas constant, T the absolute temperature, v_i the number of type i cavities per water molecule in the hydrate, and θ_j^i the occupancy factor of the cavities of type i by the guest molecule j. Occupancy factor is usually calculated thanks to a Langmuir-type approach, involving an interaction potential. In clathrate science, the most common method is the use of Kihara potential [ref]. For each guest molecule, three parameters are needed:

maximum attractive potential ε, distance between the cores at zero potential energy σ, and the hard-core radius a. These parameters need to be optimized on equilibrium data.

In this effort, Kihara parameters for cyclopentane are optimized by using CPH experimental data in NaCl solutions [28], while experimental data of CP/CO_2 hydrates in pure water [49] and in NaCl from literature [52] and from this work are used in the case of binary CP/CO_2 hydrates (see Table 5).

Again, PHREEQC is employed for water activity calculation (liquid part of equation 12). Optimized Kihara parameters are then used to predict equilibrium in other salts.

Table 5: Thermodynamic data used for Kihara parameters optimization in binary CP/CO_2 hydrates

T, K	P, MPa	NaCl concentration, % mass	Citation
281.55	0.15	0	[49]
281.95	0.18	0	[49]
283.85	0.35	0	[49]
286.05	0.70	0	[49]
286.95	0.89	0	[49]
289.15	1.48	0	[49]
290.25	1.92	0	[49]
287.25	1.88	7	This work
285.30	1.14	7	This work
288.35	2.37	7	This work
284.40	1.40	10	[52]
286.80	2.98	10	[52]
281.10	1.48	15	[52]
283.30	2.81	15	[52]
270.80	1.50	25	[52]
272.00	2.45	25	[52]

Finally, the optimized Kihara parameters for CP in the case of CPH and binary CP/CO_2 hydrates are presented in **Table 6**.

Table 6: Optimized Kihara parameters for CP in two different hydrates systems

Hydrates system	Kihara parameters		
	a, Å	σ, Å	ε/k_b, K
CPH	0.8968	2.72	265.5
CP+CO_2 hydrates	0.8968	2.641	262.38

3.4. Activity-Based Occupancy Correlation (ABOC) approach

This fourth approach is similar to the latest. However, instead of using Kihara parameters, *ergo* an interaction potential, a simpler model is used. Instead of considering a Langmuir type method for the occupancy of cavities, a correlation between the occupancy factor and water activity, $\theta = F(a_w)$, has been introduced [25,40]. By this mean, the knowledge of water activity is sufficient to estimate θ^{j}_{i}, using the equation Eq.(12), Eq.(13). This novel correlation is written as follow:

$$\theta(a_w) = m \times (a^{w}_{2}) + n \times (a^{w}) + p \quad (14)$$

where m, n and p are the empirical constants calculated by using the experimental data in the presence of NaCl. These three coefficients m, n and p have been found to be -0.0004772, 0.0004731, and 0.9998800, respectively.

Chapter IV. Thermodynamics results

This section presents a brief summary of thermodynamic results including measurements and simulations of CPH and binary CP/CO_2 hydrates equilibrium.

4.1. CPH equilibrium results

The experimental equilibrium temperatures of CPH in the presence of eight different brine solutions (NaCl, KCl, NaCl-KCl, $CaCl_2$, $MgCl_2$, $MgCl_2$-NaCl, $MgCl_2$-NaCl-KCl, or Na_2SO_4) under a wide range of salt concentrations are illustrated in both Figure 9 and Figure 10. Note that only data according to the slow dissociation procedure are provided in the figures.

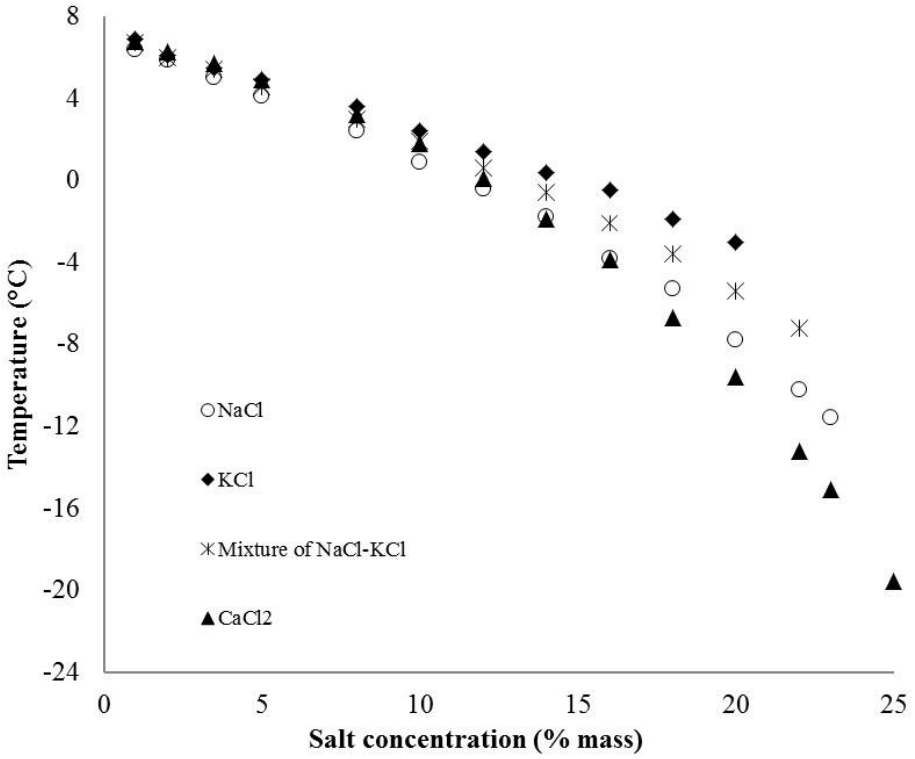

Figure 9: Equilibrium temperature of CPH in the presence of NaCl, KCl, NaCl-KCl, or $CaCl_2$ from experiments

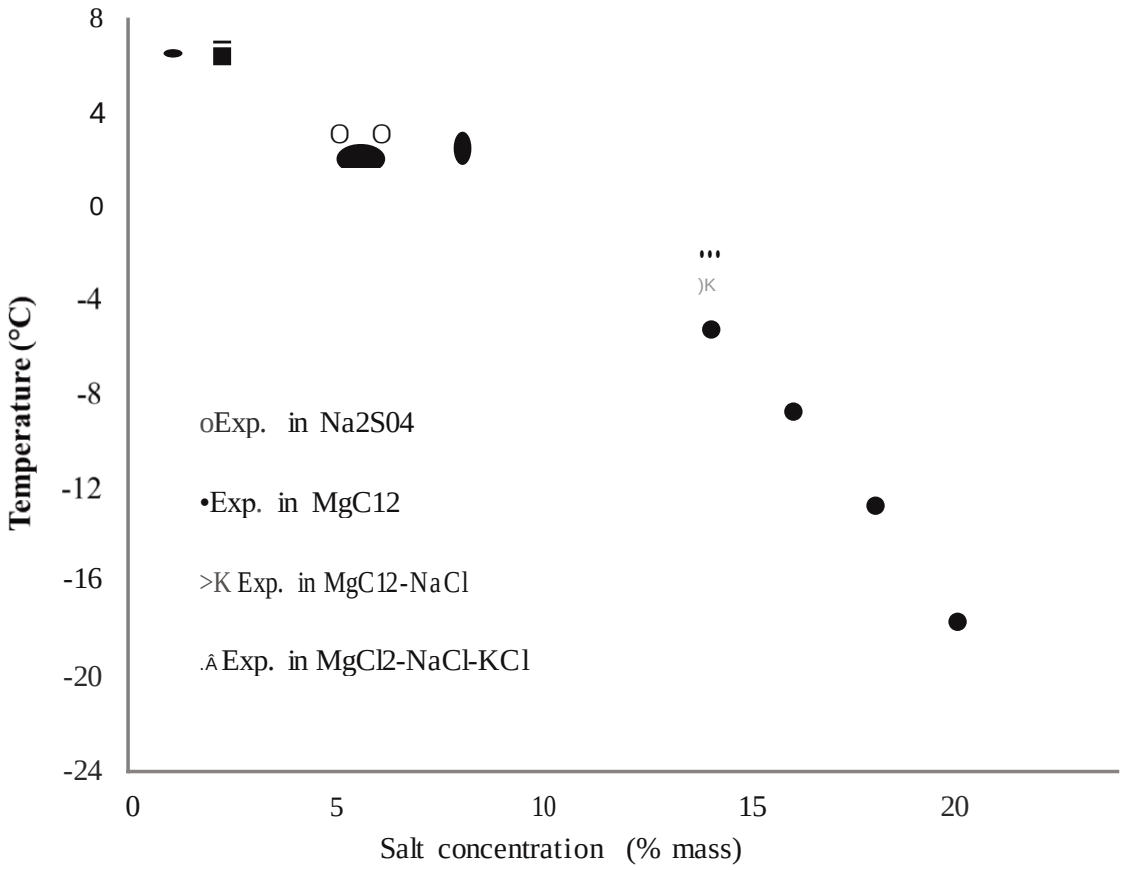

Figure 10: Equilibrium temperature of CPH in the presence of MgCh, MgCh-NaCl, MgCh-NaCl-KCl, or Na_2S0_4 from experiments

Figure 9 and Figure 10 show that salts inhibit strongly equilibrium. This inhibition is different based on the kind of tested salts. More explanations in the role of salt on equilibrium inhibition are provided in paper II and paper III of this thesis.

Then, the equilibrium data are modelled according to four approaches including SFPD, HLS, Kihara, and ABOC. The deviations (AAD) between the simulations and measurements are summarized in Table 7.

As seen in Table 7, all models are capable or predicting CPH equilibrium with AAD less than 0.7°C. Importantly, the ABOC method is the best tool to reproduce consistent CPH dissociation temperature from all examined electrolytes systems.

Table 7: Average deviation (°C) of different approaches for simulating CPH equilibrium.

Approach	Na2S04	MgClz	MgClr NaCl	MgClrNaCl-KCl	NaCl	KCl	NaCl-KCl	CaClz
SFPD	0.1	0.5	0. 4	0.3	0.3	0.3	0.2	0. 4
HLS	0.3	0.7	0. 4	0.2	0.5	0.3	0.3	0.5
Kihara	0.2	0.5	0.2	0.1	0.2	0.1	0.1	0.2
ABOC	0.1	0.2	0.1	0.1	0.1	0.1	0.1	0.2

4.2. CP/C0$_2$ hydrates equilibrium results

New experimental four-phase equilibrium data (V-Lw-Lttc-H) of mixed CP/C02 hydrates in pure water and in brine (NaCl, KCl, and a NaCl-KCl) are presented in Figure 11.

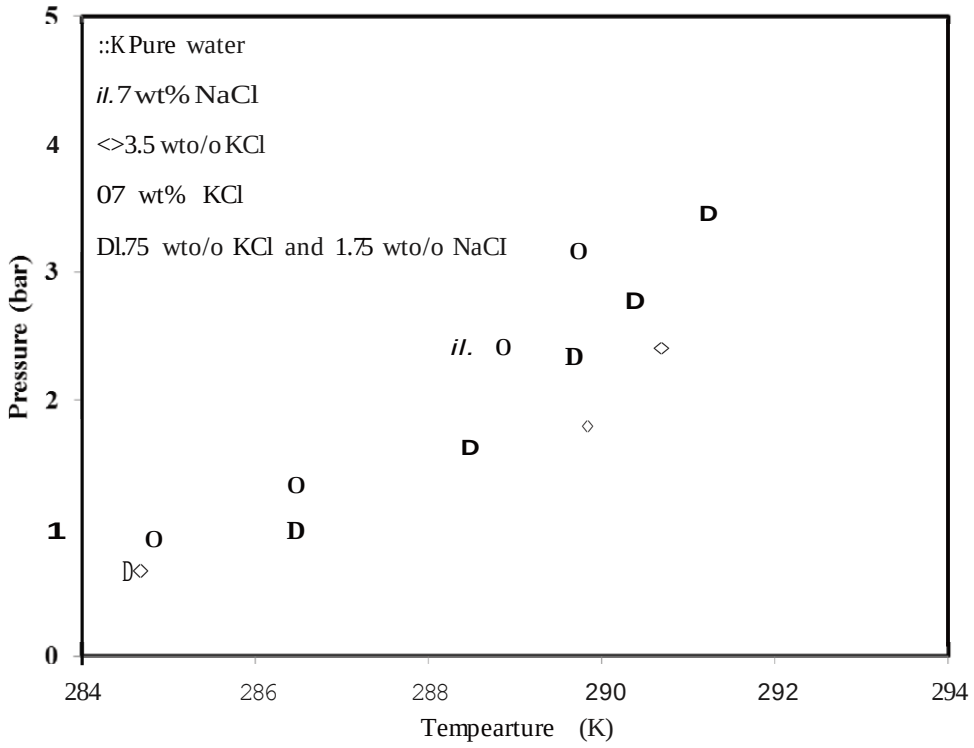

Figure 11: V-Lw-Lttc-H equilibrium data of CP/C02 hydrates in pure water and in brine

Figure **11** shows that electrolytes inhibit CP/C02 hydrates equilibrium, as seen in the case of CPH (Figure 9 and Figure 10). The equilibrium curves of CP/C02 hydrate in brine are always

located at an upper position than that in pure water. This means that, in the presence of salts, more subcooling is required for hydrate formation than that in pure water.

Again, each salt inhibit differently equilibrium. This influence on equilibrium is based on the kind of tested salt and its concentrations.

Note that some equilibrium data during the intermediate dissociation stages were recorded for each experiment. These dissociation results are also provided in details in paper VI of this thesis. However, since these results are not well reproduced by the thermodynamic approach, contrary to total dissociation points, their accuracy is questionable.

Results in presence of salts usually exhibits two exothermic peaks. Therefore, several kind of hydrates are probably formed. Indeed, during dissociation, two behavior are observed, with a change of slope in the PT curve. Consequently, pure SI CO_2 hydrate are supposed to be formed along with mixed SII CO_2/CP hydrates. However, the use of analysis tools, like Raman or FTIR spectroscopy, would be needed to ascertain this hypothesis.

After, all experimental measurements are reproduced by using the Kihara approach. The deviations between modelled data and experimental data are listed in Table 8.

Table 8: Average deviation between simulations and measurements of CP/CO_2 hydrates equilibrium.

Solution	Pure water	NaCl 7% mass	KCl 3.5% mass	KCl 7% mass	NaCl-KCl 1.5%-1.5% mass
AAD, K	0.3	0.2	0.4	0.4	0.4

As seen in Table 8, the use of Kihara approach is excellent to predict the CP/CO_2 hydrates equilibrium (considering final dissociation points). Average deviation is less than 0.4K in all systems tested.

Chapter V. Cyclopentane hydrates crystallization and morphology study

In order to optimize the CPH based desalination, knowledge on CPH crystallization like mechanisms, kinetics, or geometric shape and size of hydrate crystals are crucial. Therefore, in this work, crystallization mechanisms, hydrate layer growth rate, as well as morphology of CPH in the presence of different salts have been investigated. Mixtures of Na_2SO_4, NaCl, NaCl-$MgCl_2$, or NaCl-KCl-$MgCl_2$, under different concentrations have been considered. Three different initial subcoolings have been used. For that purpose, a small non-mixing batch-type reactor connected to a microscopy is employed.

However, since the experimental system is very specific to this study (small, no agitation), note that this approach is rather fundamental, and not process design oriented. Indeed, expectations have been focused on transfer mechanisms that occur in clathrate hydrate system, and CPH is a good model system (atmospheric pressure, separation between hydrate formers).

5.1. Apparatus description

Simplified diagram of experimental apparatus for CPH enclathration and morphology investigation is presented in Figure 12.

The main device is a batch-type jacketed reactor (1) with a volume of approximately 1.23 ml. A sapphire window (8) allows observing the solution inside the reactor with both optical microscope and Raman microscope. A chiller (6) is utilized to control the temperature of the solution. The temperature of solution is recorded by a temperature probe (4). Solution can be introduce or rejected by the input (2) and output (3), respectively. A microscope (10) linked to a camera (11) is employed to witness the crystallization through the sapphire window (8) from the top. Grams of silica gel (7) and a transparent tube (9) are utilized to dry the sapphire window surface (8). Digital data are documented by a computer (13).

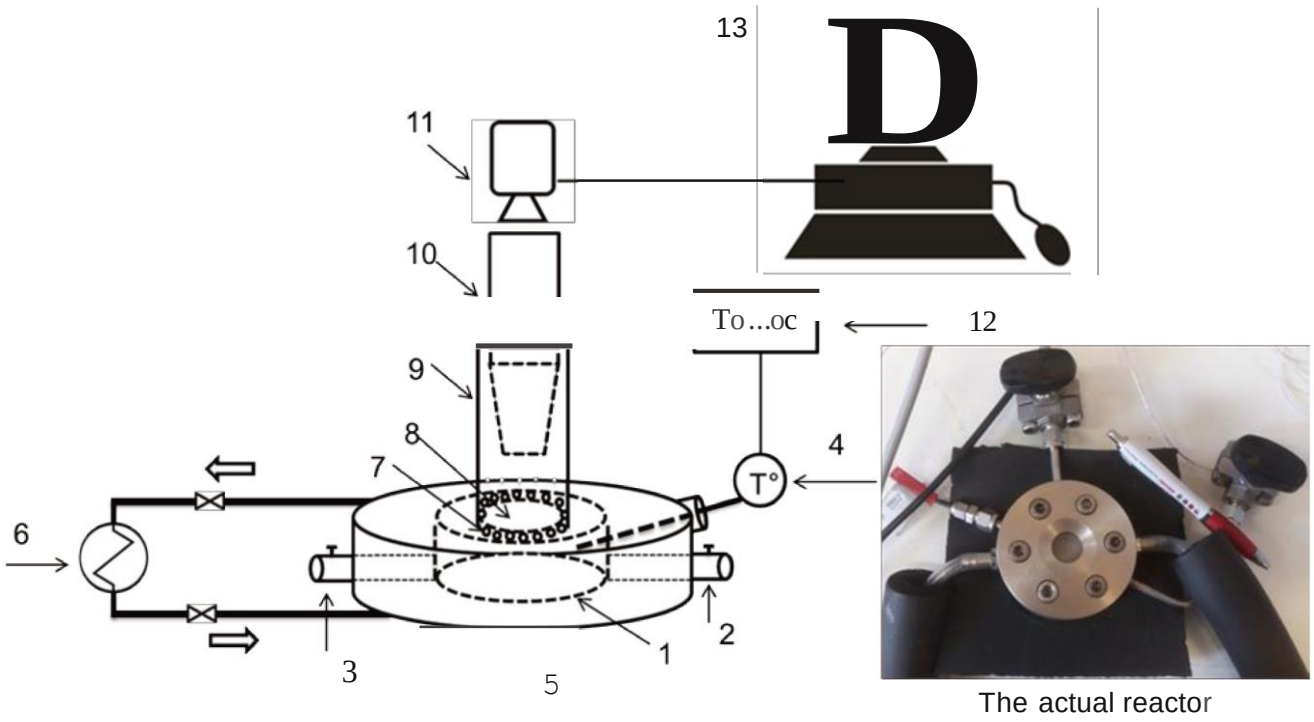

Figure 12: Schematic illustration of the experimental set-up for CPH crystallization mechanism and morphology study [106]

(1) Reactor cell; (2) input line; (3) output line; (4) Temperature probe; (5) Cooling jacket; (6) Chiller; (7) Silica gel; (8) Sapphire window; (9) Transparent tube; (10) Objective lens; (11) Camera; (12) Temperature transmitter; (13) Computer.

5.2. Experimental procedure

Before each experiment, in order to reduce the induction time, the saline solution is first used to form CPH in a bigger reactor (IL). CPH is then dissociated very slowly with the heating rate of 0.1°C/hour, up to a temperature of 0.1°C above equilibrium. At this temperature, there should not be any crystals remained in the brine. Then, approximately 0.8 ml of the solution is introduced into the reactor, followed by about 0.4 ml of CP (stoichiometric composition). Once the temperature of the solution reaches its set point, the objective of the microscope is adjusted to observe and record the interface between water and CP. Photos are taken every 5 minutes. After days, when CPH formation has completely, images of individual CPH crystals are taken and all the previous pictures are collected to make videos (see supplementary information [100]). Also, videos are made from the successive pictures at 10 FPS (hence 1second of video corresponds to 50 minutes).

5.3. Results

This section presents some main results on crystallization mechanism, growth rate, and morphology of CPH in brine. More details can be found in paper IV and V in this thesis.

The CPH crystallization mechanisrn near the liquid-liquid interface in the small reactor is desc1bed in Figure 13.

At the first stage, some nucleation site near the interface is observed (hexagonal-shaped). Then, the single crystal grows by consuming the CP traces and water (2nd stage). After, rapid nucleation and crystallization along the interface are witnessed (3rd stage). At this stage, the single crystal also reaches its final size because all CP traces are consurned totally.

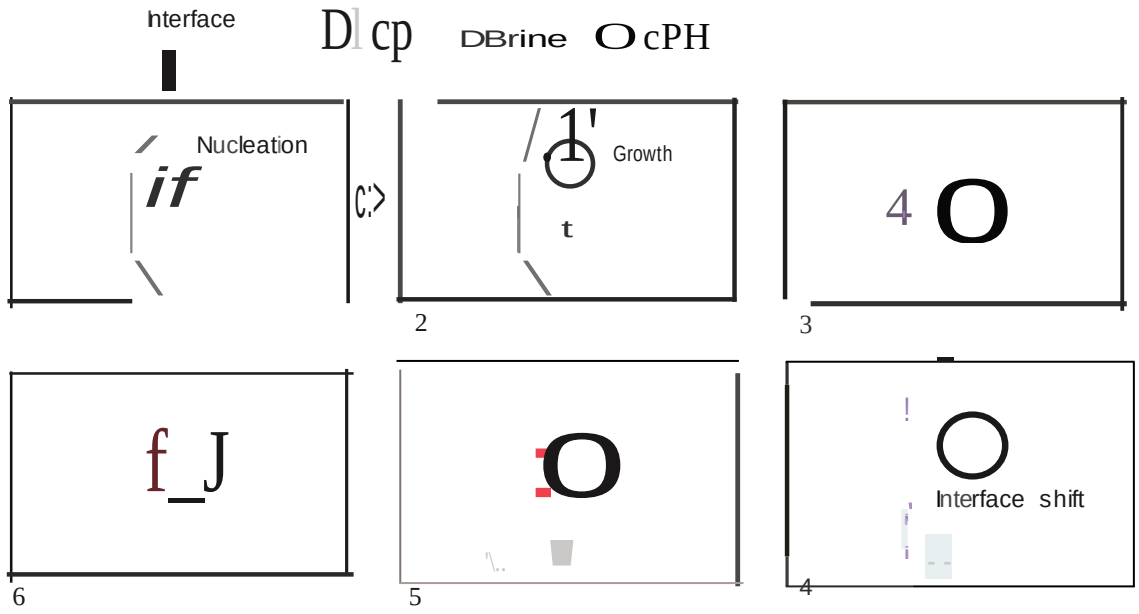

Figure 13: Simplified scheme of the CPH crystallization mechanism near the interface in the reactor cell.

In the next step, a shift of the water-CPH interface into the water phase is observed (4th stage). This is possibly because of water consumption in crystallization. Then, the hydrate layers were observed to grow mostly toward the CP phase by consuming initially water in the brine phase and also water dissolved in the CP phase near the liquid-liquid interface.

Later (5th stage and 6th stage), CPH hydrates grow into both CP and water phases. However, the growth toward CP phase is obviously faster than toward the water phase. This is probably due to the difference in mass transfer of CP and water through hydrate layer. Note that more

water is needed to form CPH according to the theory stoichiometric composition ($17H_20$ per CP). Moreover, the hydrate layer is presumably water-wet, facilitati ng the water migration.

The mass transfer mechanism of CP, water, and sait during CPH crystallization is presented in Figure 14.

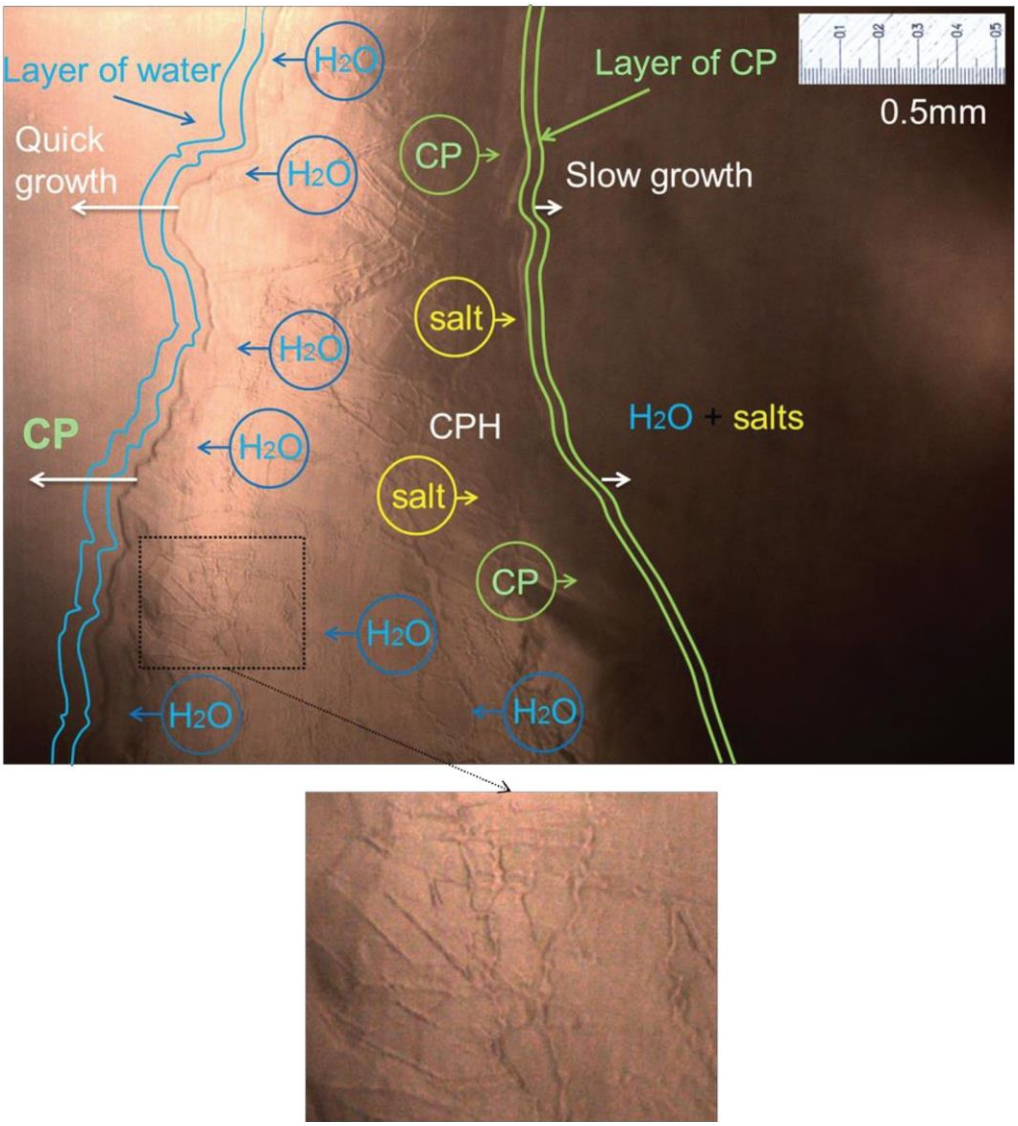

Figure 14: The mass transfer mechanism of CP, water, and salt dming CPH crystallization

As seen in Figure 14, three mass movements through the hydrate layer are observed: water advection toward the CP phase, CP advection toward the water phase, and sait diffusion toward the water phase. In addition, pores or channels (unknown geometry) generated during the hydrate formation could be the ways for these mass movements.

The hydrate layer growth rates for all tested salts are also provided. Measured growth rates highlights two important poi nts: Firstly, they increased with the increase of subcooling and decrease with salt concentration. Secondly, this growth rate decreases with time due to the increased thickness of the hydrate layer.

Then, the morphology of CPH has been investigated in brine. An example of CPH crystals morphology is presented Figure 15.

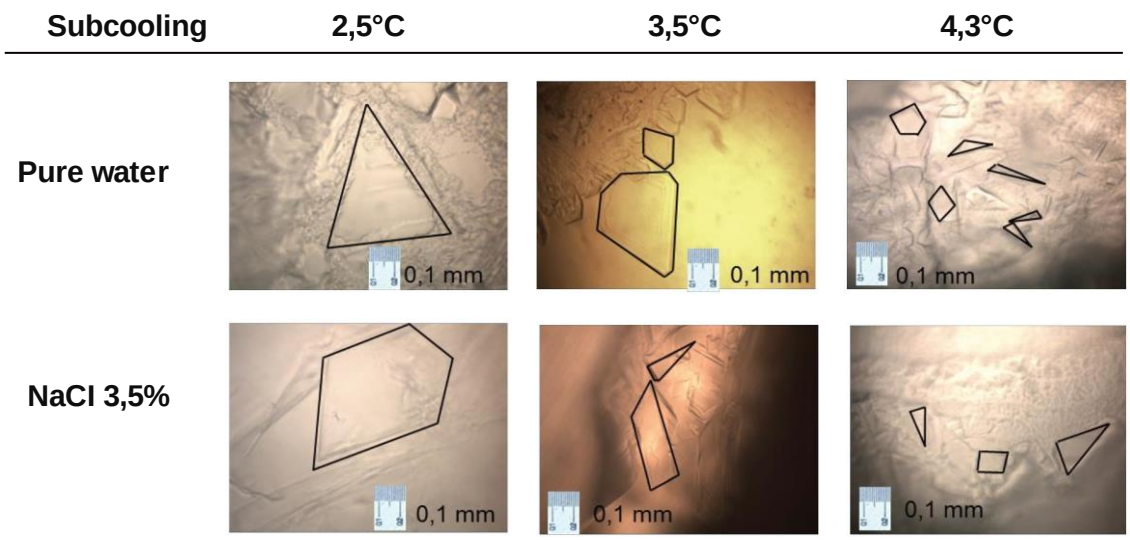

Figure 15. An example of CPH crystals morphology in pure water and in brine

We observed that the size of CPH crystals decreases strongly with the increase of the initial subcooling, while the shape is quantitatively at the same initial subcooling for all tested aqueous solutions. This indicates that the effect of subcooling on the CPH crystals morphology is more important than the effect of salt and its concentrations.

References

[1] Sloan ED, Koh CA, Clathrate hydrates of natural gases, Third edition. CRC Press, FL: Boca Raton, 2008.

[2] Sloan ED, Koh C, K.Sum A. Natural Gas Hydrate in Flow Assurance. Gulf Professional Pub./Elsevier; 2011

[3] Y.F. Makogon, Natural gas hydrates - A promising source of energy, J. Nat. Gas Sci. Eng. 2 (2010) 49–59. doi:10.1016/j.jngse.2009.12.004.

[4] A.A. Khokhar, J. Gudmundsson, ED. Sloan, Gas storage in structure H hydrates, Fluid Phase Equilib. 150–151 (1998) 383–392. doi:10.1016/S0378-3812(98)00338-0.

[5] R. Sassen, I.A.N.R. Macdonald, Evidence of structure H hydrate, Gulf of Mexico continental slope, Org. Geochem. 22 (1994) 1029–1032. doi:10.1016/0146-6380(94)90036-1.

[6] A.P. Mehta, E.D. Sloan, Structure H Hydrates : Implications for the Petroleum Industry, SPE Journal, SPE 53450, 1999, 4, 3–8.

[7] E.D. Sloan, Fundamental principles and applications of natural gas hydrates, Nature. 426 (2003) 353. doi:10.1038/nature02135.

[8] W.L. Mao, W.L. Mao, H. Mao, A.F. Goncharov, Hydrogen Clusters in Clathrate Hydrate, 2247 (2014). doi:10.1126/science.1075394.

[9] H. Mimachi, S. Takeya, A. Yoneyama, K. Hyodo, T. Takeda, Y. Gotoh, T. Murayama, Natural gas storage and transportation within gas hydrate of smaller particle: Size dependence of self-preservation phenomenon of natural gas hydrate, Chem. Eng. Sci. 118 (2014) 208–213. doi:10.1016/j.ces.2014.07.050.

[10] Z.G. Sun, R. Wang, R. Ma, K. Guo, S. Fan, Natural gas storage in hydrates with the presence of promoters, Energy Convers. Manag. 44 (2003) 2733–2742. doi:10.1016/S0196-8904(03)00048-7.

[11] A. Burnol, I. Thinon, L. Ruffine, J.M. Herri, Influence of impurities (nitrogen and methane) on the CO2 storage capacity as sediment-hosted gas hydrates - Application in the area of the Celtic Sea and the Bay of Biscay, Int. J. Greenh. Gas Control. 35 (2015) 96–109. doi:10.1016/j.ijggc.2015.01.018.

[12] H.P. Veluswamy, R. Kumar, P. Linga, Hydrogen storage in clathrate hydrates: Current state of the art and future directions, Appl. Energy. 122 (2014) 112–132. doi:10.1016/j.apenergy.2014.01.063.

[13] N.H. Duc, F. Chauvy, J.M. Herri, CO2 capture by hydrate crystallization - A potential solution for gas emission of steelmaking industry, Energy Convers. Manag. 48 (2007) 1313–1322. doi:10.1016/j.enconman.2006.09.024.

[14] J.-M. Herri, A. Bouchemoua, M. Kwaterski, P. Brântuas, A. Galfré, B. Bouillot, J. Douzet, Y. Ouabbas, A. Cameirao, Enhanced Selectivity of the Separation of CO_2 from N_2 during

Crystallization of Semi-Clathrates from Quaternary Ammonium Solutions, Oil Gas Sci. Technol. – Rev. d'IFP Energies Nouv. 69 (2014) 947–968. doi:10.2516/ogst/2013201.

[15] P.J. Herslund, K. Thomsen, J. Abildskov, N. von Solms, A. Galfré, P. Brântuas, M. Kwaterski, J.M. Herri, Thermodynamic promotion of carbon dioxide-clathrate hydrate formation by tetrahydrofuran, cyclopentane and their mixtures, Int. J. Greenh. Gas Control. 17 (2013) 397–410. doi:10.1016/j.ijggc.2013.05.022.

[16] P. Babu, P. Linga, R. Kumar, P. Englezos, A review of the hydrate based gas separation (HBGS) process forcarbon dioxide pre-combustion capture, Energy. 85 (2015) 261–279. doi:10.1016/j.energy.2015.03.103.

[17] Sloan. ED, Review article Fundamental principles and applications of natural gas hydrates, Nature. 426 (2003). doi: 10.1038/nature02135

[18] M. Darbouret, M. Cournil, J.M. Herri, Rheological study of TBAB hydrate slurries as secondary two-phase refrigerants, Int. J. Refrig. 28 (2005) 663–671. doi:10.1016/j.ijrefrig.2005.01.002.

[19] J. Douzet, M. Kwaterski, A. Lallemand, F. Chauvy, D. Flick, J.M. Herri, Prototyping of a real size air-conditioning system using a tetra-n-butylammonium bromide semiclathrate hydrate slurry as secondary two-phase refrigerant - Experimental investigations and modelling, Int. J. Refrig. 36 (2013) 1616–1631. doi:10.1016/j.ijrefrig.2013.04.015.

[20] H. Ogoshi, S. Takao, Air-Conditioning System Using Clathrate Hydrate Slurry, JFE Tech. Rep. 3 (2004) 1–5.

[21] H. Fakharian, H. Ganji, A. Naderifar, Desalination of high salinity produced water using natural gas hydrate, J. Taiwan Inst. Chem. Eng. 72 (2017) 157–162. doi:10.1016/j.jtice.2017.01.025.

[22] K.C. Kang, P. Linga, K. nam Park, S.J. Choi, J.D. Lee, Seawater desalination by gas hydrate process and removal characteristics of dissolved ions (Na^+, K^+, Mg^{2+}, Ca^{2+}, B^{3+}, Cl^-, $SO4^{2-}$), Desalination. 353 (2014) 84–90. doi:10.1016/j.desal.2014.09.007.

[23] M. Karamoddin, F. Varaminian, Water desalination using R141b gas hydrate formation, Desalin. Water Treat. 52 (2014) 2450–2456. doi:10.1080/19443994.2013.798840.

[24] P. Babu, A. Nambiar, T. He, A Review of Clathrate Hydrate Based Desalination to Strengthen Energy-Water Nexus, ACS Sustain. Chem. Eng. (2018). doi:10.1021/acssuschemeng.8b01616.

[25] H. Prakash, A. Kumar, Y. Seo, J. Dong, P. Linga, A review of solidified natural gas (SNG) technology for gas storage via clathrate hydrates, Appl. Energy. 216 (2018) 262–285. doi:10.1016/j.apenergy.2018.02.059.

[26] T.A. Strobel, K.C. Hester, C.A. Koh, A.K. Sum, E.D. Sloan, Properties of the clathrates of hydrogen and developments in their applicability for hydrogen storage, Chem. Phys. Lett. 478 (2009) 97–109. doi:10.1016/j.cplett.2009.07.030.

[27] M. Nakajima, R. Ohinura, Y.H. Mori, Clathrate hydrate formation from cyclopentane-in-water

emulsions, Ind. Eng. Chem. Res. 47 (2008) 8933–8939. doi:10.1021/ie800949k.

[28] S. Ho-Van, B. Bouillot, J. Douzet, S. Maghsoodloo, J.-M. Herri, Experimental Measurement and Thermodynamic Modeling of Cyclopentane Hydrates with NaCl, KCl, CaCl2 or NaCl-KCl Present, AIChE. J. 6 (2018) 2207-2218. doi:10.1002/aic.16067.

[29] T. He, S.K. Nair, P. Babu, P. Linga, I.A. Karimi, A novel conceptual design of hydrate based desalination (HyDesal) process by utilizing LNG cold energy, Appl. Energy. 222 (2018) 13–24. doi:10.1016/j.apenergy.2018.04.006.

[30] M.L. Martinez de Baños, Mechanisms of formation and dissociation of cyclopentane hydrates, Ph.D.Thesis, Université de Pau et des Pays de l'Adour, 2015.

[31] A. Galfré, Captage du dioxyde de carbone par cristallisation de clathrate hydrate en présence de cyclopentane : Etude thermodynamique et cinétique, Ph.D.Thesis, Ecole Nationale Supérieure des Mines de Saint-Etienne, 2014.

[32] A. Galfré, M. Kwaterski, P. Braîntuas, A. Cameirao, J.M. Herri, Clathrate hydrate equilibrium data for the gas mixture of carbon dioxide and nitrogen in the presence of an emulsion of cyclopentane in water, J. Chem. Eng. Data. 59 (2014) 592–602. doi:10.1021/je4002587.

[33] C.A. Whitman, R. Mysyk, M.A. White, Investigation of factors affecting crystallization of cyclopentane clathrate hydrate, J. Chem. Phys. 129 (2008). doi:10.1063/1.3005379.

[34] J.S. Zhang, J.W. Lee, Equilibrium of hydrogen + cyclopentane and carbon dioxide + cyclopentane binary hydrates, J. Chem. Eng. Data. 54 (2009) 659–661. doi:10.1021/je800219k.

[35] G. Zylyftari, J.W. Lee, J.F. Morris, Salt effects on thermodynamic and rheological properties of hydrate forming emulsions, Chem. Eng. Sci. 95 (2013) 148–160. doi:10.1016/j.ces.2013.02.056.

[36] S. Baek, J. Min, J.W. Lee, Equilibria of cyclopentane hydrates with varying HLB numbers of sorbitan monoesters in water-in-oil emulsions, Fluid Phase Equilib. 413 (2016) 41–47. doi:10.1016/j.fluid.2015.10.018.

[37] R. Sakemoto, H. Sakamoto, K. Shiraiwa, R. Ohmura, T. Uchida, Clathrate hydrate crystal growth at the seawater/hydrophobic-guest-liquid interface, Cryst. Growth Des. 10 (2010) 1296–1300. doi:10.1021/cg901334z.

[38] M. Mitarai, M. Kishimoto, D. Suh, R. Ohmura, Surfactant effects on the crystal growth of clathrate hydrate at the interface of water and hydrophobic-guest liquid, Cryst. Growth Des. 15 (2015) 812–821. doi:10.1021/cg501613a.

[39] H. Delroisse, J.-P. Torré, C. Dicharry, Effect of a Hydrophilic Cationic Surfactant on Cyclopentane Hydrate Crystal Growth at the Water/Cyclopentane Interface, Cryst. Growth Des. 17 (2017) 5098–5107. doi:10.1021/acs.cgd.7b00241.

[40] S. Han, J.Y. Shin, Y.W. Rhee, S.P. Kang, Enhanced efficiency of salt removal from brine for cyclopentane hydrates by washing, centrifuging, and sweating, Desalination. 354 (2014) 17–22. doi:10.1016/j.desal.2014.09.023.

[41] E.G. Dirdal, C. Arulanantham, H. Sefidroodi, M.A. Kelland, Can cyclopentane hydrate formation be used to rank the performance of kinetic hydrate inhibitors?, Chem. Eng. Sci. 82 (2012) 177–184. doi:10.1016/j.ces.2012.07.043.

[42] H. Sefidroodi, E. Abrahamsen, M.A. Kelland, Investigation into the strength and source of the memory effect for cyclopentane hydrate, Chem. Eng. Sci. 87 (2013) 133–140. doi:10.1016/j.ces.2012.10.018.

[43] R. Ambekar, Equilibrium conditions of Hydrate-forming pickering emulsions (M.S. thesis), City University of New York, New York, NY, 2012.

[44] J. Peixinho, V. Ageorges, B. Duchemin, Growth of Clathrate Hydrates from Water Drops in Cyclopentane, Energy & Fuels. (2017) acs.energyfuels.7b02740. doi:10.1021/acs.energyfuels.7b02740.

[45] M. Kishimoto, S. Iijima, R. Ohmura, Crystal growth of clathrate hydrate at the interface between seawater and hydrophobic-guest liquid: Effect of elevated salt concentration, Ind. Eng. Chem. Res. 51 (2012) 5224–5229. doi:10.1021/ie202785z.

[46] J. nan Zheng, M. jun Yang, Y. Liu, D. yong Wang, Y. chen Song, Effects of cyclopentane on CO2 hydrate formation and dissociation as a co-guest molecule for desalination, J. Chem. Thermodyn. 104 (2017) 9–15. doi:10.1016/j.jct.2016.09.006.

[47] Y. Matsumoto, T. Makino, T. Sugahara, K. Ohgaki, Phase equilibrium relations for binary mixed hydrate systems composed of carbon dioxide and cyclopentane derivatives, Fluid Phase Equilib. 362 (2014) 379–382. doi:10.1016/j.fluid.2013.10.057.

[48] P.J. Herslund, N. Daraboina, K. Thomsen, J. Abildskov, N. von Solms, Measuring and modelling of the combined thermodynamic promoting effect of tetrahydrofuran and cyclopentane on carbon dioxide hydrates, Fluid Phase Equilib. 381 (2014) 20–27. doi:10.1016/j.fluid.2014.08.015.

[49] M. Wang, Z.G. Sun, C.H. Li, A.J. Zhang, J. Li, C.M. Li, H.F. Huang, Equilibrium Hydrate Dissociation Conditions of CO2+ HCFC141b or Cyclopentane, J. Chem. Eng. Data. 61 (2016) 3250–3253. doi:10.1021/acs.jced.6b00333.

[50] A.H. Mohammadi, D. Richon, Phase equilibria of clathrate hydrates of methyl cyclopentane, methyl cyclohexane, cyclopentane or cyclohexane+carbon dioxide, Chem. Eng. Sci. 64 (2009) 5319–5322. doi:10.1016/j.ces.2009.09.048.

[51] J.H. Cha, Y. Seol, Increasing gas hydrate formation temperature for desalination of high salinity produced water with secondary guests, ACS Sustain. Chem. Eng. 1 (2013) 1218–1224. doi:10.1021/sc400160u.

[52] Y. Zhang, S.M. Sheng, X.D. Shen, X.B. Zhou, W.Z. Wu, X.P. Wu, D.Q. Liang, Phase Equilibrium of Cyclopentane + Carbon Dioxide Binary Hydrates in Aqueous Sodium Chloride Solutions, J. Chem. Eng. Data. 62 (2017) 2461–2465. doi:10.1021/acs.jced.7b00404.

[53] A. Parker, Potable water from sea-water, Nature. 149 (1942) 184–186.

[54] A.J. Barduhn, H.E. Towlson, Y.C. Hu, The properties of some new gas hydrates and their use in demineralizing sea water, AIChE J. 8 (1962) 176–183. doi:10.1002/aic.690080210.

[55] J. Sugi, S. Saito, Concentration and demineralization of sea water by the hydrate process, Desalination. 3 (1967) 27–31. doi:10.1016/S0011-9164(00)84021-7.

[56] S.L. Colten, F.S. Lin, T.C. Tsao, S.A. Stern, A.J. Barduhn, Hydrolysis losses in the hydrate desalination process: rate measurements and economic analysis, Desalination. 11 (1972) 31–59. doi:10.1016/S0011-9164(00)84047-3.

[57] D. Klass, Hydrate forming in water desalination, US3856492A , 1972.

[58] W.G. Knox, M. Hess, G.E. Jones, The hydrate process, Chem. Eng. Prog. 57 (1961) 66–71.

[59] The Koppers hydrate process for saline water conversion experimental and engineering studies, Research and development progress report No.90, US department of commerce, Office of technical services, Washington, D.C., 1964.

[60] R.A. McCormack, G.A. Niblock, Build and operate clathrate desalination pilot plant, Water Treatment Technology Program Report 31, 1998.

[61] R.W. Bradshaw, D.E. Dedrick, B.A. Simmons, J.A. Great- house, R.T. Cygan, E.H. Majzoub, Desalination Utilizing Clathrate Hydrates, Sandia National Laboratories, California, 2008.

[62] K. nam Park, S.Y. Hong, J.W. Lee, K.C. Kang, Y.C. Lee, M.G. Ha, J.D. Lee, A new apparatus for seawater desalination by gas hydrate process and removal characteristics of dissolved minerals (Na+, Mg2+, Ca2+, K+, B3+), Desalination. 274 (2011) 91–96. doi:10.1016/j.desal.2011.01.084.

[63] P. Babu, R. Kumar, P. Linga, Unusual behavior of propane as a co-guest during hydrate formation in silica sand: Potential application to seawater desalination and carbon dioxide capture, Chem. Eng. Sci. 117 (2014) 342–351. doi:10.1016/j.ces.2014.06.044.

[64] M. Yang, J. Zheng, W. Liu, Y. Liu, Y. Song, Effects of C3H8 on hydrate formation and dissociation for integrated CO2 capture and desalination technology, Energy. 93 (2015) 1971–1979. doi:10.1016/j.energy.2015.10.076.

[65] P.D. Dholabhai, N. Kalogerakis, P.R. Bishnoi, Equilibrium Conditions for Carbon Dioxide Hydrate Formation in Aqueous Electrolyte Solutions, J. Chem. Eng. Data. 38 (1993) 650–654. doi:10.1021/je00012a045.

[66] K. Ohgaki, Y. Makihara, K. Takano, Formation of CO2 hydrate in pure and sea waters, J. Chem. Eng. Japan. 26 (1993) 558–564.

[67] S. Fan, T. Guo, Hydrate Formation of CO2-Rich Binary and Quaternary Gas Mixtures in Aqueous Sodium Chloride Solutions, J. Chem. Eng. Data. 44 (1999) 829–832.

[68] M. Sarshar, a H. Sharafi, Simultaneous water desalination and CO2 capturing by hydrate formation, Desalin. Water Treat. 28 (2011) 59–64. doi:10.5004/dwt.2011.2201.

[69] M. Yang, Y. Song, L. Jiang, W. Liu, B. Dou, W. Jing, Effects of operating mode and pressure on hydrate-based desalination and CO2 capture in porous media, Appl. Energy. 135 (2014)

504–511. doi:10.1016/j.apenergy.2014.08.095.

[70] P.T. Ngema, C. Petticrew, P. Naidoo, A.H. Mohammadi, D. Ramjugernath, Experimental Measurements and Thermodynamic Modeling of the Dissociation Conditions of Clathrate Hydrates for (Refrigerant + NaCl + Water) Systems, J. Chem. Eng. Data. 59 (2014) 466–475. doi:10.1021/je400919u.

[71] A.M. Aliev, R.Y. Yusifov, A.R. Kuliev, Y.G. Yusifov, Method of Gas Hydrate Formation for Evaluation of Water Desalination, Russ. J. Appl. Chem. 81 (2008) 588–591. doi:10.1134/S1070427208040034.

[72] P. Mekala, P. Babu, J.S. Sangwai, P. Linga, Formation and Dissociation Kinetics of Methane Hydrates in Seawater and Silica Sand, Energy. 28 (2014) 2708–2716. doi: 10.1021/ef402445k

[73] Z. Rong, A. Hui, M. Chan, P. Babu, M. Yang, P. Linga, Journal of Natural Gas Science and Engineering Effect of NaCl on methane hydrate formation and dissociation in porous media, J. Nat. Gas Sci. Eng. (2015). doi:10.1016/j.jngse.2015.08.055.

[74] C. McAuliffe, Solubility in Water of Paraffin, Cycloparaffin, Olefin, Acetylene, Cycloolefin, and Aromatic Hydrocarbons1, J. Phys. Chem. 70 (1966) 1267–1275. doi: 10.1021/j100876a049.

[75] Y. Zhang, P.G. Debenedetti, R.K. Prud, B.A. Pethica, Differential Scanning Calorimetry Studies of Clathrate Hydrate Formation, Water. 108 (2004) 16717–16722. doi:10.1021/jp047421d.

[76] P.U. Karanjkar, J.W. Lee, J.F. Morris, Calorimetric investigation of cyclopentane hydrate formation in an emulsion, Chem. Eng. Sci. 68 (2012) 481–491. doi:10.1016/j.ces.2011.10.014.

[77] R.A. McCormack, R.K. Andersen, Clathrate desalination plant preliminary research study, U.S. Dept. of the Interior, Bureau of Reclamation, 1995.

[78] C.F.S. Lirio, F.L.P. Pessoa, Enthalpy of dissociation of simple and mixed carbon dioxide clathrate hydrate, Chem. Eng. Trans. 32 (2013) 577–582. doi:10.3303/CET1332097.

[79] Compositions, enthalpies of dissociation, and heat capacities in the range 85 to 270 K for clathrate hydrates of methane, ethane, and propane, and enthalpy of dissociation of isobutane hydrate, as determined by a heat-flow calorimeter, J. Chem. Thermodyn. 18 (1986) 915–921. doi:10.1016/0021-9614(86)90149-7.

[80] S. Ho-Van, B. Bouillot, J. Douzet, S. Maghsoodloo Babakhani, J.-M. Herri, Implementing Cyclopentane Hydrates Phase Equilibrium Data and Simulations in Brine Solutions, Ind. Eng. Chem. Res. 57 (2018) 14774 -14783. doi:10.1021/acs.iecr.8b02796.

[81] H. Xu, M.N. Khan, C.J. Peters, E.D. Sloan, C.A. Koh, Hydrate-Based Desalination Using Cyclopentane Hydrates at Atmospheric Pressure, J. Chem. Eng. Data. (2018) acs.jced.7b00815. doi:10.1021/acs.jced.7b00815.

[82] D. Corak, T. Barth, S. Høiland, T. Skodvin, R. Larsen, T. Skjetne, Effect of subcooling and amount of hydrate former on formation of cyclopentane hydrates in brine, Desalination. 278

(2011) 268–274. doi:10.1016/j.desal.2011.05.035.

[83] S. Han, Y.W. Rhee, S.P. Kang, Investigation of salt removal using cyclopentane hydrate formation and washing treatment for seawater desalination, Desalination. 404 (2017) 132–137. doi:10.1016/j.desal.2016.11.016.

[84] L. CAI, Desalination via formation of binary clathrate hydrates, Ph.D.Thesis 2013

[85] Y.-N. Lv, S.-S. Wang, C.-Y. Sun, J. Gong, G.-J. Chen, Desalination by forming hydrate from brine in cyclopentane dispersion system, Desalination. 413 (2017) 217–222. doi:10.1016/j.desal.2017.03.025.

[86] S. Ho-Van, J. Douzet, D. Le-Quang, B. Bouillot, J.-M. Herri, in Proc. of the Int. Conf. on Integrated Petroleum Engineering (Eds: V.A.Tran et al.), Hanoi, Vietnam, November 2016, 150-157

[87] B. Mottet, Method for treating an aqueous solution containing dissolved materials by crystallization of clathrates hydrates, US20170044024A1, 2017.

[88] F. Li, Z. Chen, H. Dong, C. Shi, B. Wang, L. Yang, Z. Ling, Promotion e ff ect of graphite on cyclopentane hydrate based desalination, Desalination. 445 (2018) 197–203. doi:10.1016/j.desal.2018.08.011.

[89] J. Lee, Y.K. Jin, Y. Seo, Characterization of cyclopentane clathrates with gaseous guests for gas storage and separation, Chem. Eng. J. 338 (2018) 572–578. doi:10.1016/J.CEJ.2018.01.054.

[90] W.L. Zhao, D.L. Zhong, C. Yang, Prediction of phase equilibrium conditions for gas hydrates formed in the presence of cyclopentane or cyclohexane, Fluid Phase Equilib. 427 (2016) 82–89. doi:10.1016/j.fluid.2016.06.044.

[91] B. Tohidi, A. Danesh, A.C. Todd, R.W. Burgass, K.K. Østergaard, Equilibrium data and thermodynamic modelling of cyclopentane and neopentane hydrates, Fluid Phase Equilib. 138 (1997) 241–250. doi:10.1016/S0378-3812(97)00164-7.

[92] D. Jianwei, L. Deqing, L. Dongliang, L. Xinjun, Experimental determination of the equilibrium conditions of binary gas hydrates of cyclopentane + oxygen, cyclopentane + nitrogen, and cyclopentane + hydrogen, Ind. Eng. Chem. Res. 49 (2010) 11797–11800. doi:10.1021/ie101339j.

[93] J.N. Zheng, M. Yang, B. Chen, Y. Song, D. Wang, Research on the CO2Gas Uptake of Different Hydrate Structures with Cyclopentane or Methyl-cyclopentane as Co-guest Molecules, Energy Procedia. 105 (2017) 4133–4139. doi:10.1016/j.egypro.2017.03.877.

[94] Q. Lv, X. Li, Raman Spectroscopic Studies on Microscopic Mechanism of CP - CH4 Mixture Hydrate, Energy Procedia. 142 (2017) 3264–3269. doi:10.1016/j.egypro.2017.12.501.

[95] A.H. Mohammadi, D. Richon, Phase Equilibria of Clathrate Hydrates of Tetrahydrofuran+Hydrogen Sulfide and Tetrahydroduran+Methane, J. Chem. Eng. Data. 55 (2009) 982–984. doi:10.1021/je9004257.

[96] J.A. Dean, LANGE'S HANDBOOK OF CHEMISTRY, Mater. Manuf. Process. 5 (1990) 687–688. doi:10.1080/10426919008953291.

[97] J.H. van der Waals, J.C. Platteeuw, Clathrate solutions, Adv. Chem. Phys. 2 (1958) 1–57. doi:10.1002/9780470143483.ch1.

[98] J.H. Hildebrand, R.L. Scott, Regular Solutions, Prentice Han, Englewood Cliffs, New York, 1962.

[99] O. Miyawaki, A. Saito, T. Matsuo, K. Nakamura, Activity and activity coefficient of water in aqueous solutions and their relationships with solution structure parameters, Biosci. Biotechnol. Biochem. 61 (1997) 466–469. doi:10.1271/bbb.61.466.

[100] B.D.L. Parkhurst, C. a J. Appelo, User's Guide To PHREEQC (version 2) — a Computer Program for Speciation, and Inverse Geochemical Calculations, Exch. Organ. Behav. Teach. J. D (1999) 326. doi:Rep. 99-4259.

[101] A. Pieroen., Gas hydrates - approximate relations between heat of formation, composition and equilibrium temperature lowering by "inhibitors, Recl. Des Trav. Chim. Des Pays-Bas. 74 (1955) 995–1002. doi:10.1002/recl.19550740808.

[102] Y. Hu, B.R. Lee, A.K. Sum, Universal correlation for gas hydrates suppression temperature of inhibited systems: I. Single salts, AIChE J. (2017). doi:10.1002/aic.15846.

[103] Y. Hu, B.R. Lee, A.K. Sum, Universal correlation for gas hydrates suppression temperature of inhibited systems: II. Mixed salts and structure type, AIChE J. 64 (2018) 2240–2250. doi:10.1002/aic.16116.

[104] J.-M. Herri, A. Bouchemoua, M. Kwaterski, A. Fezoua, Y. Ouabbas, A. Cameirao, Gas hydrate equilibria for CO2–N2 and CO2–CH4 gas mixtures—Experimental studies and thermodynamic modelling, Fluid Phase Equilib. 301 (2011) 171–190. doi:10.1016/j.fluid.2010.09.041.

[105] D. Le Quang, D. Le Quang, B. Bouillot, J.M. Herri, P. Glenat, P. Duchet-Suchaux, Experimental procedure and results to measure the composition of gas hydrate, during crystallization and at equilibrium, from N2-CO2-CH4-C2H6-C3H8-C4H10 gas mixtures, Fluid Phase Equilib. 413 (2016) 10–21. doi:10.1016/j.fluid.2015.10.022.

[106] S. Ho-van, B. Bouillot, D. Garcia, J. Douzet, A. Cameirao, S. Maghsoodloo-, Crystallization mechanisms and rates of Cyclopentane Hydrates formation in Brine, Chem. Eng. Technol. (2019) 1–21. doi:10.1002/ceat.201800746.

[107] S.L. Postel, Entering an era of water scarcity: The challenges ahead, Ecol. Appl. (2000) 941–948. doi: 10.2307/2641009.

[108] P.H. Gleick, The world's water. Volume 8 : the biennial report on freshwater resources.

[109] T. Oki, S. Kanae, Global hydrological cycles and world water resources, Science (80-.). 313 (2006) 1068–1072. doi:10.1126/science.1128845.

[110] M. Elimelech, W. Phillip, The future of seawater desalination: energy, technology, and the

environment., Science. 333 (2011) 712–7. doi:10.1126/science.1200488.

[111] K.W. Lawson, D.R. Lloyd, Membrane distillation, J. Memb. Sci. (1997) 1–25. doi:10.1016/S0376-7388(96)00236-0.

[112] P. Wang, T.S. Chung, A conceptual demonstration of freeze desalination-membrane distillation (FD-MD) hybrid desalination process utilizing liquefied natural gas (LNG) cold energy, Water Res. 46 (2012) 4037–4052. doi:10.1016/j.watres.2012.04.042.

[113] O.K. Buros, The U.S.A.I.D. Desalination Manual, International Desalination and Environmental Association, 1980.

[114] A. Subramani, J.G. Jacangelo, Emerging desalination technologies for water treatment: A critical review, Water Res. 75 (2015) 164–187. doi:10.1016/j.watres.2015.02.032.

[115] H. Yang, Z. Xu, M. Fan, R.B. Slimane, A.E. Bland, I. Wright, Progress in carbon dioxide seperation and capture: A review, J. Environ. Sci. 20 (2008) 14–27. doi:10.1016/S1001-0742(08)60002-9.

Chapter VI. Introduction to the papers

Five articles and one short article have been submitted to international journals. Three of the long articles have already been accepted and published, while the others have been submitted and are under review. The list is presented as follows:

1. Cyclopentane hydrates – a candidate for desalination?, Accepted in *Journal of Environmental Chemical Engineering*,
2. Experimental Measurement and Thermodynamic Modeling of Cyclopentane Hydrates with NaCl, KCl, $CaCl_2$, or NaCl-KCl Present, Published in *AIChE Journal*,
3. Implementing Cyclopentane Hydrates Phase Equilibrium Data and Simulations in Brine Solutions, published in *Industrial & Engineering Chemistry Research*,
4. Crystallization mechanisms and rates of Cyclopentane Hydrates formation in Brine, published in *Chemical Engineering & Technology*,
5. Morphology of Cyclopentane Hydrates in Saline Water, published in HAL as ''Document de travail'' (*i.e.* working document) ,
6. Phase equilibrium investigations of mixed cyclopentane and carbon dioxide hydrates in presence of different salt solutions, submitted to *Chemical Engineering Science* (1^{st} revision under process),

Afterward, each article is introduced and reproduced in this thesis. Finally, a conclusion summarizes and provides perspectives to this work.

6.1. Paper I: Cyclopentane hydrates – a candidate for desalination?

S.Ho-Van, B.Bouillot, J.Douzet, S. Maghsoodloo Babakhani, J.M.Herri

Accepted in: Journal of Environmental Chemical Engineering, First publication online: 12th of August, 2019.

Summary: Fresh water is an essential resource for both society and ecosystems, but it is also finite [107]. Nowadays, more than 1 billion people are living in areas facing water scarcity [108]. Certainly, the global population is forecast to grow in the next several decades, and hence water demand will augment accordingly [109]. This fact requires more clean water production processes in regard to enormous future demand. A number of methods to reduce the stresses on water demand should be mentioned such as water conservation, repair of infrastructure, and improved catchment and distribution systems [110]. Nevertheless, these measures can only improve the use of existing water resources, but not increase them. Desalination is one of the methods that can increase fresh water beyond what exists in the hydrological cycle [110]. The most common techniques which have been investigated and improved including thermal distillation, reverse osmosis, freezing, electro dialysis [111–114]. Lately, CPH based desalination is attracting considerable interest to the progressive worldwide clean water demand [40,81,83,85]. Unfortunately, no review work on CPH related to desalination application can be found in the open literature. Therefore, in this effort, we presented a systematic review that covers all the multiphase equilibria data, kinetics, morphology, and phase properties of cyclopentane hydrates required to improve an effective and sustainable hydrate-based desalination process. Moreover, this contribution describes perspectives for research and commercialization for seawater desalination via CPH crystallization. A comparison between this technique and other traditional methods demonstrate the potentiality when using CPH for desalting processes. A diagram of CPH based salt removed was also created to illustrate and define future research possibilities. Hopefully, this review contribution can suggest new ideas about advancing new technical solutions to make commercial/large scale CPH-based desalination processes a reality.

Cyclopentane hydrates – a candidate for desalination?

S.Ho-Van[1,2]*, B.Bouillot[1]*, J.Douzet[1], S. Maghsoodloo Babakhani[1], J.M.Herri[1]

[1]*SPIN Center, Ecole des Mines de Saint-Etienne, SPIN, CNRS 5307, LGF, F-42023, Saint-Etienne, France;*

[2]*Oil Refinery and Petrochemistry Department, Hanoi University of Mining and Geology,*

Duc Thang, Bac Tu Liem, Hanoi, Viet Nam

*Corresponding authors: son.ho-van@emse.fr (S.Ho-Van) and bouillot@emse.fr (B.Bouillot).

Abstract

This article presents a systematic review on the past developments of Hydrate-Based Desalination process using Cyclopentane as hydrate guest. This is the first review that covers all required fundamental data, such as multiphase equilibria data, kinetics, morphology, or physical properties of cyclopentane hydrates, in order to develop an effective and sustainable desalination process. Furthermore, this state-of-the-art describes research and commercialization perspectives. When compared to traditional applications, cyclopentane hydrate-based desalination process could be a promising solution. Indeed, it operates under normal atmospheric pressure, lower operation energies are required, etc… However, there are some challenges yet to overcome. A decision aid in the form of a diagram is proposed for a new cyclopentane hydrates-based desalination process. Hopefully, concepts reviewed in this study will suggest new ideas to advance technical solutions in order to make commercial hydrate-based desalination processes a reality.

Keywords: Review, Desalination, Clathrate Hydrates, Cyclopentane Hydrates, Seawater treatment.

1. Introduction

Seemingly abundant, clean water is a crucial resource for life on our planet. However, due to the increasing population, industrialization, global warming, agriculture activities, the shortage of clean water has become an urgent issue in many countries, especially in the Middle East and Africa [1,2]. Today, more than 1 billion people are denied the right to access clean water and about 2.6 billion people lack access to adequate sanitation [3,4]. Dirty water is the world's second biggest children killer [3]. For instance, in the Kingdom of Saudi Arabia (KSA), 60% of water demand is provided by desalination, that is to say about 10 Mm^3/day [5]. Expectations of KSA desalination demand in 2050 should be 60 Mm^3/day. Therefore, while mature technologies exist, processes for clean water production need to be optimized in regard to the enormous future demand. Because of the practical unlimited supply capacity of

sea-water, desalination has become an ever increasingly used method to produce fresh water [6]. A history of desalination research literature is detailed in Figure 1. As illustrated in figure, there has been a significant rise in research on desalination over the past decades. The most common studied methods have been: Thermal distillation, Reverse osmosis, Freezing, and Electro dialysis [7–10].

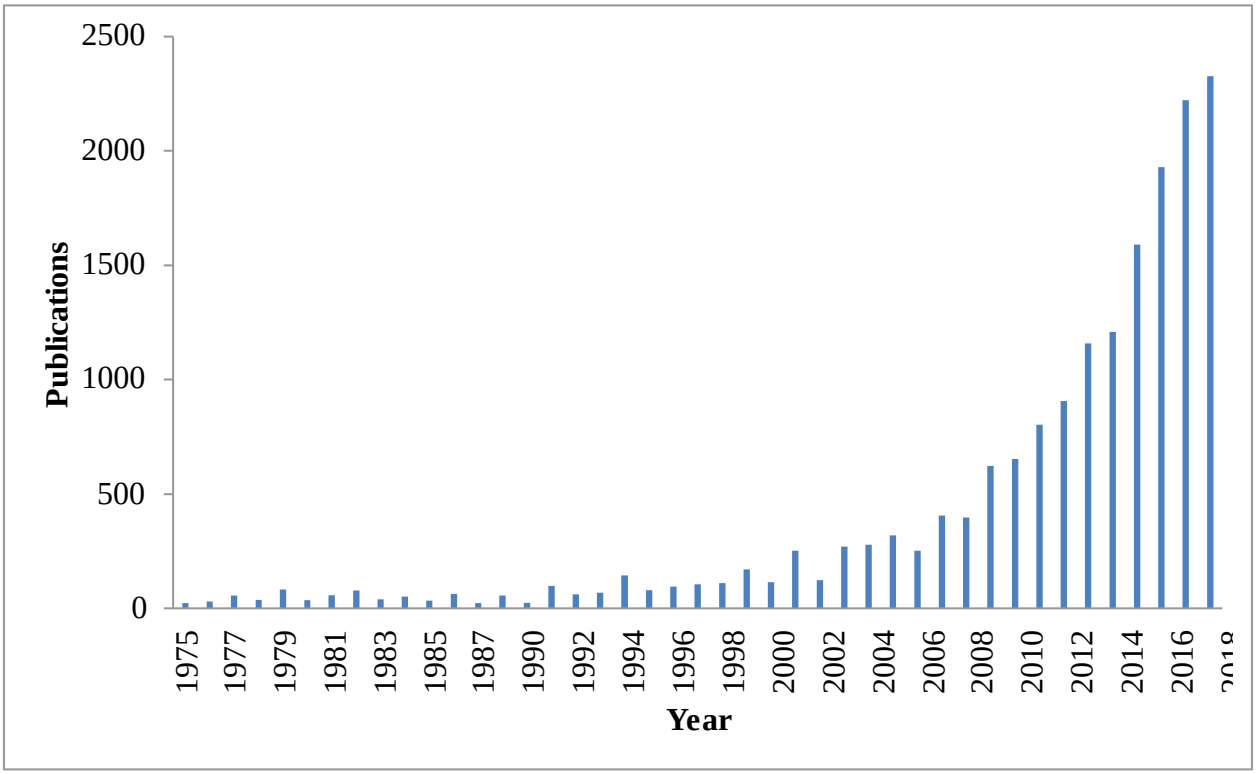

Figure 1. Frequency of desalination study in literature. Data from Web of Science with the keyword "desalination" (09/04/2019).

Recently, Clathrate hydrate–based desalination technique has attracted considerable interest [11–13]. Clathrate hydrates, or gas hydrates, are ice-like non-stoichiometric crystalline solid compounds that contain water molecules forming cages through a hydrogen-bonding system enclosing guest molecules, formed under high pressure and low temperature conditions [14]. This is usually the case for gaseous guest molecules (CO_2, CO, N_2, CH_4…). Other heavier guest molecules can form clathrate hydrates under atmospheric pressure (Cyclopentane (CP), Tetrahydrofuran…). Depending on size and nature of the guest molecules, water molecules can form different kind of cages that combine to form a crystal lattice according to three well-known structures: I, II, and H. Since water is usually present in the oil and gas flowlines, gas hydrates are well known to plug pipelines [14]. Besides, several potential applications of

clathrate hydrates have been investigated, such as gas storage [15–18], carbon dioxide capture [19,20], gas transportation [15,21], gas separation [22,23], air-conditioning [24–26], and of course seawater desalination [11,13,27,28].

Here is how water desalination works with Clathrates. During hydrate formation, water and guest molecules are incorporated into a new solid phase. It can be separated and recovered. Moreover, salts are excluded from the crystal phase. Therefore water and guest molecules can be retrieved after dissociation. If the guest is gaseous at standard conditions, only saturated gas remains inside liquid water. Consequently, clean "desalinated" water is obtained. If the guest molecule is not under vapor phase after dissociation, clean water is obtain providing that it can be separated after dissociation. Usual guest molecules studied for desalination applications are: CH_4, CO_2, C_3H_8, HCFC R141B, and CP.

As a matter of fact, gas hydrates-based desalination has been investigated for decades [10,12,29–38]. Despite that, hydrate-based technology is not used nowadays in desalination plants. There are several explanations: mostly energy consumption issues and technology immaturity [35]. However, a great deal of research has been done recently, and could provide a base for future hydrate-based desalination technology. In some studies, CP is suggested as an adequate guest candidate [39–45]. Indeed, CP forms clathrate hydrates with pure water under atmospheric pressure at 7°C. Especially, it is not miscible into water (solubility of 0.156 g/L at 25°C [46]). Therefore, it can be easily recovered from water after dissociation, and recycled for the desalination/cleaning process.

Note that CP act as a hydrate promoter for other applications, such as carbon capture, as described in detail by Herri et al. [22], or Zheng et al. [47]. It is a co-guest used to milder hydrate formation conditions when combined to other molecules such as N_2 [40,48–50], C_3H_8 [51], CO_2 [48,49,52–54], CH_4 [40,49,55,56], or H_2S [56]. Thus, the use of cyclopentane hydrates (CPH) for a combined gas capture and desalination process could be applicable and probably more interesting energetically.

Finally, this article provides a comprehensive, but non exhaustive, state-of-the-art review on CPH. It objective is to inform the scientific and industrial community the latest advances, and establishing the challenges to address when developing CPH-based desalination.

2. Phase equilibria of CPH

Phase equilibrium data of CPH in pure water and in presence of electrolytes are crucial for salt removal using CPH. Thermodynamic equilibrium data of CPH has been classified into three categories: CP+water, CP+water+electrolytes, and CP+water+other guests.

2.1. Phase equilibrium of CPH in pure water with and without surfactants

At ambient pressure, CP can form hydrate with pure water from 6.3°C to 7.7°C according to literature. The melting point varies in the literature, and can be lowered by adding surfactant such as SPAN 80. Table 1 presents literature results.

Table 1. Equilibrium temperature of CPH in pure water at atmospheric pressure with and without surfactant

Authors	Published year	Value (°C)	Method	Citation
Palmer et al.	1950	7.7	Quick dissociation	[57]
Davidson et al.	1973	7.7	Quick dissociation	[58]
Fan et al.	1999	7.07	"Pressure search" procedure	[59]
Dendy Sloan et al.	2008	7.7	Quick dissociation	[14]
Nakajima et al.	2008	6.6, 6.8, 7.1	DSC	[60]
Whitman et al.	2008	7.0	DSC	[61]
Nicholas et al.	2009	7.7	Quick dissociation	[62]
Zhang et al.	2009	7.02	DSC	[63]
Sakemoto et al.	2010	7.0[a]	Slow dissociation	[64]
Dirdal et al.	2012	7.7	Quick dissociation	[65]
Sefidroodi et al.	2012	7.7	Quick dissociation	[66]
Ambekar et al.	2012	6.3 (0.1% vol Span 80)[+]	DSC	[67]

Zylyftari et al.	2013	7.11[a]	DSC	[68]
Zylyftari et al.	2013	6.57[b] (Span 80)[+]	DSC	[68]
Han et al.	2014	7.8	Quick dissociation	[69]
Xu et al.	2014	7.7	Quick dissociation	[70]
Mitarai et al.	2015	7.1[a]	Slow dissociation	[71]
Martinez de Baños et al.	2015	7.2	*	[72]
Baek et al.	2015	6.7-7.2 (Span 20, 40, 60, 80)[+]	DSC	[73]
Brown et al.	2016	7.7	*	[74]
Peixinho et al.	2017	6.7 (no Span 80)[+]	Quick dissociation	[75]
		5.7 (0.0001 % mass Span 80)[+]	Quick dissociation	[75]
		5.5 (0.001 % mass Span 80)[+]	Quick dissociation	[75]
		7.7 (0.1 % mass Span 80)[+]	Quick dissociation	[75]
Hobeika et al.	2017	7.0	*	[76]
Delroisse et al.	2017	7.2[c]	Slow dissociation	[77]
Ho-Van et al.	2018	7.7[a]	Quick dissociation	[28]
		7.1[a]	Slow dissociation	
Delroisse et al	2018	7.05[d]	Stirred calorimetric cell	[78]

[+] in the presence of surfactant, * not acknowledge, DSC: Differential Scanning Calorimetry, Uncertainty range: [a] ±0.1°C, [b]±0.01°C, [c]±0.2, [d]±0.5°C.

Table 1 shows that there are actually two ranges of equilibrium temperatures in pure water: 7.7-7.8°C and 6.6-7.2°C. This can be explained by different experimental procedures used by the authors.

Equilibrium temperatures reported at 7.7-7.8°C range were obtain by quick dissociation method [28,65,66,69,79]. Unfortunately, the quick method tends to miss the correct dissociation temperature, because of the high dissociation rate. Therefore, the value of equilibrium temperature is usually overestimated.

One seemingly more reliable method is Differential Scanning Calorimetry (DSC) [60,61,63,68,73]. Equilibrium temperatures measured by DSC show a temperature range from 6.6°C to 7.2°C.

In addition, Sakemoto et al. [64], Mitarai et al [71], Ho-Van et al. [28], and Delroisse et al. [77] performed slow dissociation method and reported crystallization temperature of CPH of 7.0°C, 7.1°C and 7.2°C, respectively. The small variations could be attributed to heating rate differences. Sakemoto et al. [64], Mitarai et al [71], and Ho-Van et al. [28] used an increment of 0.1°C/hour, and 0.2°C/hour for Delroisse et al. [77]. Hence, equilibrium temperature reported by Delroisse et al. [77] is slightly higher. In another work, Delroisse et *al.* [78] reported the dissociation temperatures of 7.05°C (280.2 °K) by using a stirred calorimetric cell. Their method utilized an agitator to mix the fluid (CP+H_2O) in a calorimetric cell instead of static condition, as in a normal DSC method. This development is believed to provide more accurate data [78]. Martinez de Baños *et al.* [72] determined the equilibrium of 7.2°C which is very close to the values according to slow dissociation method [28,64,77], and DSC method [60,61,63,68,73]. Finally, the temperature range 6.6-7.2°C seems to be the most reliable and should be considered.

Besides, Ambekar et al. [67], Zylyftari et al. [68], Baek et al. [73], and Peixinho et al. [75] indicated that the use of a surfactant, such as Span, can reduce CPH equilibrium temperature. Indeed, hydrate crystallization is usually observed at the water – CP interface, while surfactant can modify the interfacial tension force. Hydrate formation is therefore affected by the surfactant [68,80]. Karanjkar *et al.* [81] stated that a mushy and porous structure, showing small needle-like crystals, is formed in presence of Span compared to polycrystalline shell structure in the absence of any surfactant. This porous structure hydrate may cause a reduction in dissociation point, referred to as the Gibbs–Thomson effect [68,82].

However, in the presence of 0.1% mass Span 80, corresponding to a concentration above Critical Micelle Concentration (CMC), the hydrate dissociation temperature is 7.7°C,

according to Peixinho et al. [75]. At this concentration, surfactants cover the whole water droplet and the morphology of the hydrate is hence slightly denser. Consequently, dissociation would require a higher temperature [75].

In terms of pressure dependency, by applying a pressure-search method [83], Fan et al. [59] reported that CPH formation conditions are within the temperature range of 0.21-7.07°C for a pressure range of 6.9-19.8 kPa. The measured equilibrium data are detailed in Table 2. Fan et al. indicated that the quadruple point is 7.07°C at 19.8 kPa involving four phases: liquid water (L_w), liquid CP (L_{cp}), hydrate (H), and vapor CP (V_{cp}). This point is very close to the equilibrium temperature reported elsewhere [58,60,61,63,64,68,73] at atmospheric pressure, involving only three phases: L_w - H -L_{cp}.

Table 2. Three phase (V-L_w-H) equilibrium data of CPH in pure water [59]

Phase	Temperature (±0.01°C)	Pressure (±0.1kPa)
L_w-H-V_{cp}	0.21	6.9
	1.19	8.1
	2.08	9.2
	3.34	11.2
	4.36	13.2
	5.72	16.3
	6.72	18.9
L_w- L_{cp}-H-V_{cp}	7.07	19.8*

* Upper quadruple point

In the desalination process, atmospheric pressure condition is more favorable than high pressure or even vacuum like conditions. However, the data reported by Fan et al. [59] are also very useful for salt removing from seawater under vacuum especially in association with membrane [84] or simply vacuum distillation [85].

Under higher pressures, Trueba et al. [86] reported hydrate (H) – aqueous liquid (L_w) – CP-rich liquid (L_a) phase equilibrium data. They indicated that the equilibrium temperature was

nearly independent of pressure due to the low compressibility of the two fluids and the one solid phase. This indicates that, without any gas molecule, CPH dissociation temperature is almost constant with pressure increase [86]. High pressure condition is out of the question in CPH pure based – desalination because of a significant increase in the energy required.

Table 3. CPH phase equilibrium data at high pressure

Phase	**Temperature** (±0.02°C)	**Pressure (MPa)** (±3% of reading)
L_w-H-L_a	6.75	2.55
	6.79	5.05
	6.87	7.55
	6.85	10.03
	6.88	12.55

2.2. Phase equilibrium of CPH in the presence of salts

Obviously, to design an actual CPH based-desalination process, it is essential to have sufficient phase equilibrium data of CPH in the presence of diverse salts [28]. However, only few published datasets are available.

Zylyftari et al. [68] reported a set of equilibrium data in the presence of NaCl at a wide range of concentration, from 0 up to 23% mass by using DSC method. This method was also used by Baek et al. [73] for CPH equilibrium at 3.5% mass NaCl concentration.

Kishimoto et al. [87] used slow stepwise dissociation method to determine the dissociation points with an increment of 0.1°C/h at NaCl concentration from 5 to 26.4% mass fraction. Likewise, Sakemoto at al. [64] provided results in the presence of 3.5% NaCl and synthetic seawater. Delroisse et al. [77] reported 5 dissociation temperatures with NaCl present (0, 1, 2, 3, 4% mass NaCl) by using the slow dissociation method with an increment of 0.2°C/hour. Moreover, Ho-Van et al. [28,88] reported numerous equilibrium data for CPH in the presence of NaCl, KCl, NaCl-KCl, $CaCl_2$, Na_2SO_4, $MgCl_2$, $MgCl_2$-NaCl, or $MgCl_2$-NaCl-KCl under a wide-range of salt concentrations.

CPH equilibrium data in the presence of salts in the open literature are presented in Table 4, and Figure 2.

Table 4. Literatures on equilibrium temperature of CPH in the presence of salts

Salts	Salt concentration range (% mass)	Method	Published year	Citation
NaCl	3.5	Slow dissociation[a]	2010	[64]
Synthetic seawater	*	Slow dissociation[a]	2010	[64]
NaCl	5-26.4	Slow dissociation[a]	2012	[87]
NaCl	0 – 23	DSC[a]	2013	[68]
NaCl	3.5	Quick dissociation	2014	[69]
NaCl	3.5	DSC	2016	[73]
NaCl	0 – 4	Slow dissociation[b]	2017	[77]
NaCl	0 – 23	Slow dissociation[a]	2018	[28]
KCl	0 – 20	Slow dissociation[a]	2018	[28]
NaCl-KCl	0 – 22	Slow dissociation[a]	2018	[28]
$CaCl_2$	0 – 25	Slow dissociation[a]	2018	[28]
Na_2SO_4	0 – 6	Slow dissociation[a]	2018	[88]
$MgCl_2$	0 – 20	Slow dissociation[a]	2018	[88]
$MgCl_2$-NaCl	0 – 22	Slow dissociation[a]	2018	[88]
$MgCl_2$-NaCl-KCl	0 – 22	Slow dissociation[a]	2018	[88]

* 2.6518% NaCl, 0.2447% $MgCl_2$, 0.3305% $MgSO_4$, 0.1141% $CaCl_2$, 0.0725% KCl, 0.0202% $NaHCO_3$, and 0.0083% NaBr. Uncertainty range: [a] ±0.1°C, [b] ±0.2°C.

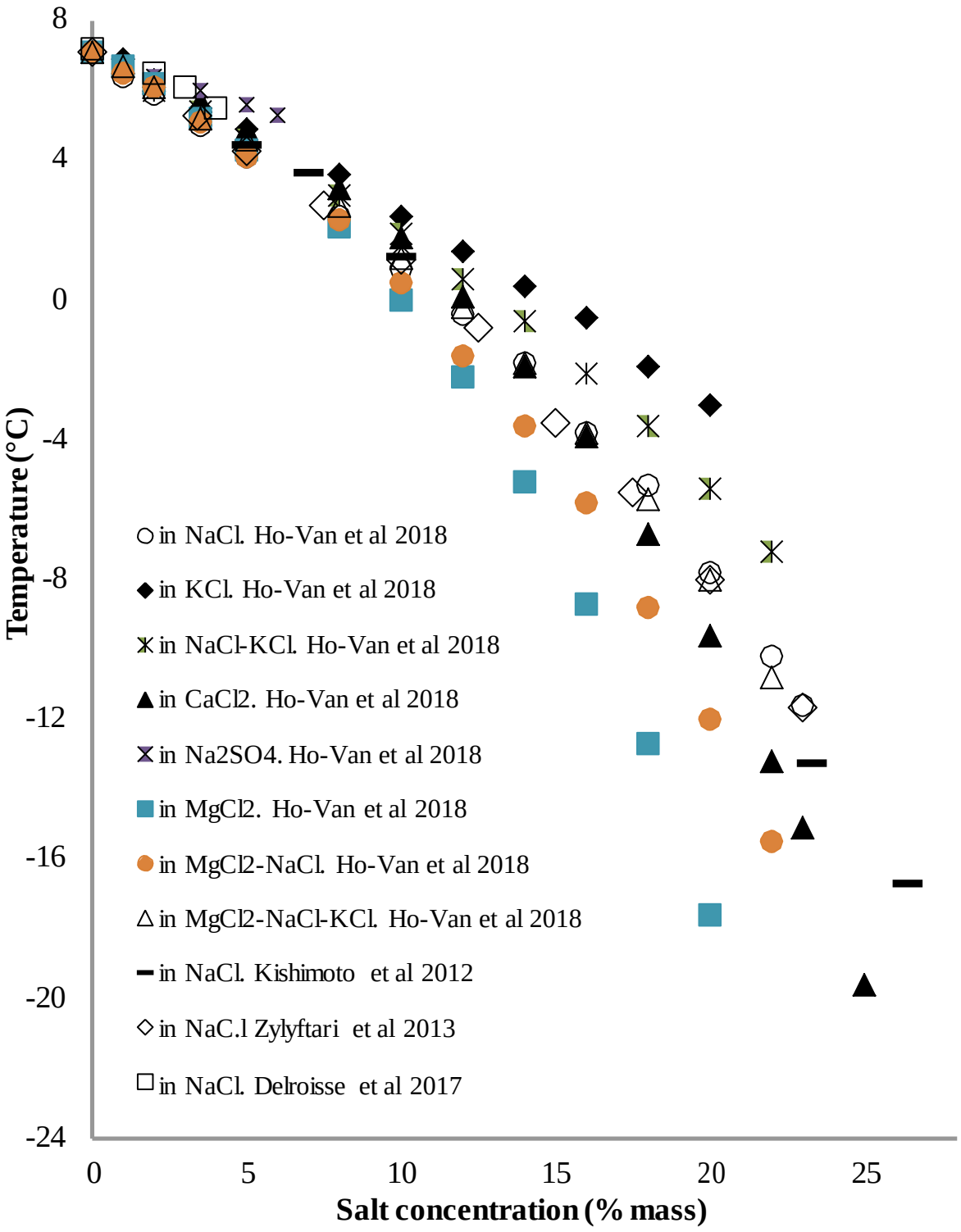

Figure 2. Equilibrium temperatures of CPH in the presence of salts from literatures [28,64,68,77,87,88]

There are slight variations concerning dissociation temperature at 3.5% NaCl between four studies of Han et al. [69], Sakemoto et al. [64], Baek et al. [73], and Ho-Van et al. [28]. Han et al. [69] used the quick dissociation procedure leading to a higher value (6.6°C) compared to

others. Among the three other data, Baek et al. [73] reported the lowest dissociation temperature of 4.57°C, while Ho-Van et al. [28] and Sakemoto et al. [64] recorded 5.0°C and 5.5°C, respectively. This is due to the presence of SPAN surfactant, used by Baek et al. [73]. It decreased the equilibrium temperature due to Gibbs–Thomson effect [82], as stated by Zylyftari et al. [68]. In addition, at 3.4% NaCl, Zylyftari et al. [68] reported that the equilibrium temperature of CPH is 5.28°C. This value is slightly higher than the value of 5.0°C at 3.5% NaCl provided by Ho-Van et al. [28].

The previous comparison indicates that the slow dissociation and DSC methods furnish more trustworthy data. Nonetheless, Delroisse et al. [77] offers a 2% NaCl dissociation temperature at 6.5°C ± 0.2°C. This is higher than the value of 5.9°C ±0.1°C reported by Ho-Van et al. [28]. This might be attributed to the higher dissociation rate (0.2°C/hour) used by Delroisse et al. [77] compared to Ho-Van et al. [28] (0.1°C/hour).

Figure 2 also points out that the hydrate formation temperature decreases quickly with increasing salt concentration, indicating that salt noticeably inhibits CPH thermodynamic equilibrium. Two well-known phenomena, "ion clustering" and "salting-out", are believed to reduce the hydrate formation temperatures, as clearly explained elsewhere [14,28,89].

Note bene: salt concentration increases during hydrate formation due to the consumption of pure water. When the salt concentration reaches saturation, precipitated salt can appear. Hence, solid salts can be recovered at the bottom of the bulk, while CPH lay above the aqueous phase. For instance, it happens easily for some salts such as Na_2SO_4 at 6% mass fraction [88], or $PbCl_2$, $CaSO_4$, and Ag_2SO_4 whose solubilities are very low into water. Therefore, their crystallization can occur quickly after CPH formation.

2.3. Phase equilibria of mixed hydrates containing CP as a co-guest

Clathrate hydrates can form in the presence of multiple guests beside CP. Therefore, some efforts used a secondary guest alongside CP for desalination process (Cha et al. [90], and Zheng et al. [47]). Results show that these mixed clathrate hydrates can improve salt removal efficiency compared to pure CPH. One promising idea is to combine CP with another guest molecule, and by this mean to couple desalination to another hydrate-based application, such as gas capture, gas hydrate exploitation (CH_4 for instance), or gas separation. Hereby, energy involved in the integrated process could be optimized, and salt removal efficiency could increase [20,47,91]. Table 5 provides range of thermodynamic equilibrium data of the mixed hydrate containing CP as a co-guest.

Table 5. Equilibrium conditions of mixed hydrate containing CP as a co-guest

Note: pure water implies distilled or only under laboratory conditions

Hydrate formers	Aqueous solution	Temperature range (K)	Pressure range (Mpa)	Citation
Binary				
CP – CO_2	Simulated produced water: 8.95 % mass	280.15 – 289.15	3.1	[90]
CP – CO_2	NaCl: 3.0% mass	271.89 – 292.21	0.55 – 3.59	[47]
CP – CO_2	NaCl: 0, 3.5, 7.0, 10.0, 15, 25% mass	269.8 – 292.4	1.18 – 3.33	[92]
CP – CO_2	Pure water	280.16 – 291.57	0.08 – 4.88	[52]
CP – CO_2	Pure water	284.6 – 291.6	0.49 – 2.58	[53]
CP – CO_2	Pure water	275.5 – 285.2	0.42 – 0.59	[20]
CP – CO_2	Pure water	284.3 – 291.8	0.35 – 2.52	[93]
CP – CO_2	Pure water	281.55 – 290.25	0.15 – 1.92	[94]
CP – CO_2	Pure water	283.5– 287.5	0.761– 1.130	[95]
CP – CH_4	NaCl : 0, 3.5, 7.0, 10.0 % mass	284.4 – 301.3	0.480 – 16.344	[96]
CP – CH_4	NaCl : 0, 3.5, 7.0% mass	288.5 – 296.9	3.26 – 1.09	[39]
CP – CH_4	NaCl : 3.5% mass	283.15 – 298.15	0.48 – 10.15	[97]
CP – CH_4	(K^+ , Na^+ , Mg^{2+} , Ca^{2+})	292.68 – 295.06	2.50 – 2.51	[98]
	(Cl^- ,SO_4^{2-})	293.75 – 295.06	2.50 – 2.51	[98]
CP – CH_4	Pure water	282.8 – 300.5	0.157 – 5.426	[40]
CP – CH_4	Pure water	284.8 – 299.3	0.321 – 4.651	[56]
CP – CH_4	Pure water	287.5 – 303.0	0.62 – 8.61	[48]
CP – CH_4	Pure water	286.70 – 300.0	0.48 – 5.69	[41]
CP – N_2	Pure water	282.9 – 289.1	0.641 – 3.496	[40]

CP – N_2	Pure water	285.9 – 302.0	1.68 – 24.45	[50]
CP – N_2	Pure water	284.7– 296.0	1.27– 10.4	[48]
CP – O_2	Pure water	289.4 – 303.3	2.27 – 21.69	[50]
CP – O_2	Pure water	286.0 – 297.1	1.03 – 9.10	[99]
CP – Methylfluoride	Pure water	287.9 – 305.9	0.138 – 2.988	[100]
CP – Kr	Pure water	283.8 – 308.5	0.116 – 7.664	[101]
CP – CH_2F_2	Pure water	280.45 - 299.75	0.027 - 1.544	[102]
CP – H_2	Pure water	280.68 – 283.72	2.70 – 11.09	[63]
CP – H_2	Pure water	281.3 – 288.3	4.34 – 32.	[50]
CP – H_2	Pure water	280.83 – 284.01	2.50 – 12.50	[86]
CP – H_2	Pure water	280.70– 284.31	2.463 – 14.005	[103]
CP – H_2	Pure water	283.4	10	[104]
CP – H_2S	Pure water	295.4 – 310.0	0.150 – 1.047	[56]
CP – Light mineral oil	NaCl : 0 – 23% mass	257.8 0– 278.55	0.101325 (Atmospheric)	[68]
Ternary				
CP – N_2 – CH_4	Pure water	283.3 – 289.5	0.310 – 1.855	[40]
CP – N_2 – CH_4	Pure water	283.4 – 288.1	0.3 – 1.2	[105]
CP – CH_4 – Trimethylene sulfide	NaCl : 0, 3.5, 5, 7, 10% mass	289.01 – 303.77	1.11 – 12.49	[106]
CP – THF – CO_2	Pure water	285.2 – 293.2	0.42 – 2.92	[53]
CP – THF – CO_2	Pure water	274.0 – 289.6	0.29 – 0.97	[20]
CP – CO_2 – N_2	Pure water	286.73 – 293.04	2.00 – 6.51	[107]
CP – CO_2 – H_2	Pure water	284 – 291	1.5 – 7.23	[108]

CP – CO_2 – H_2	Pure water	270.15 – 276.15	2.88 – 4.90	[109]
CP – O_2 – N_2	Pure water	284.0 – 296.2	1.09 – 9.45	[99]
CP – O_2 – N_2	Pure water	281.25	2.49 – 3.95	[110]
CP – Light mineral oil – Halocarbon 27	NaCl : 0 – 23% mass	258.67 – 278.54	0.101325 (Atmospheric)	[68]
Quaternary				
CP – TBAB – CO_2 – N_2	Pure water	280.20 – 290.32	2.21 – 5.71	[107]
CP – nC_5H_{10} – Methylbutane – Methylpropane	Pure water	273.35 – 279.68	5.5×10^3 – 19.5×10^3	[59]
CP – CH_4 – N_2 – O_2	Pure water	288.0 – 293.1	0.89 – 2.60	[111]
Quinary				
CP – Cyclohexane – CH_4 – N_2 – O_2	Pure water	278.6 – 286.7	1.99 – 5.08	[111]

Table 5 indicates that CO_2, CH_4, N_2, and H_2 are the four most common gases used to study mixed CPH. As seen from Figure 3, mixed CP-CH_4, CP-CH_4-O_2, CP-CH_4-N_2, CP-CH_4-TMS (Trimethylene sulfide) hydrates have been studied in pure water and in brine. Indeed, CH_4 is valuable fuel. Moreover, it is flammable and dangerously explosive at high pressure, especially when air, or just O_2, is present. As a result, CH_4 is not an auspicious hydrate former for CPH-based desalination, even though the hydrate formation conditions of the mixed CP-CH_4 hydrates are systematically milder than those of the mixed CP-CO_2, CP-O_2, CP-N_2, or CP-H_2 hydrates in fresh water and in brine.

Figure 3 also shows that CP-Kr and CP-H_2S can form mixed hydrates at the most favorable conditions [56,101] . However, Kr is a very expensive gas due to costly production process, from liquid air by a fractional distillation procedure. Plus, H_2S is a toxic, corrosive, and flammable gas. These gases cannot be considered as candidates for CPH-based desalination processes.

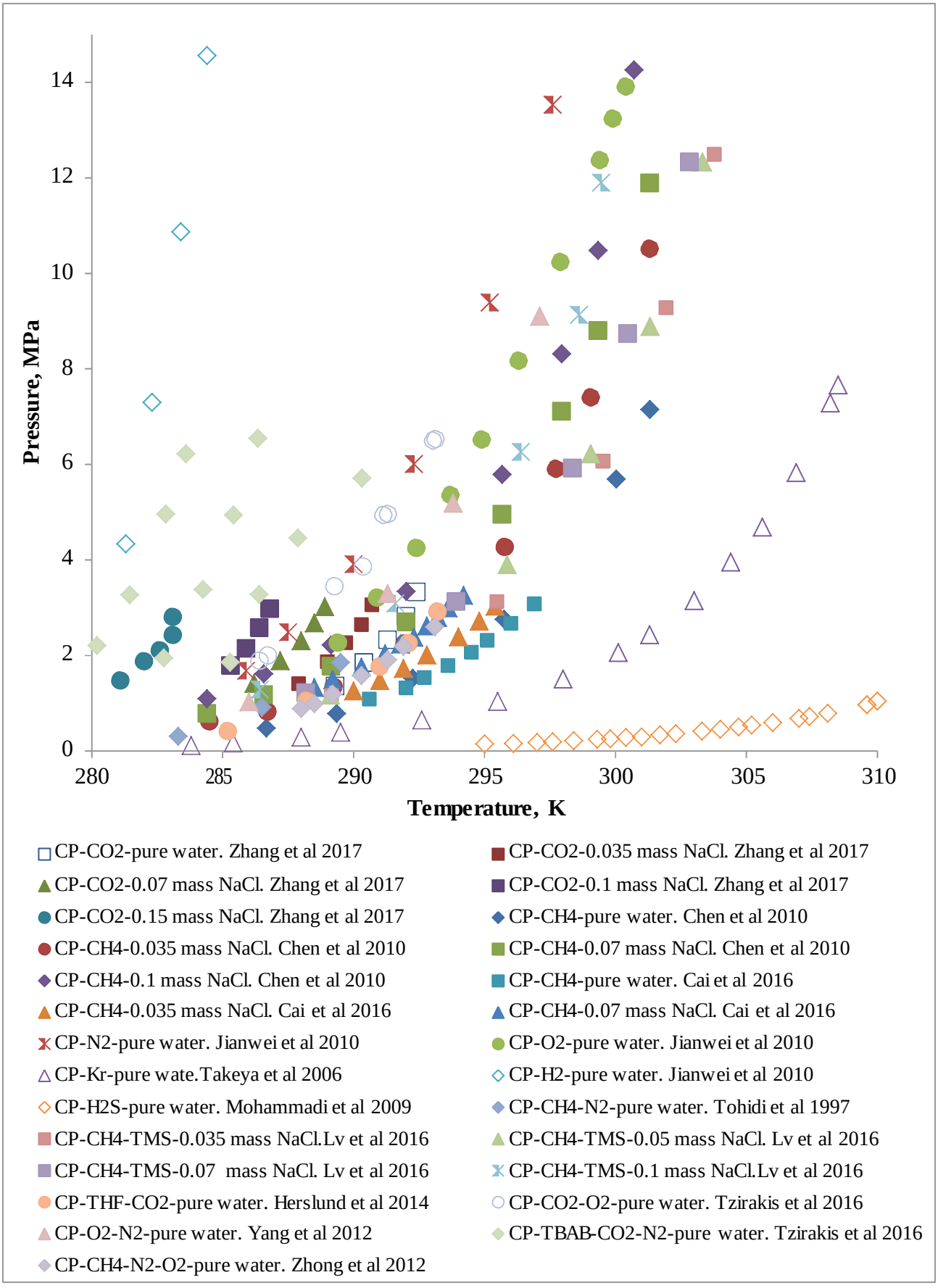

Figure 3. Equilibrium data of mixed gas hydrates containing CP in literature

Figure 3 further indicates that the hydrate formation conditions of CP-O_2, CP-N_2, and CP-H_2 are all much harder to achieve than those of CP-CO_2 in pure water. As CO_2 is the most common and arguably famous greenhouse gas, the disposal of CO_2 has become a global concerns issue [17,19,112–115]. One of the ways to mitigate CO_2 emission is gas hydrate–based capture [116]. Furthermore, pressurized CO_2 streaming from CO_2 emission sources may be favorable for hydrate formation and the cost for pressurization can be decreased [117,118]. Note that CO_2 forms hydrate SI in pure water at 278.8 K at 2.33 Mpa according to the study of Zhang et al [92]. In the presence of CP, the binary mixture of CP-CO_2 can form SII hydrate at milder condition (291.3 K at 2.33 Mpa in pure water [92]) compared to the single CO_2 gas [90,92]. In this case, CP occupies large cages while CO_2 molecules occupy small cages. Hence, CP-CO_2 binary can be used for both desalination [44,47] and carbon capture [20]. Note that, in the case of flue gas, mixed CO_2-N_2-CP hydrates would be formed, and CO_2-H_2 for pre-combustion capture. Still, more studies are needed to improve gas hydrate based desalination and CO_2 capture processes in term of energy requirement, salt removal efficiency, and CO_2 storage capacity from a gas mixture in brine.

3. Kinetics of CPH formation

Kinetics is one key parameter for a process design. It is, in the present case, correlated to the rate of crystallization, water conversion efficiency, and therefore the number of separating steps, and total operating cost. In this section, all published studies on kinetic of CPH formation are collected and investigated.

Table 6 lists the effects of several parameters on CPH formation kinetics in terms of nucleation and growth. In the next subsections, some details are provided to explain these phenomena.

3.1 Subcooling and Agitation

The rates of hydrate nucleation [14,130,142–145] and growth [79,146–153] can be increased with the raise of the subcooling. Note that subcooling, ΔT_{sub}, is related to the driving force for the crystallization and defined as the difference between the system and the equilibrium temperature [87].

Xu et al. [70,124] indicated that the duration of CPH formation from salty water decreases with both the increase of subcooling and agitation speed. Martinez de Baños et al. [72] and Ho-Van et al [123] reported that the hydrate growth rate is observed to be proportional to

subcooling. Indeed these conditions enhance mass and heat transfer between water/CP and the driving force for the hydrate formation.

Table 6. The effects of several considerations on kinetic of CPH formation

Considerations	**Nucleation**	**Growth rate**	**Citation**
Subcooling increase	↑	↑	[42,64,68,70–72,76,87,119–125]
Quantity of CP	↑	↑	[42,79,119,120,126,127]
Agitation speed increase	↑	↑	[39,60,70,119,124,125,128]
Use of ''Memory effect''	↑	NA	[61,65,66,72]
Solid additives	↑	NA	[43,61,75,129,130]
Presence of salts	↓	↓	[39,45,68,72,77,87,119]
Presence of surfactants or polymers	↑	↑	[68,71,74,126,130–136]
Presence of surfactants or polymers	↓	↓	[65,74–77,121,131,137–140]
Presence of THF (0.01 - 0.05 % mass)	↑	↑	[139]
Presence of MeOH	↓	↓	[139]
Presence of activated carbon particles	↓	↓	[51]
Presence of free resins, biding resins, and residual Asphaltenes	NA	↓	[141]

where ↑: increase; ↓: decrease; NA: Not Acknowledge.

Masoudi et al [79] stated that under mixing condition, the growth rate of CPH (1.9×10^{-5}–3.9×10^{-5} kg $m^{-2}s^{-}1$) is much higher than only flow condition (4.5×10^{-6} kg $m^{-2}s^{-}1$). Sakemoto et

al. [64] and Kishimoto et al. [87] reported that the CPH nucleation location is at the CP-water interface because of the low solubility of CP in the aqueous phase. Consequently, agitation is needed to increase the kinetic of CPH formation.

Moreover, Cai et al. [125] observed that the rate of CP-CH_4 hydrate formation improves with the increase of the agitation rate. Indeed, this increase can lead to smaller CP droplets, as well as the splitting of hydrate shells covering CP droplets. Ergo, this enhances the CP-water contact area and then enhances the hydrate formation rate.

3.2 Addition of CP

Corak et al. [42] and Lim et al. [126] showed that the kinetic of CPH depends strongly not only on subcooling, but also on the quantity of CP. Faster growth was ascertained by increasing amount of CP. In fact, increasing the quantity of hydrate former improves mass transfer, diffusion and consequently escalates the number of nucleation locations for hydrate formation. However, for desalination, CP quantity needed to be minimized in accordance with other important parameters, in order to reduce the total cost.

3.3 "Memory effect''

"Memory effect'' corresponds to the empirical reduction of induction time by using a solution that has already formed crystals. This has been observed and used in laboratories to reduce drastically the induction time, especially for crystallization without agitation in small reactors. Some authors have investigated the influence of this phenomenon on hydrate formation [14,65,142,154–157]. Sefidrood et al.[66] concluded that the "memory effect" could enhance the nucleation of CPH formation. Using a small quantity of water from dissociated CPH at a temperature 2-3°C above the equilibrium, the CPH formation rate was observed to be much faster than starting from fresh water. Consequently, in desalination, a small amount of the melted water from dissociation step can be recycled to the next CPH formation step in order to reduce the induction time. Of course, this is not a problem in case of a continuous process, or in presence of seeds.

3.4 Solid kinetic additives

Some kind of solids such as ice, silica gel, silica sand, rust, chalk, or clay have been studied to reduce hydrate nucleation time [37,65,158–161]. Zylyftari et al. [129] reported CPH formation at the ice – CP – brine phase contact line, which is believed to improve kinetics of hydrate crystallization [129]. Karanjkar et al [130] observed that, in this case, there is no

induction time and nucleation takes place instantaneously as ice dissociates into free water. This fresh free water is then converted totally into CPH. Moreover, Li et al [43] indicated that addition of graphite promotes CPH formation. The graphite particles are composed of many flat carbon sheets (graphenes) that can provide heterogeneous sites for both ice and hydrate nucleation [43]. Other studies using nanoparticules can also be found, but not in presence of CP [162–164]. Nanofluids enhance crystallization kinetics as well [165].

3.5 Influence of salts

It is known that inorganic mineral salts affects significantly not only thermodynamics of CPH but also the kinetics of hydrate formation [39,146]. In the presence of salts, the equilibrium temperature is further shifted lower [14,28,64,68,72,77,88,89]. This leads to less subcooling, reducing hydrate growth and preventing the final water-to-hydrate conversion.

Kishimoto et al. [87] described that the nucleation and the growth rates of CPH are slowed down with increasing salt concentrations at a given subcooling. Moreover, Cai et al [39] reported that the mixed CP-methane hydrate growth rate in NaCl solution is systematically lower than that in pure water for any salt concentrations. Indeed, during hydrates formation in brine, ions are mostly excluded and then accumulate at the vicinity of growing solid hydrate. Therefore, it could locally lower the driving force for hydrate growth. This is called the concentration polarization effect [39].

Finally, the quantity of accumulated salt considerably depends on the kinetic of hydrate formation and the speed of stirring. Consequently, the concentration polarization effect can be reduced by enhancing the mixing to transport salt away from the growing crystal.

3.6 Interfacial effects, surfactants

Hydrate formation kinetics is also deeply related to surface phenomena [143,166–170]. Interfacial tension of liquid-liquid or liquid-gas system plays a crucial role on the mass and heat transfers. Some additives, which affect the interfacial tension, can be used as a promotor while others can be used as an inhibitor for hydrate formation.

It is known that CP is a hydrophobic hydrocarbon. Hence it is immiscible with water. Therefore, complete conversion of water (or CP) into CPH is hard to achieve. This issue can be remedied by adding a small quantity of certain surfactants to the process [68,132,134,135,166]. Of course, it is then difficult to separate fresh water from liquid CP afterward.

Erfani et al. [134] investigated the effects of 14 surfactants and polymers on CPH formation. The results showed that the addition of surfactants can highly decrease the induction time and

enhance the hydrate formation rate. Furthermore, Lauryl Alcohol Ethoxylates with 8 ethoxylate groups (LAE8EO), TritonX-100 and Nonyl Phenol ethoxylates with 6 ethoxylate groups (NPE6EO) were found to be the best additives to increase the kinetic of hydrate formation. Erfani et al. [134] demonstrated that surfactants generating oil in water emulsion improved the kinetic of hydrate formation better than those generating water in oil emulsion.

Lo et al. [166] declared that CPH growth rate is higher in presence of sodium dodecyl sulfate (SDS) and dodecyl-trimethylammonium bromide (DTAB) than without surfactant.

Likewise, Karanjkar et al. [130] and Zylyftari et al. [68] reported that Span 80 promotes CPH formation. However, Peixinho et al [75] observed the opposite. They witnessed that addition of surfactant Span 80 (0.0001, 0.01, 0.1% mass) into water, to form water in oil emulsion, decreases kinetic time for hydrate formation. According to them, surfactant Span 80 molecules cover the CP-water interface and inhibit water and CP diffusion. Thus, the CPH formation is prevented. This variation of the influence of Span 80 on kinetics could be attributed to differences in the experimental systems. For instance, Zylyftari et al [68] studied the CPH formation in the hydrate-forming emulsion, while Peixinho et al [75] studied CPH formation in one water drop in CP phase without agitation.

Brown et al [74] reported that the CPH shell thickness is not modified when surfactants are introduced into the system. This study reveals that they have different effects on the growth rate: Dodecylbenzenesulfonic acid at a concentration of 10^{-6} mol/L (DDBSA) and Tween at 10^{-4} mol/L decrease slightly the growth rate, while DDBSA at 10^{-4} mol/L and Tween at 10^{-8} mol/L slightly increase the growth rate.

Delroisse et al. [77] indicated that the average lateral growth of CPH in the presence of 0.1% and 1% of surfactant DA 50 (benzyl-dodecyl-dimethylazanium chloride, $C_{21}H_{38}C_lN$) is about twice lower compared to pure water system.

Furthermore, Zhang et al. [140] indicated that polyvinyl pyrrolidone (PVP) and polyvinylcaprolactam (PVCap) acted as inhibitors on CPH formation. In fact, PVP and PVCap prevented CP diffusion from the bulk to the hydrate surface. This hence decreases the growth rate of CPH. Hobeika et al. [76] showed that, with PVP, PVCap, or vinylpyrrolidone/vinyl-caprolactam copolymer VP/VCap present, the CPH growth rate is much lower compared to pure water. Therefore larger subcooling is required. Moreover, among these three polymers, PVCap was found to be best to prevent hydrate formation.

Dirdal et al. [65] investigated the inhibition efficacy of various of kinetic hydrate inhibitors (KHIs) of CPH formation under atmospheric pressure. Their results exhibited that, in the

range of 100-200 ppm, considerable smaller quantities of KHIs are needed to prevent CPH formation than standard gas hydrate formation. Furthermore, Abojaladi et al [138] studied the performance of surfactants (cation, non-ionic, and anion surfactants) as low dosage hydrate inhibitors (LDHI) and anti-agglomerants (AAs) by considering CPH formation. Their results showed that no link was found between hydrophilic-lipophilic balance (HLB) value and AA performance. In addition, it was found that anionic surfactants perform insufficiently, whilst cationic surfactants exposed favorable performances in dispersing hydrate crystals.

To sum up, in desalination, surfactants which promote hydrate formation and/or reduce the induction time such as LAE8EO, TritonX-100, NPE6EO, SDS, DTAB, Span 80, DDBSA and Tween at appropriate concentrations are advantageous. However, since their presence makes the hydrate former difficult to separate after dissociation, their use probably bring more drawbacks than advantages.

3.7 Liquid co-guests influence

Li et al. [139] indicated that the presence of 0.01-0.05% mass THF increases CPH formation rate. Moreover, Mohamed et al. [171] observed that the addition of THF to the CPH system, either with or without surfactants (Span 20, Tween 20), enhances the kinetics of CHP formation. They stated that THF, a highly soluble molecule into water, is a better kinetic additive than Span 20 or Tween 20. Unfortunately, it is difficult to separate THF from water for its reuse in desalination applications. Therefore, use of THF is not recommended in CPH-based desalination processes.

3.8 Other inhibitors

Li et al. [139] elucidated that Rhamnolipid bio-surfactant (product JBR 425) and Methanol inhibit CPH formation. Moreover, Baek *et al.* [51] demonstrated that activated carbon particles act as a kinetic inhibitor for the mixed hydrate of CP and propane. At 1%mass of activated carbon particles, the particle layer covers the whole interface between hydrate formers and water, preventing mass transfer and diffusion. Therefore, hydrate growth is retarded compared to pure mixed hydrate without activated carbon particles.

Finally, Morrissy et al. [141] indicated that free resins (FR), binding resins (BR), and residual asphaltenes (RA) in the crude oil reduce CPH film growth rate with a trend in following order: RAs > BRs > FRs. Above a given concentration threshold, these additive species are suspected to settle at the water/CP interface. Consequently, this prevents the growth of CPH crystals [141].

3.9 Conclusion on kinetics

Table 6 reveals that there have been several methods to increase the hydrate formation rate such as increasing subcooling, quantity of CP, agitation speed, using memory effect, using heterogeneous nucleation by ice or graphite, and addition of appropriate surfactants. Nevertheless, the methods of increasing subcooling and agitation speed consume much more energy than other methods. Moreover, increasing the quantity of CP is also a costly method because the huge quantity of seawater or salt water employed in a real facility. The uses of memory effect and/or heterogeneous nucleation by ice or graphite are probably favorable techniques to improve CPH kinetic due to low cost and operating simplicity. Appropriate surfactants could give the impression of being good method because of their high capability to enhance kinetics of CPH formation. However, their use is a significant issue in water/CP separation since an emulsion is formed.

4. Physical properties of CPH

Crystal morphology is another important aspect of hydrate-based technologies [148], and of course CPH-based desalination [64]. Indeed, CPH crystal shape strongly influences the kinetics of the formation process and it should be taken into account in designing equipment such as reactors and transportation devices. Adhesion, cohesion, rheology, interfacial tension, yield stress, and shell property are also useful common properties of hydrates. These are essential factors that affect CPH transportation in the process. In this section, morphology and physical properties of CPH in the open literature are classified and presented.

Table 7 provides different properties of CPH in the literature. The following subsections look at different parameters in detail.

4.1 Morphology

Hobeika et al. [76] reported that the growth rate and morphology of CPH remarkably depends on subcooling. CPH grow slowly with some large crystals present at low subcooling, while CPH grow quicker with many small crystals under high subcooling. Furthermore, the morphologies of CPH are different when additives like PVP, PVCap, or VP/VCap are present. In this case, CPH particles are thinner, less glassy, and more fragile. Sakemoto et al. [64] and Kishimoto et al. [87] pointed out that the morphology of the individual CPH crystals in water, seawater and brine at any NaCl concentration are comparable at a similar subcooling. Moreover, the size of the CPH crystals are smaller at higher subcooling [87].

Table 7. CPH physical properties studied in the literature

Properties	Citation
Morphology	[42,45,64,71,74–77,87,122,126,127,129,131,171–174]
Adhesion	[42,62,80,175–180]
Cohesion	[74,137,141,175,177,181,182]
Rheology	[68,173,183–185]
Interfacial tension	[68,73,74,76,77,80,122,131,134,166,169,170,175,177,179,181]
Yield stress	[68,172]
Hydrate density	[14,60,76,77]
Wettability	[77,81,123]
Shell property	[74]
Heat of formation	[60,78,130,186,187]
Heat capacity	[186]
Torque	[174]

In addition, Mohamed et al. [171] reported that the nature of surfactants affects the morphology of CPH. Delroisse et al. [77] studied the morphology of CPH at different surfactant DA 50 concentrations. Their results showed that at 0.01% mass DA 50, small hairy hydrate crystals with a large quantity of needles and some many-sided shapes were observed. At 0.1 and 1% mass DA 50, smaller hydrate crystals with many-sided, three-sided, and sword-like shaped were observed. This was attributed to differences in the configuration of the surfactant molecules absorbed on hydrate surface, due to differences in surfactant concentration tested.

Mitarai et al [71] elucidated that, with Span surfactant present, the individual CPH crystals had a larger size compared to those in the system without Span surfactant. Their results also indicate that Span has two effects: inhibition of hydrate agglomeration; enhancement of hydrate formation.

Lim et al. [126] showed that adding SDS can modify the CPH hydrate crystal morphology. Indeed, with SDS present, the same length rectangular tree-like or fiber-like crystals were observed from hydrate deposit.

4.2 Adhesion

Aspenes et *al.* [175] investigated adhesion force between CPH and solid surface materials. Their results showed that the force of adhesion depend on the surface materials and the presence of water. Low free energy surface solids lead to the lowest adhesion. The hydrate-solid surface adhesion was more than 10 times stronger than hydrate–hydrate adhesion. Adding petroleum acids declined adhesion, while the presence of water-dissolved oil phase improved adhesion. In addition, water-wet solid surfaces were found to have the strongest adhesion.

Nicholas et al. [62] revealed that adhesion between CPH and carbon steel was found to be significantly weaker than CPH – CPH particles and were also lower than ice – carbon steel. Aman et al. [177] reported that CPH adhesion forces are 5 to 10 times stronger for calcite and quartz minerals than stainless steel, and adhesive forces are strengthened by 3 – 15 times when delaying surface contact time from 10 to 30 seconds. Finally, Aman et al. [176] demonstrated that hydrate adhesion drops significantly with Span 80, polypropylene glycol, or naphthenic acid mixture present in a mineral oil and CP continuous phase.

4.3 Cohesion

Brown et al. [182] observed that, at different temperatures, longer annealing time led to lower cohesive force. Indeed, annealing step disrupts micropores or capillaries in hydrate structures, where free water is transported from the hydrate core to the outer surface. This diminishes the water layer favorable for cohesion.

Aman et al. [181] determined cohesion force for CPH in water, hydrocarbon, and gas bulk phases. Their results showed that cohesion is different in various phases. Cohesion in gas phase is roughly twice and six times stronger than that in the hydrocarbon phase and in the water phase, respectively. Furthermore, Aman et al. [80] reported that cohesion force of the CPH particles is 9.1 ± 2.1 mN/m and 4.3 ± 0.4 mN/m at around 3°C in the gas phase (N_2 and CP vapor) and in the pure liquid CP phase, respectively.

4.4 Interfacial tension

Aman et al. [169] affirmed that the interfacial tension of CPH – water and CPH – CP is 0.32 ± 0.05 mN/m and and 47 ± 5 mN/m, respectively. Brown et al. [74] indicated that the addition of Tween 80 leads to a remarkable drop in interfacial tensions at high concentrations above

critical micelle concentration (CMC) in a water bulk phase. Nonetheless, dodecylbenzenesulfonic acid (DDBSA) showed no dependence of interfacial tension under concentrations below the CMC.

Moreover, Delroisse et al. [77] concluded that, in presence of DA 50, the interfacial tension between CPH and water increases while the interfacial tension between CPH and CP diminishes.

4.5 Rheology

In term of CPH rheology, Karanjkar et al. [183] indicated that CPH slurry viscosity is proportional to the water volume fraction. Slurry viscosity decreases (1-3 Pa.s at 8 °C) with increasing of subcooling (below freezing ice temperature). This is explained by ice formation. Indeed, more ice was observed in the CPH slurry system at lower temperatures (higher subcooling) than at higher temperature (lower subcooling), resulting in lower viscosity.

Moreover, at Span 80 concentrations of 0.5-5% (v/v), viscosity was found to be lower due to the accessibility of extra quantity of Span 80 molecules (oil-soluble surfactant) which can adsorb onto the CPH interface and weaken CPH-CPH interactions. Therefore, Span 80 can increase the flowability as an anti-agglomerant at high concentrations.

In addition, when introducing ice to the system to induce hydrate crystallization, Zylyftari et al. [129] observed that the viscosity of the mixture increases faster than by introducing CPH.

Finally, since high viscous hydrate slurry requires much more energy to be transported, methods to reduce viscosity, such as the use of surfactants or especially CPH seeds, are recommended in CPH-based desalination.

4.6 Yield stress

Ahuja et al. [172] determined that the yield stress of CPH slurry rises quickly from 5 Pa to 4600 Pa when increasing the water volume fraction (ϕ) from 16% to 30% above a critical water fraction (ϕ_c) of 15%. A power dependence of the yield stress of CPH and slurry viscosity on water volume fraction was also found, scaling as $(\phi - \phi_c)^{2.5}$.

Zylyftari et al. [68] reported that, at low water conversions (< 27%vol), the yield stress is quite small (10^{-1} Pa). At higher water conversions (42-81%vol), yield stress increases to 100 Pa. It reaches to a maximum of 145 Pa at 81%vol conversion. The behavior of yield stress as a function of the water to CPH conversion exhibits a similar tendency as the viscosity. This also illustrates the effect of capillary bridges between CPH particles. At 81% water conversion, the yield stress is maximum (145 pa), showing the optimal number of capillary bridges and CHP surface required to have the strongest network structure.

4.7 Density

Sloan et al. [14], Delroisse et al [77], Hobeika et al. [76] and Nakajima et al. [60] indicated that CPH density is about 950 to 960 kg/m^3. At standard conditions, this value is between the density of brine (>1000 kg/m^3) and CP (751 kg/m^3). Thus, CPH floats on water and sinks in liquid CP.

4.8 Wettability and shell properties

Delroisse et al. [77] reported that CPH is CP – wettable with surfactant DA 50 present. However, Karanjkar et al. [81] indicated that in the presence of Span 80, CPH is water – wettable. This requires selecting the appropriate surfactants to be used in desalination to optimize hydrate separation from the aqueous and also CP phases.

Brown et al. [74] investigated the effect of surfactants on CPH shell properties. It was found that the addition of DDBSA and Tween 80 changed the CPH properties. Indeed, the CPH shells, with DDBSA and Tween 80 present, require a much lower perforation than for pure CPH. This indicates that adding these surfactants weaken the CPH shell strength.

4.9 Thermodynamic properties

Two thermodynamic parameters including heat of formation and heat capacity have been well reported in literature [60,78,130,186,187]. These two parameters are crucial for the design and optimization of CPH-based desalination [186].

The value of heat of formation (kJ/mole of water) varies according to authors: 4.84 [130,187]; 5.098 [186]; 6.786 [78]. The CPH heat capacity was firstly approximated from the heat capacities of THF and propane hydrate according to He el al. [186] as follows:

$C_P = -124.33+3.2592T+2\times10^{-6}T^2-4\times10^{-9}T^3$ where T is the absolute temperatures (K).

4.10 Torque

The agglomeration phenomena of hydrate crystals are important in hydrate-based desalination since they are related to the transport of hydrate in the desalination process. The torque value is one of the common factors that represent the agglomeration of hydrate [89,138,159,184,188]. Delroisse et al [174] reported that, without biodegradable anti-agglomerant (called AA-LDHI [174]) in a stirred-tank reactor, the torque of CPH increases progressively to 0.3N.m until the agitator stopped at 550 min (approximately 0.7N.m). It is because of the significant increase in viscosity after the crystallization onset, when CPH crystals agglomerated *via* capillary bridges. In addition of 0.1% AA-LDHI, the torque drops significantly, about ten times. Furthermore, in the presence of AA-LDHI, when CPH crystallization started, the torque grows slightly from 0.025 N.m to 0.035 N.m and then

remains nearly constant. The results indicate that the added AA-LDHI disperses CPH particle (average diameter of 380 ± 150 µm [174]) and reduce their agglomeration during crystallization. Consequently, this is expected to facilitate the transport of CPH crystals in desalting processes.

4.11 Conclusion on CPH physical properties

In many cases, adding surfactants modifies morphology and physical properties of CPH in aqueous solution. The choice of appropriate kind and amount of surfactants could be favorable to the improvement of CPH kinetics and transport.

Besides, some issues on the use of surfactants should be prudently considered. Since they are soluble into water, and enhance CP solubility into water, it is very difficult to recover them by a simple physical method as decanting. Indeed, some techniques for removal surfactants from water could be applied such as nano-filtration [189], activated carbon/ultrafiltration hybrid process [190], coagulation [191,192], or constructed-wetland-treatment systems [193]. Bio-surfactants are also a good suggestion for CPH-based desalination since they promote hydrates formation and they are degradable [174,194,195]. However, the use of surfactants still needs more efforts to purify the dissociated water and increases the total operating cost. Therefore, minimizing quantity of the surfactants is one of the requirements for feasible CPH – based salt removal process.

5. Influence of operating conditions on CPH–based desalination efficiency

Gas hydrate formation involves high pressure conditions, and therefore appropriate equipments are required to design a hydrate–based process. Indeed, operating costs could be significantly higher compared to standard processes (distillation, reverse osmosis…). This cost drawback is the reason hydrate-based desalination has not been commercialized yet. As discussed earlier, the use of CP as guest for desalination in ~~and~~ combination with ~~to~~ other applications, such as gas capture/separation, or cold energy storage (see later in section 6.2), might be advantageous or profitable.

Remember that, with CP, hydrate crystallization occurs at only one bar under normal atmospheric pressure. In addition, CP can be recovered easily after hydrate dissociation since it is not miscible into water. This simplicity is an enormous advantage, and this is probably why CPH-based desalination is still of interest in the scientific community.

Recently, the use of CPH for desalination has been investigated at both laboratory and pilot scales [42,43,69,119,124,186,188,196–198] considering three main concerns: yield of

dissociated water from CPH, water conversion to hydrate, and salt removal efficiency. The effects of mentioned considerations on CPH-based desalination process are detailed in Table 8.

Table 8. Effect of various considerations on CPH-based desalination process

Considerations	Yield of dissociated water	Water conversion to hydrate	Salt removal efficiency	Citation
Quantity of CP:				
+ CP concentration in				
1 – 5 mol% range: ↑	NA	↑	NA	[69]
0.9 – 2.3 mol% range: ↑	NA	↑	Fluctuated	[42]
+ Water cut in				
20 – 60 vol % range: ↑	↑	NA	↓	[119]
70 - 90 vol % range: ↑	↓	NA	↑	[119]
Agitation:				
300 – 500 rpm range: ↑	↑	NA	↓	[119]
300 – 600 rpm range: ↑	NA	↑	NA	[124,197]
600 rpm	NA	NA	↑	[43]
Operating temperature:				
0.95 – 3.95°C range: ↑	↓	NA	↑	[119]
-2° – 2°C range: ↑	NA	↓	NA	[124,197]
0.4 – 2.4 °C range: ↑	NA	↓	↓	[42]

Salinity: 3 – 5% mass NaCl range: ↑	↓	NA	↑	[119]
0.17 – 5% mass NaCl range: ↑	NA	↓	NA	[124,197]
Use of graphite	↑	NA	↑	[43]
Use of filtering	NA	NA	↑	[69,124,196,197]
Use of centrifuging	NA	NA	↑	[69]
Use of washing By 3.5 % mass brine water	↑	NA	↑	[119]
By fresh water	↑	NA	↑	[119]
By fresh water	NA	NA	↑	[69,196]
By DI water	NA	NA	↑	[124,188,197]
By filtered water	NA	NA	↑	[124,197]
Ratio of washing water/dissociated water (g/g) 0.1 – 0.5 range: ↑	Fluctuated	NA	↑	[119]
0.5 – 1.2 range: ↑	Fluctuated	NA	Fluctuated	[119]
0.02 – 0.03 range: ↑	NA	NA	↑	[69]
0.03-0.05 range: ↑	NA	NA	↓	[69]
0 – 0.035 range: ↑	NA	NA	↑	[196]

0.035 – 0.05 range: ↑	NA	NA	↓	[196]
Use of sweating	NA	NA	↑	[69]
Use of gravitational separating	NA	NA	↑	[124,197]
Use of spray injecting	NA	↑	NA	[124,197]
Use of tube injecting	NA	↑	NA	[124,197]

where ↑: increase; ↓: decrease, NA: Not Acknowledge

Removal efficiency, yield of dissociated water, water conversion to hydrate, ratio of washing water/dissociated water (g/g), CP concentration, and water cut were calculated as follows:

$$\text{Yield of dissociated water} = \frac{m_1}{m_0} \times 100\% \text{ or } = \frac{V_1}{V_o} \times 100\% \quad (1)$$

where m_o/V_o are the mass/volume of initial salt solution, and m_1/V_1 are the mass/volume of melted water [43,119].

$$\text{Water conversion to hydrate} = \frac{m_c}{m_0} \times 100\% \quad (2)$$

where m_c is the mass of water converted to hydrates [42,69,124,196,197].

$$\text{Salt removal efficiency} = \frac{C_0 - C_1}{C_0} \times 100\% \quad (3)$$

where C_0 is weight percent of NaCl in prepared brine and C_1 is that in dissociated water [42,43,69,119,124,196,197].

$$\text{Ratio of washing water/dissociated water} = \frac{m_2}{m_1} \times 100\% \quad (4)$$

where m_2 is the mass of water used for washing [119]

$$\text{CP concentration} = \frac{n_{CP}}{n_{brine}} \times 100\% \quad (5)$$

where n_{CP} is the mole number of CP and n_{brine} is the mole number of initially prepared brine [42,69]. This is somewhat related to another parameter in the literature, the "Water cut".

$$\text{Water cut} = \frac{V_{brine}}{V_{brine} + V_{CP}} \times 100\% \quad (6)$$

where V_{brine} is the volume of initially prepared brine and V_{CP} is the volume of CP [119]

In the next sections, some details are provided to explain the effects of some considerations on the CPH-based desalination process.

5.1 Quantity of CP.

Water cut can be used to indicate quantity of CP as described by Equation (6). When water cut increases, quantity of CP then decreases because these two parameters are inversely proportional to each other.

Table 8 illustrates that the water conversion into hydrate increases by raising the CP concentration in the system [42,69]. Also, the salt removal efficiency varies irregularly from less than 70% to close to 90% when increasing CP concentration from 0.9 to 2.3 mol % [42]. Moreover, the water cut can affect the yield of dissociated water and the salt removal efficiency differently [119]. The yield of dissociated water first augments significantly with water cut from 20% to 60% while the removal efficiency declines inappreciably. When the water cut is in 60% - 90% range, the yield tends to lessen considerably while the removal efficiency is slightly improved. To summarize, the removal salt efficiency for different water cut varies from 75% to 85%. This demonstrates that, compared to high water cut systems (>80 vol% water or <5 mol% CP [42,69]), extra CP addition in brine could considerably improve the yield of dissociated water while the removal efficiency undergoes a relatively minor change.

The effect of CP quantity on the hydrate formation rate is described in elsewhere [42,119,126,127]. It was found that excess CP can increase notably the kinetics of hydrate formation, and hence the conversion of water to hydrate and the yield of dissociated water.

5.2 Agitation

Change in flow condition, or shear rate, is observed using various stirring rates. This leads to different mass and heat transfer rates in the system. Table 8 shows that boosting the agitation rate promotes water conversion and yield of dissociated water, as examined by different authors [39,43,60,70,119,124,125,197]. However, this comes with a decrease in salt removal efficiency [119]. Indeed, higher agitation rates may enhance the reaction kinetic and hence cause formation of smaller hydrate crystals with larger specific surface area. As a hydrate

surface is hydrophilic, more salt ions tend to attach on the crystal surfaces, leading to a difficult separation of brine from hydrate [119].

The way CP is introduced into a system can also change the hydrate formation kinetics. Xu et al [124,197] declared that, by using the CP spray injection method, higher water conversion can be achieved, due to the smaller CP droplets created by the spray injection. However, a pump is hence needed for CP injection in this case, thus more energy is required.

5.3 Operating temperature

Table 8 indicates that the operating temperature affects strongly water conversion to hydrate, yield of dissociated water, and removal efficiency. At higher operating temperature, the hydrate formation rate decreases due to decrease in the driving force (here subcooling). Thus, both water conversion and yield of dissociated water are reduced with higher operating temperature [42,119,124,197].

However, two different observations in purification efficiency when increasing operating temperature were reported by Beak et.[42] and Lv et al.[119].

One the first hand, Beak et al. elucidated that, at operating temperature of 2.4°C, the purification is less efficient than at 0.4°C. This is attributed to higher attractive force between CPH particles. Certainly, adhesion forces between CPH particles increase linearly with rising temperature [199]. Thus, at higher temperatures, growing CPH crystals adhere to each other in a stronger framework than at lower temperatures. Consequently, more brine is trapped between CPH crystals, and a post-treatment method, such as centrifuging, is required.

One the second hand, Lv et al.[119] showed that the salt removal efficiency improves when increasing operating temperature from 0.95 to 3.95°C (or 274.1 – 277.1K). It was found that the residual salinity is likely to be strongly related to the shapes and size of hydrate crystals. Kishimoto et al. [87] specified that the size of the hydrate crystals diminished with subcooling increase.

Moreover, by using the FBRM probe, Lv et al.[119] indicated that the median chord length of CPH particles after 8h formation at 0.95 °C (274.1 K) is 22.16 μm, while particles formed at 3.95°C (277.1 K) under the same other conditions exhibited a median chord length of 34.15 μm. Thus, it was supposed that at higher operating temperature (or lower subcooling), hydrate particles are bigger with a smaller specific surface area favorable to salt removal [119].

To sum up, in order to clarify the effect of operating temperature on the purification efficiency, more data at a varied range of operating temperature and salt concentration would be needed.

5.4 Salinity

Table 8 shows that the salt removal efficiency increases slightly with the salinity increase, while both water conversion to hydrate and yield of dissociated water appear to decrease considerably [119,124,197]. Indeed, when there is uptake in salt concentration, the driving force for hydrate formation decreases [28,119,124,197]. This reduces the CPH formation rate [39,68,87,119]. As a result, less water converts into hydrate under higher salt concentrations. Moreover, an enhancement in purification efficiency at high operating temperatures can be attributed the CPH crystals size change. Indeed, the hydrate formation kinetics decreases as salt concentration increases [39,68,87,119]. Thus, bigger hydrate particles with a smaller specific area are likely to form. Consequently, there is less brine trapped between CPH crystals.

5.5. Solid additives

As aforementioned, the addition of some solid additives can promote CHP formation [43,61,75,129,130]. Moreover, Li et al [43] reported that the addition of graphite not only enhances CPH formation but also boosts the salt removal efficiency. They indicated that the surface functional groups of graphite improve both hydrate nucleation and growth of CPH. Moreover, the hydrophobic surfaces of graphite could inhibit hydrate aggregation and make hydrate crystal particles more porous. Consequently, the trapped salt ions can be removed more easily by centrifuging process, thus increasing the salt removal efficiency [43]. In addition, in presence of graphite, the prolongation of hydrate formation improved the desalting efficiency [43]. The hydrophobic behavior of graphite is believed to play a crucial role in this improvement [43]. These findings present interesting perspectives for the use of graphite or carbon material surfaced in the development of CPH-base desalination techniques.

5.6 Post-treatment methods

In order to remove salts trapped onto the hydrate surfaces, some post-treatment methods are introduced, such as filtration, centrifuging, sweating, gravitational separation, and washing. Several studies concluded that all these techniques can enhance profoundly the salt removal efficiency [69,119,124,196,197].

About 60-63% of NaCl from the feed solution was removed after CPH formation with only vacuum filtration [69,196]. It means that the treated water still contained a high level of NaCl. Obviously, this level of water purification is insufficient for desalination, so further post-treatments are needed.

Han et al. [69] demonstrated that centrifuging can enhance salt removal efficiency up to 96%. However, centrifuging is very expensive for mass treatment. Sweating by melting the impure zone over time can be a potential process to enhance salt removal. Nonetheless, it reduces the quantity of water retrieved. Moreover, this process is time consuming, hence an optimal time should be determined for the sweating of CPH crystal [69].

Washing is also an effective approach to enhance salt removal [69,119,124,196,197]. The source of the wash can be fresh, DI water, filtered water, or even brine water. The effect of washing water/produced water ratio on salt removal was remarkable. Han et al. [69,196] indicated that the optimal ratio of washing water/ produced water is approximately 0.03 (g/g) with a salt removal efficiency above 90%. Lv et al. [119] suggested that this value should be 0.5 (g/g) in order to remove enough salt from CPH crystals. However, this value is extremely high for industrial scales. Therefore, more investigation is required to optimize this ratio in order to meet the requirement of water purification and reduce the costs of desalination process.

Finally, forthcoming research should combine optimization of both kinetics of CPH formation and the salt removal efficiency [119]. Post-treatment methods may include filtration or pelletizing (squeezing) at first step [11,13] in order to facilitate CPH separation from aqueous solution and transportation to dissociation devices. Furthermore, to meet potable water standards, several existing technologies like washing and sweating are needed to remove entrapped salt ions on the crystal surfaces. Of course, optimizations on these technologies are also required for the economy feasibility of the desalting process.

6. Comparison to other desalination technologies

6.1 Comparison to traditional technologies

Other processes such as multi-stage flash distillation (MSF), multiple-effect distillation (MED), solar thermal distillation (SD), freezing, reverse osmosis (RO), ecletro-dyalysis (ED), ion-exchange desalination (IE), and adsorption have been investigated, and industrially used, for seawater desalination [6,10,27,36,118,200–214].

Table 9 presents a comparison between diverse technologies based on four criteria: Thermal Energy consumption, electrical energy consumption, production cost, and product water salinity. Also, note that, in the case of clathrates, different formers can be used. Therefore, there are other opportunities than CPH to consider when discussing hydrate-based desalination. Consequently, a short comparison between different clathrate formers will be presented in the next section. Table 9 illustrate of what can be expected with other clathrate than CPH.

In term of purification level, MSF, MED, RO, adsorption, or clathrate hydrate technique can produce water with salinity lower than 10 ppm. Of course, this value varies according to the procedure and technology. For hydrate-based desalination, Subramani et al. [10] estimated that the technique can reach 100% salt removal in theory. However, such quality should not be expected. For instance, McCormack et al [32] obtained fresh water with a salinity of 100 ppm by using HCFC 141b (Dichloromonofluoroethane – CCl_2FCH_3) clathrates. In a patent, Mottet [198] evaluates that the salinity for the treated water via CPH crystallization to be 1000 ppm. By using a new batch-wise displacement washing technique in CPH-based desalting process, Cai et al [188] obtained fresh water with a salinity less than 10 ppm (<0.001% mass). Accordingly, in other efforts, Han et al. [69,196] and Lv et al. [119] indicated that CPH-based desalination technology can produce water with a salinity from 700-4400 ppm. Recently, Xu et al [197] and Li et al [43] reported values of 700 ppm and 4008 ppm, respectively.

Note that, according to World Health Organization (WHO), the palatability of water with a total dissolved solids (TDS) level less than 600 mg/l is generally considered to be good; drinking-water becomes significantly and increasingly unpalatable at TDS levels greater than 1000 mg/l [215]. Remember that seawater has an average of 35000 ppm TDS [210,216]. The high TDS value (here salinity) of product water via CPH-based desalination is strongly related to the salts trapped in the hydrate crystals [6,10,27,36,118,200–214]. This requires efforts on post-treatment process to completely remove trapped salt and therefore achieve product water with quality that meets the WHO drinking-water criterions.

Table 9. A comparison in energy consumption, production cost and product water quality between desalination technologies

Desalination technology	Thermal energy consumption (kWh/m^3)	Electrical energy consumption (kWh/m^3)	Production cost ($\$/m^3$)	Water salinity (ppm)
MSF	52.78-78.33[200]	*15.83-23.5* [200]	0.52-1.75 [200][217] 1.0785 [218] 0.77-1.64 [207]	10 [200]
MED	40.28-63.89 [200]	*12.2-19.1* [200]	0.52 -8.0 [200] 0.87-1.95 [207]	10 [200]
SD	0 [200,210]	*0* [200,210]	1.3-6.5 [200] 3.9 [210]	80 [210]
Freezing	*	9-11[219]	0.93 [219,220]	100 [210]
RO	*4.1 [5]*	4.0 [5] 3-7 [221] 8.2-9.0 [207]	0.85 [206,211] 0.45-1.72 [200] *0.64-0.76* [207]	35 [5,205] 400-500 [200] *10* [210]
ED	*	2.64-5.5 [200]	0.6-1.05 [200]	150-500 [200]
IE	*	1.1 [210] 0.29-1.04 [222]	1.05 [210]	13 [210]
Adsorption	*	1.38 [10,204,207]	0.18 [207]	7.54 [207] 10 [210] Up to 100% rejection [10]

CPH	*	0.35 [186]	*	< 10 [184] 1000 [198] 700-4400 [69,119,196] 4008 [43] 700 [197]
Other Clathrates				
HCFC 141b hydrates	*	1.58 [32,210]	0.63 [32,210] 0.46-0.52 [10]	100 [32,210] Up to 100% rejection [10]
Propane hydrates	*	0.60-0.84 [35]	2.76 [211] 1.11 [223]	100-500 [224]
CO_2 hydrates	*	*	*	7665 [11] 1100 [13] 23270 [90]
CO_2+CP hydrates	*	*	*	8055 [90]

* *Not Acknowledge*

In terms of energy consumption, Table 9 indicates that clathrate hydrate, adsorption, SD, or IE technology require the lowest amount of energy (< 2kWh/m^3), whilst MSF, MED, and Freezing consume an energy almost more than 10 kWh/m^3. The lower energy required in clathrate techniques compared others is related to its low phase change enthalpy. As clarified in Table 10, HCFC 141b hydrate or CPH requires a smaller energies (5.74 or 4.84 kJ/mol water, respectively) compared to freezing water (6.02 kJ/mol) or water evaporation (40.7 kJ/mol) [69,130,187].

Table 9 also displays that the production cost for adsorption and clathrate hydrate is much smaller than MSF, SD, freezing, and IE technologies. For instance, production costs for HCFC 141b and propane hydrates are less than 0.6 $/m^3$ and 1.11 $/m^3$, respectively. Otherwise, it is between 0.6 and 1.95 $/m^3$ for RO, MED, and ED technologies.

The above assessments indicate that clathrate hydrate and adsorption techniques could be able to produce high quality fresh water with a low energy consumption (< 2kWh/m^3) and minimum operating cost (less or around 0.6-1.11 $/$m^3$). Thus, both clathrate hydrate and adsorption technologies could be promising technologies after proper development compared to conventional processes.

However, there are some strong drawbacks concerning the adsorption technique [10]: it requires waste heat or renewable energy source for cost-effective desalination. Robustness of silica gel adsorber beds is still not known. Data are available only for demonstration-scale projects. Thus, this technique still requires more study.

6.2 Comparison between Clathrate formers for hydrate-based process

Concerning hydrate-based approach, the kind of former is crucial. It is one of the most important factors in hydrate-based desalination since the operating conditions strongly depend on the guest molecules. With a possibility to form hydrate at temperature above 0°C from seawater, CHFC 141B has been studied for desalination in the last few decades [32,33,225]. However, CHFC 141B has a solubility of 350mg/l at 15.6°C [32] higher than that for CP (156mg/l at 20°C) [28,46]. Moreover, HCFC R141B is also very volatile (boiling point of 32.2°C) [32]. This leads to an ozone-depletion problem when released into the atmosphere [226]. International concern over relatively high global warming potential of HCFC has caused some European countries to abandon it for many applications such as refrigerants or as a cleaning agent [226]. HCFC compounds, such as R141b, are hence restricted by current environmental regulations and are no longer practical candidates for a hydrate desalination process, despite their ease of use [33].

Recently, He et al [35,227], Nambiar et al [228], and Chong et al [223], proposed a propane-hydrate based desalination process using LNG cold energy. When compared to MSF, RO, and freezing techniques, Babu et al [229] demonstrated that this technology (the HyDesal process) can be economically attractive. As shown in Table 9, this process requires a remarkably low

energy (0.60-0.84 kWh/m^3) compared to others. The cost of potable water was found to be approximately $1.11/m3 with LNG cold energy integration [223]. LNG cold energy from the LNG regasification terminals replaces the external refrigeration cycle. Of course, this desalination technique still needs a stable LNG cold energy source. High-pressure devices (0.4 Mpa) are also required to form propane hydrate. Lastly, it should be noticed that LNG and propane are flammable and explosive gases at high pressure. Thus, although its economic feasibility, estimated by Chong et al [223], an industrial-scale testing of this process is not yet available.

In addition, Table 10 shows that CPH have a lower phase change enthalpy compared to CHFC 141B hydrate, CO_2 hydrate, and propane hydrate. The energy required for CPH-based desalination is hence likely less than for CHFC 141B hydrate, CO_2 hydrate, or propane hydrate based desalination.

Newly, He et al [186] investigated the techno-economic of CPH-based desalination utilizing LNG cold energy. Their results indicate that CPH-based desalination technique requires a specific energy consumption of 0.35 kWh/m^3, which is 58% lower than desalting technology utilizing propane hydrates. The Fixed Capital Investment (FCI) of the CPH-based desalination process was estimated to be $6,113,751 (for 0.75 m^3/h of pure water) which is again lower than with propane hydrates ($ 9.6 million for 1.3 m^3/h of pure water [223]). Moreover, the FCI augments from $6,113,751 to $9,559,668 when decreasing the CPH formation temperature from 277.15 K to 273.15 K. Finally, He et al [186] stated that the escalation of the water recovery rate of the CPH can lead to a decline in the SEC and FCI, and to a rise in the pure water flow rate and exergy efficiency. Consequently, improving the water recovery rate of CPH is crucial to enable fresh water production from this technique.

Furthermore, based on the fact that CPH-based desalination requires relatively low temperatures (less than 7°C) for hydrate nucleation and growth, this desalting technique would be more cost-effective if we can use the low temperature of actual seawater instead of utilizing a cryostat. For that purpose, Li et al [43] worked with actual seawater in winter at -10°C. Their results show that the crystallization occurred rapidly over 7h, with a salt removal efficiency of 70% and a water conversation rate of 56%. This indicates one more time the economy feasibility of CPH-based desalting technique when utilizing cold seawater.

Table 10. Latent heat of phase change of several techniques in desalination

Method of desalination	Latent heat of phase change, kJ/mol	Citation
CPH	4.84	[69,130,187]
CO_2 hydrates	57.7±1.8 to 63.6±1.8	[230]
	53.29	[231]
	66.8	[232]
Propane hydrates	27 ±0.33	[233]
Mixed hydrate CP + C_3H_8	2.23	[51]
Mixed hydrate CP + CH_4	131.70 – 121.74	[41]
Form R141 b hydrate	6.19	[225,234]
	5.74	[32]
Freezing water	6.02	[69]
Water distillation	40.7	[69]

7 Example of CPH technological approach

Based on the literature, hydrate-based desalination requires a relative low energy and it is theoretically more competitive economically than other standard processes (distillation, freezing, and RO technologies). To apply that at a commercial and industrial scale, there are still various challenges that need to be addressed. One of the most difficult trials concerns the improvement of two crucial limiting factors: salt removal efficiency and water to hydrate conversion. As detailed in Table 8, these two parameters are usually inversely proportional to each other. There is a need to investigate the best method to transport CPH after formation. Filtration and pelletizing seem to be appropriate to facilitate this transportation step. A washing method is necessary to enhance the salt removal capacity. However, improving the

ratio of washing water/dissociated water is also required to make this process economical feasible.

Utilizing LNG cold energy during the regasification process in the LNG regasification terminals for CPH-based desalination is one of the promising approaches to minimize the energy consumption and hence Strengthen Energy-Water Nexus [186]. Of course, this technique requires more experimental explorations before commercial readily-available in the freshwater production industry.

Furthermore, the idea of combining CO_2 capture and desalination can be advantageous when a hydrate mixture of CO_2 + CP is used. Indeed, merging two energy demanding processes can optimize energy use [23,90,92]. However, this procedure is more complicated with the added requirements of higher pressure equipment.

To recap, based on the analysis of all of the articles reviewed, a diagram of CPH-based desalination, with all proposed required steps and apparatus is proposed in Figure 4.

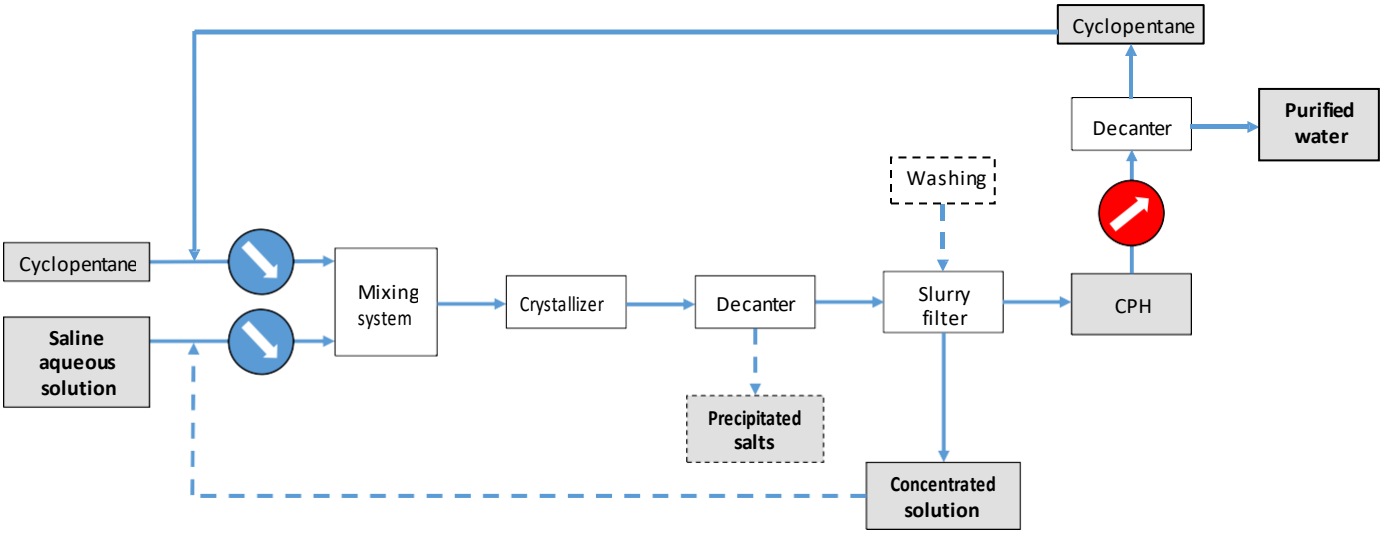

Figure 4. CPH-based desalination process diagram (inspired by [198])

Figure 4 presents a continuous system of water treatment. A mixing system is fed with both cooled CP and saline solution. This mixer, also called an emulsifier is critical to design as it governs the size of the CP droplets in water. The second piece of equipment is crystallizer, where the formation of CPH occurs. Since this is a continuous process; there is no induction time to consider. However, the residence time to complete hydrate formation in the crystallizer is optimized based on the device configuration design in order to reduce the

process capital cost. The slurry is then transferred to a decanter, allowing the growth of hydrate particles and the separation of different phases, notably the possible precipitation of the salts. Then, the slurry filter separates CPH and a concentrated solution. This concentrated solution is waste. However it can be partially re-injected to the mixing system if the aim is to produce saturated solution and precipitated salts. CPH crystals are melted with a heat exchanger and are introduced in a decanter allowing the separation of the CP (on the top) and purified water (on the bottom). The CP is then re-used at the beginning of the process in a closed loop.

A washing step can be also added to the slurry filter. This drives out the concentrated solution trapped between CPH particles. Nonetheless, a less concentrated solution is required. This can be the initial saline aqueous solution or a fraction of the purified water, depending on the rate of purification expected. Although by using a fraction of purified water, while a better purification rate can be obtained, unfortunately the yield of the system decreases.

As seen on figure 4, there are cooling and heating systems in the process. An optimization by energy recovery between the two types of heat exchangers could be considered in order to reduce the energy consumption still further.

From a technological point of view, this flow diagram summarizing all required steps and apparatus for a CPH based desalination process is inspired by the one proposed by BGH Company (France) [198].

According to Mottet [194], here are some advantages to this process:

- CPH can act as both a water purifier and a concentrator of dissolved materials (salts). Interestingly, Ho-van et al [88] reported the precipitation of salts (6% mass Na_2SO_4 at less than 5.3°C) during CPH crystallization. As solid materials, the precipitated salts can be then removed easily by a physical method since their high density compared to others (CPH, CP, brine).
- This is a "no discharge method", since simultaneous production valorized salts and pure water
- High yield, more than 95%
- This technique can treat highly-salty water (impossible for RO method).
- No pressure requirement, and reasonable operating temperature from -20°C to 7°C
- Less energy consumed than both evaporation and Ice EFC (Eutectic Freeze Crystallization) methods.

- This method is technically more reliable than the Ice EFC as the crystallization of water is internal and direct when CP is added.
- This is a continuous process

Obviously, before hydrate desalination becomes a practical commercial technology, the vital issues of controlled hydrate nucleation, formation rate, phase properties, amount of entrapped salt and its removal efficiency must be thoroughly understood and optimized [33]. As aforementioned, CPH has been recently studied in terms of thermodynamic, kinetic, and phase properties. A relatively sufficient database of CPH for desalination is now available in the literature as provided in this present review.

8 Conclusions

Numerous investigations have been being conducted on CPH for decades. Records on thermodynamic, kinetic, phase properties, and use of CPH for desalination were presented. A comparison between CPH based desalination and other techniques has also been provided. After analyzing vital factors such as energy consumption, product water quality, and economy of desalination plant, conclusions show that Clathrate hydrates present potential for new desalination technique. The use of CP as hydrate former is a promising idea, supported by recent researches in that field. While hydrate technology has not been yet fully developed in the industry, the combination of water desalination to other applications, such as cold energy storage, or even gas separation and storage, makes it again an encouraging idea compared to other competing technologies like distillation, freezing, and reverse osmosis. Of course, other clathrates formers, instead or in addition to CP molecule, could be more suitable for future water treatment applications. However, a diagram of CPH based salt removed has been suggested to illustrate future directions. Finally, some challenges, such as the best economic compromise between salt efficiency and water-to-hydrate conversion need to be addressed before industrial development and implantation.

References

[1] M. Pedro-Monzonís, A. Solera, J. Ferrer, T. Estrela, J. Paredes-Arquiola, A review of water scarcity and drought indexes in water resources planning and management, J. Hydrol. 527 (2015) 482–493. doi:10.1016/j.jhydrol.2015.05.003.

[2] S. Lu, X. Zhang, H. Bao, M. Skitmore, Review of social water cycle research in a changing environment, Renew. Sustain. Energy Rev. 63 (2016) 132–140. doi:10.1016/j.rser.2016.04.071.

[3] K. Watkins, Human Development Report 2006 - Beyond scarcity: Power, poverty and the global water crisis, 2006. doi:10.1016/S1352-0237(02)00387-8.

[4] M.A. Montgomery, M. Elimelech, Water And Sanitation in Developing Countries: Including Health in the Equation, Environ. Sci. Technol. 41 (2007) 17–24. doi:10.1021/es072435t.

[5] U. Caldera, D. Bogdanov, S. Afanasyeva, C. Breyer, Role of Seawater Desalination in the Management of an Integrated Water and 100% Renewable Energy Based Power Sector in Saudi Arabia, Water. 10 (2017) 3. doi:10.3390/w10010003.

[6] A.D. Khawaji, I.K. Kutubkhanah, J.M. Wie, Advances in seawater desalination technologies, Desalination. 221 (2008) 47–69. doi:10.1016/j.desal.2007.01.067.

[7] K.W. Lawson, D.R. Lloyd, Membrane distillation, J. Memb. Sci. (1997) 1–25. doi:10.1016/S0376-7388(96)00236-0.

[8] P. Wang, T.S. Chung, A conceptual demonstration of freeze desalination-membrane distillation (FD-MD) hybrid desalination process utilizing liquefied natural gas (LNG) cold energy, Water Res. 46 (2012) 4037–4052. doi:10.1016/j.watres.2012.04.042.

[9] O.K. Buros, The U.S.A.I.D. Desalination Manual, International Desalination and Environmental Association, 1980.

[10] A. Subramani, J.G. Jacangelo, Emerging desalination technologies for water treatment: A critical review, Water Res. 75 (2015) 164–187. doi:10.1016/j.watres.2015.02.032.

[11] K. nam Park, S.Y. Hong, J.W. Lee, K.C. Kang, Y.C. Lee, M.G. Ha, J.D. Lee, A new apparatus for seawater desalination by gas hydrate process and removal characteristics of dissolved minerals (Na^+, Mg^{2+}, Ca^{2+}, K^+, B^{3+}), Desalination. 274 (2011) 91–96. doi:10.1016/j.desal.2011.01.084.

[12] H. Lee, H. Ryu, J.-H. Lim, J.-O. Kim, J. Dong Lee, S. Kim, An optimal design approach of gas hydrate and reverse osmosis hybrid system for seawater desalination, Desalin. Water Treat. 57 (2016) 9009–9017. doi:10.1080/19443994.2015.1049405.

[13] K.C. Kang, S.Y. Hong, S.J. Cho, D.H. Kim, J.D. Lee, Evaluation of Desalination by Nanostructured Hydrate Formation and Pellet Production Process, J. Nanosci. Nanotechnol. 17 (2017) 4059–4062. doi:10.1166/jnn.2017.13383.

[14] Sloan ED, Koh CA, Clathrate hydrates of natural gases, Third edition. CRC Press, FL: Boca Raton, 2008.

[15] H. Mimachi, S. Takeya, A. Yoneyama, K. Hyodo, T. Takeda, Y. Gotoh, T. Murayama, Natural gas storage and transportation within gas hydrate of smaller particle: Size dependence of self-preservation phenomenon of natural gas hydrate, Chem. Eng. Sci. 118 (2014) 208–213. doi:10.1016/j.ces.2014.07.050.

[16] Z.G. Sun, R. Wang, R. Ma, K. Guo, S. Fan, Natural gas storage in hydrates with the presence of promoters, Energy Convers. Manag. 44 (2003) 2733–2742. doi:10.1016/S0196-8904(03)00048-7.

[17] A. Burnol, I. Thinon, L. Ruffine, J.M. Herri, Influence of impurities (nitrogen and methane) on the CO_2 storage capacity as sediment-hosted gas hydrates - Application in the area of the Celtic

Sea and the Bay of Biscay, Int. J. Greenh. Gas Control. 35 (2015) 96–109. doi:10.1016/j.ijggc.2015.01.018.

[18] H.P. Veluswamy, R. Kumar, P. Linga, Hydrogen storage in clathrate hydrates: Current state of the art and future directions, Appl. Energy. 122 (2014) 112–132. doi:10.1016/j.apenergy.2014.01.063.

[19] N.H. Duc, F. Chauvy, J.M. Herri, CO_2 capture by hydrate crystallization - A potential solution for gas emission of steelmaking industry, Energy Convers. Manag. 48 (2007) 1313–1322. doi:10.1016/j.enconman.2006.09.024.

[20] P.J. Herslund, K. Thomsen, J. Abildskov, N. von Solms, A. Galfré, P. Brântuas, M. Kwaterski, J.M. Herri, Thermodynamic promotion of carbon dioxide-clathrate hydrate formation by tetrahydrofuran, cyclopentane and their mixtures, Int. J. Greenh. Gas Control. 17 (2013) 397–410. doi:10.1016/j.ijggc.2013.05.022.

[21] Z. Taheri, M.R. Shabani, K. Nazari, A. Mehdizaheh, Natural gas transportation and storage by hydrate technology: Iran case study, J. Nat. Gas Sci. Eng. 21 (2014) 846–849. doi:10.1016/j.jngse.2014.09.026.

[22] J.-M. Herri, A. Bouchemoua, M. Kwaterski, P. Brântuas, A. Galfré, B. Bouillot, J. Douzet, Y. Ouabbas, A. Cameirao, Enhanced Selectivity of the Separation of CO_2 from N_2 during Crystallization of Semi-Clathrates from Quaternary Ammonium Solutions, Oil Gas Sci. Technol. – Rev. d'IFP Energies Nouv. 69 (2014) 947–968. doi:10.2516/ogst/2013201.

[23] P. Babu, P. Linga, R. Kumar, P. Englezos, A review of the hydrate based gas separation (HBGS) process forcarbon dioxide pre-combustion capture, Energy. 85 (2015) 261–279. doi:10.1016/j.energy.2015.03.103.

[24] M. Darbouret, M. Cournil, J.M. Herri, Rheological study of TBAB hydrate slurries as secondary two-phase refrigerants, Int. J. Refrig. 28 (2005) 663–671. doi:10.1016/j.ijrefrig.2005.01.002.

[25] J. Douzet, M. Kwaterski, A. Lallemand, F. Chauvy, D. Flick, J.M. Herri, Prototyping of a real size air-conditioning system using a tetra-n-butylammonium bromide semiclathrate hydrate slurry as secondary two-phase refrigerant - Experimental investigations and modelling, Int. J. Refrig. 36 (2013) 1616–1631. doi:10.1016/j.ijrefrig.2013.04.015.

[26] H. Ogoshi, S. Takao, Air-Conditioning System Using Clathrate Hydrate Slurry, JFE Tech. Rep. 3 (2004) 1–5.

[27] H. Fakharian, H. Ganji, A. Naderifar, Desalination of high salinity produced water using natural gas hydrate, J. Taiwan Inst. Chem. Eng. 72 (2017) 157–162. doi:10.1016/j.jtice.2017.01.025.

[28] S. Ho-Van, B. Bouillot, J. Douzet, S. Maghsoodloo, J.-M. Herri, Experimental Measurement and Thermodynamic Modeling of Cyclopentane Hydrates with NaCl, KCl, $CaCl_2$ or NaCl-KCl Present, AIChE. J. 6 (2018) 2207-2218. doi:10.1002/aic.16067.

[29] S.L. Colten, F.S. Lin, T.C. Tsao, S.A. Stern, A.J. Barduhn, Hydrolysis losses in the hydrate desalination process: rate measurements and economic analysis, Desalination. 11 (1972) 31–59. doi:10.1016/S0011-9164(00)84047-3.

[30] J. Sugi, S. Saito, Concentration and demineralization of sea water by the hydrate process, Desalination. 3 (1967) 27–31. doi:10.1016/S0011-9164(00)84021-7.

[31] R.A. McCormack, N.G. A. Build and operate clathrate desalination pilot plant, U.S. Dept. of the Interior, Bureau of Reclamation, 1998.

[32] R.A. McCormack, R.K. Andersen, Clathrate desalination plant preliminary research study, U.S. Dept. of the Interior, Bureau of Reclamation, 1995.

[33] R.W. Bradshaw, D.E. Dedrick, B.A. Simmons, J.A. Great- house, R.T. Cygan, E.H. Majzoub, Desalination Utilizing Clathrate Hydrates, Sandia National Laboratories, California, 2008.

[34] M.D. Max, Hydrate desalination for water purification, US 6991722 B2, 2006.

[35] T. He, S.K. Nair, P. Babu, P. Linga, I.A. Karimi, A novel conceptual design of hydrate based desalination (HyDesal) process by utilizing LNG cold energy, Appl. Energy. 222 (2018) 13–24. doi:10.1016/j.apenergy.2018.04.006.

[36] P. Englezos, The Freeze Concentration Process and its Applications, Dev. Chem. Eng. Miner. Process. 2 (1994) 3–15. doi:10.1002/apj.5500020102.

[37] P. Babu, R. Kumar, P. Linga, Unusual behavior of propane as a co-guest during hydrate formation in silica sand: Potential application to seawater desalination and carbon dioxide capture, Chem. Eng. Sci. 117 (2014) 342–351. doi:10.1016/j.ces.2014.06.044.

[38] A.J. Barduhn, H.E. Towlson, Y.C. Hu, The properties of some new gas hydrates and their use in demineralizing sea water, AIChE J. 8 (1962) 176–183. doi:10.1002/aic.690080210.

[39] L. Cai, B.A. Pethica, P.G. Debenedetti, S. Sundaresan, Formation of cyclopentane methane binary clathrate hydrate in brine solutions, Chem. Eng. Sci. 141 (2016) 125–132. doi:10.1016/j.ces.2015.11.001.

[40] B. Tohidi, A. Danesh, A.C. Todd, R.W. Burgass, K.K. Østergaard, Equilibrium data and thermodynamic modelling of cyclopentane and neopentane hydrates, Fluid Phase Equilib. 138 (1997) 241–250. doi:10.1016/S0378-3812(97)00164-7.

[41] Q.N. Lv, X. Sen Li, Z.Y. Chen, J.C. Feng, Phase equilibrium and dissociation enthalpies for hydrates of various water-insoluble organic promoters with methane, J. Chem. Eng. Data. 58 (2013) 3249–3253. doi:10.1021/je4007025.

[42] D. Corak, T. Barth, S. Høiland, T. Skodvin, R. Larsen, T. Skjetne, Effect of subcooling and amount of hydrate former on formation of cyclopentane hydrates in brine, Desalination. 278 (2011) 268–274. doi:10.1016/j.desal.2011.05.035.

[43] F. Li, Z. Chen, H. Dong, C. Shi, B. Wang, L. Yang, Z. Ling, Promotion e ff ect of graphite on cyclopentane hydrate based desalination, Desalination. 445 (2018) 197–203. doi:10.1016/j.desal.2018.08.011.

[44] S. Hong, S. Moon, Y. Lee, S. Lee, Y. Park, Investigation of thermodynamic and kinetic effects of cyclopentane derivatives on CO2 hydrates for potential application to seawater desalination, Chem. Eng. J. 363 (2019) 99–106. doi:10.1016/j.cej.2019.01.108.

[45] Q. Wang, D. Han, Z. Wang, Q. Ma, D. Wang, D. Wang, Lattice Boltzmann modeling for hydrate formation in brine Dalian University of Technology, Chem. Eng. J. (2019). doi:10.1016/j.cej.2019.02.060.

[46] C. McAuliffe, Solubility in Water of Paraffin, Cycloparaffin, Olefin, Acetylene, Cycloolefin, and Aromatic Hydrocarbons1, J. Phys. Chem. 70 (1966) 1267–1275. doi:DOI: 10.1021/j100876a049.

[47] J. nan Zheng, M. jun Yang, Y. Liu, D. yong Wang, Y. chen Song, Effects of cyclopentane on CO2 hydrate formation and dissociation as a co-guest molecule for desalination, J. Chem. Thermodyn. 104 (2017) 9–15. doi:10.1016/j.jct.2016.09.006.

[48] J. Lee, Y.K. Jin, Y. Seo, Characterization of cyclopentane clathrates with gaseous guests for gas storage and separation, Chem. Eng. J. 338 (2018) 572–578. doi:10.1016/J.CEJ.2018.01.054.

[49] W.L. Zhao, D.L. Zhong, C. Yang, Prediction of phase equilibrium conditions for gas hydrates formed in the presence of cyclopentane or cyclohexane, Fluid Phase Equilib. 427 (2016) 82–89. doi:10.1016/j.fluid.2016.06.044.

[50] D. Jianwei, L. Deqing, L. Dongliang, L. Xinjun, Experimental determination of the equilibrium conditions of binary gas hydrates of cyclopentane + oxygen, cyclopentane + nitrogen, and cyclopentane + hydrogen, Ind. Eng. Chem. Res. 49 (2010) 11797–11800. doi:10.1021/ie101339j.

[51] S. Baek, J. Min, J.W. Lee, Inhibition effects of activated carbon particles on gas hydrate formation at oil–water interfaces, RSC Adv. 5 (2015) 58813–58820. doi:10.1039/C5RA08335D.

[52] Y. Matsumoto, T. Makino, T. Sugahara, K. Ohgaki, Phase equilibrium relations for binary mixed hydrate systems composed of carbon dioxide and cyclopentane derivatives, Fluid Phase Equilib. 362 (2014) 379–382. doi:10.1016/j.fluid.2013.10.057.

[53] P.J. Herslund, N. Daraboina, K. Thomsen, J. Abildskov, N. von Solms, Measuring and modelling of the combined thermodynamic promoting effect of tetrahydrofuran and cyclopentane on carbon dioxide hydrates, Fluid Phase Equilib. 381 (2014) 20–27. doi:10.1016/j.fluid.2014.08.015.

[54] J.N. Zheng, M. Yang, B. Chen, Y. Song, D. Wang, Research on the CO_2Gas Uptake of Different Hydrate Structures with Cyclopentane or Methyl-cyclopentane as Co-guest Molecules, Energy Procedia. 105 (2017) 4133–4139. doi:10.1016/j.egypro.2017.03.877.

[55] Q. Lv, X. Li, Raman Spectroscopic Studies on Microscopic Mechanism of CP - CH_4 Mixture Hydrate, Energy Procedia. 142 (2017) 3264–3269. doi:10.1016/j.egypro.2017.12.501.

[56] A.H. Mohammadi, D. Richon, Phase Equilibria of Clathrate Hydrates of Tetrahydrofuran+Hydrogen Sulfide and Tetrahydroduran+Methane, J. Chem. Eng. Data. 55 (2009) 982–984. doi:10.1021/je9004257.

[57] Palmer, H. A. Characterization of hydrocarbon-type hydrates. Ph.D.Thesis, University of Oklahoma, Norman, OK, 1950.

[58] D.W.Davidson, Clathrate Hydrates, in: F. Franks (Ed.), Water Cryst. Hydrates Aqueous Solut. Simple Nonelectrolytes, 2nd ed., Springer Science+Business Media, New York, 1973.

[59] S.S. Fan, D.Q. Liang, K.H. Guo, Hydrate equilibrium conditions for cyclopentane and a quaternary cyclopentane-rich mixture, J. Chem. Eng. Data. 46 (2001) 930–932. doi:10.1021/je010026l.

[60] M. Nakajima, R. Ohinura, Y.H. Mori, Clathrate hydrate formation from cyclopentane-in-water emulsions, Ind. Eng. Chem. Res. 47 (2008) 8933–8939. doi:10.1021/ie800949k.

[61] C.A. Whitman, R. Mysyk, M.A. White, Investigation of factors affecting crystallization of cyclopentane clathrate hydrate, J. Chem. Phys. 129 (2008). doi:10.1063/1.3005379.

[62] J.W. Nicholas, L.E. Dieker, E.D. Sloan, C.A. Koh, Assessing the feasibility of hydrate deposition on pipeline walls-Adhesion force measurements of clathrate hydrate particles on carbon steel, J. Colloid Interface Sci. 331 (2009) 322–328. doi:10.1016/j.jcis.2008.11.070.

[63] J.S. Zhang, J.W. Lee, Equilibrium of hydrogen + cyclopentane and carbon dioxide + cyclopentane binary hydrates, J. Chem. Eng. Data. 54 (2009) 659–661. doi:10.1021/je800219k.

[64] R. Sakemoto, H. Sakamoto, K. Shiraiwa, R. Ohmura, T. Uchida, Clathrate hydrate crystal growth at the seawater/hydrophobic-guest-liquid interface, Cryst. Growth Des. 10 (2010) 1296–1300. doi:10.1021/cg901334z.

[65] E.G. Dirdal, C. Arulanantham, H. Sefidroodi, M.A. Kelland, Can cyclopentane hydrate formation be used to rank the performance of kinetic hydrate inhibitors?, Chem. Eng. Sci. 82 (2012) 177–184. doi:10.1016/j.ces.2012.07.043.

[66] H. Sefidroodi, E. Abrahamsen, M.A. Kelland, Investigation into the strength and source of the memory effect for cyclopentane hydrate, Chem. Eng. Sci. 87 (2013) 133–140. doi:10.1016/j.ces.2012.10.018.

[67] R. Ambekar, Equilibrium conditions of Hydrate-forming pickering emulsions (M.S. thesis), City University of New York, New York, NY, 2012.

[68] G. Zylyftari, J.W. Lee, J.F. Morris, Salt effects on thermodynamic and rheological properties of hydrate forming emulsions, Chem. Eng. Sci. 95 (2013) 148–160. doi:10.1016/j.ces.2013.02.056.

[69] S. Han, J.Y. Shin, Y.W. Rhee, S.P. Kang, Enhanced efficiency of salt removal from brine for cyclopentane hydrates by washing, centrifuging, and sweating, Desalination. 354 (2014) 17–22. doi:10.1016/j.desal.2014.09.023.

[70] Hongfei Xu. Hydrate Desalination Using Cyclopentane Hydrates At Atmospheric Pressure.

M.S. Thesis, Colorado School of Mines, U.S.A, 2014.

[71] M. Mitarai, M. Kishimoto, D. Suh, R. Ohmura, Surfactant effects on the crystal growth of clathrate hydrate at the interface of water and hydrophobic-guest liquid, Cryst. Growth Des. 15 (2015) 812–821. doi:10.1021/cg501613a.

[72] M.L. Martinez de Baños, O. Carrier, P. Bouriat, D. Broseta, Droplet-based millifluidics as a new tool to investigate hydrate crystallization: Insights into the memory effect, Chem. Eng. Sci. 123 (2015) 564–572. doi:10.1016/j.ces.2014.11.018.

[73] S. Baek, J. Min, J.W. Lee, Equilibria of cyclopentane hydrates with varying HLB numbers of sorbitan monoesters in water-in-oil emulsions, Fluid Phase Equilib. 413 (2016) 41–47. doi:10.1016/j.fluid.2015.10.018.

[74] E.P. Brown, C.A. Koh, Micromechanical measurements of the effect of surfactants on cyclopentane hydrate shell properties., Phys. Chem. Chem. Phys. 18 (2016) 594–600. doi:10.1039/c5cp06071k.

[75] J. Peixinho, V. Ageorges, B. Duchemin, Growth of Clathrate Hydrates from Water Drops in Cyclopentane, Energy & Fuels. (2017) acs.energyfuels.7b02740. doi:10.1021/acs.energyfuels.7b02740.

[76] N. Hobeika, M.L. Martinez De Baños, P. Bouriat, D. Broseta, R. Brown, High-Resolution Optical Microscopy of Gas Hydrates, in: Gas Hydrates 1, 2017: pp. 113–144. doi:10.1002/9781119332688.ch3.

[77] H. Delroisse, J.-P. Torré, C. Dicharry, Effect of a Hydrophilic Cationic Surfactant on Cyclopentane Hydrate Crystal Growth at the Water/Cyclopentane Interface, Cryst. Growth Des. 17 (2017) 5098–5107. doi:10.1021/acs.cgd.7b00241.

[78] H. Delroisse, F. Plantier, L. Marlin, C. Dicharry, L. Frouté, R. André, J. Torré, Determination of thermophysical properties of cyclopentane hydrate using a stirred calorimetric cell, J. Chem. Thermodyn. 125 (2018) 136–141. doi:10.1016/j.jct.2018.05.023.

[79] A. Masoudi, P. Jafari, M. Nazari, V. Kashyap, B. Eslami, P. Irajizad, P. Jafari, M. Nazari, V. Kashyap, B. Eslami, P. Irajizad, An in situ method on kinetics of gas hydrates An in situ method on kinetics of gas hydrates, Rev. Sci. Instrum. 035111 (2019). doi:10.1063/1.5082333.

[80] Z.M. Aman, E.P. Brown, E.D. Sloan, A.K. Sum, C. a. Koh, Interfacial mechanisms governing cyclopentane clathrate hydrate adhesion/cohesion, Phys. Chem. Chem. Phys. 13 (2011) 19796. doi:10.1039/c1cp21907c.

[81] P.U. Karanjkar, J.W. Lee, J.F. Morris, Surfactant Effects on Hydrate Crystallization at the Water–Oil Interface: Hollow-Conical Crystals, Cryst. Growth Des. 12 (2012) 3817–3824. doi:10.1021/cg300255g.

[82] M. Perez, Gibbs-Thomson effects in phase transformations, Scr. Mater. 52 (2005) 709–712. doi:10.1016/j.scriptamat.2004.12.026.

[83] S.-S. Fan, T.-M. Guo, Hydrate Formation of CO_2-Rich Binary and Quaternary Gas Mixtures in

Aqueous Sodium Chloride Solutions, J. Chem. Eng. Data. 44 (1999) 829–832. doi:10.1021/je990011b.

[84] J.P. Mericq, S. Laborie, C. Cabassud, Vacuum membrane distillation of seawater reverse osmosis brines, Water Res. 44 (2010) 5260–5273. doi:10.1016/j.watres.2010.06.052.

[85] T.J. Itsuno, K.H. Amabe, Vacuum Distillation System Aiming to Use Solar-Heat for Desalination, J. Arid L. Stud. 155 (2012) 153–155.

[86] A.T. Trueba, L.J. Rovetto, L.J. Florusse, M.C. Kroon, C.J. Peters, Phase equilibrium measurements of structure II clathrate hydrates of hydrogen with various promoters, Fluid Phase Equilib. 307 (2011) 6–10. doi:10.1016/j.fluid.2011.04.025.

[87] M. Kishimoto, S. Iijima, R. Ohmura, Crystal growth of clathrate hydrate at the interface between seawater and hydrophobic-guest liquid: Effect of elevated salt concentration, Ind. Eng. Chem. Res. 51 (2012) 5224–5229. doi:10.1021/ie202785z.

[88] S. Ho-Van, B. Bouillot, J. Douzet, S. Maghsoodloo Babakhani, J.-M. Herri, Implementing Cyclopentane Hydrates Phase Equilibrium Data and Simulations in Brine Solutions, Ind. Eng. Chem. Res. 57 (2018) 14774 -14783. doi:10.1021/acs.iecr.8b02796.

[89] Sloan D, Koh C, K.Sum A. Natural Gas Hydrate in Flow Assurance. Gulf Professional Pub./Elsevier; 2011.

[90] J.H. Cha, Y. Seol, Increasing gas hydrate formation temperature for desalination of high salinity produced water with secondary guests, ACS Sustain. Chem. Eng. 1 (2013) 1218–1224. doi:10.1021/sc400160u.

[91] Q.N. Lv, X. Sen Li, Z.Y. Chen, Formation of cyclopentane - methane hydrates in brine systems and characteristics of dissolved ions, Appl. Energy. 184 (2016) 482–490. doi:10.1016/j.apenergy.2016.10.035.

[92] Y. Zhang, S.M. Sheng, X.D. Shen, X.B. Zhou, W.Z. Wu, X.P. Wu, D.Q. Liang, Phase Equilibrium of Cyclopentane + Carbon Dioxide Binary Hydrates in Aqueous Sodium Chloride Solutions, J. Chem. Eng. Data. 62 (2017) 2461–2465. doi:10.1021/acs.jced.7b00404.

[93] A.H. Mohammadi, D. Richon, Phase equilibria of clathrate hydrates of methyl cyclopentane, methyl cyclohexane, cyclopentane or cyclohexane+carbon dioxide, Chem. Eng. Sci. 64 (2009) 5319–5322. doi:10.1016/j.ces.2009.09.048.

[94] M. Wang, Z.G. Sun, C.H. Li, A.J. Zhang, J. Li, C.M. Li, H.F. Huang, Equilibrium Hydrate Dissociation Conditions of CO_2+ HCFC141b or Cyclopentane, J. Chem. Eng. Data. 61 (2016) 3250–3253. doi:10.1021/acs.jced.6b00333.

[95] A. Galfré, M. Kwaterski, P. Braîntuas, A. Cameirao, J.M. Herri, Clathrate hydrate equilibrium data for the gas mixture of carbon dioxide and nitrogen in the presence of an emulsion of cyclopentane in water, J. Chem. Eng. Data. 59 (2014) 592–602. doi:10.1021/je4002587.

[96] Z.Y. Chen, Q.P. Li, Z.Y. Yan, K.F. Yan, Z.Y. Zeng, X. Sen Li, Phase equilibrium and dissociation enthalpies for cyclopentane + methane hydrates in NaCl aqueous solutions, J.

Chem. Eng. Data. 55 (2010) 4444–4449. doi:10.1021/je100597e.

[97] Q. Lv, Y. Song, X. Li, Kinetic study on the process of cyclopentane + methane hydrate formation in NaCl solution, Energy & Fuels. 30 (2016) 1310–1316. doi:10.1021/acs.energyfuels.5b02634.

[98] Q. Lv, X. Zang, X. Li, G. Li, Effect of seawater ions on cyclopentane-methane hydrate phase equilibrium, Fluid Phase Equilib. 458 (2018) 272–277. doi:10.1016/j.fluid.2017.11.031.

[99] H. Yang, S. Fan, X. Lang, Y. Wang, X. Sun, Hydrate dissociation conditions for mixtures of air + tetrahydrofuran, air + cyclopentane, and air + tetra-n-butyl ammonium bromide, J. Chem. Eng. Data. 57 (2012) 1226–1230. doi:10.1021/je201330j.

[100] S. Takeya, K. Yasuda, R. Ohmura, Phase equilibrium for structure II hydrates formed with methylfluoride coexisting with cyclopentane, fluorocyclopentane, cyclopentene, or tetrahydropyran, J. Chem. Eng. Data. 53 (2008) 531–534. doi:10.1021/je700624q.

[101] S. Takeya, R. Ohmura, Phase Equilibrium for Structure II Hydrates Formed with Krypton Co-existing with Cyclopentane, Cyclopentene, or Tetrahydropyran, J. Chem. Eng. Data. 51 (2006) 1880–1883. doi:10.1021/je060233r.

[102] S. Imai, K. Okutani, R. Ohmura, Y.H. Mori, Phase Equilibrium for Clathrate Hydrates Formed with Difluoromethane + either Cyclopentane or Tetra- n -butylammonium Bromide, J. Chem. Eng. Data. 50 (2005) 1783–1786. doi:10.1021/je050212h.

[103] H. Komatsu, H. Yoshioka, M. Ota, Phase Equilibrium Measurements of Hydrogen− Tetrahydrofuran and Hydrogen− Cyclopentane Binary Clathrate Hydrate Systems, J. Chem. Eng. Data. (2010) 2214–2218. doi:10.1021/je900767h.

[104] P. Di Profio, V. Canale, R. Germani, S. Arca, A. Fontana, Reverse micelles enhance the formation of clathrate hydrates of hydrogen, J. Colloid Interface Sci. 516 (2018) 224–231. doi:10.1016/j.jcis.2018.01.059.

[105] D.L. Zhong, N. Daraboina, P. Englezos, Recovery of CH4 from coal mine model gas mixture (CH_4/N_2) by hydrate crystallization in the presence of cyclopentane, Fuel. 106 (2013) 425–430. doi:10.1016/j.fuel.2013.01.029.

[106] Q. Lv, L. Li, X. Li, Z. Chen, Clathrate hydrate dissociation conditions and structure of the methane + cyclopentane + trimethylene sulfide hydrate in NaCl aqueous solution, Fluid Phase Equilib. 425 (2016) 305–311. doi:10.1016/j.fluid.2016.06.020.

[107] F. Tzirakis, P. Stringari, N. von Solms, C. Coquelet, G. Kontogeorgis, Hydrate equilibrium data for the CO_2+ N_2 system with the use of tetra-n-butylammonium bromide (TBAB), cyclopentane (CP) and their mixture, Fluid Phase Equilib. 408 (2016) 240–247. doi:10.1016/j.fluid.2015.09.021.

[108] J. Zhang, P. Yedlapalli, J.W. Lee, Thermodynamic analysis of hydrate-based pre-combustion capture of CO_2, Chem. Eng. Sci. 64 (2009) 4732–4736. doi:10.1016/j.ces.2009.04.041.

[109] H. Liu, J. Wang, G. Chen, B. Liu, A. Dandekar, B. Wang, X. Zhang, C. Sun, Q. Ma, High-

efficiency separation of a CO_2/H_2 mixture via hydrate formation in W/O emulsions in the presence of cyclopentane and TBAB, Int. J. Hydrogen Energy. 39 (2014) 7910–7918. doi:10.1016/j.ijhydene.2014.03.094.

[110] S. Li, S. Fan, J. Wang, X. Lang, Y. Wang, Clathrate hydrate capture of CO_2 from simulated flue gas with cyclopentane/water emulsion, Chinese J. Chem. Eng. 18 (2010) 202–206. doi:10.1016/S1004-9541(08)60343-2.

[111] D.L. Zhong, K. Ding, C. Yang, Y. Bian, J. Ji, Phase equilibria of clathrate hydrates formed with $CH_4 + N_2 + O_2$ in the presence of cyclopentane or cyclohexane, J. Chem. Eng. Data. 57 (2012) 3751–3755. doi:10.1021/je301024v.

[112] J.-M. Herri, A. Bouchemoua, M. Kwaterski, A. Fezoua, Y. Ouabbas, A. Cameirao, Gas hydrate equilibria for CO_2–N_2 and CO_2–CH_4 gas mixtures—Experimental studies and thermodynamic modelling, Fluid Phase Equilib. 301 (2011) 171–190. doi:10.1016/j.fluid.2010.09.041.

[113] H. Yang, Z. Xu, M. Fan, R.B. Slimane, A.E. Bland, I. Wright, Progress in carbon dioxide seperation and capture: A review, J. Environ. Sci. 20 (2008) 14–27. doi:10.1016/S1001-0742(08)60002-9.

[114] X. Sen Li, C.G. Xu, Z.Y. Chen, J. Cai, Synergic effect of cyclopentane and tetra-n-butyl ammonium bromide on hydrate-based carbon dioxide separation from fuel gas mixture by measurements of gas uptake and X-ray diffraction patterns, Int. J. Hydrogen Energy. 37 (2012) 720–727. doi:10.1016/j.ijhydene.2011.09.053.

[115] P.J. Herslund, Thermodynamic and Process Modelling of Gas Hydrate Systems in CO_2 Capture Processes, Technical University of Denmark, 2013.

[116] J. Zheng, Z. Bao-yong, Q. Wu, P. Linga, Kinetic evaluation of cyclopentane as a promoter for CO_2 capture via clathrate process employing different contact modes, Sustain. Chem. Eng. (2018). doi:10.1021/acssuschemeng.8b02187.

[117] M. Yang, J. Zheng, W. Liu, Y. Liu, Y. Song, Effects of C3H8 on hydrate formation and dissociation for integrated CO_2 capture and desalination technology, Energy. 93 (2015) 1971–1979. doi:10.1016/j.energy.2015.10.076.

[118] M. Sarshar, a H. Sharafi, Simultaneous water desalination and CO_2 capturing by hydrate formation, Desalin. Water Treat. 28 (2011) 59–64. doi:10.5004/dwt.2011.2201.

[119] Y.-N. Lv, S.-S. Wang, C.-Y. Sun, J. Gong, G.-J. Chen, Desalination by forming hydrate from brine in cyclopentane dispersion system, Desalination. 413 (2017) 217–222. doi:10.1016/j.desal.2017.03.025.

[120] L.C. Ho, P. Babu, R. Kumar, P. Linga, HBGS (hydrate based gas separation) process for carbon dioxide capture employing an unstirred reactor with cyclopentane, Energy. 63 (2013) 252–259. doi:10.1016/j.energy.2013.10.031.

[121] M.L. Martinez de Baños, Mechanisms of formation and dissociation of cyclopentane hydrates, Ph.D.Thesis, Université de Pau et des Pays de l'Adour, 2015.

[122] M. Li, J. Tian, C. Liu, K. Geng, Effects of sorbitan monooleate on the interactions between cyclopentane hydrate particles and water droplets, J. Dispers. Sci. Technol. 39 (2018) 360–366. doi:10.1080/01932691.2017.1318706.

[123] S. Ho-van, B. Bouillot, D. Garcia, J. Douzet, A. Cameirao, S. Maghsoodloo-, Crystallization mechanisms and rates of Cyclopentane Hydrates formation in Brine, Chem. Eng. Technol. (2019) 1–21. doi:10.1002/ceat.201800746.

[124] H. Xu, M.N. Khan, C.J. Peters, E.D. Sloan, A.K. Sum, C.A. Koh, Hydrate Desalination Using Cyclopentane Hydrates At Atmospheric Pressure, in: Proc. 8th Int. Conf. Gas Hydrates, Beijing, China, 2014: pp. 1–7.

[125] L. Cai, B.A. Pethica, P.G. Debenedetti, S. Sundaresan, Formation kinetics of cyclopentane-methane binary clathrate hydrate, Chem. Eng. Sci. 119 (2014) 147–157. doi:10.1016/j.ces.2014.08.025.

[126] Y.A. Lim, P. Babu, R. Kumar, P. Linga, Morphology of carbon dioxide-hydrogen-cyclopentane hydrates with or without sodium dodecyl sulfate, Cryst. Growth Des. 13 (2013) 2047–2059. doi:10.1021/cg400118p.

[127] Q. Lv, L. Li, X. Li, Z. Chen, Formation Kinetics of Cyclopentane + Methane Hydrates in Brine Water Systems and Raman Spectroscopic Analysis, Energy and Fuels. 29 (2015) 6104–6110. doi:10.1021/acs.energyfuels.5b01416.

[128] C.J. Brown, X. Ni, Evaluation of rate of cyclopentane hydrate formation in an oscillatory baffled column using laser induced fluorescence and energy balance, Chem. Eng. J. 157 (2010) 131–139. doi:10.1016/j.cej.2009.11.019.

[129] G. Zylyftari, A. Ahuja, J.F. Morris, Nucleation of cyclopentane hydrate by ice studied by morphology and rheology, Chem. Eng. Sci. 116 (2014) 497–507. doi:10.1016/j.ces.2014.05.019.

[130] P.U. Karanjkar, J.W. Lee, J.F. Morris, Calorimetric investigation of cyclopentane hydrate formation in an emulsion, Chem. Eng. Sci. 68 (2012) 481–491. doi:10.1016/j.ces.2011.10.014.

[131] K. Dann, L. Rosenfeld, J. Accepted, Surfactant effect on hydrate crystallization at oil-water interface, Langmuir. (2018). doi:10.1021/acs.langmuir.8b00333.

[132] C. Lo, J.S. Zhang, a. Couzis, P. Somasundaran, J.W. Lee, Adsorption of Cationic and Anionic Surfactants on Cyclopentane Hydrates, J. Phys. Chem. C. 114 (2010) 13385–13389. doi:10.1021/jp102846d.

[133] C. Lo, J.S. Zhang, P. Somasundaran, S. Lu, a. Couzis, J.W. Lee, Adsorption of Surfactants on Two Different Hydrates, Langmuir. 24 (2008) 12724–12726. doi:10.1021/la802362m.

[134] A. Erfani, F. Varaminian, Kinetic promotion of non-ionic surfactants on cyclopentane hydrate formation, J. Mol. Liq. 221 (2016) 963–971. doi:10.1016/j.molliq.2016.06.058.

[135] Li, Huijuan, Du, Jianwei and Wang, Liguang (2013). Effect of surfactant-coated particles on clathrate hydrate formation. In: Chemeca 2013: Challenging Tomorrow. Chemeca 2013:

Australasian Conference on Chemical Engineering, Brisbane, QLD, Australia, (1-5). 29 September-2 October, 2013.

[136] C. Lo, J. Zhang, P. Somasundaran, J.W. Lee, Raman spectroscopic studies of surfactant effect on the water structure around hydrate guest molecules, J. Phys. Chem. Lett. 1 (2010) 2676–2679. doi:10.1021/jz1009967.

[137] R.Z.J. Wu, Experimental studies of gas hydrate formation, Ph.D.Thesis, The University of Western Australia, 2014.

[138] N. Abojaladi, M.A. Kelland, Can cyclopentane hydrate formation be used to screen the performance of surfactants as LDHI anti-agglomerants at atmospheric pressure?, Chem. Eng. Sci. 152 (2016) 746–753. doi:10.1016/j.ces.2016.06.067.

[139] X. Li, L. Negadi, A. Firoozabadi, Anti-agglomeration in cyclopentane hydrates from bio-and co-surfactants, Energy and Fuels. 24 (2010) 4937–4943. doi:10.1021/ef100622p.

[140] J.S. Zhang, C. Lo, A. Couzis, P. Somasundaran, J. Wu, J.W. Lee, Adsorption of kinetic inhibitors on clathrate hydrates, J. Phys. Chem. C. 113 (2009) 17418–17420. doi:10.1021/jp907796d.

[141] S.A. Morrissy, A.J. McKenzie, B.F. Graham, M.L. Johns, E.F. May, Z.M. Aman, Reduction of Clathrate Hydrate Film Growth Rate by Naturally Occurring Surface Active Components, Energy & Fuels. 31 (2017) 5798–5805. doi:10.1021/acs.energyfuels.6b02942.

[142] R. Ohmura, M. Ogawa, K. Yasuoka, Y.H. Mori, Statistical Study of Clathrate-Hydrate Nucleation in a Water/Hydrochlorofluorocarbon System: Search for the Nature of the "Memory Effect," J. Phys. Chem. B. 107 (2003) 5289–5293. doi:10.1021/jp027094e.

[143] P. Englezos, Clathrate Hydrates., Ind. Eng. Chem. Res. 32 (1993) 1251–1274. doi:10.1021/ie00019a001.

[144] D. Kashchiev, A. Firoozabadi, Induction time in crystallization of gas hydrates, J. Cryst. Growth. 250 (2003) 499–515. doi:10.1016/S0022-0248(02)02461-2.

[145] L.C. Jacobson, W. Hujo, V. Molinero, Nucleation pathways of clathrate hydrates: Effect of guest size and solubility, J. Phys. Chem. B. 114 (2010) 13796–13807. doi:10.1021/jp107269q.

[146] T. Uchida, I.Y. Ikeda, S. Takeya, T. Ebinuma, J. Nagao, H. Narita, CO_2 hydrate film formation at the boundary between CO_2 and water: Effects of temperature, pressure and additives on the formation rate, J. Cryst. Growth. 237–239 (2002) 383–387. doi:10.1016/S0022-0248(01)01822-X.

[147] K. Saito, A.K. Sum, R. Ohmura, Correlation of Hydrate-Film Growth Rate at the Guest / Liquid-Water Interface to Mass Transfer Resistance, Society. 7 (2010) 7102–7103. doi:Doi 10.3390/En5010092.

[148] K. Saito, M. Kishimoto, R. Tanaka, R. Ohmura, Crystal growth of clathrate hydrate at the interface between hydrocarbon gas mixture and liquid water, Cryst. Growth Des. 11 (2011) 295–301. doi:10.1021/cg101310z.

[149] E.M. Freer, M.S. Selim, E.D.S. Jr, Methane hydrate film growth kinetics, Fluid Phase Equilib. 185 (2001) 65–75. doi: 10.1016/S0378-3812(01)00457-5.

[150] B.Z. Peng, A. Dandekar, C.Y. Sun, H. Luo, Q.L. Ma, W.X. Pang, G.J. Chen, Hydrate film growth on the surface of a gas bubble suspended in water, J. Phys. Chem. B. 111 (2007) 12485–12493. doi:10.1021/jp074606m.

[151] C.J. Taylor, K.T. Miller, C.A. Koh, E.D. Sloan, Macroscopic investigation of hydrate film growth at the hydrocarbon/water interface, Chem. Eng. Sci. 62 (2007) 6524–6533. doi:10.1016/j.ces.2007.07.038.

[152] M. Karamoddin, F. Varaminian, Water purification by freezing and gas hydrate processes, and removal of dissolved minerals (Na^+, K^+, Mg^{2+}, Ca^{2+}), J. Mol. Liq. 223 (2016) 1021–1031. doi:10.1016/j.molliq.2016.08.099.

[153] S.R. Davies, J.W. Lachance, E.D. Sloan, C.A. Koh, High-Pressure Differential Scanning Calorimetry Measurements of the Mass Subcooling, Industrial & Engineering Chemistry Research. 49 (2010) 12319–12326. doi: 10.1021/ie1017173

[154] S. Takeya, A. Hori, T. Hondoh, T. Uchida, Freezing-memory effect of water on nucleation of CO_2 hydrate crystals, J. Phys. Chem. B. 104 (2000) 4164–4168. doi:10.1021/jp993759+.

[155] J.S. PARENT, P. BISHNOI, Investigations Into the Nucleation Behaviour of Methane Gas Hydrates, Chem. Eng. Commun. 144 (1996) 51–64. doi:10.1080/00986449608936444.

[156] C. Duchateau, C. Dicharry, J.-L. Peytavy, P. Glénat, T.-E. Pou, M. Hidalgo, Laboratory Evaluation of Kinetic Hydrate Inhibitors : a New Procedure for Improving the Reproducibility of Measurements, Icgh2008. 23 (2008) 962–966.

[157] C. Duchateau, P. Glénat, T.E. Pou, M. Hidalgo, C. Dicharry, Hydrate precursor test method for the laboratory evaluation of kinetic hydrate inhibitors, Energy and Fuels. 24 (2010) 616–623. doi:10.1021/ef900797e.

[158] L. Jensen, K. Thomsen, N. Von Solms, Inhibition of structure I and II gas hydrates using synthetic and biological kinetic inhibitors, Energy and Fuels. 25 (2011) 17–23. doi:10.1021/ef100833n.

[159] M. a Kelland, History of the Development of Low Dosage Hydrate Inhibitors, Energy Fuels. 20 (2006) 825–847. doi:10.1021/ef050427x.

[160] Y. Xie, K. Guo, D. Liang, S. Fan, J. Gu, J. Chen, Gas hydrate fast nucleation from melting ice and quiescent growth along vertical heat transfer tube, Sci. China Ser. B Chem. 48 (2005) 75–82. doi:10.1007/BF02990916.

[161] E.D. Sloan, F. Fleyfel, A Molecular Mechanism for Gas Hydrate Nucleation from Ice, AIChE J. 37 (1991) 1281–1292. doi:10.1002/aic.690370902

[162] M. Rahmati-abkenar, M. Manteghian, H. Pahlavanzadeh, Nucleation of ethane hydrate in water containing silver nanoparticles, Mater. Des. 126 (2017) 190–196. doi:10.1016/j.matdes.2017.04.051.

[163] S. Abedi-farizhendi, M. Rahmati-abkenar, M. Manteghian, J.S. Yekshaveh, V. Zahmatkeshan, Kinetic study of propane hydrate in the presence of carbon nanostructures and SDS, J. Pet. Sci. Eng. 172 (2019) 636–642. doi:10.1016/j.petrol.2018.04.075.

[164] O. Nashed, B. Partoon, B. Lal, K.M. Sabil, A. Mohd, Review the impact of nanoparticles on the thermodynamics and kinetics of gas hydrate formation, 55 (2018) 452–465. doi:10.1016/j.jngse.2018.05.022.

[165] S. Said, V. Govindaraj, J. Herri, Y. Ouabbas, A study on the influence of nanofluids on gas hydrate formation kinetics and their potential: Applicatin to the CO_2 capture process, J. Nat. Gas Sci. Eng. 32 (2016) 95–108. doi:10.1016/j.jngse.2016.04.003.

[166] C.Y. Lo, The role of surface active agents on hydrate formation. Ph.D.Thesis, The City University of New York, 2011.

[167] A.N. Nesterov, A.M. Reshetnikov, A.Y. Manakov, T. V. Rodionova, E.A. Paukshtis, I.P. Asanov, S.P. Bardakhanov, A.I. Bulavchenko, Promotion and inhibition of gas hydrate formation by oxide powders, J. Mol. Liq. 204 (2015) 118–125. doi:10.1016/j.molliq.2015.01.037.

[168] B. Zarenezhad, Accurate prediction of the interfacial tension of surfactant/fluid mixtures during gas hydrate nucleation: The case of SDS surfactant-based systems near ethylene hydrate formation region, J. Mol. Liq. 191 (2014) 161–165. doi:10.1016/j.molliq.2013.12.005.

[169] Z.M. Aman, K. Olcott, K. Pfeiffer, E.D. Sloan, A.K. Sum, C.A. Koh, Surfactant adsorption and interfacial tension investigations on cyclopentane hydrate, Langmuir. 29 (2013) 2676–2682. doi:10.1021/la3048714.

[170] Z.M. Aman, C.A. Koh, Interfacial phenomena in gas hydrate systems, Chem. Soc. Rev. 45 (2016) 1678–1690. doi:10.1039/C5CS00791G.

[171] BMH Abdulkader, Cyclopentane Hydrate for Hydrate Wetting Studies, M.S. Thesis, University of Bergen, 2013.

[172] A. Ahuja, G. Zylyftari, J.F. Morris, Yield stress measurements of cyclopentane hydrate slurry, J. Nonnewton. Fluid Mech. 220 (2015) 116–125. doi:10.1016/j.jnnfm.2014.11.007.

[173] G. Zylyftari, A. Ahuja, J.F. Morris, Modeling Oilfield Emulsions: Comparison of Cyclopentane Hydrate and Ice, Energy and Fuels. 29 (2015) 6286–6295. doi:10.1021/acs.energyfuels.5b01431.

[174] H. Delroisse, G. Barreto, J. Torré, C. Dicharry, Evaluation of the Performance of a New Biodegradable AA-LDHI in Cyclopentane Hydrate and CH_4/C_3H_8 Gas Hydrate Systems, in: SPE Middle East Oil Gas Show Conf., Manama, 2019: pp. 1–13. doi:10.2118/195054-MS.

[175] G. Aspenes, L.E. Dieker, Z.M. Aman, S. Høiland, A.K. Sum, C.A. Koh, E.D. Sloan, Adhesion force between cyclopentane hydrates and solid surface materials, J. Colloid Interface Sci. 343 (2010) 529–536. doi:10.1016/j.jcis.2009.11.071.

[176] Z.M. Aman, L.E. Dieker, G. Aspenes, A.K. Sum, E.D. Sloan, C.A. Koh, Influence of model oil

with surfactants and amphiphilic polymers on cyclopentane hydrate adhesion forces, Energy and Fuels. 24 (2010) 5441–5445. doi:10.1021/ef100762r.

[177] Z. Aman, J.L. William, G. Grasso, E.D. Sloan, A.K. Sum, C.A. Koh, Adhesion Force between Cyclopentane Hydrate and Mineral Surfaces, Langmuir. 29 (2013) 15551–15557. doi:dx.doi.org/10.1021/la403489q.

[178] L.E. Dieker, C.J. Taylor, C.A. Koh, D. Sloan, Micromechanical adhesion force measurements between cyclopentane hydrate particles, Conf. Gas Hydrates. (2011) 2011. doi:http://dx.doi.org/10.1016/j.jcis.2006.10.078.

[179] Zachary M. Aman, Luis E. Zerpa, Giovanny Grasso, William E. Leith, E. Dendy Sloan, Amadeu K. Sum, and Carolyn A. Koh, Interfacial Tension and Mineral Adhesion Properties of Cyclopentane Hydrate. Unconventional Resources Technology Conference, Denver, Colorado, 12-14 August 2013: pp. 2265-2268. doi:10.1190/urtec2013-235.

[180] A. Das, T.A. Farnham, S. Bengaluru Subramanyam, K.K. Varanasi, Designing Ultra-Low Hydrate Adhesion Surfaces by Interfacial Spreading of Water-Immiscible Barrier Films, ACS Appl. Mater. Interfaces. 9 (2017) 21496–21502. doi:10.1021/acsami.7b00223.

[181] Z.M. Aman, S.E. Joshi, E.D. Sloan, A.K. Sum, C.A. Koh, Micromechanical cohesion force measurements to determine cyclopentane hydrate interfacial properties, J. Colloid Interface Sci. 376 (2012) 283–288. doi:10.1016/j.jcis.2012.03.019.

[182] E. Brown, M.N. Khan, D. Salmin, J. Wells, S. Wang, C.J. Peters, C.A. Koh, Cyclopentane hydrate cohesion measurements and phase equilibrium predictions, J. Nat. Gas Sci. Eng. 35 (2016) 1435–1440. doi:10.1016/j.jngse.2016.05.016.

[183] P.U. Karanjkar, A. Ahuja, G. Zylyftari, J.W. Lee, J. F. Morris, Rheology of cyclopentane hydrate slurry in a model oil-continuous emulsion, Rheol. Acta. 55 (2016) 235–243. doi:10.1007/s00397-016-0911-1.

[184] B.C. Leopercio, Kinetics of cyclopentane hydrate formation - an interfacial rheology study, M.S. Thesis, Pontifical Catholic University of Rio de Janeiro, PUC-Rio, Brazil. 2016.

[185] A. Ahuja, G. Zylyftari, J.F. Morris, Calorimetric and rheological studies on cyclopentane hydrate-forming water-in-kerosene emulsions, J. Chem. Eng. Data. 60 (2015) 362–368. doi:10.1021/je500609q.

[186] T. He, Z.R. Chong, P. Babu, P. Linga, Techno-economic Evaluation of Cyclopentane Hydrate-Based Desalination with LNG Cold Energy Utilization, Energy Technol. (2019). doi:10.1002/ente.201900212.

[187] Y. Zhang, P.G. Debenedetti, R.K. Prud, B.A. Pethica, Differential Scanning Calorimetry Studies of Clathrate Hydrate Formation, Water. 108 (2004) 16717–16722. doi:10.1021/jp047421d.

[188] L. CAI, Desalination via formation of binary clathrate hydrates, Ph.D.Thesis 2013. Princeton University. USA.

[189] A.C. Archer, A.M. Mendes, R.A. Boaventura, Separation of an Anionic Surfactant by Nanofiltration, Environ. Sci. Technol. 33 (1999) 2758–2764. doi: 10.1021/es980737c.

[190] M. Zahoor, Separation of surfactants from water by granular activated carbon/ultrafiltration hybrid process, Desalin. Water Treat. 3994 (2016). doi:10.1080/19443994.2014.979242.

[191] P. Taylor, J. Kaleta, M. Elektorowicz, The removal of anionic surfactants from water in coagulation process, Env. Technol. (2012) 37–41. doi:10.1080/09593330.2012.733415.

[192] E. Onder, An alternative method for the removal of surfactants from water : Electrochemical coagulation, Sep. Purif. Technol. 52 (2007) 527–532. doi:10.1016/j.seppur.2006.06.006.

[193] J. Sima, M. Havelka, V. Holcova, Removal of Anionic Surfactants from Wastewater Using a Constructed Wetland, Chem. Biodivers. 6 (2009) 1350–1363. doi:10.1002/cbdv.200900108.

[194] A. Arora, S.S. Cameotra, R. Kumar, C. Balomajumder, Biosurfactant as a Promoter of Methane Hydrate Formation : Thermodynamic and Kinetic Studies, Sci. Rep. (2016) 1–13. doi:10.1038/srep20893.

[195] R.E. Rogers, C. Kothapalli, M.S. Lee, J.R. Woolsey, Catalysis of Gas Hydrates by Biosurfactants in Seawater-Saturated Sand/Clay, Can. J. Chem. Eng. 81 (2003) 973–980. doi:10.1002/cjce.5450810508.

[196] S. Han, Y.W. Rhee, S.P. Kang, Investigation of salt removal using cyclopentane hydrate formation and washing treatment for seawater desalination, Desalination. 404 (2017) 132–137. doi:10.1016/j.desal.2016.11.016.

[197] H. Xu, M.N. Khan, C.J. Peters, E.D. Sloan, C.A. Koh, Hydrate-Based Desalination Using Cyclopentane Hydrates at Atmospheric Pressure, J. Chem. Eng. Data. (2018) acs.jced.7b00815. doi:10.1021/acs.jced.7b00815.

[198] B. Mottet, Method for treating an aqueous solution containing dissolved materials by crystallization of clathrates hydrates, US20170044024A1, 2017.

[199] A.G. Ogienko, A.Y. Manakov, A. V Kurnosov, E. V Grachev, E.G. Larionov, Direct measurement of stoichiometry of the structure H argon gas hydrate synthesized at high pressure, J. Struct. Chem. 46 (2005) 65–69. doi:10.1007/s10947-006-0153-7.

[200] A. Al-Karaghouli, L.L. Kazmerski, Energy consumption and water production cost of conventional and renewable-energy-powered desalination processes, Renew. Sustain. Energy Rev. 24 (2013) 343–356. doi:10.1016/j.rser.2012.12.064.

[201] M. Mahdavi, A.H. Mahvi, S. Nasseri, M. Yunesian, Application of Freezing to the Desalination of Saline Water, Arab. J. Sci. Eng. 36 (2011) 1171–1177. doi:10.1007/s13369-011-0115-z.

[202] M. Ameri, S.S. Mohammadi, M. Hosseini, M. Seifi, Effect of design parameters on multi-effect desalinationsystem specifications, Desalination. 245 (2009) 266–283. doi:10.1016/j.desal.2008.07.012.

[203] J. Imbrogno, J.J. Keating, J. Kilduff, G. Belfort, Critical aspects of RO desalination: A combination strategy, Desalination. 401 (2017) 68–87. doi:10.1016/j.desal.2016.06.033.

[204] K.C. Ng, K. Thu, Y. Kim, A. Chakraborty, G. Amy, Adsorption desalination: An emerging low-cost thermal desalination method, Desalination. 308 (2013) 161–179. doi:10.1016/j.desal.2012.07.030.

[205] M. Elimelech, W.A. Phillip, The Future of Seawater and the Environment: Energy, Technology, and the Environment, Science (80-.). 333 (2011) 712–718. doi:10.1126/science.1200488.

[206] M. Park, N. Park, H. Park, B. Kim, An economic analysis of desalination for potential applicaiton in Korea, Desalination. 114 (1997) 209–221. doi:10.1016/S0011-9164(98)00013-7

[207] K. THU, Adorption desalination: Theory & Experiments, Ph.D.Thesis, National University of Singapore, 2010.

[208] S.A. Kalogirou, Seawater desalination using renewable energy sources, Prog. Energy Combust. Sci. 31 (2005) 242–281. doi:10.1016/j.pecs.2005.03.001.

[209] M.A. Shannon, P.W. Bohn, M. Elimelech, J.G. Georgiadis, B.J. Marĩas, A.M. Mayes, Science and technology for water purification in the coming decades, Nature. 452 (2008) 301–310. doi:10.1038/nature06599.

[210] P.G. Youssef, R.K. Al-Dadah, S.M. Mahmoud, Comparative analysis of desalination technologies, Energy Procedia. 61 (2014) 2604–2607. doi:10.1016/j.egypro.2014.12.258.

[211] J. Javanmardi, M. Moshfeghian, Energy consumption and economic evaluation of water desalination by hydrate phenomenon, Appl. Therm. Eng. 23 (2003) 845–857. doi:10.1016/S1359-4311(03)00023-1.

[212] M. Sangwai, J. S., Patel, R. S., Mekala, P., Mech, D., & Busch, Desalination of Seawater Using Gas Hydrate Technology–Current Status and Future Direction, 18th Conf. Hydraul. Water Resiources, Coast. Environ. Eng. (2013) 434–440.

[213] H. Fakharian, H. Ganji, A. Naderifar, Saline Produced Water Treatment Using Gas Hydrates, J. Environ. Chem. Eng. (2017). doi:10.1016/j.jece.2017.08.008.

[214] P.S. Goh, T. Matsuura, A.F. Ismail, N. Hilal, Recent trends in membranes and membrane processes for desalination, Desalination. 391 (2016) 43–60. doi:10.1016/j.desal.2015.12.016.

[215] Edition, F. (2008). Guidelines for drinking-water quality. WHO Chronicle, 1(3), 334–415.

[216] H.T. El-Dessouky, H.M. Ettouney, Fundamentals of salt water desalination, Elsevier, 2002.

[217] I.C. Karagiannis, P.G. Soldatos, Water desalination cost literature : review and assessment, Desalination. 223 (2008) 448–456. doi:10.1016/j.desal.2007.02.071.

[218] C.S. Bandi, R. Uppaluri, A. Kumar, Global optimization of MSF seawater desalination processes, Desalination. 394 (2016) 30–43. doi:10.1016/j.desal.2016.04.012.

[219] P.M. Williams, M. Ahmad, B.S. Connolly, D.L. Oatley-Radcliffe, Technology for freeze concentration in the desalination industry, Desalination. 356 (2015) 314–327. doi:10.1016/j.desal.2014.10.023.

[220] M.S. Rahman, M. Ahmed, X.D. Chen, Freezing-melting process and desalination: I. review of

the state-of-the-art, Sep. Purif. Rev. 35 (2006) 59–96. doi:10.1080/15422110600671734.

[221] A. Alkaisi, R. Mossad, A. Sharifian-Barforoush, A Review of the Water Desalination Systems Integrated with Renewable Energy, Energy Procedia. 110 (2017) 268–274. doi:10.1016/j.egypro.2017.03.138.

[222] J. Hu, Y. Chen, L. Guo, X. Chen, Chemical-free ion exchange and its application for desalination, Desalination. 365 (2015) 144–150. doi:10.1016/j.desal.2015.02.033.

[223] Z.R. Chong, T. He, P. Babu, J. Zheng, P. Linga, Economic evaluation of energy e ffi cient hydrate based desalination utilizing cold energy from lique fi ed natural gas (LNG), Desalination. 463 (2019) 69–80. doi:10.1016/j.desal.2019.04.015.

[224] B.B. Buchanan, Removing salt from sea water, US3027320A, 1962.

[225] M. Karamoddin, F. Varaminian, Water desalination using R141b gas hydrate formation, Desalin. Water Treat. 52 (2014) 2450–2456. doi:10.1080/19443994.2013.798840.

[226] B.O. Bolaji, Z. Huan, Ozone depletion and global warming: Case for the use of natural refrigerant - A review, Renew. Sustain. Energy Rev. 18 (2013) 49–54. doi:10.1016/j.rser.2012.10.008.

[227] T. He, Z. Rong, J. Zheng, Y. Ju, P. Linga, LNG cold energy utilization : Prospects and challenges, Energy. 170 (2019) 557–568. doi:10.1016/j.energy.2018.12.170.

[228] A. Nambiar, P. Babu, Improved Kinetics and Water Recovery with Propane as Co-Guest Gas on the Hydrate-Based Desalination (HyDesal) Process, Chemengineering. (2019). doi:10.3390/chemengineering3010031.

[229] P. Babu, A. Nambiar, T. He, A Review of Clathrate Hydrate Based Desalination to Strengthen Energy-Water Nexus, ACS Sustain. Chem. Eng. (2018). doi:10.1021/acssuschemeng.8b01616.

[230] G.K. Anderson, Enthalpy of dissociation and hydration number of carbon dioxide hydrate from the Clapeyron equation, J. Chem. Thermodyn. 35 (2003) 1171–1183. doi:10.1016/S0021-9614(03)00093-4.

[231] Q. Nasir, K.K. Lau, B. Lal, Enthalpies of Dissociation of Pure Methane and Carbon Dioxide Gas Hydrate, Int. J. Chem. Nucl. Metall. Mater. Eng. 8 (2014) 785–788.

[232] C.F.S. Lirio, F.L.P. Pessoa, Enthalpy of dissociation of simple and mixed carbon dioxide clathrate hydrate, Chem. Eng. Trans. 32 (2013) 577–582. doi:10.3303/CET1332097.

[233] Compositions, enthalpies of dissociation, and heat capacities in the range 85 to 270 K for clathrate hydrates of methane, ethane, and propane, and enthalpy of dissociation of isobutane hydrate, as determined by a heat-flow calorimeter, J. Chem. Thermodyn. 18 (1986) 915–921. doi:10.1016/0021-9614(86)90149-7.

[234] Y. Bi, T. Guo, T. Zhu, S. Fan, D. Liang, L. Zhang, Influence of volumetric-flow rate in the crystallizer on the gas-hydrate cool-storage process in a new gas-hydrate cool-storage system, Appl. Energy. 78 (2004) 111–121. doi:10.1016/j.apenergy.2003.08.003.

6.2. Paper II: Experimental Measurement and Thermodynamic Modeling of Cyclopentane Hydrates with NaCl, KCl, $CaCl_2$, or NaCl-KCl Present

S.Ho-Van, B.Bouillot, J.Douzet, S. Maghsoodloo Babakhani, J.M.Herri

Published in: AIChE journal, Volume: 64, Issue: 6, Pages: 2207-2218, First published: 28 December 2017.

Summary: Obviously, in order to design a CPH based desalting plant, accurate phase equilibrium data of CPH in brine are crucial. However, experimental equilibrium data and thermodynamic simulation tools are completely limited in the open literature. Therefore, in this contribution we proposed a method to produce numerous consistent equilibrium data for CPH in the presence of NaCl, KCl, $CaCl_2$, or equi-weight mixture of NaCl-KCl under a wide range of salt concentrations. Moreover, we developed three thermodynamic models to simulate the equilibrium. The first is based on the standard freezing point depression equation. The two others are based on van der Waals and Platteuw model. While the second utilizes optimized Kihara parameters from this work, the third uses an innovative correlation between the occupancy factor and water activity. All three methods have a good capability to predict CPH formation temperatures in brine. The new correlation between occupancy factor and water activity is the most recommended simulation tool to achieve quick, consistent, and accurate dissociation temperature of CPH in brine.

Experimental Measurement and Thermodynamic Modeling of Cyclopentane Hydrates with NaCl, KCl, $CaCl_2$, or NaCl-KCl Present

S. Ho-Van
SPIN Center, Ecole Nationale Supérieure des Mines de Saint-Etienne, 42023 Saint-Étienne, France

Oil Refinery and Petrochemistry Department, Hanoi University of Mining and Geology, Duc Thang, Bac Tu Liem, Hanoi, Vietnam

B. Bouillot, J. Douzet, S. Maghsoodloo Babakhani, and J. M. Herri
SPIN Center, Ecole Nationale Supérieure des Mines de Saint-Etienne, 42023 Saint-Étienne, France

DOI 10.1002/aic.16067
Published online January 14, 2018 in Wiley Online Library (wileyonlinelibrary.com)

Consistent phase equilibrium data for cyclopentane hydrates in presence of salts are vitally important to many industries, with particular interest to the field of hydrate-based water separation via cyclopentane hydrate crystallization such as desalination. However, there are very little experimental equilibrium data, and no thermodynamic prediction tools. Hence, we set up a method to generate a great deal of much needed equilibrium data for cyclopentane hydrates in diverse saline solutions with a wide range of salt concentrations. Our method does furnish verified, reliable and accurate equilibrium data. Plus, three thermodynamic approaches are developed to predict equilibrium, and provide tools for simulations, by considering the kind of salt and concentrations. All three models are in very good accordance with experimental data. One method, using a new correlation between occupancy factor and water activity, might be the best way to obtain consistent, quick, and accurate dissociation temperatures of cyclopentane hydrate in brine. © 2018 American Institute of Chemical Engineers *AIChE J*, 64: 2207–2218, 2018
Keywords: cyclopentane hydrates, equilibrium, experimental, modeling, salts

Introduction

Clathrate hydrates, henceforth termed hydrates, are crystalline solids composed of water and guest molecules.[1] They are cage-like structures, formed by hydrogen-bonded water molecules that enclose different guest molecules. Guest compounds can be small molecules, such as CO_2, H_2, CH_4, C_2H_6, N_2 or relatively large molecules such as Neohexane, Tetrahydrofuran (THF), Tetra-n-butyl ammonium bromide (TBAB), or cyclopentane (CP). There are three different standard polymorphic structures, well described in the literature: Structure I, Structure II, and Structure H.[1]

Hydrates have been widely studied the past decades. Indeed, their formation is a common nuisance in the oil and gas industry.[2,3] Nevertheless, there are many new and potentially profitable applications such as natural gas storage,[4–6] hydrogen storage,[7] carbon dioxide capture,[8–10] gas separation,[2,11] and air-conditioning, and cold thermal energy.[12–14]

Like any crystallization process, hydrate formation can be used as a separation technique. It can separate guest molecules, as well as remove water from an aqueous solution, or even water vapor. Consequently, better understanding, controlling, and or modifying the hydrate crystallization process may prove to be crucial for desalination processes,[15–18] solute separation or purification,[19] metal recovery,[20] or even wastewater treatment.[21] Moreover, some authors have suggested to use CP as large guest molecules for the hydrate-based separation process. Indeed, CP is a promising candidate. As it is not miscible with water, hence it is easily recovered. In addition, as it crystallizes with pure water at about 7°C at atmospheric pressure, no special high-pressure equipment is necessary.[1,22]

Most of the time, these novel techniques involve electrolytes, which are natural hydrate inhibitors, in the aqueous medium. However, even if gas hydrate formation from seawater in deep sea ocean sediments, or in pipelines, has been studied widely in the past, to the best of our knowledge there are very few applicable publications on CPH in presence of salts (and in absence of gas).

Among the relevant articles on CPH in brine, the works of Kishimoto et al.[23] (morphology of CPH in presence of NaCl), Zylyftari et al.[24] (rheological and thermodynamic influences of NaCl on CPH), Corak et al.[25] (effect of subcooling and amount of hydrate former on formation of CPH in brine), Han et al.[15] (efficiency of salt removal from brine by CPH using three secondary treatment methods: washing, centrifuging, and sweating), Lv et al.[26] (desalination by forming hydrate

Additional Supporting Information may be found in the online version of this article.

Correspondence concerning this article should be addressed to S. Ho-Van at son.ho-van@emse.fr or B. Bouillot at bouillot@emse.fr.

Table 1. Purity of Initial Material Used.

Material	Chemical Formula	Mol. Weight (g mol^{-1})	Solubility in Water (g/L)	Purity
Cyclopentane	C_5H_{10}	70.1	0.156 (25°C)[27]	98.0%
Sodium chloride	NaCl	58.4	360 (20°C)[28]	99.5%
Potassium chloride	KCl	74.55	344 (20°C)[28]	99.0%
Calcium chloride	$CaCl_2$	110.978	745 (20°C)[28]	99.0%

from brine in CP dispersion systems) should be mentioned. Unfortunately, while Nakajima et al.[22] determined the heat of dissociation, as well as the equilibrium temperature of CPH formed from a mixture of CP-in-water emulsions, no salts were used.

Considering the limited available data, the first objective of this study is to provide new experimental results in presence of electrolytes. Three salts were considered, with a wide range of concentrations: NaCl (0–23% mass), KCl (0–20% mass), an equimass mixture of NaCl-KCl (0–22% mass), and $CaCl_2$ (0–25% mass). Two procedures, quick and slow, were applied in this study. The aim of the quick procedure is to provide an initial estimate of the equilibrium temperatures. Then, the slow procedure obtains more accurate data.

Second, three thermodynamic modeling approaches are presented to determine CPH equilibrium temperatures in presence of salt with accuracy. Thank to this, simple methods can subsequently be used to model water separation processes via CPH in salty water.

Experimental Section

Chemicals

All chemicals were supplied by Sigma-Aldrich (see details and purity in Table 1). Ultrapure water is provided by Milli-Q® Advantage A10 Water Purification System. This system can produce water with a conductivity $\sigma \leq 0.055$ μS.cm^{-1} and TOC (total organic carbon content) less than 5 ppm.

Apparatus

The experimental apparatus is presented in Figure 1. The reactor is a jacketed batch glass vessel (1) provided by Verre Equipments (France) with an approximate volume of one liter.

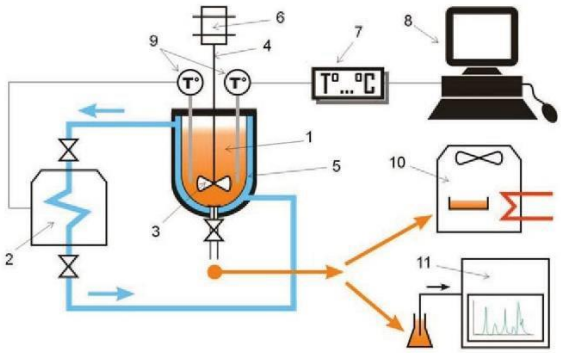

Figure 1. Simplified schematic of the main experimental apparatus.1-Vessel, 2-Chiller, 3-Impeller, 4-Agitator, 5-Cooling jacket, 6-Motor, 7-Temp transmitter, 8-Computer, 9-Temperature probe, 10-Drying oven, 11-Ion chromatography.

[Color figure can be viewed at wileyonlinelibrary.com]

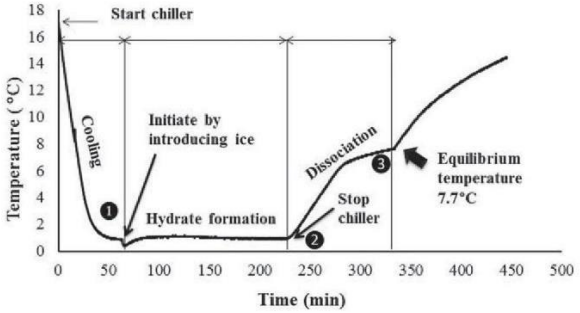

Figure 2. Temperature profile in hydrate formation and dissociation in pure water following the quick procedure.

The vessel is equipped with a double jacket to constantly and uniformly controls the temperature of the solution using a chiller (2). This chiller, Ministat 240, supplied by Huber, has an operating temperature range of (–45°C to 200°C) with a temperature stability of ±0.02°C. The coolant of the chiller is a solution of water and ethylene glycol (44% mass fraction).

The impeller (3) inside the vessel is powered by a motor (6) to mix the injected solution. The temperature of the aqueous mixture is monitored by two temperature probes (one for the coolant system, another for the acquisition system). The data are transferred to a computer thanks to a transmitter (7). LabVIEW is employed to observe and record the digital information throughout the course of experiments.

A drying oven (Binder) (10) and an ion chromatography (Dionex DX-500 IC) system (11) are also used to measure salt concentration of the liquid samples taken at the end of the hydrate dissociation process.

Quick dissociation procedure

The objective is to provide a quick approximation of the total dissociation temperature. This can be described as follows:

For each experiment, a solution containing 500 g of deionized water and a certain quantity of salt based on desired salt concentration is mixed for 10 min. The solution is then introduced into the vessel, followed by 114.38 g of CP according to a theoretical stoichiometric composition for CPH (the molar ratio of water:CP is supposed to be 17:1).[1]

The solution is agitated continuously throughout the course of experiment at a rate of 300–400 rpm to increase heat and mass transfer rates. To cooling down the solution, the chiller is started at a set-point above the freezing-point of the salt solution to ensure that no ice is present in solution. When the temperature of solution reaches a value close to the set-point, hydrate formation is initiated by introducing approximately 3 g of ice (made previously from deionized water), and an appropriate quantity of salt to keep salt concentration of the solution constant (point (1) on Figure 2). Seeding directly with CPH is also an option. Visual observations are also performed by both direct observation and a camera. After approximately 1 to 2 h, when a sufficient amount of CPH has formed, the chiller is stopped (point (2) on Figure 2). CPH then dissociates due to ambience heat-transfer. When the CPH has dissociated completely, there is a sharp increase of temperature (point (3) on Figure 2). This point corresponds presumably to the equilibrium temperature at the initial salt concentration. This equilibrium temperature is recorded for all the experiments.

Mixing is stopped to separate the aqueous solution with the CP solution (above). Then, two samples, 1 and 5 mL, of the salt solution are taken at the bottom of the vessel to measure salt concentration by both ion chromatography and drying oven. The objective of this step is to validate the accuracy of the equilibrium temperature recorded. If the initial salt concentration (before the experiment) and the final salt concentration (at the end of the hydrate dissociation process) are identical, then this shows that all CPH have dissociated. Therefore, the recorded temperature either corresponds to the equilibrium temperature or is slightly above the equilibrium temperature. Hence, the uncertainty on the equilibrium temperature can be significant, from 0.3 to 3.6 K (see in the result section). This vagueness can be resolved by the use of a longer slow dissociation procedure.

Note that, $CaCl_2$ will form salt hydrates after water evaporation. Indeed, after drying $CaCl_2$ salt solution at 60°C (set temperature of drying oven for all experiments), both $CaCl_2.2H_2O$ and $CaCl_2.H_2O$ are obtained instead of pure solid $CaCl_2$ as desired. Therefore, the drying oven is not employed with $CaCl_2$.

Slow dissociation procedure

Following each experiment with the quick procedure, an identical experiment is conducted but with the slow procedure. The aim is to provide more accurate data, based on the estimation obtained from the previous procedure.

The slow procedure is very similar to the quick procedure, but the dissociation method is different since the chiller is never stopped. Plus, the hydrate dissociation process is controlled differently as follow:

After a sufficient quantity of hydrate is formed, the chiller is controlled manually according to this temperature program: the temperature inside the vessel is increased at an increment of 0.1°C instead of being heating by its surroundings. The temperature is then kept constant for at least 1 hour. If there is still a significant amount of CPH after 1 h, the temperature is increased. Of course, stirring is used and kept constant at 300–400 rpm to make sure that the system is homogeneous in terms of concentration and temperature. This process is iterated until a few hydrate particles remain in the reactor. Then, temperature is increased of 0.1°C, and is preserved for a longer time (half a day up to a day) to make sure that equilibrium is reached. If there are still crystals inside the vessel, this last step is repeated. The phase equilibrium of CPH is supposed to be observed during penultimate step just before the final one as all three phases (CP, CPH, and aqueous) exist, and its temperature is the equilibrium temperature of CPH within 0.1°C uncertainty.

To detect the presence of hydrate particles, images of the solution are taken at every step through a small window by a camera. The images are analyzed and compared in order to determine the final step in which only two transparent phases of salt solution and CP can be observed as seen in the initial condition.

Moreover, to make sure that there are no CPH anymore in the bulk at the final step of the procedure, two samples of 1 and 5 mL are also taken from the bottom of the vessel. These samples are used to compare the initial (before cooling) and the final (dissociation point) salt concentrations. Analysis are performed through ion chromatography (1 mL sample) and drying oven (5 mL sample).

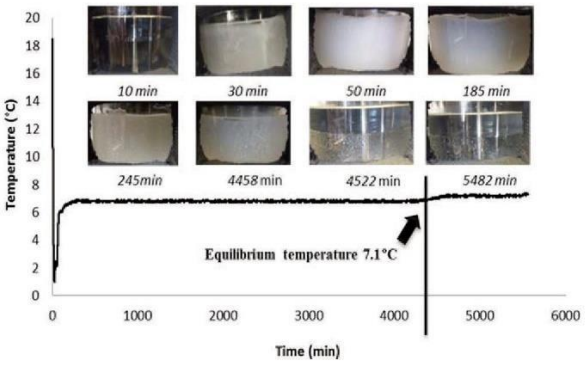

Figure 3. Temperature profile in hydrate formation and dissociation in pure water following the slow procedure.

[Color figure can be viewed at wileyonlinelibrary.com]

At last, we did an uncertainty analysis (see Supporting Information appendix). Temperature uncertainty is 0.1 K, while the uncertainty on the salts concentration is about: 0.002% mass due to weighing; 0.2% mass due to drying oven; and 0.015% mass due to ion chromatography. Figure 3 shows the slow procedure and the visual observation for each temperature step.

Experimental Results

Comparison of two procedures in pure water

The temperature profiles in CPH formation and dissociation in pure water following the quick and the slow procedures are detailed in the Figures 2 and 3. The horizontal axis indicates the time-lapse in minute throughout the course of experiment. That the temperature decreased rapidly at the beginning due to the cooling by the chiller is confirmed in Figure 2. After introducing ice (point 1), hydrates formed, which led to a small increase of temperature as a result of the exothermic nature of crystallization. A significant increase in the quantity of hydrate was then observed.

After stopping the chiller (point 2), the temperature increased quickly due to heat-transfer from the surroundings. The temperature then remained nearly stable when hydrate dissociated intensively because of the endothermic nature of this process. Theoretically, during this period, the temperature should remain constant. The unexpected nonconstant temperature dissociation can be explained only by nonequilibrium dissociation: the heat-transfer rate from the surrounding to the liquid phase is higher than the heat-transfer rate from the liquid to the hydrate crystals.

When the hydrate could no longer be observed inside the vessel, the temperature increased suddenly because of heat-transfer from the environment (point 3). The equilibrium temperature was recorded simultaneously at 7.7°C.

In comparison with literature, this value is totally identical to the data published by Dendy Sloan et al.,[1] Dirdal et al.,[29] Sefidroodi et al.,[30] Davidson et al.[31] and Palmer,[32] while Han et al.[15] reported a small different value of 7.8°C. This comparison indicates that this value is popular in the community of researchers and can probably be considered as a benchmark for the equilibrium condition of CPH. However, quick dissociation entails a risk of missing the accurate equilibrium

temperature due to the high rate of dissociation. Notwithstanding, this method provides a first valuable estimate.

Figure 3 shows the same temperature history compared to the quick procedure during the period from the cooling to hydrate formation. This time, 30 min after hydrate formation, the temperature was increased firstly up to 6°C, near the equilibrium temperature estimated from the quick procedure (7.7°C). It was then increased stepwise and was remained constant at least within 1 h. The dissociation process therefore took a relatively long time (nearly 4 days). Indeed, this typical behavior is expected in the slow procedure as the equilibrium temperatures were then determined accurately based on this behavior.

Both direct observation and a camera to take photos are used at each interval of dissociation process. In order to observe clearly any change, the solution, the mixing rate was decreased down to approximately 120 rpm at the time of taking photos. It can be plainly discerned from Figure 3 that in the cooling process, the solution was clear due to the absence of hydrate crystals (*image at 10 min*). By contrast, it became turbid (or cloudy) when hydrate formed because of the presence of suspended small-crystals of hydrate in the solution which were invisible to the naked eye (*image at 30 min*). Then color became more and more white and opaque due to the formation of more hydrate (*image at 50 min*). The color of solution was cloudy again when hydrate dissociated (*image at 185 min*). The turbidity of the aqueous solution including hydrate crystals and salt solution changed throughout the time with a gradual increase of the temperature. The solution was clearer after each step with an increment of 0.1°C/h due to the dissociation of hydrate crystals (*images at 4458 and 4522 min*). At the final step, the phases were totally clear without any turbidity (*image at 5482 min*) and the equilibrium temperature was recorded of 7.1°C.

Obviously, the value of the equilibrium temperature provided by slow dissociation procedure was less than the value given by the quick dissociation procedure. Of course, a quick dissociation procedure will presumably miss the total dissociation temperature. In comparison with literature, the equilibrium temperature in pure water following the slow procedure from our study, 7.1°C, is very close to the value of 7.11°C reported by Zylyftari et al.[24] and 6.6°C, 6.8°C, 7.1°C reported by Masahiro et al.[22] using the Differential Scanning Calorimetry method (hereafter abbreviated as DSC), and the value of 7.07°C for the quadruple point (liquid water-liquid CP-vapor CP- hydrate) reported by Fan et al.[33] based on the "pressure search" procedure.[34] The DSC method has been also used in the studies of Baek et al.,[35] Whitman et al.[36] and Zhang et al.[37] Baek et al.[35] reported that the equilibrium temperature has the values from approximately 6.7°C to 7.2°C in the presence of Sorbian monoester surfactant (HLB 4.3 to 8.6); Whitman et al.[36] indicated the melting temperature of CPH at 7°C, while Zhang et al.[37] showed this value to be 7.02°C.

From this comparison, it can be seen that the slow procedure provides data that is the same or very close to the data determined by the accurate DSC method in the literature.[22,24,35–37] In fact, the DSC method requires more complex devices and more steps to measure the heat of melting and the melting point. There is also the very real difficulty in transferring the hydrate sample from the reactor to the test cell due to the dissociation of hydrate at room temperature. The slow dissociation procedure has simple principles and is easy to perform without the need of complex devices. Therefore, the slow procedure is a promising and consistent method to determine the equilibrium temperature of CPH in brine.

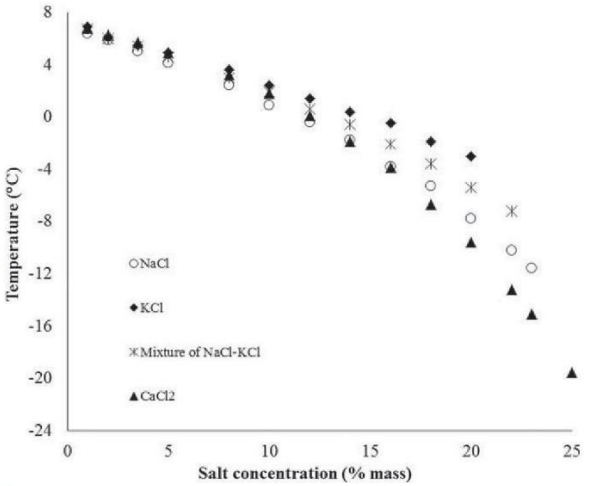

Figure 4. Equilibrium temperature of CPH in the presence of salts from experiments (slow procedure).

Equilibrium temperatures in the presence of salts

Results of measured equilibrium temperatures of CPH in presence of salts are offered in Figure 4 and Table 2. The literature data reported by Zylyftari et al.[24] and Kishimoto et al.[23] are also listed in Table 2 in order to compare them with our measured data.

It is clear from Figure 4 that the equilibrium temperatures drop significantly with an increase in salt concentration. This demonstrates that salt affects strongly phase equilibria. Actually, salt molecules act as inhibitors like glycols or alcohols to hydrate formation.[1] The salt ionizes in water and interacts with the dipoles of the water molecules with a greater Coulombic bond than both the hydrogen bond and the van der Waals forces that cause clustering around the apolar solute molecule, preventing the water inclusion into the hydrate structures. This is the same phenomenon in principle as the lowering of the freezing-point of pure water when salt is added. Conversely, the presence of salt causes a reduction in the solubility of CP in water, a phenomenon known as "salting-out." Both ion clustering and salting-out lead a shift in equilibrium temperatures to lower values.[1,3]

There is a slight temperature difference between the quick and the slow procedures for all salts as detailed in Table 2. The equilibrium temperatures following the slow dissociation are systematically lower than those following the quick procedure at the same concentrations. Again, as in the case of pure water with the quick procedure, the "equilibrium temperature" is recorded slightly late and hence is higher than actual because of the different in heat-transfer rates between solution and hydrate crystals. While, the solution temperature reaches equilibrium, the temperature inside hydrate crystals is still less than this value. Therefore, the hydrate needs a longer time to homogenize temperature and then to dissociate in the bulk solution.

In comparison with literature, Table 2 verifies that at 5%, 10%, 20%, and 23% of NaCl, the equilibrium temperatures in our experiments following the slow procedure have almost the same values reported by Zylyftari et al.[24] and Kishimoto

Table 2. Equilibrium Dissociation Temperatures[a] of CPH in the Presence of NaCl, KCl, an Equiweight Mixture of NaCl-KCl and $CaCl_2$.

Salinity[bcd] (% mass)	$T_{e\text{-quick}}$ in NaCl (°C)	$T_{e\text{-slow}}$ in NaCl (°C)	T_e in NaCl (°C)[24]	T_e in NaCl (°C)[23]	$T_{e\text{-quick}}$ in KCl (°C)	$T_{e\text{-slow}}$ in KCl (°C)	$T_{e\text{-quick}}$ in NaCl-KCl (°C)	$T_{e\text{-slow}}$ in NaCl-KCl (°C)	$T_{e\text{-quick}}$ in $CaCl_2$ (°C)	$T_{e\text{-slow}}$ in $CaCl_2$, (°C)
0 (pure water)	7.7	7.1	7.11	–	7.7	7.1	7.7	7.1	7.7	7.1
1	6.9	6.4	–	–	7.2	6.9	7	6.7	7.1	6
2	6.3	5.9	–	–	6.6	6.1	6.5	6.0	6.8	6.3
3.5	5.7	5	–	–	6	5.5	5.9	5.4	6.2	5.6
5	4.9	4.1	–	4.45	5.4	4.9	5.1	4.6	5.5	4.9
8	3.5	2.4	–	–	4.2	3.6	3.6	3.0	3.9	3.3
10	2	0.9	1.16	1.25	3.6	2.4	2.4	1.9	2.5	1.8
12	0.9	−0.4	–	–	2.3	1.4	1.5	0.6	1.5	0.1
14	−1	−1.8	–	–	1.2	0.4	−0.2	−0.6	−1.0	−1.9
16	−2.7	−3.8	–	–	0.6	−0.5	−1.2	−2.1	−2.7	−4
18	−5	−5.3	–	–	−1	−1.9	−3	−3.6	−5.5	−6.7
20	−7.2	−7.8	−8.00	–	−2.1	−3	−4.6	−5.4	−8.1	−9.6
22	−9.7	−10.2	–	–	–	–	−6.1	−7.2	−12.0	−13.2
23	−11	−11.6	−11.66	–	–	–	–	–	−13.0	−15.1
25	–	–	–	–	–	–	–	–	−16.0	−19.6

where $T_{e\text{-quick}}$ and $T_{e\text{-slow}}$ are the equilibrium temperatures following the quick and the slow procedures.
[a]Uncertainty of the temperature measurements: ±0.1 K.
[b]Uncertainty due to weighing: ±0.002% mass.
[c]Uncertainty due to drying oven: ±0.2% mass.
[d]Relative uncertainty due to ion chromatography: 1.5%, see the Supporting Information appendix.

et al.[23] in which both the very accurate DSC method and low dissociation rate method were applied, respectively. In the study of Kishimoto and his coworkers, the equilibrium temperature was considered as the final dissociation point. The temperature of solution was increased stepwise 0.1°C/h and then was kept steady at least for one hour to observe the dissociation process of hydrate. The equilibrium temperature was considered reached and recorded once hydrate was no longer visible.

Moreover, notice that in Table 2 all the equilibrium temperatures in presence of NaCl are lower than those with either KCl or a mixture of NaCl-KCl. Whilst $CaCl_2$ shows the greatest impact on the equilibria at concentrations from and above 16%. Indeed, NaCl and $CaCl_2$ have a significant influence on the water activity, and hence on the equilibrium temperature.

The accuracy of the equilibrium measurements depends on initial and final salt concentrations. If these two amounts are almost equal (all hydrate crystals have dissociated), then hypothetically, the results are valuable and accurate. Our results indicate that for all the experiments, the initial and the final salt concentrations are approximately identical.

Modelling CPH thermodynamic equilibrium

Three different thermodynamic approaches were used to model phase equilibria of CPH in presence of salts. The first approach (no. 1) is based on Hildebrand and Scott's equation[38] and the two others (no. 2 and no. 3) on van der Waals and Platteuw model.[39]

Each method establishes the equilibrium state by equalizing the chemical potential of water in liquid and hydrate phases

$$\mu_w^L = \mu_w^H \tag{1}$$

where μ_w^L and μ_w^H are the chemical potentials of water in liquid and CPH phase, respectively.

Approach no. 1

Water activity in salt solution with the presence of CPH is expressed from the freezing point depression using Hildebrand and Scott's equation which is usually applied for modeling solid–liquid equilibria of a pure solute in a solvent. The standard equation is expressed as follows

$$\ln a_w = \frac{\Delta H_{fm}}{R}\frac{(T_f - T)}{T_f T} + \frac{\Delta C_{fm}}{R}\left[\frac{(T_f - T)}{T} - \ln\left(\frac{T_f}{T}\right)\right] \tag{2}$$

where T_f is the fusion temperature in K, ΔH_{fm} is the molar enthalpy of fusion in J/mole, ΔC_{fm} is the change of molar specific heat between the subcooled liquid and the solid in J/mole K, and a_w is the water activity. Actually, this is a standard method to predict freezing of pure water in the presence of salts.[40,41] In this case, the solid phase is just ice, and there are no other molecules involved in crystallization.

Let us consider in our approach that water crystallizes alone in the form of CPH (structure II hydrate). CP molecule is "neglected'' as its chemical potential will not be considered. It is a complete separate phase. Indeed, CP is not very soluble in water. Its influence on the equilibrium will be included (hidden) in the values of ΔH_{fm}, T_f, and ΔC_{fm}. Moreover, CP's influence on water activity is negligible (molar solubility less than 4.10^{-4}), especially in presence of electrolytes, and CP can be considered as a limiting reactant, in contact with the aqueous phase. Of course, this means that the used reference state for Eq. 2 is the equilibrium between CPH and its dissociated form (pure liquid water) and CP molecules in stoichiometric proportions according the following reaction

$$C_5H_{10} + 17H_2O = C_5H_{10}.17H_2O \ (\text{CPH}) \tag{3}$$

The fusion temperature of CPH was determined from our experiments, and literature (279.95K).[22] ΔHm_f was acquired from Nakajima et al.[22] and Zhang et al.[42] (we chose the value of 283.9 kJ/kg hydrate reported by Nakajima et al.[22] because it is more accurate), and R is the well-known gas constant. Only ΔCm_f is unknown. As we work at a temperature close to T_f, we concluded that ΔCm_f could not be neglected because the results would not be accurate. Hence, this work, a correlation for $\Delta Cm_f(T)$ was established using our experimental data from NaCl-water mixture (only). The geochemical model PHREEQC[43] provided water activity in salt solution with the PITZER database.

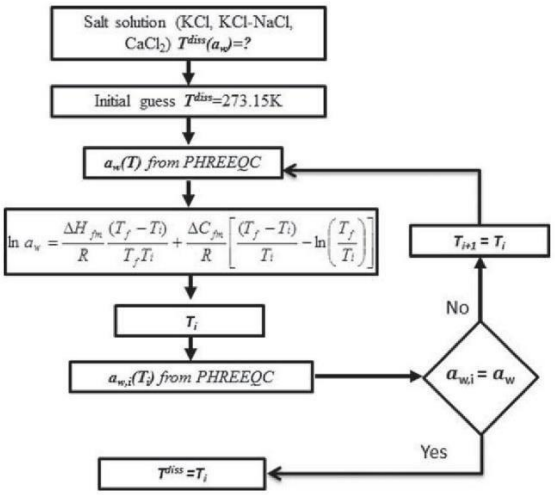

Figure 5. The algorithm of equilibrium temperature calculation in the approach no. 1.

The equilibrium temperatures of CPH in salts are then calculated using both Eq. 2 and the new correlation $\Delta Cm_f(T)$. Water activity is temperature-dependent and needs to be calculated at the onset. The value of water activity in the presence of salts at 273.15 K is first used in Eq. 2. At each following step, after predicting the equilibrium temperature, PHREEQC recalculates the new water activity via the predicted-equilibrium temperatures. This new water activity is then used to repredict the equilibrium temperature. The calculation is iterated until PHREEQC provides the same value of water activity as at the penultimate step. The final predicted-equilibrium temperature is then recorded. The procedure to predict the equilibrium temperatures is illustrated in Figure 5.

The absolute average deviation (AAD) is defined as follows

$$AAD=\frac{1}{N}\sum_{i=1}^{N}|T_{i,pred}-T_{i,\exp}| \tag{4}$$

where N is the number of experimental data points, $T_{i,\text{pred}}$ (K) is the predicted-equilibrium temperature, and $T_{i,\text{exp}}$ (K) is the experimental equilibrium temperature.

Note that Hu et al. (2017) succeeded in using a quite similar equation to correlate suppression temperature of gas hydrate in single salt inhibited system, although they neglect ΔC_p, and provide an equation for $\Delta T/T_0T$ (ΔT being the suppression temperature, T and T_0 being the equilibrium temperature with and without inhibitor, respectively).[44]

Approach no. 2

The CPH equilibrium is described by van der Waals and Platteuw model.[39] This method is based on classic thermodynamics for the water liquid phase and statistical thermodynamics for hydrate phase with the following assumptions:

Each cavity encloses at most one guest molecule.

The interaction between guest molecule and the cavity can be described by a pair potential function of the pair guest-molecule.

Cavities are perfectly sphere-shaped.

Guest molecules do not deform cavities.

There is no interaction between the guest molecules in different cavities.

In the thermodynamic equilibrium, the equality of chemical potential of water in the hydrate phase and liquid phase can be written by introducing references states. For the hydrate, the reference state is a hypothetical phase β written by the van der Waals and Platteuw model corresponding to the empty cavities

$$\Delta\mu_w^{\beta-H}=\Delta\mu_w^{\beta-L} \tag{5}$$

where $\Delta\mu_w^{\beta-H}$ and $\Delta\mu_w^{\beta-L}$ are the differences of the chemical potentials between water in the reference phase (β) and water in the hydrate or liquid phase, respectively.

While $\Delta\mu_w^{\beta-L}$ can be expressed using the Gibbs-Duhem equation,[45] $\Delta\mu_w^{\beta-H}$ is calculated from statistical Thermodynamics, from van der Waals and Platteuw method

$$\Delta\mu_w^{\beta-H}=-RT\sum_i v_i\ln\left(1-\sum_j\theta_j^i\right) \tag{6}$$

where R is the universal constant, T is the absolute temperature, v_i is the number of type i cavities per water molecule in the hydrate (8/136 for CPH), and θ_j^i is the occupancy factor ($\theta_j^i\in$ [0, 1]) of the cavities of type i by the guest molecule j (the guest molecule here is CP). θ_j^i can be written by the Langmuir adsorption model and is expressed as follows

$$\theta_j^i=\frac{C_j^i f_j(T,P)}{1+\sum_j C_j^i f_j(T,P)} \tag{7}$$

where f_j is the fugacity of the guest j (CP). C_j^i is the Langmuir constant of guest j in cavity i. It is usual to obtain C_j^i from the integration of the Kihara interaction potential as follows

$$C_j^i=\frac{4\pi}{kT}\int_0^{R-a}\exp\left(\frac{-w(r)}{kT}\right)r^2dr \tag{8}$$

where k is the Boltzmann constant, r is the distance from the center of the cavity, R is the empty cavity radius, $w(r)$ is the interaction potential between the cavity and the guest molecule, and $\mathfrak{a}$ is the core radius defined in the Kihara potential. The interaction potential $w(r)$ is determined by the Parrish and Prausnitz model[46] and can be expressed as follows

$$w(r)=2z\varepsilon\left[\frac{\sigma^{12}}{R^{11}r}\left(\delta^{10}+\frac{a}{R}\delta^{11}\right)-\frac{\sigma^6}{R^5r}\left(\delta^4+\frac{a}{R}\delta^5\right)\right] \tag{9}$$

$$\delta^N=\frac{1}{N}\left[\left(1-\frac{r}{R}-\frac{a}{R}\right)^{-N}-\left(1+\frac{r}{R}-\frac{a}{R}\right)^{-N}\right] \tag{10}$$

Parameters ε, σ, $\mathfrak{a}$ are so-called Kihara parameters. ε corresponds to the maximum attractive potential and σ is the distance between the cores at zero potential energy. They can be calculated from experimental data by fitting the model equations to correspond the equilibrium experimental one.[10,47–50] In this description, the interaction potential is dependent on only the properties of guest molecule (via Kihara parameters), and geometrical properties of the cavities (via the coordination number z and radius R).

In the end, both chemical potentials are function of the temperature and the salt concentration. Conversely, the liquid part, the pressure is atmospheric, and does not affect the equilibrium significantly. Only the temperature and the water activity (hence the salt concentration) are the major variables. Of course, property parameters are needed. We worked with the parameters from Handa and Tse[51] after verifying they correspond the best.[45]

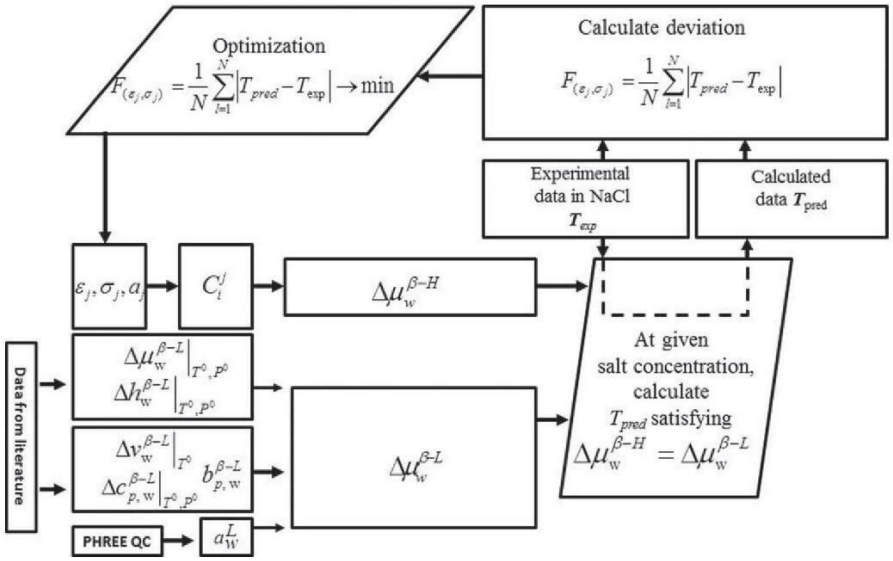

Figure 6. Procedure to optimize the Kihara parameters.

Conversely, the hydrate potential is a function of the CP fugacity, as the Kihara parameters are constant for a given guest. CP fugacity should be the same in all phases: liquid, hydrate, and vapor. As liquid CP can be considered as a pure phase (very low solubility of water in CP), fugacity was calculated from its vapor pressure. Therefore, a standard Antoine's equation was used, assuming that $f_{CP} = P_{CP}^{sat}$ (f_{CP} and P_{CP}^{sat} being the fugacity and the saturated pressure of CP, respectively). This fugacity is only temperature dependent.

The calculation of the temperature from a given salt concentration, or the opposite, can be obtained from the van der Waals equation. But first, we needed to get the Kihara parameters of CP molecule. A deviation function between the predicted-temperatures and the experimental ones was used to obtain epsilon (ε) and sigma (σ)

$$F_{(\varepsilon_j,\sigma_j)} = \frac{1}{N}\sum_{l=1}^{N}|T_{\text{pred}} - T_{\text{exp}}| \rightarrow \min \tag{11}$$

The procedure to optimize the Kihara parameters is presented in Figure 6.[45] The calculation can determine a set of Kihara parameters ε, σ, and a which provide the smallest $F_{(\varepsilon_j,\sigma_j)}$.

The value of a was determined based on the method described by Tee et al.[52] The values of $\Delta\mu_w^{L-\beta}|_{T^0,P^0}$, $\Delta h_w^{L-\beta}|_{T^0,P^0}$, $b_{p,w}^{L-\beta}$, $\Delta C_{p,w}^{L-\beta}|_{T^0,P^0}$, and $\Delta v_w^{L-\beta}|_{T0}$ can be found in the literature detailed in Tables 3 and 4 as cited by Sloan.[1,53]

As clarified on the Figure 6, at the first step of the optimization, for a given set of Kihara parameters ε_j, σ_j and a given experimental temperature in NaCl (conforming to a given salt concentration or water activity, a_w^L), we calculated the interaction potential $w(r)$ in Eq. 9, the Langmuir constant C_j^i in Eq. 8, and then $\Delta\mu_w^{\beta-H}$ in Eq. 6. The predicted-equilibrium temperature T_{pred} at a given salt concentration corresponds to the value at which $\Delta\mu_w^{\beta-H} = \Delta\mu_w^{\beta-L}$.

Table 3. Parameters used for the Hydrate-Phase and Ice (for Hydrate Structure II only).

$\Delta\mu_w^{\beta-L}\|_{T^0,p0}$(J mol)	$\Delta h_w^{\beta-I}\|_{T^0,P0}$(J mol)	Citation
1068	764	Handa and Tse[51]

The second step selects the Kihara parameters to fit with the experimental data in NaCl. In this optimization, σ is ranged from 2 to 4 (Å), while $\frac{\varepsilon}{k}$ is ranged from 200 to 300 K.

Approach no. 3

The third approach is similar to the second one (no. 2) in principle, however, Kihara parameters were not used. The main drawback of using these parameters is to provide accurate values that other authors could work with. Unfortunately, the difference in each code usually leads to differing simulation results.[45] So, we suggest modeling only the occupancy of CP in the hydrate cavities (θ). We chose to correlate the occupancy factor to the water activity, $\theta = F(a_w)$. This approach is not rigorous as occupancy factor is of course dependent on the guest molecule. However, we managed to obtain a correlation that fits well the experimental results considering only water activity. Therefore, CP influence on hydrate chemical potential is hidden in the correlation parameters.

Equations 5 and 6, and experimental data were used to obtain an adequate correlation. PHREEQC provided the water activity required to calculate, as before.

Finally, the occupancy factor can be expressed as a function of the water activity as follows

$$\theta = F(a_w) = m \times (a_w^2) + n \times (a_w) + p \tag{12}$$

where m, n, and p are the empirical constants depending on the experimental data chosen for the correlation in Eq. 12. The

Table 4. Reference Properties of Hydrate from Sloan[1,53] (for Hydrate Structure II only).

Parameters	Unit	Value
$\Delta h_w^{\beta-L}\|_{T^0,P^0}$ [a]	J mol^{-1}	$\Delta\mu_w^{l-\beta}\|_{T^0,P^0}$_6011
$\Delta C_{p,w}^{\beta-L}\|_{T^0,P^0}$	J $mol^{-1}.K^{-1}$	−38.12
$b_{p,w}^{\beta-L}$	J $mol^{-1}.K^{-2}$	0.141
$\Delta v_w^{\beta-L}\|_{T0}$	$10^{-6}m^3$ mol^{-1}	4.99644

[a] $\Delta h_w^{\beta-L}|_{T^0,P^0} = \Delta\mu_w^{\beta-I}|_{T^0,P^0}$−6011, where 6011 is the enthalpy of ice (J mol^{-1}).

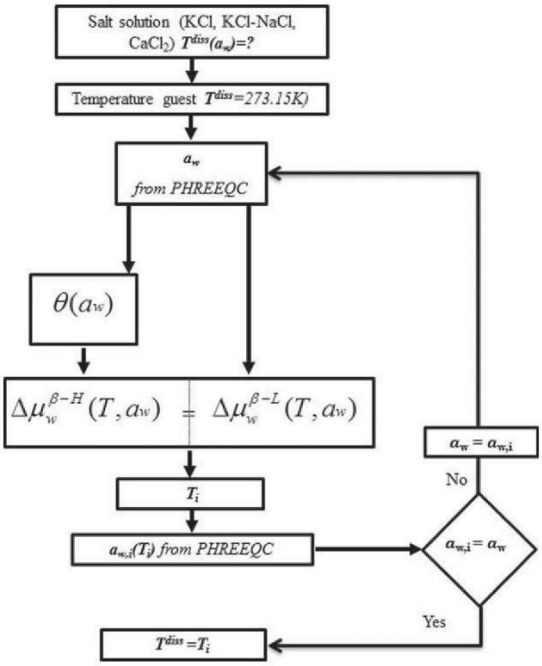

Figure 7. Procedure to predict the equilibrium temperatures using the correlation $\theta = F(a_w)$.

procedure to predict the equilibrium temperature is detailed in Figure 7.

Only data in the presence of NaCl was used at first to get the empirical parameters. Then, the method was applied to other systems, with other salts (KCl, a mixture of NaCl-KCl and $CaCl_2$). As mentioned in the first approach, as the water activity is temperature-dependent, the value of water activity at 273.15 K is used at the first step. Subsequently, PHREEQC provides the water activity at each following step. The predicted-equilibrium temperature is recorded once PHREEQC provides the same value of water activity as at the penultimate step.

Modeling Results

Approach no. 1

Using the experimental data of CPH in the presence of NaCl following the slow dissociation, the correlation for ΔCm_f was expressed as follow

$$\Delta C_{mf} = F(T) = a \times \exp(b \times T) \quad (13)$$

As stated previously, this term cannot be neglected since we work at a temperature close to the pure CPH dissociation temperature. If we ignored ΔCm_f, then any simulations would be significantly less accurate, when compared to experiments.

Figure 8 presents the experimental and predicted dissociation temperatures following the approach no. 1. Correlation coefficients are also included. Absolute average deviations were in NaCl: 0.3K, KCl: 0.3K, a mixture of NaCl-KCl: 0.2K, and $CaCl_2$: 0.4K. This indicates that the phase equilibrium temperature conditions are well reproduced using the new correlation $\Delta Cm_f(T)$ for CPH not only in the presence of NaCl but also in the presence of KCl, and a mixture of NaCl-KCl.

In the case of $CaCl_2$, at low concentrations from 1% to 18%, the predicted data are very close to the experimental results. However, at concentrations from 20% to above, there is a relatively considerable gap between the predicted and experimental data. The mean absolute difference at these high concentrations is approximately 0.9 K compared to a value of 0.2 K at the lower concentrations. This unexpected dissimilarity is probably due to the equilibrium temperature at high concentrations of $CaCl_2$ is out of range of the equilibrium data in the presence of NaCl used to discover the new correlation $\Delta Cm_f(T)$.

Approach no. 2

Three Kihara parameters of CP have been determined. They are the spherical nucleus radius a, the distance between the molecule and the cavity wall at null potential σ, and the maximum attraction potential ε. The value of a was determined based on the second virial coefficient of CP based on the method described by Tee *el al.*[52] The remaining two Kihara parameters (epsilon and sigma) were optimized by minimizing the absolute average deviation between the predicted and measured equilibrium temperatures of CPH in the presence of NaCl. Figure 9 presents average deviation between the equilibrium and predicted temperature as a function of σ and ε/k. A huge range of σ and ε/k were tested to optimize the best set of Kihara parameters for CP.

As clarified on the Figure 9, when the value of σ is less than 2.4 or more than 3.6 regardless the value of ε/k_b (k_b being the Boltzmann constant), the average deviation is enormous. Hence, the Kihara parameters of CP can be found in the two valleys of Figure 9.

To be clearer, the two valleys of Figure 9 have been presented in Figure 10 in only two dimensions. For a chosen value of σ between 2 and 4 (with an increment of 0.002), different values of ε/k_b from 200 to 300 (with an increment of 0.1) were tested and the best values which provide the smallest deviation are plotted. The Figure 10 illustrates that the average deviation is close to zero where the value of σ belongs to either a range from 2.46 to 2.81 corresponding to the value of ε/k_b between 263.5 and 300 or a range from 3.0 to 3.56 corresponding to the value of ε/k_b between 237 and 300. From these ranges of σ and ε/k_b, we chose among the best set of

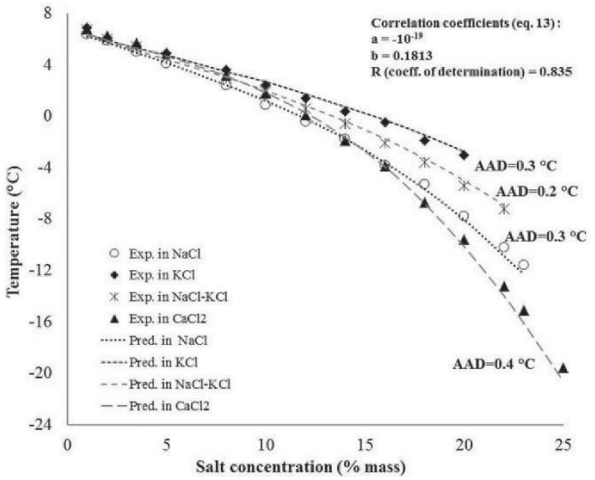

Figure 8. Experimental and predicted dissociation temperature of CPH in the presence of salts, and correlation coefficients for approach no. 1 from Eq. 13 obtained from data in the presence of NaCl.

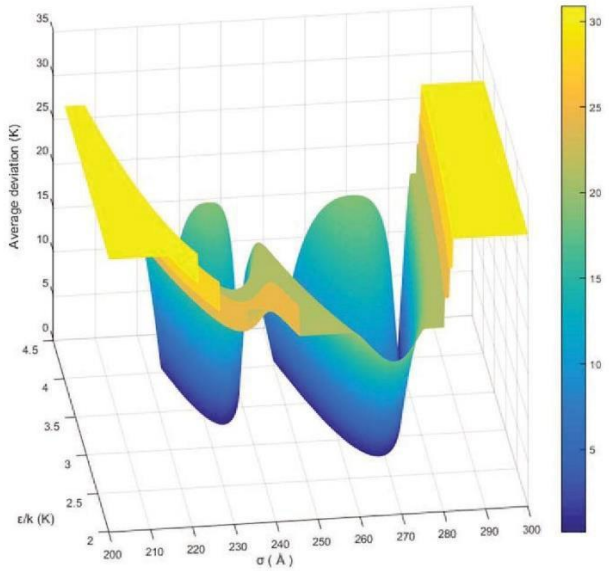

Figure 9. Typical form of the deviation between the predicted and the experimental data as a function of the Kihara parameters.

x and y axes correspond respectively to Kihara parameters σ and ε/k_b. The best set of value σ and ε is the one that minimizes the objective function F (in Eq. 11). [Color figure can be viewed at wileyonlinelibrary.com]

parameters $\sigma = 2.72$ Å, $\varepsilon/k_b = 265.5$ K. The hard-core radius was taken from the literature,[54] $a = 0.8968$ Å.

Figure 11 shows the experimental and predicted hydrate equilibrium temperatures of CPH based on the obtained Kihara parameters for CP. The agreement between experimental data and predictions is very excellent and the maximum average deviation in predicting the equilibrium temperature is about 0.2 K in the presence of either NaCl or $CaCl_2$. This value is 0.1 K for a mixture of NaCl-KCl and KCl, indicating that the hydrate formation temperatures are very well reproduced in the presence of other kinds of salts, especially in the presence of KCl and a mixture of NaCl-KCl.

Approach no. 3

As mentioned in the 4th section, in the approach no. 3, the occupancy factor is expressed as a function of the water

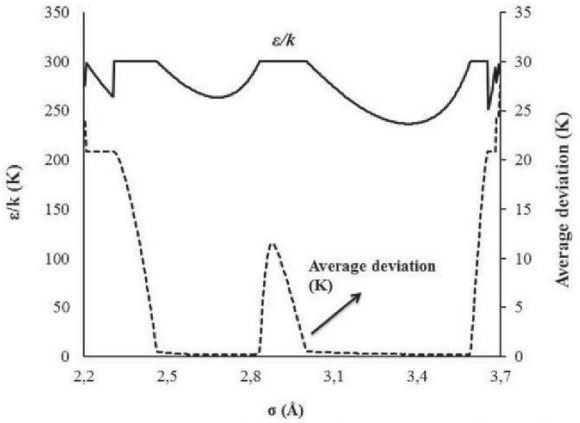

Figure 10. ε/k vs. σ at the minimum deviation from experimental data in NaCl.

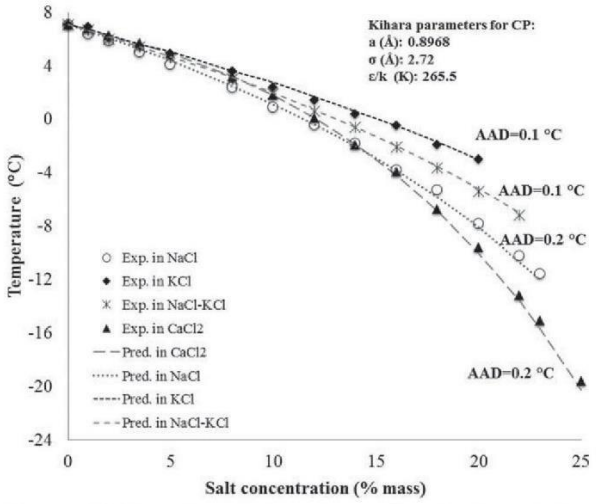

Figure 11. Experimental and predicted dissociation temperature of CPH in the presence of salts, and Kihara parameters for CP.

activity by Eq. 12. In this equation, the fitting parameters (m, n, and p) are all determined by using the experimental equilibrium data in the presence of NaCl.

The correlation coefficients in Eq. 12 and predicted CPH equilibrium temperatures in the presence of salts according to the approach no. 3 are presented in Figure 12. It can be seen that the predicted results concur well with the experimental data. The maximum absolute error in predicting the hydrate formation temperature is not greater than 0.4 K for either KCl or NaCl-KCl and not greater than 0.6 K for $CaCl_2$. The average absolute deviations are 0.1 K in the presence of NaCl, KCl and a mixture of NaCl-KCl, and 0.2 K in the presence of $CaCl_2$. This indicates that the approach no. 3 duplicates very well the equilibrium temperatures for CPH in the presence whatever salts.

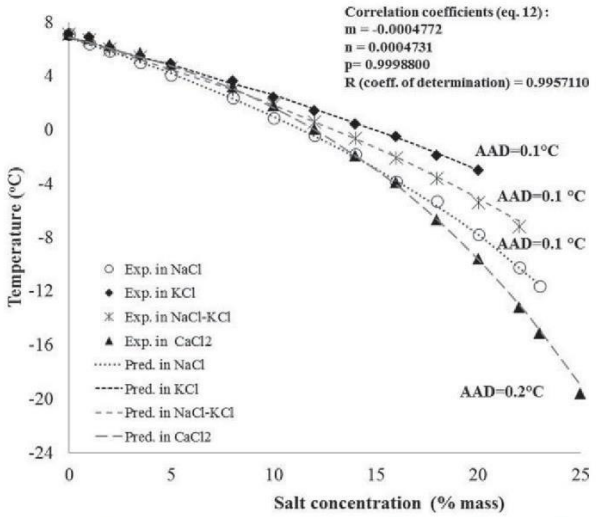

Figure 12. Experimental and predicted dissociation temperature of CPH in the presence of salts, and correlation coefficients for approach no. 3 from Eq. 12 obtained from experimental data in NaCl.

Table 5. Average Deviation (in °C or K) of Different Approaches for Predicting CPH Equilibrium Temperature

	NaCl	KCl	NaCl-KCl	$CaCl_2$
Approach no. 1	0.3	0.3	0.2	0.4
Approach no. 2	0.2	0.1	0.1	0.2
Approach no. 3	0.1	0.1	0.1	0.2

Summary and results on the models

Three approaches have been modified and used to predict the phase equilibrium of CPH in presence of various salts. The results of simulation are listed in Table 5.

As shown in this table, all three approaches are capable of satisfactorily predicting hydrate formation temperature of CP in presence of different salts. The average deviations are less than, or equal to 0.4 K in all cases.

Moreover, using the Kihara parameters in the approach no. 2 and the new correlation of occupancy factor and water activity for van der Waals and Platteuw model in the approach no. 3 are an excellent suggestion as the deviation is less than, or equal to 0.2 K, for any of the salts tested. However, approach no. 2 requires the integration of the Kihara potential, which can lead to different final values depending on the code and is also influenced by the use of the Antoine equation for CP vapor pressure. Therefore, approach no. 3 is the most accurate and simplest method to obtain quick and consistent dissociation temperatures of CPH from brine. As an added plus it is not code-dependent.

Conclusion

Two procedures were applied to determine experimentally the dissociation temperatures of CPH in presence of NaCl, KCl, an equimass mixture of NaCl-KCl, and $CaCl_2$. One was at high dissociation rate, for quick estimation completed in a few hours. Conversely, the second method occurred at a lower dissociation rate, for more accurate measurements, and took place over days.

Based on the results, a temperature shift between the equilibrium temperatures following two procedures was observed. As the quick procedure tends to miss the right temperature, its results are slightly above the right value.

Slow procedure provides results that are very close to the data reported in the literature in pure water and also brine. This indicates that this method is excellent to determine CPH dissociation temperatures.

The results also show that the equilibrium temperatures dropped significantly with an increase in salt concentration, whatever the kinds of salt used due to both ion clustering and salting-out phenomenon. In addition, the equilibrium temperatures of CPH in the presence of NaCl were always lower than the equilibrium temperatures in the presence of KCl and a mixture of KCl-NaCl at the same concentration. Whilst $CaCl_2$ shows the greatest impact on the equilibrium temperatures at concentrations from and above 16% in mass fraction compared to the other salts. This is due to the great influence on water activity of both NaCl and $CaCl_2$, and hence on the hydrate formation equilibrium temperatures.

Moreover, the experimental data have been described by three thermodynamic approaches. The first is based on the Hildebrand and Scott's equation to discover a new correlation for the change of specific heat of CPH and the dissociation points. The two others are based on van der Waals and Platteuw model. While the second one uses optimized Kihara parameters from this work, the third utilizes a new correlation between the occupancy factor and water activity.

At first, experimental data in presence of NaCl were used to fit the needed parameters. Then, each method was compared to other experimental data, with different salts. Finally, all three approaches have a good capability to predict CPH dissociation temperatures in presence of various salts. Average deviations are less than, or equal to, 0.4 K in all cases. The use of van der Waals and Platteuw method is even more accurate, with a deviation below 0.2 K. The new correlation between occupancy factor and water activity is probably the best to obtain quick, consistent, and accurate dissociation temperature of CPH in brine.

Acknowledgments

This study has been supported by ARMINES (Association pour la recherche et le developpement des methodes et processus industriels), Vietnam Ministry of Education and Training, and Hanoi University of Mining and Geology. The authors thank all the members of the GasHyDyn team for their constant support, especially our laboratory technician, Fabien Chauvy. The authors would like also to thank Christopher Yukna very much for his advice on English and proofreading.

Notation

a = activity (–) or Kihara parameter, spherical nucleus radius (m), coefficients (–) for the correlation of the change of molar specific heat
b = coefficient linear temperature dependency of the heat capacity (J mol^{-1} K^{-2}), and coefficients (–) for the correlation of is the change of molar specific heat
C = Langmuir constant of cavity (L mol^{-1}) or molar heat capacity (J mol^{-1} K^{-1})
f = fugacity, Pa
h = molar enthalpy, J mol^{-1}
k = or, k_b: Boltzmann constant, J K^{-1}
m = coefficient of the correlation of the cage occupancy
N = number of points of a given set of data
n = mole number, coefficient of the correlation of the cage occupancy
P = pressure, Pa
p = coefficient of the correlation of the cage occupancy
R = gas molecule equivalent radius (m), or universal gas constant (8.314472 m^2 kg s^{-2} K^{-1} mol^{-1}), or coefficient of determination, –
r = distance between the molecule and the wall of the cavity, m
T = temperature, K
V = volume, m^3
v = (partial) molar volume, $m^3.mol^{-1}$

Greek letters

ε = Kihara parameter, maximum attraction potential, –
μ = Chemical potential, J mol^{-1}
υ = number of cavities per molecules of water, –
θ = occupation rate of cavity/gas
ρ = (mass) density of water, kg m^{-3}
σ = Kihara parameter, distance between the molecules and the cavity wall, at null potential, m

Superscripts

I = ice phase
H = hydrate phase
L = liquid phase
β = hypothetical reference phase for the hydrate phase corresponding to empty lattice
β–φ = referring to the difference between the reference β phase and any φ phase

Literature Cited

1. Sloan ED, Koh CA. *Clathrate Hydrate of Natural Gases*, 3rd ed. CRC Press, FL: Boca Raton, 2008.
2. Sloan ED Jr. Fundamental principles and applications of natural gas hydrates. *Nature*. 2003;426:353–363.
3. Sloan ED, Koh C, Sum AK, Ballard AL, Creek J, Eaton M, Lachance J, Mcmullen N, Palermo T, Shoup G, Talley L. *Natural Gas Hydrate in Flow Assurance*. Amsterdam, Netherlands: Gulf Professional Pub./Elsevier, 2011.
4. Mimachi H, Takeya S, Yoneyama A, Hyodo K, Takeda T, Gotoh Y, Murayama T. Natural gas storage and transportation within gas hydrate of smaller particle: size dependence of self-preservation phenomenon of natural gas hydrate. *Chem Eng Sci*. 2014;118:208–213.
5. Sun ZG, Wang R, Ma R, Guo K, Fan S. Natural gas storage in hydrates with the presence of promoters. *Energy Convers Manag*. 2003;44(17):2733–2742.
6. Burnol A, Thinon I, Ruffine L, Herri JM. Influence of impurities (nitrogen and methane) on the CO_2 storage capacity as sediment-hosted gas hydrates—application in the area of the Celtic Sea and the Bay of Biscay. *Int J Greenh Gas Control*. 2015;35:96–109.
7. Veluswamy HP, Kumar R, Linga P. Hydrogen storage in clathrate hydrates: current state of the art and future directions. *Appl Energy*. 2014;122:112–132.
8. Duc NH, Chauvy F, Herri JM. CO_2 capture by hydrate crystallization—a potential solution for gas emission of steelmaking industry. *Energy Convers Manag*. 2007;48(4):1313–1322.
9. Herri J-M, Bouchemoua A, Kwaterski M, Brântuas P, Galfré A, Bouillot B, Douzet J, Ouabbas Y, Cameirao A. Enhanced selectivity of the separation of CO_2 from N_2 during crystallization of semi-clathrates from quaternary ammonium solutions. *Oil Gas Sci Technol Rev d'IFP Energies Nouv*. 2014;69(5):947–968.
10. Herslund PJ, Thomsen K, Abildskov J, von Solms N, Galfré A, Brântuas P, Kwaterski M, Herri J-M. Thermodynamic promotion of carbon dioxide–clathrate hydrate formation by tetrahydrofuran, cyclopentane and their mixtures. *Int J Greenhouse Gas Control*. 2013;17:397 Vol
11. Babu P, Linga P, Kumar R, Englezos P. A review of the hydrate based gas separation (HBGS) process for carbon dioxide pre-combustion capture. *Energy*. 2015;85:261–279.
12. Darbouret M, Cournil M, Herri JM. Rheological study of TBAB hydrate slurries as secondary two-phase refrigerants. *Int J Refrig*. 2005;28(5):663–671.
13. Douzet J, Kwaterski M, Lallemand A, Chauvy F, Flick D, Herri JM. Prototyping of a real size air-conditioning system using a tetra-n-butylammonium bromide semiclathrate hydrate slurry as secondary two-phase refrigerant—experimental investigations and modelling. *Int J Refrig*. 2013;36(6):1616–1631.
14. Ogoshi H, Takao S. Air-conditioning system using clathrate hydrate slurry. *JFE Tech Rep*. 2004;3(3):1–5.
15. Han S, Shin JY, Rhee YW, Kang SP. Enhanced efficiency of salt removal from brine for cyclopentane hydrates by washing, centrifuging, and sweating. *Desalination*. 2014;354:17–22.
16. Cha JH, Seol Y. Increasing gas hydrate formation temperature for desalination of high salinity produced water with secondary guests. *ACS Sustain Chem Eng*. 2013;1(10):1218–1224.
17. Kang KC, Hong SY, Cho SJ, Kim DH, Lee JD. Evaluation of desalination by nanostructured hydrate formation and pellet production process. *J Nanosci Nanotechnol*. 2017;17(6):4059–4062.
18. Hongfei X. Hydrate desalination using cyclopentane hydrates at atmospheric pressure. M.S. Thesis, Colorado School of Mines, CO, 2014.
19. Willson RC, Bulot E, Cooney CL. Use of hydrates for aqueous solution treatment. United States Patent, Patent Number: US 4678583, 1987.
20. Song Y, Dong H, Yang L, Yang M, Li Y, Ling Z, Zhao J. Hydrate-based heavy metal separation from aqueous solution. *Sci Rep*. 2016; 6:21389.
21. Mottet B. Method for purification of water by direct osmosis and crystallisation of clathrate hydrates. EP20150305505 20150403, *European Patent Office*, 2016.
22. Nakajima M, Ohmura R, Mori YH. Clathrate hydrate formation from cyclopentane-in-water emulsions. *Ind Eng Chem Res*. 2008; 47(22):8933–8939.
23. Kishimoto M, Iijima S, Ohmura R. Crystal growth of clathrate hydrate at the interface between seawater and hydrophobic-guest liquid: effect of elevated salt concentration. *Ind Eng Chem Res*. 2012; 51(14):5224–5229.
24. Zylyftari G, Lee JW, Morris JF. Salt effects on thermodynamic and rheological properties of hydrate forming emulsions. *Chem Eng Sci*. 2013;95:148–160.
25. Corak D, Barth T, Høiland S, Skodvin T, Larsen R, Skjetne T. Effect of subcooling and amount of hydrate former on formation of cyclopentane hydrates in brine. *Desalination*. 2011;278(1–3):268–274.
26. Lv Y-N, Wang S-S, Sun C-Y, Gong J, Chen G-J. Desalination by forming hydrate from brine in cyclopentane dispersion system. *Desalination*. 2017;413:217–222.
27. McAuliffe C. Solubility in water of paraffin, cycloparaffin, olefin, acetylene, cycloolefin, and aromatic hydrocarbons1. *J Phys Chem*. 1966;70(4):1267–1275.
28. Dean JA. Lange's handbook of chemistry. *Mater Manuf Process*. 1990;5(4):687–688.
29. Dirdal EG, Arulanantham C, Sefidroodi H, Kelland MA. Can cyclopentane hydrate formation be used to rank the performance of kinetic hydrate inhibitors? *Chem Eng Sci*. 2012;82:177–184.
30. Sefidroodi H, Abrahamsen E, Kelland MA. Investigation into the strength and source of the memory effect for cyclopentane hydrate. *Chem Eng Sci*. 2013;87:133–140.
31. Davidson DW. Clathrate hydrates. In: F. Franks, editor. *Water in Crystalline Hydrates Aqueous Solutions of Simple Nonelectrolytes*. 2nd ed. New York: Springer Science+Business Media, 1973.
32. Palmer HA. Characterization of hydrocarbon-type hydrates. Ph.D. Thesis, University of Oklahoma, Norman, OK, 1950.
33. Fan SS, Liang DQ, Guo KH. Hydrate equilibrium conditions for cyclopentane and a quaternary cyclopentane-rich mixture. *J Chem Eng Data*. 2001;46(4):930–932.
34. Fan S-S, Guo T-M. Hydrate formation of CO_2-Rich Binary and quaternary gas mixtures in aqueous sodium chloride solutions. *J Chem Eng Data*. 1999;44(4):829–832.
35. Baek S, Min J, Lee JW. Equilibria of cyclopentane hydrates with varying HLB numbers of sorbitan monoesters in water-in-oil emulsions. *Fluid Phase Equilib*. 2016;413:41–47.
36. Whitman CA, Mysyk R, White MA. Investigation of factors affecting crystallization of cyclopentane clathrate hydrate. *J Chem Phys*. 2008;129(17):174502
37. Zhang JS, Lee JW. Equilibrium of hydrogen + cyclopentane and carbon dioxide + cyclopentane binary hydrates. *J Chem Eng Data*. 2009;54(2):659–661.
38. Hildebrand JH, Scott RL. *Regular Solutions*. Prentice-Hall, NJ: Englewood Cliffs, 1962.
39. van der Waals JH, Platteeuw JC. Clathrate solutions. *Adv Chem Phys*. 1958;2:1–57.
40. Miyawaki O, Saito A, Matsuo T, Nakamura K. Activity and activity coefficient of water in aqueous solutions and their relationships with solution structure parameters. *Biosci Biotechnol Biochem*. 1997; 61(3):466–469.
41. Chandrasekaran SK, King CJ. Solid-liquid phase equilibria in multicomponent aqueous sugar solutions. *J Food Sci*. 1971;36(4):699–704.
42. Zhang Y, Debenedetti PG, Prud RK, Pethica BA. Differential scanning calorimetry studies of clathrate hydrate formation. *Water*. 2004; 108(43):16717–16722.
43. Parkhurst BDL, Appelo CAJ. User's guide to PHREEQC (version 2)—a computer program for speciation, and inverse geochemical calculations. *Exch Organ Behav Teach J*. 1999; D(Version 2):326.
44. Hu Y, Lee BR, Sum AK. *Universal Correlation for Gas Hydrates Suppression Temperature of Inhibited Systems: I. Single Salts. AIChE J*. 2017;63:5111–5124.
45. Herri J-M, Bouchemoua A, Kwaterski M, Fezoua A, Ouabbas Y, Cameirao A. Gas hydrate equilibria for CO_2–N_2 and CO_2–CH_4 gas mixtures—experimental studies and thermodynamic modelling. *Fluid Phase Equilib*. 2011;301(2):171–190.
46. Parrish WR, Prausnitz JM. Dissociation pressures of gas hydrates formed by gas mixtures. *Ind Eng Chem Process Des Dev*. 1972; 11(1):26–35.
47. Chassefière E, Dartois E, Herri J-M, Tian F, Schmidt F, Mousis O, Lakhlifi A. CO_2–SO_2 clathrate hydrate formation on early Mars. *Icarus*. 2013;223(2):878–891.
48. Herri J-M, Chassefière E. Carbon dioxide, argon, nitrogen and methane clathrate hydrates: thermodynamic modelling, investigation of their stability in Martian atmospheric conditions and variability of methane trapping. *Planet Space Sci*. 2012;73(1):376–386.

49. Muromachi S, Nagashima HD, Herri JM, Ohmura R. Thermodynamic modeling for clathrate hydrates of ozone. *J Chem Thermodyn*. 2013;64:193–197.
50. Le Quang D, Le Quang D, Bouillot B, Herri JM, Glenat P, Duchet-Suchaux P. Experimental procedure and results to measure the composition of gas hydrate, during crystallization and at equilibrium, from N_2-CO_2-CH_4-C_2H_6-C_3H_8-C_4H_{10} gas mixtures. *Fluid Phase Equilib*. 2016;413:10–21.
51. Handa YP, Tse JS. Thermodynamic properties of empty lattices of structure I and structure II clathrate hydrate. *J Phys Chem*. 1986; 90(22):5917
52. Tee LS, Gotoh S, Stewart WE. Molecular parameters for normal fluids. Kihara potential with spherical core. *Ind Eng Chem Fundam*. 1966;5(3):363–367.
53. Sloan E Jr. *Clathrate Hydrates of Natural Gases*, 2nd ed. Vol 14. New York City, NY: Marcel Dekker, Inc. 1998.
54. Takeuchi F, Ohmura R, Yasuoka K. Statistical-thermodynamics modeling of clathrate-hydrate-forming systems suitable as working media of a hydrate-based refrigeration system. *Int J Thermophys*. 2009;30(6):1838–1852.

Manuscript received Sep. 21, 2017, and revision received Nov. 22, 2017.

6.3. Paper III: Implementing Cyclopentane Hydrates Phase Equilibrium Data and Simulations in Brine Solutions

S.Ho-Van, B.Bouillot, J.Douzet, S. Maghsoodloo Babakhani, J.M.Herri

Published in: Industrial & Engineering Chemistry Research, Volume: 57, Issue: 43, Pages: 14774-14783, Publication Date: October 4th, 2018

Summary: In this paper we extended experimental equilibrium data of CPH to four common salt systems including Na_2SO_4, $MgCl_2$, equi-weight mixture of $MgCl_2$-NaCl, or equi-weight mixture of $MgCl_2$-NaCl-KCl with various salt concentrations. As in the paper II, three thermodynamic approaches are again employed to predict equilibrium. Moreover, one simulation model based on the Hu-Lee-Sum (HLS) correlation was also developed for CPH system to predict and compare to this new set of experimental data. Interestingly, all models exhibit an adequate agreement between simulations and measurements. Again, the ABOC method is the best model to regenerate rapid and consistent equilibrium data of CPH in brine, whatever the electrolytes involved.

I&EC research
Industrial & Engineering Chemistry Research

Article

Cite This: Ind. Eng. Chem. Res. 2018, 57, 14774−14783

pubs.acs.org/IECR

Implementing Cyclopentane Hydrates Phase Equilibrium Data and Simulations in Brine Solutions

Son Ho-Van,*[,†,‡] Baptiste Bouillot,*[,†] Jérôme Douzet,[†] Saheb Maghsoodloo Babakhani,[†] and Jean-Michel Herri[†]

[†]Ecole Nationale Supérieure des Mines de Saint-Etienne, SPIN, CNRS 5307, LGF, F-42023 Saint-Etienne, France

[‡]Oil Refinery and Petrochemistry Department, Hanoi University of Mining and Geology, Duc Thang, Bac Tu Liem, Hanoi, Vietnam

ABSTRACT: Cyclopentane hydrate-based salt removal is considered to be a possible promising technology for desalination. In order to optimize such processes, phase equilibrium data of cyclopentane hydrates (CPH) in saline solutions are crucial. Lamentably, these data sets are still incomplete. Therefore, earlier we published a limited experimental and modeling study on CPH equilibrium with some salts present. This study extends experimental equilibrium to four more common brine systems: Na_2SO_4, $MgCl_2$, $MgCl_2$−NaCl, or $MgCl_2$−NaCl−KCl at various salt concentrations. Importantly, four thermodynamic approaches (the standard freezing point depression equation based (SFPD), Hu−Lee−Sum (HLS) correlation, and the two van der Waals and Platteuw-based Kihara and activity-based occupancy correlation (ABOC) methods) are compared to this new set of experimental data. Results show that simulations agree adequately with measured data. Nonetheless, the ABOC method is the best model to reproduce rapid and consistent equilibrium data of CPH in brine, whatever the electrolytes involved.

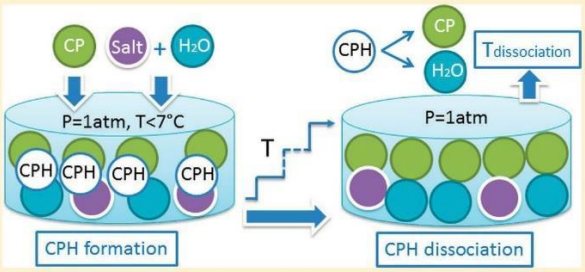

INTRODUCTION

Clathrate hydrates are nonstoichiometric ice-like crystalline compounds formed by combination of a lattice of water molecules, and guest molecules. These guests are small molecules, capable of fitting into the lattice cavities, such as CO_2, CH_4, N_2, cyclopentane, etc.[1] Three main polymorphs of clathrate hydrate are well-known as structures I (sI), II (sII), and H (sH), composed of a certain number of cavities formed by water molecules through a hydrogen bonding system.[1]

Clathrate hydrates present many prospective applications, such as gas separation,[2,3] gas storage,[4,5] air-conditioning,[6−8] carbon dioxide capture,[9,10] and desalination.[1,11,12] Recently, hydrate-based desalination has attracted significant interest due to international fresh water increasing demand.[13−17]

In hydrate-based desalination, solid salts and dissolved ions are excluded from hydrate crystals during crystallization. Hydrate crystals can then be separated from the aqueous solution using a solid−liquid filter. Fresh water and guest molecules can be isolated after hydrate dissociation. If the guest molecules are gaseous at standard conditions, or hydrophobic, they can easily be removed from fresh water. Afterward, they can be recycled into the desalination process.

Certainly, thehydrate-based desalination method has been studied widely and intensively for many years (since the 1960s).[13,15,18−25] Nevertheless, this technology is not ready for industrial scale use yet. As stated in the review work by Babu et al.,[16] there are still some challenges yet to overcome: high energy consumption issues, separating hydrate crystals from highly concentrated saltwater without impurities, and slow kinetics. Recently, He et al.[15] suggested a new hydrate based desalination system using liquefied natural gas (LNG) cold energy. Compared to multistage flash distillation (MSF), reverse osmosis (RO), and freezing desalination processes, this technology can be attractive since LNG cold energy replaces the external refrigeration cycle and hence reduces the specific energy consumption.[15] Obviously, this novel technology still requires a large and steady source of LNG cold energy. A high-pressure reactor is also needed because propane is utilized to form hydrate.

Cyclopentane with water forms sII clathrate hydrates at around 7.1 °C under atmospheric pressure.[1,26] Because of its capability to form clathrate hydrates under such mild conditions, cyclopentane hydrates (CPH) is a promising candidate for water treatment applications, such as desalination. Recently, some authors have attempted to use CPH for desalination: Corak et al.[27] (optimize the subcooling for CPH-based desalination), Han et al.[28,29] (use post treatment methods: washing, centrifuging, and sweating to remove excessive brine from CPH crystals), Cai et al.[30] (desalination by using cyclopentane methane binary hydrate), Lv et al.[31] (optimize kinetic of CPH-based desalination conditions), Xu et al.[17] (use a three-step separation method, including gravitational separation, filtration, and a washing step with a salt removal efficiency of 81%).

Received: June 22, 2018
Revised: August 28, 2018
Accepted: October 4, 2018
Published: October 4, 2018

DOI: 10.1021/acs.iecr.8b02796
Ind. Eng. Chem. Res. 2018, 57, 14774−14783

However, before this CPH-based desalination technique is commercially ready, some important issues such as kinetic, thermodynamic (phase equilibrium data), entrapped salt quantity, and salt removal efficiency remain. They must be comprehensively understood and optimized. Unfortunately, in terms of CPH thermodynamics in the presence of salts, there are still few experimental data available in the literature. Therefore, we previously compiled and verified equilibrium temperatures of CPH in the presence of NaCl, KCl, NaCl−KCl, or $CaCl_2$. Moreover, three thermodynamic methods were applied to simulate them.[26] Nonetheless, more phase equilibrium data in other salts are still required, and thermodynamic approaches still need to be compared to a wider range of experimental data.

Consequently, this effort extends experimental dissociation temperature to four other brine systems: Na_2SO_4, $MgCl_2$, an equiweight mixture of $MgCl_2$−NaCl, and an equiweight mixture of $MgCl_2$−NaCl−KCl under wide ranges of salt concentrations. Then, our three previously developed thermodynamic models based on the standard freezing point depression method, or the van der Waals and Platteuw approaches, are again compared to this new data set. Moreover, a brand new method, the Hu−Lee−Sum (HLS) correlation is considered.

EXPERIMENTAL SECTION

Chemicals. All chemicals used in this work were provided by Sigma-Aldrich Company. A water purification system was utilized to produce high-purity water with a conductivity $\sigma \leq 0.055\ \mu S\ cm^{-1}$ and TOC (total organic carbon content) less than 5 ppm. Details of the chemicals are listed in Table 1.

Table 1. Purity of Initial Material Used

material	chemical formula	mol weight (g mol^{-1})	solubility in water (g/L)	purity (% mol)
cyclopentane	C_5H_{10}	70.1	0.156 (25 °C)[32]	98.0
sodium chloride	NaCl	58.4	360 (20 °C)[33]	99.5
potassium chloride	KCl	74.55	344 (20 °C)[33]	99.0
magnesium chloride	$MgCl_2$	95.21	54.6 (20 °C)[33]	99.5
sodium sulfate	Na_2SO_4	142.04	19.5 (20 °C)[33]	99.5

Apparatus. Experimental apparatus is detailed in Figure 1. A jacketed glass reactor (1) with a volume of 1 L is provided by Verre Equipment (France). A chiller Ministat 240 (2) controls constantly and homogeneously the temperature of the solution and has an operating temperature range of −45 to +200 °C with a stability of ±0.02 °C. The coolant used is a mixture of water and ethylene glycol (44% mass). The solution inside the reactor is mixed by an impeller (3) powered by a motor (6). Two temperature probes (9) are utilized to monitor the aqueous mixture. A transmitter (7) transfers temperature data to a computer (8). LabVIEW observes and records the digital information throughout the course of experiments. To measure the salt concentration of the solution, an ionic chromatography (Dionex DX-500 IC) system (11) was utilized. A drying oven (Binder) (10) was employed only for a second salt concentration measurement in the experiments with Na_2SO_4 solution.

Procedure. To determine the CPH dissociation temperatures, two procedures (quick and slow) are used as described in more detail in a previous article.[26]

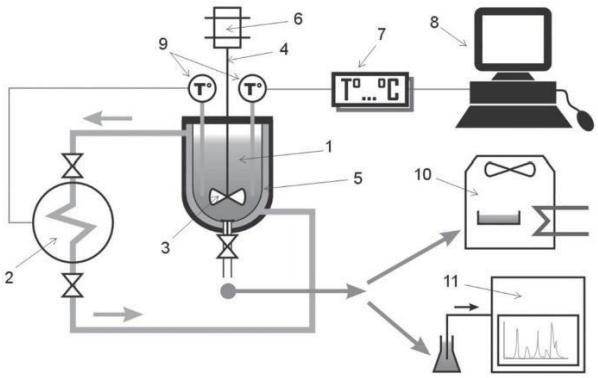

Figure 1. Diagram of the experimental apparatus: 1, vessel; 2, chiller; 3, impeller; 4, agitator; 5, cooling jacket; 6, motor; 7, temp transmitter; 8, computer; 9, temperature probe; 10, drying oven; 11, ion chromatography.

Quick Procedure. In the reactor are introduced 500 g of pure water, a chosen amount of salt, and 114.38 g of CP (corresponding to the hydrate molar ratio water/CP = 17:1). Then, the solution is cooled to a temperature above the freezing point of the salt solution. Crystallization is triggered by introducing grams of ice and a corresponding amount of salt to keep a constant salinity. After 1−2 h of crystallization, the chiller is stopped. CPH then dissociates progressively. A sharp rise in temperature is observed when no hydrate is present in the reactor. This point corresponds presumably to the dissociation temperature of CPH. Aliquots of 1 and 5 mL of brine solution are taken to measure salt concentration by ion chromatography and drying oven. This step is necessary to make sure all CPH have dissociated.

Of course, due to the high heating rate, this procedure is not quite accurate enough. However, it provides a stepping stone for the next procedure.

Note that $MgCl_2$ should form salt hydrates ($MgCl_2 \cdot 6H_2O$) after water evaporation at 60 °C (set temperature of drying oven for all experiments).[34,35] Therefore, the drying oven was not employed with solutions containing $MgCl_2$ andionic chromatography only was used instead.

Slow Procedure. A duplicate experiment is performed with a different dissociation procedure. After 1−2 h of crystallization, the chiller functions manually as follows:

The first heating step increases the temperature to a temperature of 4 °C below the prior dissociation temperature recorded by the quick procedure. After stabilization, the temperature inside the reactor is increased at an increment of 0.1 °C. Then, the temperature remains constant for at least 1 h. If no significant CPH dissociation is observed after 1 h, the temperature is augmented again by the same increment. This process is iterated until a small amount of hydrate is observed. The temperature is then kept steady for a longer time (12−24 h) to ensure that equilibrium is reached. The last step is required when hydrate is still present. The CPH dissociation temperature is recorded during next to last step as all three phases (CP, CPH, and brine) exist.

Images of the aqueous mixture are taken at every step. These images are then compared in order to determine the final step in which only two transparent phases of brine solution and CP can be observed as seen in the initial condition (pictures provided in the previous study[26]).

DOI: 10.1021/acs.iecr.8b02796
Ind. Eng. Chem. Res. 2018, 57, 14774−14783

Moreover, to make sure that there are no longer any CPH in the bulk at the final step, 1 and 5 mL of brine solution are sampled to measure salt concentration.

EXPERIMENTAL RESULTS

All experimental results on phase equilibrium data of CPH following the slow dissociation procedure are provided in Table 2 and Figure 2. Note that the mass ratio $MgCl_2$/NaCl is 1:1 in the equiweight mixture of $MgCl_2$–NaCl and the mass ratio $MgCl_2$/NaCl/KCl is 1:1:1 in the equiweight mixture of $MgCl_2$–NaCl–KCl.

Table 2. Equilibrium Temperatures[a] of CPH in the Presence of Na_2SO_4, $MgCl_2$, an Equiweight Mixture of $MgCl_2$–NaCl, or an Equiweight Mixture of $MgCl_2$–NaCl–KCl (Slow Dissociation Procedure)

salinity[b,c,d] (% mass)	in Na_2SO_4 (°C)	in $MgCl_2$ (°C)	in $MgCl_2$–NaCl (°C)	in $MgCl_2$–NaCl–KCl, (°C)
0	7.1	7.1	7.1	7.1
1	6.7	6.7	6.5	6.7
2	6.4	6.2	6.1	6.1
3.5	6.0	5.2	5.1	5.2
5	5.6	4.3	4.1	4.6
6	5.3[e]			
8		2.1	2.3	2.7
10		0	0.5	1.2
12		−2.2	−1.6	−0.2
14		−5.2	−3.6	−1.8
16		−8.7	−5.8	−3.8
18		−12.7	−8.8	−5.7
20		−17.6	−12	−8
22			−15.5	−10.8

[a]Uncertainty of the temperature measurements: ±0.1 °C. [b]Uncertainty due to weighing: ±0.002% mass. [c]Uncertainty due to drying oven: ±0.2% mass. [d]Relative uncertainty due to ion chromatography: 1.5% (see the Supporting Information from Ho-Van et al.[26] for all uncertainty estimations). [e]Corresponds to eutectic point.

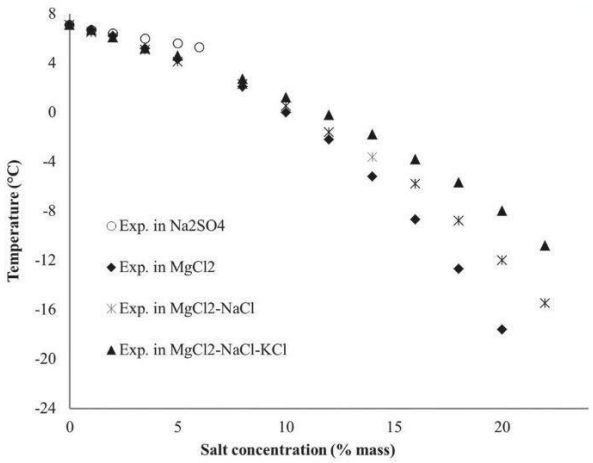

Figure 2. Experimental equilibrium temperature of CPH in the presence of salts (slow procedure only).

Our measure results show that the equilibrium temperatures obtained by the slow dissociation procedure (T^{slow}) are systematically lower than those provided by the quick dissociation procedure (T^{quick}). This difference between the measured data from both procedures ($\Delta T = T^{quick} - T^{slow}$) ranges from 0.3 up to 3.2 °C. We believe that a quick dissociation procedure likely misses the total dissociation temperature, i.e., the equilibrium temperature, as stated by Ho-Van et al.[26] Hence, the slower process furnishes more trustworthy and consistent equilibrium data than the quick one.

Figure 2 indicates that the equilibrium temperatures considerably decrease with higher salt concentrations. Of course, electrolytes in solution significantly affect the water activity, and hence the CPH phase equilibria. Both phenomena of clustering and salting-out lower the equilibrium temperature of CPH.[1,26,36] Moreover, the influence on equilibrium temperature is different for each salt. For instance, Table 2 reveals that the measured dissociation temperatures for Na_2SO_4 are higher than those for $MgCl_2$, $MgCl_2$–NaCl, or $MgCl_2$–NaCl–KCl. This can be attributed to the lower water activity and molality in the presence of Na_2SO_4 compared to those in the presence of other salts at the same concentrations (in % mass) (see Appendix I, Table A1).

Indeed, as seen in Table A1 (in Appendix I), $MgCl_2$–NaCl and $MgCl_2$–NaCl–KCl mixtures have approximately the same molality at the same salt concentration (in % mass). Therefore, the variance in the dissociation point between these two brine solutions can be observed through the role of each salt when ions interact with water molecules. Table 2 illustrates that the equilibrium temperatures in the brine system of $MgCl_2$–NaCl are lower than those in the brine system of $MgCl_2$–NaCl–KCl. This means the effect of NaCl on phase equilibria is stronger than KCl. In addition, $MgCl_2$ shows the significant impact on the equilibria at concentration above 8% mass. This is because $MgCl_2$ has a considerable influence on water activity even at lower molality at the same salt concentration (see Appendix I, Table A1).

In fact, the effect of each salt on hydrate phase equilibria depends on ion charge density. Observations showed that small cations with high charge density can lead to powerful electrostatic interaction between the cations and water molecules. This weakens hydrogen bonding interaction between water molecules, inhibiting the hydrate formation.[37,38]

The ionic radius of Mg^{2+} (+2 charge), Na^+ (+1 charge), and K^+ (+1 charge) are 0.78, 1.02, and 1.38 Å, respectively.[37,38] Hence, the charge density of Mg^{2+} is higher than Na^+ or K^+. According to Sabil et al.[37] and Cha et al.,[38] the hydrate inhibiting strength rises in the following order: $Mg^{2+} > Na^+ > K^+$. This agrees well with our observation in the presence of $MgCl_2$ (above 8% mass), $MgCl_2$–NaCl, and $MgCl_2$–NaCl–KCl.

Then, at 8% mass Na_2SO_4, when hydrate formed, coprecipitation of salt hydrates was observed at the bottom of the reactor (at temperatures less than 7 °C; see Figure 3). Indeed, according to phase diagram of Na_2SO_4 with water,[39] we expect Na_2SO_4 to form $Na_2SO_4{\cdot}10H_2O$ hydrates in the system under these conditions. Indeed, both CPH and $Na_2SO_4{\cdot}10H_2O$ hydrates dissociate concurrently with increasing temperature. When no CPH was observed, the temperature of the system was recorded to be 5.4 °C following the slow procedure (see Figure 4). Therefore, 5.3 °C was recorded to be the dissociation point for CPH phase. However, Na_2SO_4 hydrates were still present at the bottom of the reactor. Consequently, the salt concentration in aqueous phase was not 8% mass. At this moment, two samples of 1 and 5 mL were then taken by a syringe Rhizon with a mean pore size of the porous part of 0.15 μm in order to separate salts solid or any crystal from the aqueous

DOI: 10.1021/acs.iecr.8b02796
Ind. Eng. Chem. Res. 2018, 57, 14774−14783

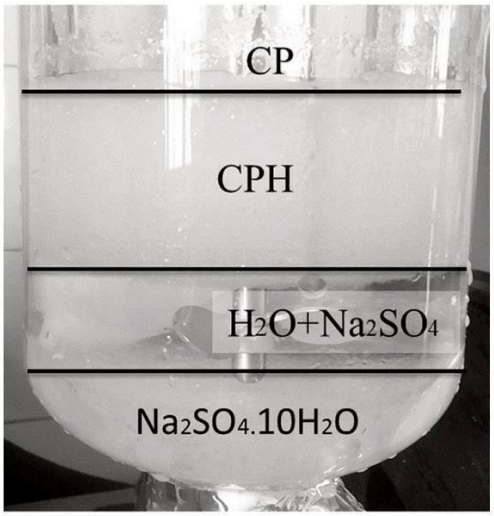

Figure 3. Photo of the experiment with Na_2SO_4 at 8%, 5.2 °C following the slow procedure.

Figure 4. Photo of the experiment with Na_2SO_4 at 8%, 5.4 °C following the slow procedure.

solution (see Figure 4). Both drying oven and ionic chromatography provided an identical measured salt concentration of 6%. Therefore, 5.3 °C at 6% salt concentration is the eutectic point of the four-phase system (Na_2SO_4 + H_2O, Na_2SO_4·$10H_2O$, CP, and CPH). This means that if the temperature is decreased below 5.3 °C at 6% mass salt concentration, CPH and Na_2SO_4·$10H_2O$ will form simultaneously.

■ MODELING CPH THERMODYNAMIC EQUILIBRIUM

In this effort, four different approaches are utilized to model phase equilibria of CPH in the presence of salts. The first approach is based on the standard freezing point depression equation.[40,41] The second is a new correlation by Hu et al.,[42,43] called HLS correlation. It is a derivation of the freezing point depression equation developed especially to calculate gas hydrate suppression temperatures in the presence of single salts (Hu et al.[42]), or salt mixtures (Hu et al.[43]). The two others methods are based on the van der Waals and Platteuw model.[44] As aforementioned, these approaches are described in detail in our previous article.[26]

In the following, average absolute deviation (AAD) between experimental and simulated results is defined as follows:

$$\mathrm{AAD} = \frac{1}{N}\sum_{i=1}^{N} |T_{i,\mathrm{pred}} - T_{i,\mathrm{exp}}| \tag{1}$$

where N is the number of experimental data points, $T_{\mathrm{i,pred}}$ (K) is the predicted-equilibrium temperature, and $T_{\mathrm{i,exp}}$ (K) is the experimental equilibrium temperature.

Standard Freezing Point Depression (SFPD) Approach. In this approach, the water activity in brine with the CPH present is expressed as follows:[40,41]

$$\ln a_w = \frac{\Delta H_{\mathrm{fm}}}{R}\frac{(T_f - T)}{T_f T} + \frac{\Delta C_{\mathrm{fm}}}{R}\left[\frac{(T_f - T)}{T} - \ln\left(\frac{T_f}{T}\right)\right] \tag{2}$$

where T_f is the dissociation temperature in K,[45] ΔH_{fm} is the molar enthalpy of dissociation in J/mol,[45] ΔC_{fm} is the change of molar specific heat between the subcooled liquid and the crystals in (J/mol)/K, and a_w is the water activity. PHREEQC[46] was employed to calculate water activity in brine using the PITZER database.

ΔCm_f is only unknown and could not be ignored. Therefore, a correlation for ΔCm_f was established previously[26] using experimental data in the presence of NaCl under the form as follows:

$$\Delta C_{\mathrm{fm}} = F(T) = a \times \exp(b \times T) \tag{3}$$

The equilibrium temperatures of CPH in other brine solutions (Na_2SO_4, $MgCl_2$, $MgCl_2$−NaCl, or $MgCl_2$−NaCl−KCl) are then calculated by using both eqs 2 and 3.

Hu−Lee−Sum (HLS) Correlation. Hu et al.[42,43] observed that $\frac{nR}{\Delta H_{\mathrm{diss}}}$ remains constant, while $\frac{\Delta T}{T_0 T}$ only depends on the effective mole fraction. Therefore, they developed a new correlation for the suppression temperature ($\Delta T = T_0 - T$) based on eq 2 as follows:[42,43,47]

$$\frac{\Delta T}{T_0 T} = -\frac{nR}{\Delta H_{\mathrm{diss}}}\ln a_w = C_1 X + C_2 X^2 + C_3 X^3 \tag{4}$$

where T_0 and T are the hydrate equilibrium temperatures in pure water and brine solution, respectively. ΔH_{diss} is the hydrate dissociation enthalpy, n the hydration number, and a_w the water activity. C_1, C_2, and C_3 are fitted coefficients, and X is the effective mole fraction. X can be expressed as follows:[43]

$$X = \sum_{\mathrm{j=salts}}\sum_{\mathrm{i=ions}} |z_{j,i}| x_{j,i} \tag{5}$$

where i and j represent the ion and salt, respectively. z is the ion charge number, and x is the mole fraction. In the end, the hydrate formation temperature is

$$T = T_0\left[1 + \left(\frac{\Delta T}{T_0 T}\right)T_0\right]^{-1} \tag{6}$$

Equation 4 was originally developed for structure I hydrates but has been derived for salt mixtures and structure II hydrates

DOI: 10.1021/acs.iecr.8b02796
Ind. Eng. Chem. Res. 2018, 57, 14774−14783

lately.[43] To account for sII hydrates, the authors suggested a new parameter α:

$$\alpha = \frac{\left(\frac{\Delta T}{T_0 T}\right)_{sII}}{\left(\frac{\Delta T}{T_0 T}\right)_{sI}} \tag{7}$$

so that

$$T = T_0\left[1 + \alpha\left(\frac{\Delta T}{T_0 T}\right)_I T_0\right]^{-1} \tag{8}$$

By this means, the sII hydrate suppression temperature is correlated to sI suppression temperature. In our work, the studied system is different since no gas molecules are considered. Instead, cyclopentane is the guest molecule, and the pressure dependency of CPH is negligible. Therefore, we first checked Hu et al.'s assumption in water + CP + salt systems considering the same salts {NaCl, KCl, $CaCl_2$, $MgCl_2$}. Figure 5 shows that $\frac{\Delta T}{T_0 T}$ is indeed strongly correlated

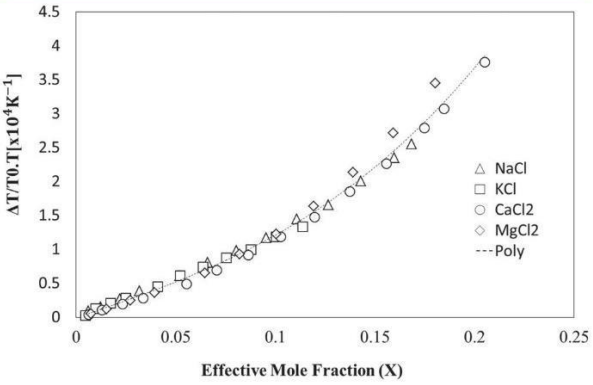

Figure 5. CPH hydrate depression temperature versus the effective mole fraction of NaCl, KCl, $CaCl_2$, and $MgCl_2$.

to the effective mole fraction (see also eq 4), although there is a slight deviation for the $MgCl_2$ system at high concentrations ($X > 0.15$).

Since the parameters furnished by Hu et al.[42] have not led to satisfactory simulation for CPH formation temperature (see Appendix II), data from Figure 5 have been used to optimize C_1, C_2, and C_3 coefficients. Note that, on Figure 5, dissociation points of CPH in the presence of NaCl, KCl, and $CaCl_2$ come from Ho-Van et al.[26] and results involving $MgCl_2$ come from the present work. Figure 5 shows the CPH depression temperature versus the effective mole fraction of NaCl, KCl, $CaCl_2$, and $MgCl_2$. On the basis of Figure 5, and Hu et al., $\frac{\Delta T}{T_0 T}$ can be expressed as a fitted function of X as follow (regression coefficient $R = 0.990$):

$$\frac{\Delta T}{T_0 T} = 0.000956623X + 0.00059779X^2 + 0.01897593X^3 \tag{9}$$

Hence, C_1, C_2, and C_3 for CPH are now determined to be 0.000956623, 0.00059779, and 0.01897593, respectively.

Kihara Approach. The van der Waals and Platteeuw model[44] is a standard approach in clathrate science.[1] Its use for CPH crystallization from brine has been explained by Ho-Van et al.[2] Therefore, it will not be detailed in this section. However, for the sake of understanding, here is some basic information.

The equilibrium is calculated by searching uniform chemical potentials of water in both liquid and hydrate phases. A reference state (β) is used: the empty clathrate. Hence, it can be expressed as follows:

$$\Delta\mu_w^{\beta\text{-H}} = \Delta\mu_w^{\beta\text{-L}} \tag{10}$$

$\Delta\mu_w^{\beta\text{-L}}$, the difference between chemical activity of water in β state and liquid phase can be expressed from the Gibbs–Duhem equation,[48] while $\Delta\mu_w^{\beta\text{-H}}$, the difference between the β state and hydrate phase can be calculated via the van der Waals and Platteeuw model as follows:

$$\Delta\mu_w^{\beta\text{-H}} = -RT\sum_i \nu_i \ln\left(1 - \sum_j \theta_j^i\right) \tag{11}$$

where R is the universal gas constant, T is the absolute temperature, ν_i is the number of type i cavities per water molecule in the hydrate (just 8/136 for CPH since cyclopentane only occupies large cavities of sII), and θ_j^i is the occupancy factor ($\theta_j^i \varepsilon [0,1]$) of the cavities of type i by the guest molecule j (the guest molecule here is CP). Occupancy factor θ_j^i can be obtained from integration of the Kihara potential (Parrish et al.[49]) and the fugacity of guest molecules. It will not be developed hereafter. However, the reader should now be aware that calculation of $\Delta\mu_w^{\beta\text{-H}}$ is possible under the condition that Kihara parameters (maximum attractive potential ε, distance between the cores at zero potential energy σ, and the hard-core radius a) are available. In our previous work, optimization of these parameters for cyclopentane has been performed for ε and a (the hard-core radius is supposed to be known). Results are presented in Figure 8.

In this approach, the activity of water is needed for the chemical potential of water in the liquid phase, as well as specific thermodynamic properties. Like the first approach, PHREEQC has been used for water activity. The others parameters have been chosen, and taken from literature, on the basis of previous work and observation (Herri et al.[48] and Ho-Van et al.[26]).

■ ACTIVITY-BASED OCCUPANCY CORRELATION (ABOC) APPROACH

The fourth approach is similar to the latest. However, instead of using Kihara parameters, ergo an interaction potential, a more simple approach has been used. Instead of considering a Langmuir type method for the occupancy of cavities, an elementary correlation between the occupancy factor and water activity, $\theta = F(a_w)$, can be used.[26] By this means, the knowledge of water activity (with PHREEQC, or any activity coefficient method, for instance) is enough to estimate θ. The correlation is expressed as follows:

$$\theta(a_w) = m \times (a_w{}^2) + n \times (a_w) + p \tag{12}$$

where m, n, and p are the empirical constants reported by Ho-Van et al.:[26] −0.0004772, +0.0004731, and +0.9998800, respectively. Note that these constants have been obtained from CPH equilibrium points in water + NaCl mixtures only.

DOI: 10.1021/acs.iecr.8b02796
Ind. Eng. Chem. Res. 2018, 57, 14774−14783

MODELING RESULTS

SFPD Approach. Figure 6 illustrates the experimental and predicted equilibrium temperatures according to the SFPD approach. Absolute average deviations are 0.1 °C in Na_2SO_4, 0.3 °C in $MgCl_2$−NaCl−KCl, 0.4 °C in $MgCl_2$−NaCl, and 0.5 °C in $MgCl_2$. Results indicate that dissociation temperatures are relatively well reproduced using the $\Delta Cm_f(T)$ correlation for CPH.

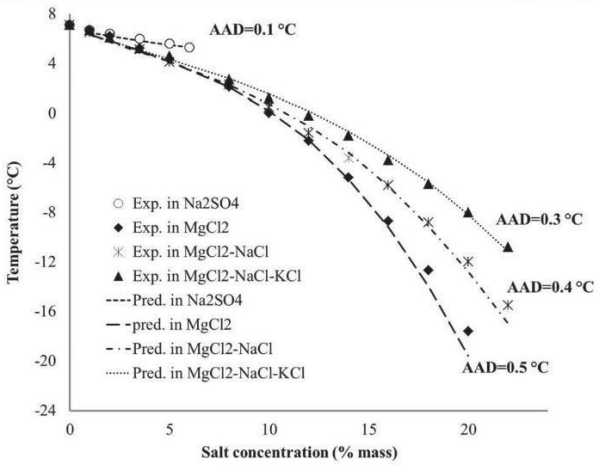

Figure 6. Experimental and predicted dissociation temperature of CPH in the presence of salts according to the SFPD approach.

Unfortunately, there is a significant gap between the modeling and experimental data in the presence of $MgCl_2$ (≥18% mass) and a $MgCl_2$−NaCl mixture (≥20% mass). This might be due to water activity calculations. However, since our fourth approach (ABOC) provides better results using the same estimation tool (PHREEQC), deviations seem to be due to the method itself and its simplified hypothesis (considering CPH as a pure water crystal with its specific thermodynamic properties).

HLS Correlation. The CPH equilibrium temperatures in brine solutions of $MgCl_2$−NaCl, $MgCl_2$−NaCl−KCl, or Na_2SO_4 have been predicted by eq 6 using the three coefficients obtained earlier (eq 9). Simulated results are presented in Figure 7. They are in relatively good agreement with the measured data. Average absolute deviations are 0.3 °C for Na_2SO_4, 0.2 °C for $MgCl_2$−NaCl−KCl, 0.4 °C for $MgCl_2$−NaCl, and 0.7 °C for $MgCl_2$.

HLS correlation is, however, less comfortable with $MgCl_2$.[42] This is not surprising when looking at Figure 5. Indeed, there is a behavior deviation from eq 9 (higher $\frac{\Delta T}{T_0 T}$ than for the correlation curve for $X > 0.15$).

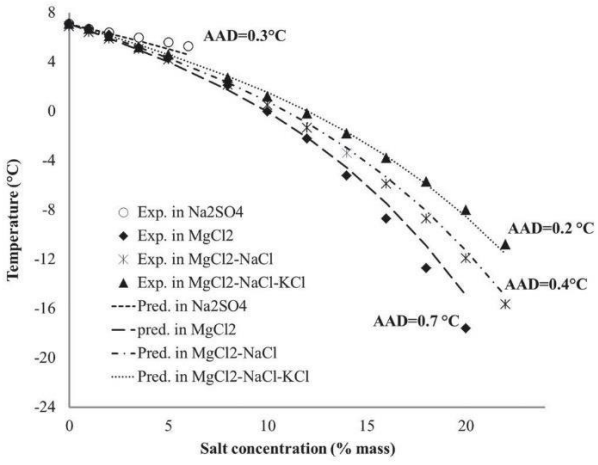

Figure 7. Experimental and predicted dissociation temperature of CPH in the presence of salts according to the HLS approach

Kihara Approach. Figure 8 reveals the experimental and predicted hydrate equilibrium temperatures of the Kihara-based method. In this case, the simulated results agree reasonably well with the experimental data. Average absolute deviations are less than 0.2 °C in the presence of Na_2SO_4, $MgCl_2$−NaCl, or $MgCl_2$−NaCl−KCl, and regrettably about 0.5 °C in the presence of $MgCl_2$.

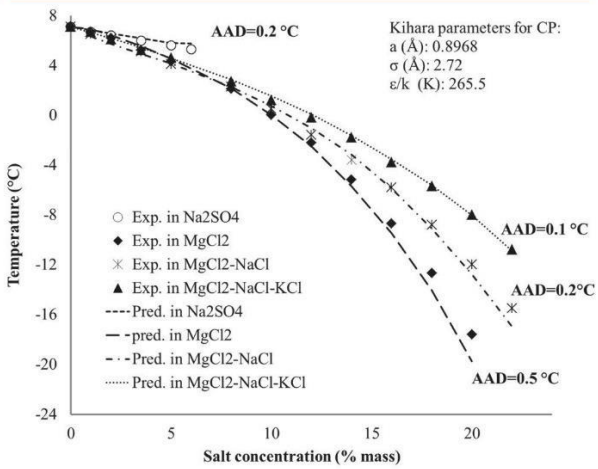

Figure 8. Experimental and predicted dissociation temperature of CPH in the presence of salts, and Kihara parameters for CP obtained by using the experimental data in NaCl.

Activity-Based Occupancy Correlation (ABOC). The simulated results of th CPH phase equilibrium with the ABOC method are presented in Figure 9. Predicted results agree well

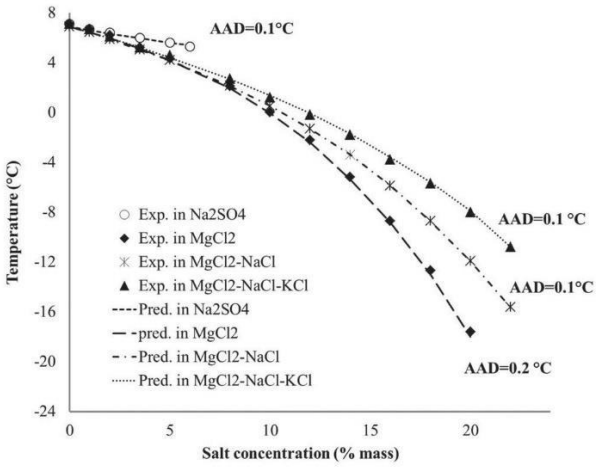

Figure 9. Experimental and predicted dissociation temperature of CPH in the presence of salts according to the ABOC approach.

DOI: 10.1021/acs.iecr.8b02796
Ind. Eng. Chem. Res. 2018, 57, 14774−14783

Table 4. Average Deviation (°C or K) of Different Approaches for Predicting CPH Equilibrium Temperature

approach	Na_2SO_4	$MgCl_2$	$MgCl_2$−NaCl	$MgCl_2$−NaCl−KCl	NaCl[26]	KCl[26]	NaCl−KCl[26]	$CaCl_2$[26]
SFPD	0.1	0.5	0.4	0.3	0.3	0.3	0.2	0.4
HLS	0.3	0.7	0.4	0.2	0.5	0.3	0.3	0.5
Kihara	0.2	0.5	0.2	0.1	0.2	0.1	0.1	0.2
ABOC	0.1	0.2	0.1	0.1	0.1	0.1	0.1	0.2

with the experimental data. Importantly, the average absolute deviation is about 0.1 °C for either Na_2SO_4 or $MgCl_2$−NaCl or $MgCl_2$−NaCl−KCl and about 0.2 °C for $MgCl_2$. This shows that the ABOC approach reproduces successfully the experimental dissociation temperatures for CPH in all cases. Note that it was already the recommended approach to use in the previous study[26] and here its application is extended. These superb new results solidify that activity-based occupancy correlation (ABOC) is the best method to use so far.

Discussion on the Models. The average deviation between the present simulation and the experimental data and from Ho-Van et al.[26] are listed in Table 4. Note that HLS deviations for the former systems (NaCl, KCl, or $MgCl_2$) have been calculated and are presented in Appendix III. As highlighted in this table, all three approaches can reproduce acceptably the CPH phase equilibrium temperature. The average deviations are reported to be less than or equal to 0.7 °C in all brine systems.

In addition, the Kihara (except for $MgCl_2$) and ABOC methods predict satisfactorily the CPH formation temperature. As stated by Ho-Van et al.,[26] the weakness of the Kihara method is that it requires Kihara potential integration. This can lead to different final values depending on the calculation code, and it is also influenced by the use of the Antoine equation for CP vapor pressure. Consequently, the ABOC approach is the strongest model to achieve a rapid and consistent CPH equilibrium temperature from different brine systems.

Finally, HLS correlation, while being also useful and very simple to use, seems to be less versatile in terms of systems (especially $MgCl_2$) since it is based on effective mole fraction. However, this correlation seems promising because of the excellent results the authors obtained for gas hydrates. Maybe new developments of this correlation for heavier nongaseous guest molecules, such as cyclopentane, are necessary to provide a more accomplished tool.

■ CONCLUSION

The dissociation temperature of CPH in four different brine systems Na_2SO_4, $MgCl_2$, $MgCl_2$−NaCl, or $MgCl_2$−NaCl−KCl were determined experimentally following two different procedures: quick and slow. First essential approximations on CPH phase equilibrium data were obtained by the quick procedure, and then more trustworthy and consistent measurements were provided by the slow dissociation. A temperature gap between the dissociation temperatures following two procedures was observed. Because the quick procedure is likely to misjudge the correct value, its recorded measurements were hence slightly higher than the right dissociation point in all brine systems tested.

Results also point to the fact that the CPH dissociation temperature decreased considerably with increasing brine concentration due to two well-known phenomena: clustering and salting-out. In addition, differing brine systems show dissimilar effects on the dissociation temperature: Na_2SO_4 exhibits the smallest effect at concentrations from 1% to 5% mass while $MgCl_2$ displays the great impact on the equilibria at concentrations above 8%. Furthermore, the equilibrium temperatures in the brine system of $MgCl_2$−NaCl are reported to be lower than those in the brine system of $MgCl_2$−NaCl−KCl at any salt concentration. This means the effect of NaCl on the phase equilibria is stronger than the effect of KCl. In addition, the eutectic point of the four-phase system Na_2SO_4 + H_2O, $Na_2SO_4{\cdot}10H_2O$, CP, and CPH was also recorded at 6% mass Na_2SO_4 at 5.3 °C.

Lastly, four thermodynamic approaches were employed, including the novel HLS correlation from Hu et al.[42,43] to predict CPH dissociation temperatures. Simulated results show that all four approaches reproduced adequately the CPH dissociation temperature with an average deviation less than 0.7 °C. However, the activity-based occupancy correlation (ABOC) method is overall better. This is the recommended method to achieve rapid and reliable equilibrium temperatures of CPH in different brine systems, with a deviation less than 0.2 °C.

■ APPENDIX I: MOLALITY, EFFECTIVE MOLE FRACTION, AND WATER ACTIVITY

See Table A1.

■ APPENDIX II: USE OF HLS CORRELATION WITH HU ET AL. COEFFICIENTS

The first thing we did when utilizing HLS correlation was to use the Hu et al. parameter.[42] Since cyclopentane is the guest, and not methane or another light hydrocarbon, and since CPH forms structure II, the second work from Hu et al.[43] was considered. In this effort, the sII hydrate suppression temperature is written:

$$\left(\frac{\Delta T}{T_0 T}\right)_{II} = \alpha\left(\frac{\Delta T}{T_0 T}\right)_{I} = \alpha(C_1 X + C_2 X^2 + C_3 X^3) \tag{13}$$

and the hydrate dissociation temperature can be calculated from

$$T = T_0\left[1 + \alpha\left(\frac{\Delta T}{T_0 T}\right)_{I} T_0\right]^{-1} \tag{14}$$

Coefficient α can be estimated from the ratio β_2/β_1:

$$\frac{\left(\frac{\Delta T}{T_0 T}\right)_{II}}{\left(\frac{\Delta T}{T_0 T}\right)_{I}} = \frac{R\ln(a_w)\left(\frac{n}{\Delta H_{diss}}\right)_{II}}{R\ln(a_w)\left(\frac{n}{\Delta H_{diss}}\right)_{I}} = \frac{\beta_2}{\beta_1} = \alpha \tag{15}$$

This ratio accounts for the hydrate structure difference. Two methods are suggested by Hu et al.[43] to calculate α: optimization from experimental data, or evaluation of hydrate dissociation heat and hydration number for direct calculation. We first tried to optimize α as a constant using equilibrium data in {water + NaCl} solutions, using C_1, C_2, and C_3

DOI: 10.1021/acs.iecr.8b02796
Ind. Eng. Chem. Res. 2018, 57, 14774−14783

Table A1. Molality, Effective Mole Fraction (X), and Water Activity (Calculated by Using PHREEQC[46] at the CPH Dissociation Point) of Four Brine Solutions

	Na_2SO_4			$MgCl_2$			$MgCl_2$–NaCl			$MgCl_2$–NaCl–KCl		
salinityin (% mass)	molality	X	water activity	molality	X	water activity	molality	X	water activity	molality	X	water activity
0	0.000	0.000	1.000	0.000	0.000	1.000	0.000	0.000	1.000	0.000	0.000	1.000
1	0.071	0.005	0.997	0.106	0.008	0.995	0.140	0.007	0.995	0.138	0.006	0.995
2	0.144	0.010	0.994	0.214	0.015	0.990	0.282	0.014	0.989	0.279	0.013	0.990
3.5	0.255	0.018	0.990	0.381	0.027	0.981	0.501	0.025	0.980	0.496	0.022	0.982
5	0.371	0.027	0.986	0.553	0.039	0.971	0.727	0.036	0.971	0.720	0.032	0.973
6	0.449	0.032	0.984									
8				0.913	0.065	0.947	1.201	0.058	0.949	1.190	0.053	0.955
10				1.167	0.082	0.926	1.535	0.074	0.932	1.520	0.067	0.941
12				1.432	0.101	0.902	1.884	0.090	0.913	1.865	0.082	0.926
14				1.710	0.119	0.872	2.249	0.107	0.892	2.227	0.097	0.909
16				2.001	0.139	0.838	2.631	0.125	0.867	2.606	0.113	0.890
18				2.306	0.159	0.798	3.032	0.143	0.839	3.003	0.129	0.870
20				2.626	0.181	0.751	3.453	0.161	0.808	3.420	0.146	0.847
22							3.896	0.181	0.773	3.858	0.163	0.822

Table A2. Optimization with α Constant and Not Constant

			optimization					
			α constant			α not constant		
salinity (% mass)	X	T_{exp}, °C	α	$\frac{\Delta T}{T_0 T}$	T_{pred}, °C	α	$\frac{\Delta T}{T_0 T}$	T_{pred}, °C
0	0.0000	7.1	1.036	0	7.1	1.036	0	7.1
1	0.0062	6.4	1.036	5.72184×10^{-6}	6.6	1.562	5.72184×10^{-6}	6.4
2	0.0125	5.9	1.036	1.13631×10^{-5}	6.2	1.350	1.13631×10^{-5}	5.9
3.5	0.0221	5	1.036	1.97746×10^{-5}	5.5	1.362	1.97746×10^{-5}	5.0
5	0.0319	4.4	1.036	2.828×10^{-5}	4.8	1.227	2.828×10^{-5}	4.4
8	0.0522	2.4	1.036	4.63777×10^{-5}	3.4	1.312	4.63777×10^{-5}	2.4
10	0.0662	0.9	1.036	6.00107×10^{-5}	2.3	1.345	6.00107×10^{-5}	0.9
12	0.0806	−0.7	1.036	7.56778×10^{-5}	1.1	1.350	7.56778×10^{-5}	−0.7
14	0.0955	−1.8	1.036	9.41771×10^{-05}	−0.4	1.243	9.41771×10^{-5}	−1.8
16	0.1108	−3.3	1.036	0.000116441	−2.1	1.181	0.000116441	−3.3
18	0.1267	−5.3	1.036	0.000143558	−4.1	1.151	0.000143558	−5.3
20	0.1430	−7.8	1.036	0.000176795	−6.6	1.133	0.000176795	−7.8
22	0.1599	−10.2	1.036	0.000217627	−9.6	1.079	0.000217627	−10.2
23	0.1685	−11.3	1.036	0.000241416	−11.3	1.039	0.000241416	−11.3
				AAD	**0.8**		**AAD**	**0.0**

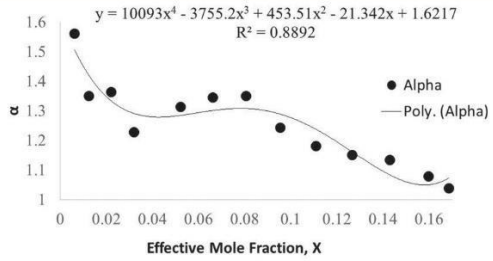

Figure A1. α vs effective mole fraction.

parameters from Hu et al.[42] In our opinion, results were not satisfactory (AAD = 0.8; see Table A2).

Then, we optimized α for each equilibrium point, trying to find a correlation under the form $\alpha = \alpha(X)$. Table A2 presents the results for water + NaCl system. Obviously, since α was adjusted for each point, the new predictions fit perfectly the experimental data (AAD = 0). However, our intention was to find an appropriate correlation for α, under the form $\alpha = \alpha(X)$. Unfortunately, the correlation $\alpha(X)$ remains under a complicated form, as shown in Figure A1. This is why we chose to optimize C_1, C_2, C_3 coefficients in our work.

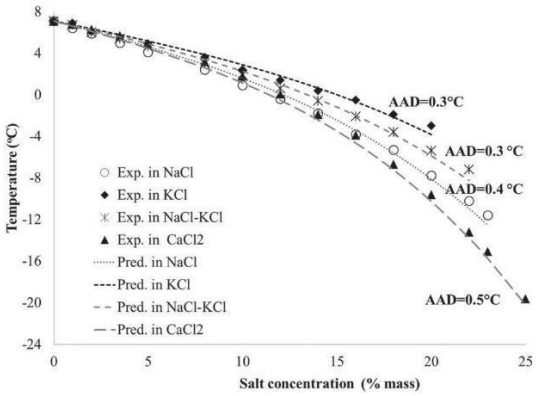

Figure A2. Experimental and predicted dissociation temperature of CPH in the presence of salts according to HLS approach for the four brine solutions from Ho-Van et al.[26]

DOI: 10.1021/acs.iecr.8b02796
Ind. Eng. Chem. Res. 2018, 57, 14774–14783

APPENDIX III: HLS APPROACH COMPARED TO THE FORMER SYSTEM[26]

Predicted results present a higher AAD than ABOC method. However, to fit C_1, C_2, and C_3 parameters, data from {water + $MgCl_2$} solutions were also considered. Since there is a deviation from the standard behavior ($\frac{\Delta T}{T_0 T} = f(X)$), it is probable that the use of such data lead to worse simulation results for NaCl, KCl, or $CaCl_2$ salts (Figure A2).

AUTHOR INFORMATION

Corresponding Authors

*E-mail: son.ho-van@emse.fr (S. Ho-Van).
*E-mail: bouillot@emse.fr (B. Bouillot).

ORCID

Son Ho-Van: 0000-0001-7276-0517

Notes

The authors declare no competing financial interest.

ACKNOWLEDGMENTS

The authors thank Christopher Yukna very much for his advice on English and proofreading.

NOTATION

a = water activity [−] or Kihara parameter, spherical nucleus radius [m], coefficients [−] for the correlation of the change of molar specific heat
b = coefficient linear temperature dependency of the heat capacity [J mol^{-1} K^{-2}], and coefficients [−] for the correlation of the change of molar specific heat
C = fitted coefficient in the HLS approach
H = molar enthalpy [J mol^{-1}]
m = coefficient of the correlation of the cage occupancy
N = number of points of a given set of data
n = mole number, coefficient of the correlation of the cage occupancy
P = pressure [Pa]
p = coefficient of the correlation of the cage occupancy
R = universal gas constant [8.314472 m^2 kg s^{-2} K^{-1} mol^{-1}]
T = temperature [K]
x = mole fraction
X = effective mole fraction
z = ion charge number

GREEK LETTERS

ε, Kihara parameter, maximum attraction potential [−]
μ, chemical potential [J mol−1]
υ, number of cavities per molecules of water [−]
θ, occupation rate of cavity/gas
σ, Kihara parameter, distance between the molecules and the cavity wall, at null potential [m]
α, Hu−Lee−Sum parameter accounts for the hydrate structure difference [−]
β, Hu−Lee−Sum parameter represents the hydrate suppression temperature [−]

SUPERSCRIPTS

H, hydrate phase
L, liquid phase
β, hypothetical reference phase for the hydrate phase corresponding to empty lattice

REFERENCES

(1) Sloan, E. D., Koh, C. A. *Clathrate Hydrate of Natural Gases*, 3rd ed.; CRC Press: Boca Raton, FL, 2008.
(2) Babu, P.; Linga, P.; Kumar, R.; Englezos, P. A review of the hydrate based gas separation (HBGS) process forcarbon dioxide pre-combustion capture. *Energy* **2015**, *85*, 261−279.
(3) Ho, L. C.; Babu, P.; Kumar, R.; Linga, P. HBGS (hydrate based gas separation) process for carbon dioxide capture employing an unstirred reactor with cyclopentane. *Energy* **2013**, *63*, 252−259.
(4) Burnol, A.; Thinon, I.; Ruffine, L.; Herri, J. M. Influence of impurities (nitrogen and methane) on the CO2 storage capacity as sediment-hosted gas hydrates - Application in the area of the Celtic Sea and the Bay of Biscay. *Int. J. Greenhouse Gas Control* **2015**, *35*, 96−109.
(5) Taheri, Z.; Shabani, M. R.; Nazari, K.; Mehdizaheh, A. Natural gas transportation and storage by hydrate technology: Iran case study. *J. Nat. Gas Sci. Eng.* **2014**, *21*, 846−849.
(6) Douzet, J.; Kwaterski, M.; Lallemand, A.; Chauvy, F.; Flick, D.; Herri, J. M. Prototyping of a real size air-conditioning system using a tetra-n-butylammonium bromide semiclathrate hydrate slurry as secondary two-phase refrigerant - Experimental investigations and modelling. *Int. J. Refrig.* **2013**, *36* (6), 1616−1631.
(7) Darbouret, M.; Cournil, M.; Herri, J. M. Rheological study of TBAB hydrate slurries as secondary two-phase refrigerants. *Int. J. Refrig.* **2005**, *28* (5), 663−671.
(8) Ogoshi, H.; Takao, S. Air-Conditioning System Using Clathrate Hydrate Slurry. *JFE Tech Rep.* **2004**, 3 (3), 1−5.
(9) Duc, N. H.; Chauvy, F.; Herri, J. M. CO2 capture by hydrate crystallization - A potential solution for gas emission of steelmaking industry. *Energy Convers. Manage.* **2007**, *48* (4), 1313−1322.
(10) Li, S.; Fan, S.; Wang, J.; Lang, X.; Wang, Y. Clathrate hydrate capture of CO2 from simulated flue gas with cyclopentane/water emulsion. *Chin. J. Chem. Eng.* **2010**, *18* (2), 202−206.
(11) Englezos, P. Clathrate Hydrates. *Ind. Eng. Chem. Res.* **1993**, *32*, 1251−1274.
(12) Javanmardi, J.; Moshfeghian, M. Energy consumption and economic evaluation of water desalination by hydrate phenomenon. *Appl. Therm. Eng.* **2003**, *23* (7), 845−857.
(13) Park, K.; Hong, S. Y.; Lee, J. W.; et al. A new apparatus for seawater desalination by gas hydrate process and removal characteristics of dissolved minerals ($Na^+Mg^{2+}Ca^{2+}K^+B^{3+}$). *Desalination* **2011**, *274* (1−3), 91−96.
(14) Lee, H.; Ryu, H.; Lim, J.-H.; Kim, J.-O.; Dong Lee, J.; Kim, S. An optimal design approach of gas hydrate and reverse osmosis hybrid system for seawater desalination. *Desalin. Water Treat.* **2016**, *57* (19), 9009−9017.
(15) He, T.; Nair, S. K.; Babu, P.; Linga, P.; Karimi, I. A. A novel conceptual design of hydrate based desalination (HyDesal) process by utilizing LNG cold energy. *Appl. Energy* **2018**, *222* (March), 13−24.
(16) Babu, P.; Nambiar, A.; He, T. A Review of Clathrate Hydrate Based Desalination to Strengthen Energy-Water Nexus. *ACS Sustainable Chem. Eng.* **2018**, *6*, 8093.
(17) Xu, H.; Khan, M. N.; Peters, C. J.; Sloan, E. D.; Koh, C. A. Hydrate-Based Desalination Using Cyclopentane Hydrates at Atmospheric Pressure. *J. Chem. Eng. Data* **2018**, *63*, 1081.
(18) Subramani, A.; Jacangelo, J. G. Emerging desalination technologies for water treatment: A critical review. *Water Res.* **2015**, *75*, 164−187.
(19) Colten, S. L.; Lin, F. S.; Tsao, T. C.; Stern, S. A.; Barduhn, A. J. Hydrolysis losses in the hydrate desalination process: rate measurements and economic analysis. *Desalination* **1972**, *11* (1), 31−59.
(20) Sugi, J.; Saito, S. Concentration and demineralization of sea water by the hydrate process. *Desalination* **1967**, 3 (1), 27−31.
(21) McCormack, R. A. *N.G. A. Build and operate clathrate desalination pilot plant*; Bureau of Reclamation, U.S. Dept. of the Interior, 1998.
(22) McCormack, R. A.; Andersen, R. K. *Clathrate desalination plant preliminary research study*; Bureau of Reclamation, U.S. Dept. of the Interior, 1995.

DOI: 10.1021/acs.iecr.8b02796
Ind. Eng. Chem. Res. 2018, 57, 14774−14783

(23) Bradshaw, R. W.; Dedrick, D. E.; Simmons, B. A.; Great-House, J. A.; Cygan, R. T.; Majzoub, E. H. *Desalination Utilizing Clathrate Hydrates*; Sandia National Laboratories, 2008.
(24) Max, M. D. Hydrate desalination for water purification. US 6991722 B2, 2006.
(25) Englezos, P. The Freeze Concentration Process and its Applications. *Dev. Chem. Eng. Miner. Process.* **1994**, *2* (1), 3−15.
(26) Ho-Van, S.; Bouillot, B.; Douzet, J.; Maghsoodloo, S.; Herri, J.-M. Experimental Measurement and Thermodynamic Modeling of Cyclopentane Hydrates with NaCl, KCl, CaCl2 or NaCl−KCl Present. *AIChE J.* **2018**, *64*, 2207.
(27) Corak, D.; Barth, T.; Høiland, S.; Skodvin, T.; Larsen, R.; Skjetne, T. Effect of subcooling and amount of hydrate former on formation of cyclopentane hydrates in brine. *Desalination* **2011**, *278* (1−3), 268−274.
(28) Han, S.; Shin, J. Y.; Rhee, Y. W.; Kang, S. P. Enhanced efficiency of salt removal from brine for cyclopentane hydrates by washing, centrifuging, and sweating. *Desalination* **2014**, *354*, 17−22.
(29) Han, S.; Rhee, Y. W.; Kang, S. P. Investigation of salt removal using cyclopentane hydrate formation and washing treatment for seawater desalination. *Desalination* **2017**, *404*, 132−137.
(30) Cai, L. Desalination via formation of binary clathrate hydrates. Ph.D. Thesis, Princeton University, NJ, 2016.
(31) Lv, Y.-N.; Wang, S.-S.; Sun, C.-Y.; Gong, J. Chen G-J. Desalination by forming hydrate from brine in cyclopentane dispersion system. *Desalination* **2017**, *413*, 217−222.
(32) McAuliffe, C. Solubility in Water of Paraffin, Cycloparaffin, Olefin, Acetylene, Cycloolefin, and Aromatic Hydrocarbons1. *J. Phys. Chem.* **1966**, *70* (4), 1267−1275.
(33) Dean, J. A. LANGE'S HANDBOOK OF CHEMISTRY. *Mater. Manuf. Processes* **1990**, *5* (4), 687−688.
(34) Han, H.; Dong, O.; Li, D.; Zeng, D. Phase diagram of the NaCl−MgCl2−H2O system at 25−75°C and its application for MgCl2 · 6H2O purification. *Russ J. Phys. Chem. A* **2017**, *91* (7), 1255−1259.
(35) Huang, Q.; Lu, G.; Wang, J.; Yu, J. Thermal decomposition mechanisms of MgCl2·6H2O and MgCl2·H2O. *J. Anal. Appl. Pyrolysis* **2011**, *91* (1), 159−164.
(36) Sloan, D.; Koh, C. A.; Sum, A. K. *Natural Gas Hydrate in Flow Assurance*; Gulf Professional Pub./Elsevier, 2011.
(37) Sabil, K. M.; Román, V. R.; Witkamp, G. J.; Peters, C. J. Experimental observations on the competing effect of tetrahydrofuran and an electrolyte and the strength of hydrate inhibition among metal halides in mixed CO_2 hydrate equilibria. *J. Chem. Thermodyn.* **2010**, *42* (3), 400−408.
(38) Cha, M.; Hu, Y.; Sum, A. K. Methane hydrate phase equilibria for systems containing NaCl, KCl, and NH_4Cl. *Fluid Phase Equilib.* **2016**, *413*, 2−9.
(39) Wells, R. C.. Sodium sunphate: its sources and uses. *United States Geol Surv.* **1923**.
(40) Hildebrand, J. H.; Scott, R. L. *Regular Solutions*; Prentice-Hall: Englewood Cliffs, NJ, 1962.
(41) Miyawaki, O.; Saito, A.; Matsuo, T.; Nakamura, K. Activity and activity coefficient of water in aqueous solutions and their relationships with solution structure parameters. *Biosci., Biotechnol., Biochem.* **1997**, *61* (3), 466−469.
(42) Hu, Y.; Lee, B. R.; Sum, A. K. Universal correlation for gas hydrates suppression temperature of inhibited systems: I. Single salts. *AIChE J.* **2017**, *63*, 5111.
(43) Hu, Y.; Lee, B. R.; Sum, A. K. Universal correlation for gas hydrates suppression temperature of inhibited systems: II. Mixed salts and structure type. *AIChE J.* **2018**, *64* (6), 2240−2250.
(44) van der Waals, J. H.; Platteeuw, J. C. Clathrate solutions. *Adv. Chem. Phys.* **2007**, *2*, 1−57.
(45) Nakajima, M.; Ohinura, R.; Mori, Y. H. Clathrate hydrate formation from cyclopentane-in-water emulsions. *Ind. Eng. Chem. Res.* **2008**, *47* (22), 8933−8939.
(46) Parkhurst, D. L., Appelo, C. A. J., 1999. User's guide to PHREEQC (version 2) − a computer program for speciation, batchreaction, one-dimensional transport, and inverse geochemical calculations, *Water-Resour. Invest. Rep. 99-4259*; US Geol. Survey: Denver, CO.
(47) Pieroen, A. Gas hydrates - approximate relations betvveen heat. *Recl des Trav Chim des Pays-Bas.* **1955**, *74*, 995−1002.
(48) Herri, J.-M.; Bouchemoua, A.; Kwaterski, M.; Fezoua, A.; Ouabbas, Y.; Cameirao, A. Gas hydrate equilibria for CO2−N2 and CO2−CH4 gas mixtures—Experimental studies and thermodynamic modelling. *Fluid Phase Equilib.* **2011**, *301* (2), 171−190.
(49) Parrish, W. R.; Prausnitz, J. M. Dissociation Pressures of Gas Hydrates Formed by Gas Mixtures. *Ind. Eng. Chem. Process Des. Dev.* **1972**, *11* (1), 26−35.

DOI: 10.1021/acs.iecr.8b02796
Ind. Eng. Chem. Res. 2018, 57, 14774−14783

6.4. Paper IV: Crystallization mechanisms and rates of Cyclopentane Hydrates formation in Brine

S.Ho-Van, B.Bouillot, D.Garcia, J.Douzet, A.Cameirao, S.Maghsoodloo-Babakhani, J.M.Herri

Published in: Chemical Engineering & Technology, 42, 28 March 2019.

Summary: Beside thermodynamic phase equilibria, better understanding the crystallization mechanisms of CPH when salts are present may prove to be crucial for desalination via CPH formation. However, there are not so many experimental studies on CPH formation mechanisms at the interface and the mass diffusion rate. Hence, in this contribution we focused on CPH formation mechanisms. Unlike other studies, the experimental set-up is a non-agitated small system. Moreover, this system geometry presents a vertical interface between water and cyclopentane, allowing a top view of the lateral hydrate growth under a microscope. There are two objectives: to measure the CPH formation rate from a two-phase system (brine-cyclopentane), and to discuss the crystallization mechanism. Moreover, both the influence on the aqueous electrolyte (four salt systems including NaCl, NaCl-$MgCl_2$, NaCl-KCl-$MgCl_2$, Na_2SO_4) and the influence of initial subcooling (2.5°C, 3.5°C, and 4.3°C) on the hydrate layer growth rate were explored.

Chemical Engineering & Technology Research Article 1

Son Ho-Van[1,2,*]
Baptiste Bouillot[1,*]
Daniel Garcia[3]
Jérome Douzet[1]
Ana Cameirao[1]
Saheb Maghsoodloo-Babakhani[1]
Jean-Michel Herri[1]

Crystallization Mechanisms and Rates of Cyclopentane Hydrates Formation in Brine

Clathrate hydrates most often grow at the interface between liquid water and another fluid phase (hydrocarbon) acting as a provider for the hydrate guest molecules, and some transfer through this shell is required for the hydrate growth to proceed, thus self-limiting the reaction rate. An optical microscope and a horizontal reaction cell are utilized to capture the shell growth phenomenology and to estimate the hydrate layer growth rates from sequential pictures. Cyclopentane (CP) is chosen as the hydrate-forming molecule to obtain hydrates at low pressure. Experimental hydrate layer growth rates are provided for the CP+brine system, using various combinations of salts and degrees of subcooling.

Keywords: Brine, Clathrate hydrates, Crystallization, Cyclopentane, Mass transfer

Received: December 20, 2018; *revised:* March 25, 2019; *accepted:* March 27, 2019

DOI: 10.1002/ceat.201800746

Supporting Information available online

1 Introduction

Clathrate hydrates are ice-like and non-stoichiometric compounds consisting of water molecules forming polyhedral hydrogen-bonded cavities that enclose guest molecules such as CO_2, CH_4, C_2H6, C_3H_8, or even cyclopentane (CP) [1]. The clathrate hydrates usually form at high pressures and at low temperatures depending on the guest molecules. These compounds have been widely studied over decades to understand and prevent hydrate plugging in pipelines [2]. More recently, clathrate hydrates have gained increasing attention due to their many potential applications, e.g., gas transportation [3–5], gas storage [6–12], gas separation [13–15], refrigeration [16, 17], or desalination [18–23].

In order to develop innovative clathrate hydrate-based techniques, and to better manage hydrate formation in multiphase flow, not only the formation conditions, phase equilibrium, are necessary, but also the crystallization mechanisms: nucleation, growth, agglomeration. In former studies, our group focused on cyclopentane hydrates (CPHs) for water treatment/desalination application [18, 19]. The formation temperature in brine have therefore been experimentally obtained and modeled. The present contribution focuses on CPH formation mechanisms and rates using a small unstirred cell under microscope.

CPHs form structure II clathrates at 7.1 °C under atmospheric pressure. They are composed of 17 water molecules per cyclopentane (CP) molecule. Since CP is not miscible with water (solubility of 156 mg L^{-1} at 25 °C [24]), the hydrate formers can be easily separated in a hydrate-based industrial application. Moreover, CPH formation from water+liquid CP may be viewed as a model analogue of gas hydrate crystallization in a water-oil emulsion under mild conditions. Therefore, it is an interesting system to study hydrate crystallization mechanisms, especially the mass transfer of the former species in the different phases, without the need of a pressurized experimental setup.

In literature, many studies addressed mass transfer phenomena in clathrate hydrate formation [25–41]. In the most usual case, crystallization occurs at an interface between water and another liquid phase, acting as a reservoir of the guest species. Therefore, specific attention has been paid to mass transfer phenomena through this interface and the crystal layer that is formed. In quiescent systems, the crystalline layer prevents direct contact between water and guest molecules and inhibits the hydrate formation (hydrate crust, or hydrate shell [34, 42, 43]. Hence, the mass transfer of water and/or guest molecules across the hydrate layer is a potential rate-limiting factor that controls the hydrate growth. Understanding the mass transfer through the hydrate layer is thus needed.

It is worth mentioning here the early experimental studies that addressed the crystal growth rates and mass transfer rates through the hydrate layer [31, 44–50], provide models [25, 26, 28, 34, 35, 41, 51], or perform molecular dynamics (MD) simulations [33, 38]. The pioneering work of Mori and co-workers [25, 26] explored theoretically the evolution of a hydrate layer thickness at the interface between water and another non-miscible phase of guest molecules. They showed

[1]Son Ho-Van, Dr. Baptiste Bouillot, Dr. Jérome Douzet, Prof. Ana Cameirao, Dr. Saheb Maghsoodloo-Babakhani, Prof. Jean-Michel Herri
son.ho-van@emse.fr, bouillot@emse.fr
Univ Lyon, Mines Saint-Etienne, CNRS, UMR 5307 LGF, Centre SPIN, 42023 Saint-Etienne, France.

[2]Son Ho-Van
Hanoi University of Mining and Geology, Oil Refinery and Petrochemistry Department, Duc Thang, Bac Tu Liem, 100000 Hanoi, Vietnam.

[3]Prof. Daniel Garcia
Univ Lyon, Univ Jean Moulin, Univ Lumière, Univ Jean Monnet, Mines Saint-Etienne, ENTPE, INSA Lyon, ENS Lyon, CNRS, UMR 5600 EVS, Centre SPIN, 42023 Saint-Etienne, France.

that a porous solid plate model is more realistic than the diffuse layer model due to the permeability of the hydrate film [25, 26].

Later, in 2010, Sun et al. [34] measured experimentally the hydrate film growth, and considered Mori's model as well as later developments [52]. They concluded that the numerous factors that influence the hydrate layer growth rate in the model make the simulation very challenging. Abe et al. [45] also measured the hydrate film thickness growth for CO_2 hydrates and suggested a model.

In the 2010s, Davies and co-workers conducted valuable experimental studies. They used differential scanning calorimetry to study the mass transfer phenomenon through a methane hydrate layer at the interface in a non-mixing reactor [31]. They found that, at the beginning, hydrate layers at the gas-water interface are porous, which facilitates the mass transfers. In addition, the mass transfer rate decreases with time, as the hydrate cavities are filled with guest molecules. Then, they utilized Raman spectroscopy to investigate the mass transfer mechanism across a methane hydrate film [30]. Their results indicate that water molecules are more moveable than gas molecules in the hydrate layer, and that the growth of gas hydrate is controlled by the water movement in the interior of the hydrate layer.

Li and co-workers [47, 48] reported the crystal growth of gas hydrates from methane and ethane by suspending a single gas bubble in water under different subcoolings. Their showed that, under low subcoolings, the growth of hydrate film is dominated by the film thickening, but not by lateral film growth. Importantly, simple kinetic models, as function of the subcoooling, could be used to correlate film growths

In another of their efforts, Li et al. [32] also concluded that hydrate layer thickening at the interface is controlled by the outward transport of water across hydrate film, while the lateral growth is controlled by the mass transfer of the guest molecules (CH_4). Based on this understanding, Kishimoto et al. [35] proposed a correlation of the lateral growth rate to mass transfer resistance.

Very recently, Sun et al. [28, 41, 51] published a remarkable series of articles for modeling the mass transfer in the hydrate shell. While their system is not a liquid-liquid interface, they looked into details at the interface between gas bubbles and water, and of course the inside of the hydrate shell. All mass and heat transfer equations are written to represent the problem of the hydrate crystallization and growth at the interface between a gas bubble and water.

Finally, MD simulations have been performed to investigate molecular mobility of interstitial H_2O molecules across hydrate cavities [33, 38]. Liang et al. [38] found that interstitial molecules diffusion could be a key mechanism for the mass transfer of H_2O across the hydrate layer. Lo et al. [33] explored the water vacancy-driven diffusion of guest molecules through a hydrate layer, and estimated the guest (CO_2) diffusivity.

This short review highlights two important points: there are not so many experimental studies that provide a local insight of the hydrate growth at the interface and furnish interface growth rates, or mass diffusion rates. Secondly, the modeling of such system is challenging.

In the present contribution, a new experimental insight is explored. Unlike other studies, the experimental setup is a non-agitated small system. Moreover, this system geometry presents a vertical interface between water and cyclopentane, allowing a top view of the lateral hydrate growth under a microscope. There are two objectives: to measure the CPH formation rate from a two-phase system (brine-CP) and to discuss the crystallization mechanism. Moreover, both the influence on the aqueous electrolyte (four saline solutions of NaCl, NaCl-$MgCl_2$, NaCl-KCl-$MgCl_2$, Na_2SO_4) and the influence of subcooling (2.5 °C, 3.5 °C, and 4.3 °C) on the hydrate layer growth rate are explored.

2 Experimental

2.1 Materials

In this study, materials utilized were CP (purity 98 %), NaCl (purity 99.5 %), KCl (purity 99.0 %), Na_2SO_4 (purity 99.5 %), and $MgCl_2$ (purity 99.5 %). They were all provided by Sigma-Aldrich. Distilled water (conductivity $< 0.055\ \mu S\ cm^{-1}$) was obtained from a Milli-Q® decontamination system.

2.2 Experimental Apparatus

A simplified diagram of the experimental apparatus is presented in Fig. 1.

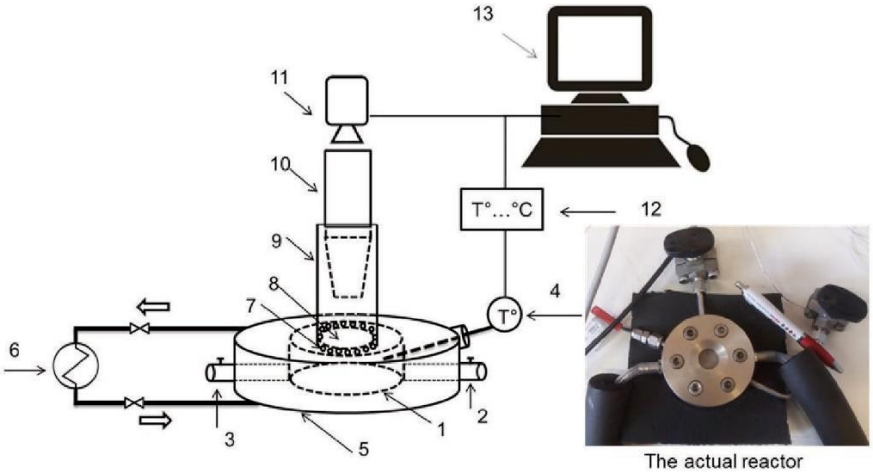

Figure 1. Schematic illustration of the experimental setup. (1) Reactor cell; (2) input line; (3) output line; (4) temperature probe; (5) cooling jacket; (6) chiller; (7) silica gel; (8) sapphire window; (9) transparent tube; (10) objective lens; (11) camera; (12) temperature transmitter; (13) computer.

The main device is a horizontal jacketed reactor cell (1) with a volume of approximately 1.23 mL. This reactor has a height of 4 mm and a diameter of 19.8 mm. The metal on the bottom and sides is Inox. On the top is a sapphire window (8) in order to observe the system with both optical microscope and Raman microscope. A chiller (6), Ministat 240-Huber, with a temperature uncertainty of 0.02 °C, is used to control the temperature of the inside solution. The coolant is a mixture of water and absolute ethanol (50 vol %). A temperature probe (4) is utilized to monitor the solution temperature inside the reactor. Input (2) and output (3) lines are employed to introduce and also reject the solutions. A microscope (10), connected to a camera (11), is applied to observe the crystallization of CPH through the transparent sapphire window (8) from the top.

Because this reactor system usually works at low temperatures (0–5 °C), grams of silica gel (7) is used to absorb condensed water on the sapphire window surface in order to achieve quality images of crystallization. A transparent tube (9) prevents air from coming in and to keep a low humidity level above the reactor. Digital data, including microscope images and temperature, are recorded by a computer (13) with a rate of 1 image every 5 min.

2.3 Experimental Protocol

Before each experiment, the chiller is set at a temperature according to the desired subcooling. Note that subcooling, ΔT_{sub}, is defined as the difference between the equilibrium temperature and the reactor temperature. The equilibrium temperatures of CPH in the presence of salts have been previously determined [18, 19] and are presented in Tab. 1.

At the beginning, in order to reduce the induction time of the crystallization, the saline solution is first used to form CPHs in a bigger reactor (1 L). Once CPHs have been crystallized that way, hydrates are melted slowly with the heating rate of 0.1 °C/h, up to a temperature of 0.1 °C above equilibrium. At this temperature, there should not be any crystals left the brine. Therefore, the initial salt concentration is regenerated in a solution close to thermodynamic equilibrium with liquid CP. Then, approximately 0.8 mL of the solution is introduced into the reactor cell, followed by about 0.4 mL of CP. It was observed that this "water preconditioning" reduces significantly the induction time, compared to the use of fresh water [53].

After stabilization, the microscope is set up to observe the water-CP interface. Photos are taken every 5 min. Hopefully, the first moments of the nucleation and growth are detected. After 3–4 days, when CPH has formed completely, videos are made from the previous pictures.

Table 1. CPH equilibrium temperatures in different solutions [18, 19].

Solutions	Salinity[a,b,c] [% mass]	CPH equilibrium temperature, ± 0.1 °C
Pure water	–	7.1
NaCl	3.5	5.5
NaCl-$MgCl_2$	3.5	5.1
NaCl-KCl-$MgCl_2$	3.5	5.2
NaCl-KCl-$MgCl_2$	5.0	4.6
Na_2SO_4	3.5	6.0
Na_2SO_4	5.0	5.6

[a)]Uncertainty due to weighing: ± 0.002 % mass; [b)]uncertainty due to drying oven: ± 0.2 % mass; [c)]relative uncertainty due to ion chromatography: 1.5 % (see the Supporting Information from Ho-Van et al. [19] for all uncertainty estimations).

3 Experimental Observations

3.1 Experimental Layout

Seven mixtures at three different initial subcoolings have been considered. However, since the occurrence of crystallization is not easy to detect, only three selected runs will be discussed in detail: in pure water at 2.5 °C subcooling and in 5 % equi-mass mixture of NaCl-KCl-$MgCl_2$ at 3.5 °C and 4.3 °C initial subcoolings. Note that in the case of salty mixtures only the initial subcooling is controlled. Indeed, with the CPH crystallization, the average salinity of the aqueous phase changes, hence the subcooling. Since the objective is to investigate a batch process at constant temperature, this is normal.

The recorded videos are available online in Supplementary Information (S1, S2, and S3). The speed of these videos is 50 min s^{-1}, corresponding to ten frames per second, one picture every 5 min. Video S1: CPH formation in pure water at a subcooling of 2.5 °C; Video S2: CPH formation in the presence of NaCl-KCl-$MgCl_2$ 5 % mass at a subcooling of 3.5 °C; Video S3: CPH formation in the presence of NaCl-KCl-$MgCl_2$ 5 % mass at a subcooling of 4.3 °C.

3.2 Interface Shape

Note that whatever the experiment, the interface shape is similar (see Fig. 2). Unexpectedly, the interface is not horizontal, even though CP is less dense than water. In the next pictures, the CP phase is always on the left side, while the water phase is on the right side. The liquid-liquid interface clearly separates the two phases into two adjacent regions. Apparently, there is neither a droplet of CP into water, nor a droplet of water into CP. This is based on two observations: from microscopy, since the interface can be optically tracked by varying the focal length, but also from Raman spectroscopy. Indeed, the use of a Raman spectroscope (Horiba Xplora, 532 nm laser) demonstrated that close to the CP-water interface no water was detected between the substrates and the CP phase (points A and B in Fig. 2), and likewise no CP was found between the substrates and brine (point C). Therefore, this infers that there is not a water film, respectively CP film, on the substrate surfaces in the CP phase, respectively brine phase.

The physicochemistry of components and interfaces (water-CP, walls-components) is the probable reason for such an atypical geometry. Of course,

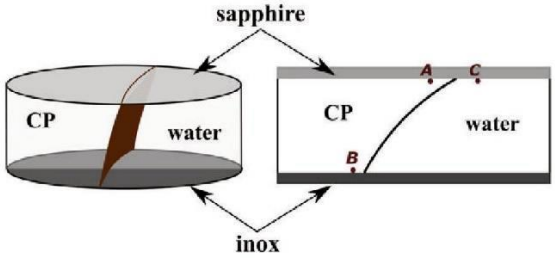

Figure 2. Schematic illustration of the hydrate layer in the reactor cell.

the configuration of the reactor cell (non-mixing, flat cylinder-shaped, very small height of 4 mm), is the plausible reason why phase inversion cannot occur. Moreover, note that the process of injection is another determining factor. Indeed, the sequence of injection can change the final geometry. Hence, in order to obtain a clear vertical interface, water is always injected first.

3.3 Experimental Phenomenology of CPH Growth

Fig. 3 illustrates the first interesting example (see also video S1). At the beginning appears a CPH nucleus in the CP phase (left). Apparently, some droplets of water are present in the CP phase, but without hydrates around them. There seem to be no CP droplets in the water phase, although this is possible out of the focus range. From stage 1 to stage 3, a triangle-shaped "single crystal" grows, and successive layers can be observed on the surfaces of the crystal with time. At some moment, there is a sudden crystallization at the water-CP interface. Remember that the solution is supersaturated in CPH, and it is not surprising to see such a rapid crystallization in the first steps. Then, step 4 corresponds to a growth of this interface, mostly toward the CP phase. Note that the growth is not parallel to the interface, showing some preferential direction for the crystallization in the beginning. Later on, the interface shifts abruptly to the right. Then, in step 5, there is a CPH growth on both sides, but still quicker toward the CP phase. At this moment, the growth seems to be parallel to the interface at the same speed in all directions although there are some exceptions. Moreover, there is a dramatic decrease of the crystal growth on the left side at the very end of the video, when the hydrate thickness is the most significant. In the end, CPH covers the whole observation plan.

A second key experiment (video S2) is illustrated in Fig. 4. This presents the CPH formation from a 5 % equi-mass NaCl-KCl-$MgCl_2$ aqueous phase under a 3.5 °C initial subcooling. In this scenario, a CPH nucleus appears first in the water phase. Its shape is hexagonal and it grows rapidly in the very beginning, hence its size stabilizes (step 2 to 3). During step 3, there is still a quick crystallization at the water-CP interface and the interface becomes rough. The CPH is then observed to grow volumetrically, but mostly at the expense of the CP liquid phase, between a CP-CPH "front" moving to the left and a CPH-bine interface that almost preserves the position of the initial CP-brine contact. Suddenly (stage 4), the CP-CPH and the CPH-brine interfaces are shifted to the right, and their abrupt displacement is recorded thanks to the fixed reference given by the early formed hexagonal crystal. Later on, the crystallization proceeds mostly towards the CP phase (stage 5) and less towards the water phase, layer by layer, at a varying speed with occasional oscillation. Finally, note that the crystallization does not occur only in the microscope focus plan, showing blurry crystals above or beneath the crystallization front.

A last experiment, illustrated in Fig. 5, explores the same system as before, but at 4.3 °C initial subcooling. Most of the previous observations can be made and the steps are quite similar. However, there is one exception. Between the quick interface crystallization and the interface shift+growth, there is a significant pause. This suggests that the interface shift is required by the volumetric changes linked to the ongoing reaction, but delayed by some mechanical resistance to displacement: a shear stress must be superrated for the displacement to occur; hence,

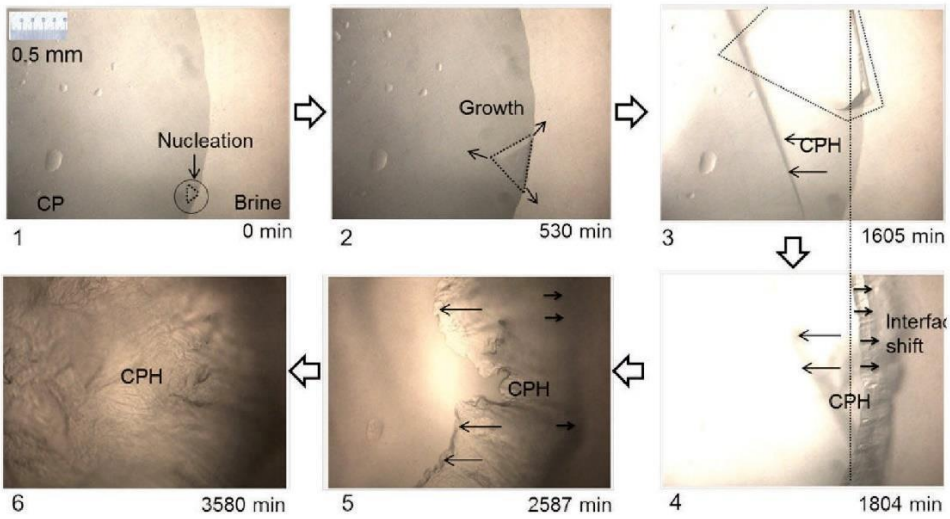

Figure 3. CPH crystallization mechanism in the presence of pure water at an initial subcooling of 2.5 °C. Arrows indicate moving crystal boundaries (single crystal growth) or interface boundary.

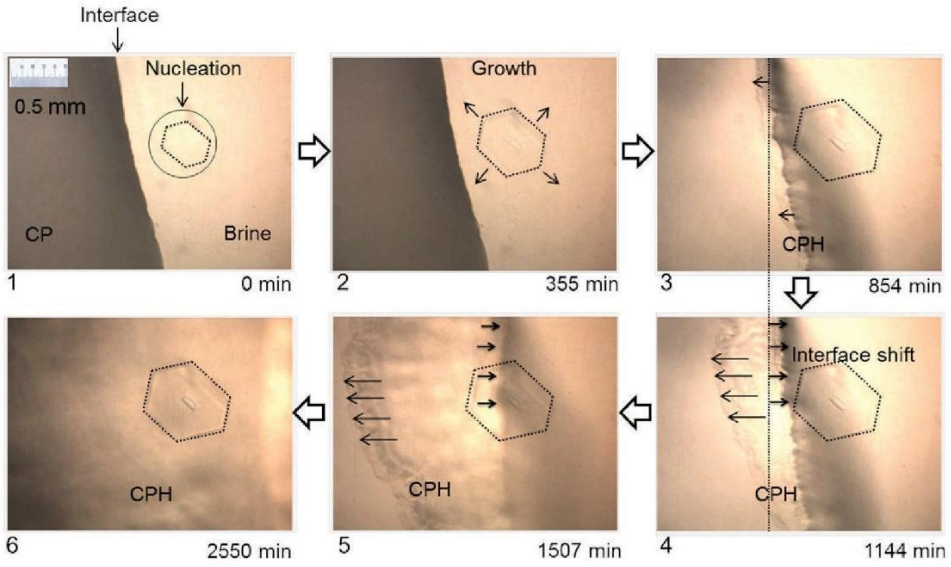

Figure 4. CPH crystallization mechanism in the presence of NaCl-KCl-$MgCl_2$ 5 % at an initial subcooling of 3.5 °C.

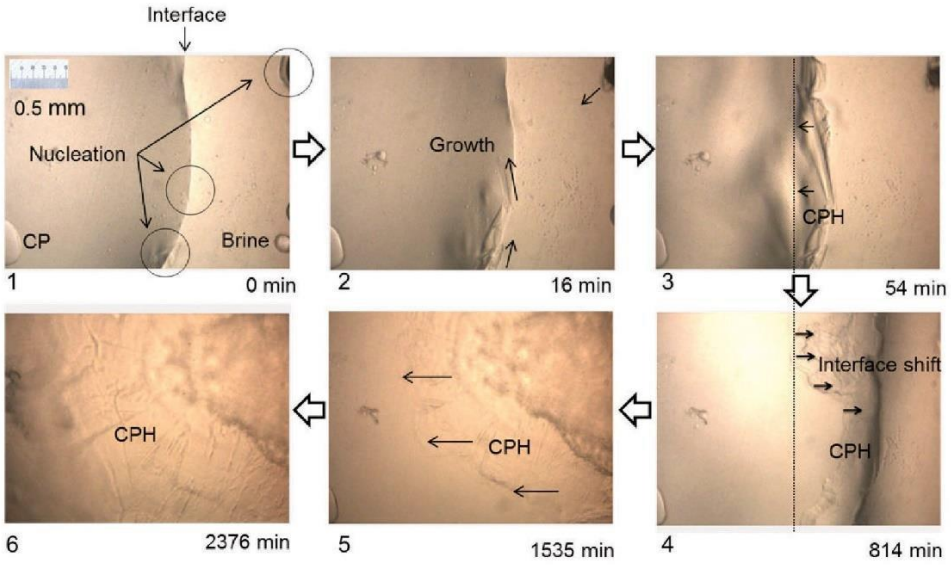

Figure 5. CPH crystallization mechanism in the presence of NaCl-KCl-$MgCl_2$ 5 % at an initial subcooling of 4.3 °C.

when this stress is superated, the volume variation is accomodated and the interface shifts to the right.

After this breakage, a growth toward the CP phase is observed. Again, the reaction front remains roughly parralel to the interface, although maybe not everywhere. Also, at this moment, the interface shift is not really noticeable. Nevertheless, at the final stage (6) there is a blurry phase growing and moving to the right, probably CPH formation above or below.

3.4 CPH-Forming Front Displacement Velocity

In order to investigate the kinetics of CPH formation and the effect of salt on it, the hydrate layer growth rate of crystallization with and without salts under different concentrations and initial subcoolings has been measured. The CHP layer growth rate, r[1)], is calculated as follows:

$$r = l/\Delta t \tag{1}$$

where l is the distance of the hydrate layer propagation and Δt is the duration for this propagation.

Note that this rate r represents either a time-averaged growth rate by considering a significant Δt, or an instantaneous growth rate if $r(t) = \mathrm{d}l/\mathrm{d}t$. If the first possibility is easy to obtain, the calculation of the instantaneous hydrate layer growth rate $r(t)$ is more complicated since all the pictures need to be workable,

1) List of symbols at the end of the paper.

which is rarely the case. In these calculations, the starting time is taken to be the beginning of the crystallization at the CP-water interface. Moreover, an average of ten different values of the CPH layer thickness *l* at ten different positions of the CP-CPH interfaces in plain view was used. Fig. 6 illustrates such calculations in pure water at subcooling of 4.3 °C. Tab. 2 provides numerical results of all calculations for different salt concentrations and initial subcoolings, for three crystallization durations (60, 120, and 180 min).

As expected, the CPH layer growth rate decreases over time. Note that our results agree well with the report on the thickness of CPH versus time according to Taylor et al. [54]. Their results pointed out that the CPH layer thickening rate is much higher at the first 0–40 min compared to that in the later periods. Moreover, the CPH layer growth rate increases with higher initial subcooling for all aqueous systems, i.e., pure water and electrolyte solutions, at the same crystallization time.

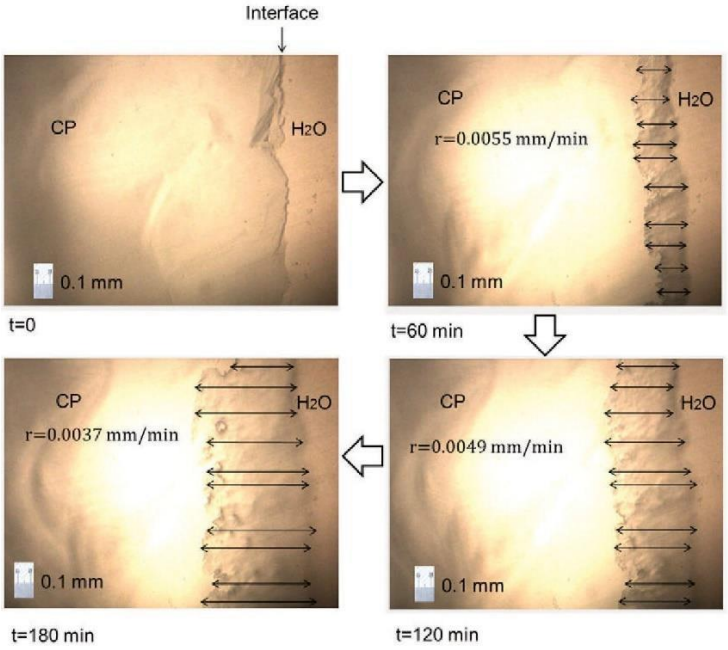

Figure 6. CPH layer growth rate in pure water at 4.3 °C subcooling after 60 min, 120 min, and 180 min.

4 Discussion on Growth Rate of the CPH Layer

Subcooling is related to the driving force of crystallization. Therefore, when it rises, the speed of hydrate formation increases. This phenomenon has been described in details elsewhere [47, 48, 52–57].

The decrease of the CPH layer growth rate with longer crystallization time can be explained as follows. In salty systems, the driving force for the crystallization changes with the increase in salinity due to the water consumption. Hence, the growth rate is expected to decline with time. Also, a reduction of the growth speed is expected because of the increasing resistance to the mass transfers, especially water.

Furthermore, the growth rates in pure water are almost unsurprisingly higher than those in the presence of salts (except

Table 2. Measured CPH layer growth rate in different subcoolings and brine solutions with time.

Aqueous solution	Propagation rate [mm min^{-1}]								
	ΔT_{sub} = 2.5 °C			ΔT_{sub} = 3.5 °C			ΔT_{sub} = 4.3 °C		
	60 min	120 min	180 min	60 min	120 min	180 min	60 min	120 min	180 min
Pure water	0.0035± 0.0004	0.0033± 0.0002	0.0025± 0.0002	0.0039± 0.0002	0.0036± 0.0004	NA	0.0055± 0.0005	0.0049± 0.0006	0.0037± 0.0003
NaCl 3.5 % mass	0.0024± 0.0004	0.0018± 0.0003	0.0016± 0.0003	0.0040± 0.0005	0.0027± 0.0002	0.0020± 0.0002	0.0046± 0.0005	NA	NA
NaCl-$MgCl_2$ 3.5 % mass	0.0022± 0.0003	0.0017± 0.0005	0.0014± 0.0002	0.0045± 0.0005	0.0033± 0.0002	NA	0.0063± 0.0006	0.0041± 0.0006	0.0041± 0.0008
NaCl-KCl-$MgCl_2$ 3.5 % mass	0.0013± 0.0002	0.0009± 0.0002	NA	0.0039± 0.0008	0.0031± 0.0004	0.0023± 0.0004	0.0054± 0.0005	NA	NA
NaCl-KCl-$MgCl_2$ 5 % mass	0.0011± 0.0002	0.0008± 0.0001	0.0006± 0.0001	0.0016± 0.0003	0.0011± 0.0004	0.0008± 0.0001	0.0020± 0.0001	0.0014± 0.0002	0.0011± 0.0001
Na_2SO_4 3.5 % mass	0.0009± 0.0001	0.0006± 0.0001	0.0006± 0.0001	0.0018± 0.0003	0.0012± 0.0002	0.0010± 0.0002	0.0020± 0.0002	0.0013± 0.0003	0.0010± 0.0001
Na_2SO_4 5 % mass	0.0009± 0.0001	0.0007± 0.0001	0.0005± 0.0001	0.0040± 0.0001	0.0038± 0.0001	NA	0.0089± 0.0002	NA	NA

NA: not available

some particular cases: NaCl-$MgCl_2$ 3.5 % mass and Na_2SO_4 5 % mass) at the same subcoolings and the same crystallization durations. Indeed, salts affect strongly both thermodynamics [19, 44, 57–59] and kinetics [57] of CPH formation. The exception of the NaCl-$MgCl_2$ 3.5 % mass and Na_2SO_4 5 % mass found no explanation.

In addition, the hydrate layer growth rates are different when considering different brines at the same subcoolings and same crystallization durations. This indicates that salts affect differently the kinetic of CPH formation. The reason of this variance is probably attributed to the varying role of each salt in inhibiting the hydrate formation. Indeed, each salt has a different influence in weakening water hydrogen bonding and reducing CP solubility due to the difference in their solubility, salt ion charge density, and importantly water activity [60, 61]. Thus, the formation of CPH is inhibited differently. Certainly, more experiments are required to discover clearly each salt effect on the kinetic of CPH formation.

In comparison with literature, the lateral CPH crystal growth rate in pure water reported by Sakemoto et al. [44] is approximately 0.0070–0.0090 mm min^{-1} and 0.0420–0.0440 mm min^{-1} under a subcooling of 2.4 °C and 4.2 °C, respectively. While the first number is quite similar to our results (0.0035 mm min^{-1} under 2.5 °C subcooling at 60 min), the second is significantly lower (0.0055 mm min^{-1} under 4.3 °C subcooling at 60 min; see Tab. 2). Nevertheless, their system is different and presents a horizontal interface in a bigger volume.

However, in the presence of NaCl 3.5 % mass, Sakemoto et al. [44] described a lateral hydrate crystal growth rate of 0.0020–0.0040 mm min^{-1} at an initial subcooling of 2.4 °C, while our result calculation is 0.0024 mm min^{-1} at 2.5 °C initial subcooling at 60 min. If the numbers are quite close (same order of magnitudes), this also reveals that the hydrate crystal growth rates reported by Sakemoto et al. [44] are usually higher than our observations.

In addition, Taylor el al. [54] found that the final CPH film thickness is approximately 15.2 µm after 200 min at a subcooling of 3.8 °C in pure water, indicating that the average thickening rate is about 0.076×10^{-3} mm min^{-1}. Our observations (see Tab. 2) present a rate of 0.0039 mm min^{-1} at 60 min or 0.0036 mm min^{-1} at 120 min at a subcooling of 3.5 °C, which is much higher than the value from Taylor et al. [54].

These differences in the growth rate can be attributed to the varying experimental systems and calculations. Indeed, Sakemoto et al. [44] defined this growth rate as an 1D growth rate of an individual hydrate crystal. Taylor el al. [54] measured the final thickness of the interface in 200 min; the average thickening rate was then calculated based on this measurement. In this work, the 2D polycrystalline hydrate layer growth rate in the nearly perpendicular direction to the water surface and CP surface are considered and not individual crystals (Fig. 6). It was found that the hydrate growth in the perpendicular direction to the liquid-liquid interface is usually much more difficult than the lateral growth rate due to the slow mass transfer rate of water and CP across the hydrate layer [53]. Consequently, the growth rates from this present study and from Taylor et al. [54] are significantly lower than the individual crystal growth rate stated by Sakemoto et al. [44].

5 Discussion on CPH Formation Mechanism

5.1 First Steps

To begin with, Fig. 7 is an attempt to capture what has been observed previously, except the apparent "hydrate breakage".

At the beginning, some nucleation sites near the liquid-liquid interface, either in the CP phase or in the water phase, are witnessed. Sometimes, it can even be in both phases (1st stage). Indeed, the nucleation site is stochastic [62–65], and any impurity near the liquid-liquid interface can be an active nucleation center. Moreover, remember that the water used for the experiment is taken from a previous crystallization process. Therefore, it is a possibility that hydrate clusters remain in the water phase. Also, traces of CP (CP droplets) on the reactor surfaces, in the water phase, could be a source of formation of an individual hydrate crystal (hexagonal-shaped in Figs. 4 and 7). Note that water droplets can also be present in the CP phase, leading to a nucleus (see Fig. 5). In order to simplify the mechanism, Fig. 7 only illustrates a nucleus in the water phase.

Later, the individual crystal grows by consuming the CP traces and water (2nd stage). Quick nucleation and crystallization along the interface are then observed (3rd stage). At this stage, the individual crystal also reaches its final size since all CP traces could have been consumed completely.

The hydrate layers grow mainly toward the CP phase by consuming initially water in the brine phase and also water dissolved in the CP phase near the liquid-liquid interface. Obvi-

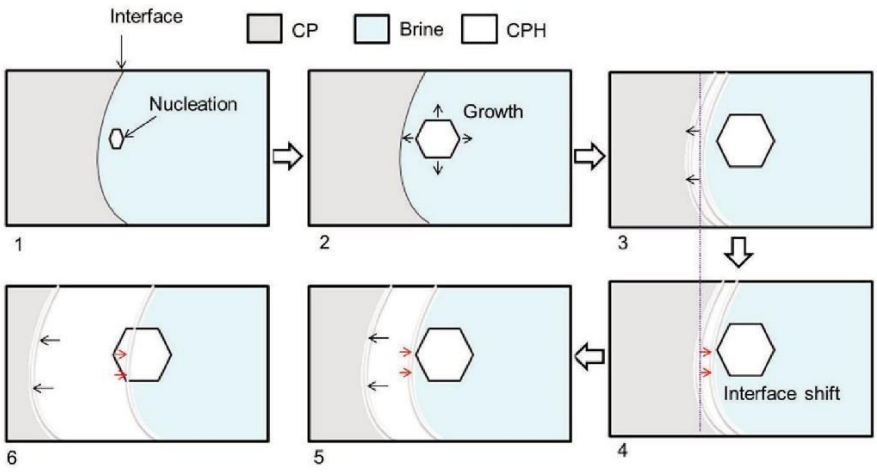

Figure 7. Simplified scheme of the CPH crystallization mechanism near the interface in the reactor cell.

ously, over time, the dissolved water becomes depleted, and water is hence required from the aqueous phase (discussed further). Accordingly, at the very beginning of the interface growth, there is only a growth toward the CP phase, without interface shift. This comes right after.

5.2 Interface Shift and Volume Balance

In the next step, a shift of the water-CPH interface into the water phase is observed (4th stage). This is probably due to water consumption of crystallization. Remember that CP and water form a hydrate structure II according to the following reaction:

$$C_5H_{10}(CP)+17H_2O = C_5H_{10}\cdot 17H_2O(CPH) \quad (2)$$

Eq. (2) indicates that one CP molecule combines with 17 H_2O molecules to form one CPH cell. Therefore, a large quantity of water is needed for the crystallization, leading to a strong reduction in the volume of the water phase.

Considering the volume balance of the process, the density of pure water at 4 °C is close to 1000 kg m^{-3}; the presence of salt reduces this density. The standard density of CP is 745 kg m^{-3}. Finally, the CPH density, assuming full occupancy of large SII cavities, can be calculated to be 950–970 kg m^{-3} [42, 53, 59, 66, 67], i.e., less than the liquid water phase and more than liquid CP. Based on these estimations, the volume balance is:

$$\begin{cases} V_m(CPH) - [V_m(CP) + 17.V_m(H_2O)] = \Delta V_m \\ 3.92.10^{-1} - (9.41.10^{-2} + 17.1.8.10^{-2}) = 8.33.10^{-3}\,\text{L mol}^{-1} \end{cases} \quad (3)$$

Therefore, the volume diminution is about 8.3 mL mol^{-1} of CP. Since about 0.8 mL of water is here introduced, a quick estimation indicates a volume change up to 22 µL, for full water consumption. As a consequence, this volume reduction can induce a pressure difference between the two sides of the interface.

This pressure difference has not been investigated in details. An evaluation would be needed in the case of a modeling. Nevertheless, this is consistent with the study of Li et al. [32] reporting the sinking of the hydrate shell into a water droplet, in which the difference between inner and outside pressure is large enough due to the water permeation out the shell for crystallization. Finally, it is not surprising that an interface shift toward the water phase is observed since the ration 17:1 for the CPH crystallization corresponds to nearly 76 % of the volume change occurring in the water phase.

5.3 Hydrate Growth and Mass Transfers

Later (step 5 and after), CPH hydrates grow into both CP and water phases. However, the growth toward CP phase is obviously faster than toward the water phase. As discussed before, more water is needed to form CPH. However, this growth on both sides demonstrates that water and CP molecules are migrating, probably inside the hydrate phase.

Several possibilities can be considered. First, the water phase and CP phase could always be in contact. This particular situation corresponds to a droplet of water in CP, or the opposite, based on the kind of substrates. This is the situation of the lateral growth on a substrate. Martínez de Baños et al. [53, 68] especially observed and discussed this phenomenon for the water-CP system. They stated an initial fast crystallization at the water-CP interface and then the spread of a "halo" on a non-hydrophobic substrate due to a water film between the substrate and CP. In this case, the limiting factor is the water mass transfer in this film. Since such water film was not observed in our system (see the discussion in the interface shape section), this is not the mechanism expected in our apparatus, unless the water amount is so low that the Raman signal was not noticeable.

In the other case, CPHs form a wall between the two former species. The growth is therefore not substrate-related. In order to observe the CPH growth, on both sides, former molecules need to cross this wall. Accordingly, this means that the hydrate phase is a porous medium, which is not surprising and documented in literature [30].

CPH is believed to be more water-wettable than oil-wettable [59, 69–71]. This means that the water phase can move more easily through the hydrate pore network than CP, proving much more water for crystallization on the CP side than CP molecules for crystallization on the brine side, hence, a faster growth toward the CP phase. This observation agrees well with other studies. Davies et al. [30] stated that the hydrate layer is initially porous and could be favorable to water transportation. In addition, their results illustrate that the growth of hydrate is controlled by the water migration within the hydrate layer. Also, Li et al. [32] concluded from their experiments that hydrate layer thickening is controlled by the outward mass transport of water molecules across the hydrate layer.

Another transport mechanism can be considered. Based on MD simulations, Liang et al. [38] reported that the interstitial water molecules are mobile entities in the interior of a hydrate. However, to our knowledge, the rate difference of these two phenomena was not determined.

An illustration of the mass transfers across the hydrate layer is presented in Fig. 8. With the hydrate formation at the interface appears a wall. The interface is all covered by the polycrystalline hydrate and then it plays as a barrier to prevent water from contacting with guest molecules (CP) and vice versa, as described in literature [2, 15, 34, 51, 54, 72–77]. Moreover, the salinity then increases in the bulk of the brine phase because salts are excluded from hydrate crystallization [29, 78, 79]. Consequently, this shifts the thermodynamic equilibrium temperatures of CPH to lower values [18, 19, 23]. Thus, the crystallization rate is expected to decrease over time [44, 57].

Fig. 8 illustrates that there are three likely mass movements through the hydrate layer: water advection toward the CP phase, CP advection toward the water phase, and salt diffusion toward the water phase. Water and/or CP phase migration can only be driven by pressure gradients within the phase of interest. By definition, a capillary pressure is not a pressure gradient, but a pressure difference between two phases. Water or CP molecules (not phases) can migrate by transport and/or diffusion within any phase. The drive for advective transport is

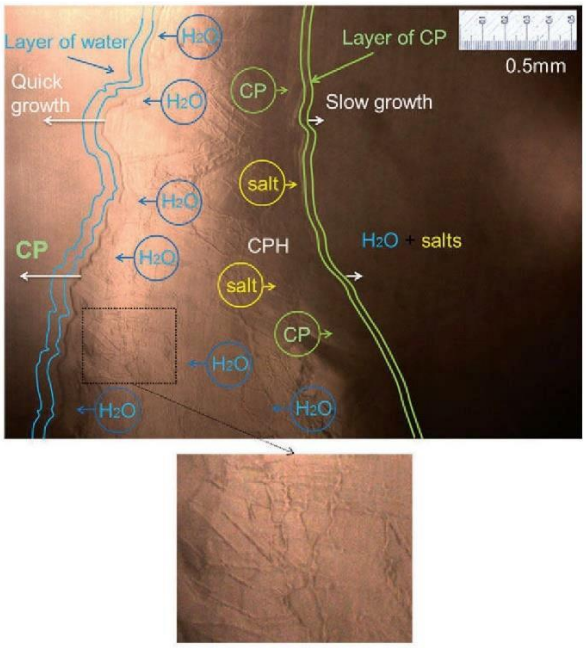

Figure 8. Mass transfer at the CPH interface during crystallization. Illustration based on the photo taken from the experiment with NaCl-KCl-$MgCl_2$ 5 % mass at subcooling 2.5 °C.

always a pressure gradient and a chemical potential gradient for diffusive transport. Salt diffusion is driven by a gradient in the chemical potential of salt in the bulk of the brine phase and in the filled hydrate pores. Certainly, because salts are excluded from crystallization, the salinity in the hydrate layer is higher than in the bulk of the brine phase. Thus, salts tend to diffuse from hydrate pores to the saline solution.

As aforementioned, there is a quick growth toward the CP phase and a slow growth toward the water phase. This difference in growth rate is related to the migration mechanism of CP and water, and also salts across the hydrate layer. Indeed, during the hydrate formation process, individual hydrate grains can join and generate some spaces, pores or channels (unknown geometry), in which water, CP, and salts can move. According to the numerical study of Mori et al. [25], water permeates through the hydrate layer filling the capillaries. The driving force for this water permeation is the capillary pressure due to the hydrophilic characteristic of the hydrate surface. This agrees well with the observations using Raman spectrometry reported by Davies et al. [30]. They stated that in the polycrystalline hydrate layer numerous visible pores or capillaries could be the mean for a relatively high mobility of water and also hydrate former migration across the hydrate film.

Our observations also indicate that the growth of the crystal interface remained somehow parallel to the CPH interface, without any obvious preferential direction, especially in the later steps. Therefore, it is suspected that the limiting step is the mass transfer. Pressure gradients are not negligible. When it is not the case, probably in the first steps, the crystal growth can be expected to be the limiting step.

From a modeling viewpoint, mass transfer across a hydrate layer was numerically explored by Mori et al. [25, 26]. However, these authors assumed a steady state where the hydrate layer forms at the hydrate-guest interface while it melts at the water-hydrate interface, thus maintaining a constant thickness. This is not strictly speaking a growth model, but the main concept to be retained from Mori et al. [25] is that because gas hydrates are (presumably) hydrophilic, the pore space in the hydrate layer is (presumably) water-wet, hence, a sustained water flux may be driven through the hydrate layer by the combined effects of capillary forces and the consumption of water at the hydrate-guest interface where the hydrate actually grows.

In the presence of salts, there is also a mass transport of salt within the hydrate layer and the bulk of saline water. Obviously, hydrate formation excludes salt into saline solution and enhances the local salinity. Recently, the salt diffusion during hydrate crystallization was investigated by Meyer et al. [29]. Salt diffusion is necessary to observe the hydrate growth in the CP-CPH interface and therefore needs to be taken into account.

6 Conclusions

The formation of CPH between brine and liquid CP was explored using a non-agitated small cell and a microscope allowing a top view of the processes and an evaluation of the lateral growth rate of the hydrate layer, under a variety of driving conditions and brine compositions.

The phenomenology of hydrate formation involves the early formation of single crystals near the interface as a likely consequence of the preparation of the system where water is produced by melting previous CP hydrate. The volumetric hydrate layer formation starts by a flash nucleation at the water-CP interface, then hydrate grows mostly, but not exclusively, at the expense of the CP phase, at a rate well recorded by the position of the CP-CPH interface in time. Accordingly, the hydrate formation mechanism involves the advective transfer of the water phase through the porous hydrate layer which is, presumably, water-wet.

Not surprisingly, the measured growth rates increase linearly with rising driving force (i.e., undercooling) and decreases with salt concentrations. This rate also declines with time, in relation to the increased thickness of the hydrate layer and its higher resistance to the water transfer.

The authors have declared no conflict of interest.

Symbols used

l	[mm]	distance of the hydrate layer propagation
r	[mm min^{-1}]	cyclopentane hydrates layer growth rate
t	[min]	hydrate layer propagation time
V_m	[L mol^{-1}]	molar volume

Abbreviations

CP	cyclopentane
CPH	cyclopentane hydrate
MD	molecular dynamics

References

[1] E. D. Sloan, C. A. Koh, *Clathrate Hydrate of Natural Gases*, 3rd ed., CRC Press, Boca Raton, FL **2008**.

[2] E. D. Sloan, C. A. Koh, A. K. Sum, *Natural Gas Hydrates in Flow Assurance*, Gulf Professional Publishing, Oxford, UK **2011**.

[3] H. Mimachi, S. Takeya, A. Yoneyama, K. Hyodo, T. Takeda, Y. Gotoh, T. Murayama, *Chem. Eng. Sci.* **2014**, *118*, 208–213. DOI: https://doi.org/10.1016/j.ces.2014.07.050

[4] Z. Taheri, M. R. Shabani, K. Nazari, A. Mehdizaheh, *J. Nat. Gas Sci. Eng.* **2014**, *21*, 846–849. DOI: https://doi.org/10.1016/j.jngse.2014.09.026

[5] E. D. Sloan, *Nature* **2003**, *426*, 353–359. DOI: https://doi.org/10.1038/nature02135

[6] Z. G. Sun, R. Wang, R. Ma, K. Guo, S. Fan, *Energy Convers. Manage.* **2003**, *44*, 2733–2742. DOI: https://doi.org/10.1016/S0196-8904(03)00048-7

[7] J. Lee, Y. K. Jin, Y. Seo, *Chem. Eng. J.* **2018**, *338*, 572–578. DOI: https://doi.org/10.1016/J.CEJ.2018.01.054

[8] H. P. Veluswamy, W. I. Chin, P. Linga, *Int. J. Hydrogen Energy* **2014**, *39*, 16234–16243. DOI: https://doi.org/10.1016/j.ijhydene.2014.01.054

[9] M. Sarshar, A. H. Sharafi, *Desalin. Water Treat.* **2011**, *28*, 59–64. DOI: https://doi.org/10.5004/dwt.2011.2201

[10] A. Burnol, I. Thinon, L. Ruffine, J. M. Herri, *Int. J. Greenhouse Gas Control* **2015**, *35*, 96–109. DOI: https://doi.org/10.1016/j.ijggc.2015.01.018

[11] A. Galfré, M. Kwaterski, P. Braîntuas, A. Cameirao, J. M. Herri, *J. Chem. Eng. Data* **2014**, *59*, 592–602. DOI: https://doi.org/10.1021/je4002587

[12] S. Muromachi, H. D. Nagashima, J. M. Herri, R. Ohmura, *J. Chem. Thermodyn.* **2013**, *64*, 193–197. DOI: https://doi.org/10.1016/j.jct.2013.05.020

[13] L. C. Ho, P. Babu, R. Kumar, P. Linga, *Energy* **2013**, *63*, 252–259. DOI: https://doi.org/10.1016/j.energy.2013.10.031

[14] H. Liu, J. Wang, G. Chen, B. Liu, A. Dandekar, B. Wang, X. Zhang, C. Sun, Q. Ma, *Int. J. Hydrogen Energy* **2014**, *39*, 7910–7918. DOI: https://doi.org/10.1016/j.ijhydene.2014.03.094

[15] P. Babu, P. Linga, R. Kumar, P. Englezos, *Energy* **2015**, *85*, 261–279. DOI: https://doi.org/10.1016/j.energy.2015.03.103

[16] J. Douzet, M. Kwaterski, A. Lallemand, F. Chauvy, D. Flick, J. M. Herri, *Int. J. Refrig.* **2013**, *36*, 1616–1631. DOI: https://doi.org/10.1016/j.ijrefrig.2013.04.015

[17] M. Darbouret, M. Cournil, J. M. Herri, *Int. J. Refrig.* **2005**, *28*, 663–671. DOI: https://doi.org/10.1016/j.ijrefrig.2005.01.002

[18] S. Ho-Van, B. Bouillot, J. Douzet, S. Maghsoodloo Babakhani, J.-M. Herri, *Ind. Eng. Chem. Res.* **2018**, *57 (43)*, 14774–14783. DOI: https://doi.org/10.1021/acs.iecr.8b02796

[19] S. Ho-Van, B. Bouillot, J. Douzet, S. Maghsoodloo, J.-M. Herri, *Am. Inst. Chem. Eng. J.* **2018**, *64 (6)*, 2207–2218. DOI: https://doi.org/10.1002/aic.16067

[20] T. He, S. K. Nair, P. Babu, P. Linga, I. A. Karimi, *Appl. Energy* **2018**, *222*, 13–24. DOI: https://doi.org/10.1016/j.apenergy.2018.04.006

[21] S. H. B. Yang, P. Babu, S. F. S. Chua, P. Linga, *Appl. Energy* **2016**, *162*, 1131–1140. DOI: https://doi.org/10.1016/j.apenergy.2014.11.052

[22] P. Babu, A. Nambiar, T. He, *ACS Sustainable Chem. Eng.* **2018**, *6 (7)*, 1893–1907. DOI: https://doi.org/10.1021/acssuschemeng.8b01616

[23] S. Ho-Van, J. Douzet, D. Le-Quang, B. Bouillot, J.-M. Herri, in *Proc. of the Int. Conf. on Integrated Petroleum Engineering* (Eds: V. A. Tran et al.), Hanoi University of Mining and Geology, Hanoi **2016**, 150–157.

[24] C. McAuliffe, *J. Phys. Chem.* **1966**, *70*, 1267–1275. DOI: https://doi.org/10.1021/j100876a049

[25] Y. H. Mori, T. Mochizuki, *Chem. Eng. Sci.* **1997**, *52*, 3613–3616. DOI: https://doi.org/10.1016/S0009-2509(97)00169-3

[26] Y. H. Mori, T. Mochizuki, in *Proc. of the 2nd Int. Conf. on Natural Gas Hydrates* (Ed: J. P. Monfort), PROGREP-NGH, Toulouse **1996**, 267–274.

[27] Y. N. Lv, C. Y. Sun, B. Liu, G. J. Chen, J. Gong, *AIChE J.* **2017**, *63*, 1010–1023. DOI: https://doi.org/10.1002/aic.15436

[28] X. Sun, B. Sun, Z. Wang, L. Chen, Y. Gao, *Chem. Eng. Sci.* **2017**, *173*, 168–178. DOI: https://doi.org/10.1016/j.ces.2017.07.040

[29] D. W. Meyer, P. B. Flemings, D. Dicarlo, K. You, S. C. Phillips, T. J. Kneafsey, *J. Geophys. Res. Solid Earth* **2018**, *123 (7)*, 5350–5371. DOI: https://doi.org/10.1029/2018JB015748

[30] S. R. Davies, E. D. Sloan, A. K. Sum, C. A. Koh, *J. Phys. Chem. C* **2010**, *114*, 1173–1180. DOI: https://doi.org/10.1021/jp909416y

[31] S. R. Davies, J. W. Lachance, E. D. Sloan, C. A. Koh, *Ind. Eng. Chem. Res.* **2010**, *49*, 12319–12326. DOI: https://doi.org/10.1021/ie1017173

[32] S. L. Li, Y. F. Wang, C. Y. Sun, G. J. Chen, B. Liu, Z. Y. Li, Q. L. Ma, *Chem. Eng. Sci.* **2014**, *135*, 412–420. DOI: https://doi.org/10.1016/j.ces.2015.01.057

[33] H. Lo, M. T. Lee, S. T. Lin, *J. Phys. Chem. C* **2017**, *121*, 8280–8289. DOI: https://doi.org/10.1021/acs.jpcc.7b00853

[34] C. Y. Sun, B. Z. Peng, A. Dandekar, Q. L. Ma, G. J. Chen, *Annu. Rep. Prog. Chem. Sect. C: Phys. Chem.* **2010**, *106*, 77–100. DOI: https://doi.org/10.1039/b811053k

[35] M. Kishimoto, R. Ohmura, *Energies* **2012**, *5*, 92–100. DOI: https://doi.org/10.3390/en5010092

[36] C. Wang, X. Zhang, J. Li, L. Wang, L. Jioa, *Adv. Mater. Res.* **2013**, *616–618*, 902–906. DOI: https://doi.org/10.4028/www.scientific.net/AMR.616-618.902

[37] J. D. Sundramoorthy, K. M. Sabil, B. Lal, P. Hammonds, *Cryst. Growth Des.* **2015**, *15*, 1233–1241. DOI: https://doi.org/10.1021/cg501626h

[38] S. Liang, P. G. Kusalik, *J. Am. Chem. Soc.* **2011**, *133*, 1870–1876. DOI: https://doi.org/10.1021/ja108434h

[39] S. L. Li, C. Y. Sun, G. J. Chen, Z. Y. Li, Q. L. Ma, L. Y. Yang, A. K. Sum, *Chem. Eng. Sci.* **2014**, *116*, 109–117. DOI: https://doi.org/10.1016/j.ces.2014.04.009

[40] T. Mochizuki, Y. H. Mori, *Chem. Eng. Sci.* **2017**, *171*, 61–75. DOI: https://doi.org/10.1016/j.ces.2017.05.015

[41] X. Sun, B. Sun, Z. Wang, L. Chen, Y. Gao, *Int. J. Heat Mass Transfer* **2018**, *117*, 940–950. DOI: https://doi.org/10.1016/j.ijheatmasstransfer.2017.10.045

[42] N. Hobeika, M. L. Martinez De Baños, P. Bouriat, D. Broseta, R. Brown, in: *Gas Hydrates 1* (Eds: D. Broseta, L. Ruffine, A. Desmedt), Wiley-ISTE, London **2017**, 113–144. DOI: https://doi.org/10.1002/9781119332688.ch3

[43] D. Daniel-David, F. Guerton, C. Dicharry, J. P. Torré, D. Broseta, *Chem. Eng. Sci.* **2015**, *132*, 118–127. DOI: https://doi.org/10.1016/j.ces.2015.04.015

[44] R. Sakemoto, H. Sakamoto, K. Shiraiwa, R. Ohmura, T. Uchida, *Cryst. Growth Des.* **2010**, *10*, 1296–1300. DOI: https://doi.org/10.1021/cg901334z

[45] Y. Abe, X. Ma, T. Yanai, K. Yamane, *AIChE J.* **2016**, *62*, 4078–4089. DOI: https://doi.org/10.1002/aic.15304

[46] X. Ma, Y. Abe, A. Kaneko, K. Yamane, *Energy Procedia* **2014**, *63*, 5925–5932. DOI: https://doi.org/10.1016/j.egypro.2014.11.628

[47] S. Li, C. Sun, B. Liu, Z. Li, G. Chen, A. K. Sum, *Sci. Rep.* **2014**, *1–6*. DOI: https://doi.org/10.1038/srep04129

[48] S. Li, C. Sun, B. Liu, X. Feng, F. Li, L. Chen, G. Chen, *AIChE J.* **2013**, *59 (6)*, 2145–2154. DOI: https://doi.org/10.1002/aic.13987

[49] M. Mitarai, M. Kishimoto, D. Suh, R. Ohmura, *Cryst. Growth Des.* **2015**, *15*, 812–821. DOI: https://doi.org/10.1021/cg501613a

[50] K. Saito, M. Kishimoto, R. Tanaka, R. Ohmura, *Cryst. Growth Des.* **2011**, *11*, 295–301. DOI: https://doi.org/10.1021/cg101310z

[51] X. Sun, Z. Wang, B. Sun, L. Chen, J. Zhang, *Chem. Eng. J.* **2018**, *331*, 221–233. DOI: https://doi.org/10.1016/j.cej.2017.08.105

[52] B. Z. Peng, A. Dandekar, C. Y. Sun, H. Luo, Q. L. Ma, W. X. Pang, G. J. Chen, *J. Phys. Chem. B* **2007**, *111*, 12485–12493. DOI: https://doi.org/10.1021/jp074606m

[53] M. L. Martinez de Baños, *Ph. D. Thesis*, Université de Pau et des Pays de l'Adour, Pau, France **2015**.

[54] C. J. Taylor, K. T. Miller, C. A. Koh, E. D. Sloan, *Chem. Eng. Sci.* **2007**, *62*, 6524–6533. DOI: https://doi.org/10.1016/j.ces.2007.07.038

[55] E. M. Freer, M. S. Selim, E. D. S. Jr, *Fluid Phase Equilib.* **2001**, *185*, 65–75.

[56] K. Saito, A. K. Sum, R. Ohmura, *Society* **2010**, *7*, 7102–7103. DOI: https://doi.org/10.3390/En5010092

[57] M. Kishimoto, S. Iijima, R. Ohmura, *Ind. Eng. Chem. Res.* **2012**, *51*, 5224–5229. DOI: https://doi.org/10.1021/ie202785z

[58] G. Zylyftari, J. W. Lee, J. F. Morris, *Chem. Eng. Sci.* **2013**, *95*, 148–160. DOI: https://doi.org/10.1016/j.ces.2013.02.056

[59] H. Delroisse, J.-P. Torré, C. Dicharry, *Cryst. Growth Des.* **2017**, *17*, 5098–5107. DOI: https://doi.org/10.1021/acs.cgd.7b00241

[60] K. M. Sabil, V. R. Román, G. J. Witkamp, C. J. Peters, *J. Chem. Thermodyn.* **2010**, *42*, 400–408. DOI: https://doi.org/10.1016/j.jct.2009.09.012

[61] M. Cha, Y. Hu, A. K. Sum, *Fluid Phase Equilib.* **2016**, *413*, 2–9. DOI: https://doi.org/10.1016/j.fluid.2015.08.010

[62] P. Pirzadeh, P. G. Kusalik, *J. Am. Chem. Soc.* **2013**, *135*, 7278–7287. DOI: https://doi.org/10.1021/ja400521e

[63] E. Dendy Sloan Jr, *Nature* **2003**, *426*, 353–363.

[64] L. C. Jacobson, W. Hujo, V. Molinero, *J. Phys. Chem. B* **2010**, *114*, 13796–13807. DOI: https://doi.org/10.1021/jp107269q

[65] C. Duchateau, P. Glénat, T. E. Pou, M. Hidalgo, C. Dicharry, *Energy Fuels* **2010**, *24*, 616–623. DOI: https://doi.org/10.1021/ef900797e

[66] E. D. Sloan Jr, *Clathrate Hydrates of Natural Gases*, 2nd ed., Marcel Dekker, New York **2000**, Vol. 14.

[67] M. Nakajima, R. Ohinura, Y. H. Mori, *Ind. Eng. Chem. Res.* **2008**, *47*, 8933–8939. DOI: https://doi.org/10.1021/ie800949k

[68] M. L. M. De Banos, N. Hobeika, P. Bouriat, D. Broseta, E. Enciso, F. Clément, R. Brown, *Cryst. Growth Des.* **2016**, *16*, 4360–4373. DOI: https://doi.org/10.1021/acs.cgd.6b00471

[69] P. U. Karanjkar, A. Ahuja, G. Zylyftari, J. W. Lee, J. F. Morris, *Rheol. Acta* **2016**, *55*, 235–243. DOI: https://doi.org/10.1007/s00397-016-0911-1

[70] G. Aspenes, L. E. Dieker, Z. M. Aman, S. Høiland, A. K. Sum, C. A. Koh, E. D. Sloan, *J. Colloid Interface Sci.* **2010**, *343*, 529–536. DOI: https://doi.org/10.1016/j.jcis.2009.11.071

[71] E. P. Brown, S. Hu, J. Wells, X. Wang, C. A. Koh, *Energy Fuels* **2018**, *32*, 6619–6626. DOI: https://doi.org/10.1021/acs.energyfuels.8b00803

[72] M. Sugaya, Y. H. Mori, *Chem. Eng. Sci.* **1996**, *51*, 3505–3517. DOI: https://doi.org/10.1016/0009-2509(95)00404-1

[73] T. Y. Makogon, R. Larsen, C. A. Knight, E. D. Sloan, *J. Cryst. Growth.* **1997**, *179*, 258–262.

[74] X. Sen Li, C. G. Xu, Z. Y. Chen, H. J. Wu, *Energy* **2011**, *36*, 1394–1403. DOI: https://doi.org/10.1016/j.energy.2011.01.034

[75] P. U. Karanjkar, J. W. Lee, J. F. Morris, *Chem. Eng. Sci.* **2012**, *68*, 481–491. DOI: https://doi.org/10.1016/j.ces.2011.10.014

[76] P. Linga, R. Kumar, P. Englezos, *Chem. Eng. Sci.* **2007**, *62*, 4268–4276. DOI: https://doi.org/10.1016/j.ces.2007.04.033

[77] H. Dong, Z. Fan, B. Wang, S. Xue, J. Zhao, Y. Song, *Energy Procedia* **2017**, *105*, 4706–4712. DOI: https://doi.org/10.1016/j.egypro.2017.03.1020

[78] X. Liu, P. B. Flemings, *Earth Planet. Sci. Lett.* **2006**, *241*, 211–226. DOI: https://doi.org/10.1016/j.epsl.2005.10.026

[79] R. Hesse, W. E. Harrison, *Earth Planet. Sci. Lett.* **1981**, *55*, 453–462. DOI: https://doi.org/10.1016/0012-821X(81)90172-2

Research Article: Cyclopentane hydrates are considered to be a candidate for hydrate-based desalination, so the mechanism of cyclopentane hydrate crystallization in pure water and in brine is crucial. Various salts at different concentrations and under three driving forces (subcooling) were considered to explore the phenomenology of hydrate formation by microscopy. The hydrate growth speeds were also determined.

Crystallization Mechanisms and Rates of Cyclopentane Hydrates Formation in Brine

S. Ho-Van*, B. Bouillot*, D. Garcia, J. Douzet, A. Cameirao, S. Maghsoodloo-Babakhani, J.-M. Herri

Chem. Eng. Technol. **2019**, *42 (XX)*, **XXX … XXX**

DOI: 10.1002/ceat.201800746

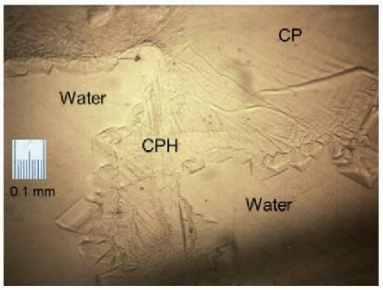

Supporting Information available online

6.5. Paper V: Morphology of Cyclopentane Hydrates in Saline Water

S.Ho-Van, B.Bouillot, D.Garcia, J.Douzet, A.Cameirao, S.Maghsoodloo-Babakhani, J.M.Herri

Published in HAL as ''Document de travail'' (*i.e.* working document):

https://hal.archives-ouvertes.fr/hal-02197257, July 30, 2019.

Summary: In this contribution we provided the observations on the morphology of individual CPH crystals in the presence of saline solutions as considered previously in the paper IV by using the same mili-reactor system. Three different driving forces (here are subcoolings: 2.5°C, 3.5°C, and 4.3°C) are considered. Various salinities are also tested to discover the effect of elevated salt concentrations on hydrate crystals morphology. Our observations demonstrate that the CPH crystals morphology is approximately comparable at the same driving force, while the size of the individual crystals drops significantly with increasing of subcooling, whatever the electrolytes involved and their concentrations. Accordingly, subcooling might be used as a standard for classification the morphology of individual hydrate crystals.

Morphology of Cyclopentane Hydrates in Saline water

S.Ho-Van[1,2]*, B.Bouillot[1]*, D.Garcia[3], J.Douzet[1], A.Cameirao[1], S.Maghsoodloo-Babakhani[1], J.M.Herri[1]

[1]*Mines Saint-Etienne, Univ Lyon, CNRS, UMR 5307 LGF, Centre SPIN, F - 42023 Saint-Etienne France;*

[2]*Oil Refinery and Petrochemistry Department, Hanoi University of Mining and Geology,*

Duc Thang, Bac Tu Liem, Hanoi, Viet Nam

[3]*Mines Saint-Etienne, Univ Lyon, Univ Jean Moulin, Univ Lumière, Univ Jean Monnet, ENTPE, INSA Lyon, ENS Lyon, CNRS, UMR 5600 EVS, Centre SPIN, F - 42023 Saint-Etienne France*

*Corresponding authors: son.ho-van@emse.fr and bouillot@emse.fr

Abstract

This effort focuses on morphology of cyclopentane hydrates formed from pure and saline water. Different brine solutions of Na_2SO_4, NaCl, NaCl-$MgCl_2$, or NaCl-KCl-$MgCl_2$ are considered at different concentrations and subcoolings. Especially, a small close reactor cell was used under a microscope with neither agitation nor seeds. Results show that the CPH crystals morphology is approximately comparable at the same subcooling, while the size of the individual crystals drops significantly with increasing of subcooling, regardless the type of salts and their concentrations.

Keywords: Clathrates; Cyclopentane Hydrates; Crystallization; Saline; Morphology.

1. Introduction

Cyclopentane hydrates (CPH) morphology is crucial in CPH-based desalination, or water treatment, applications since this affect strongly the desalting process and of course the equipment design. A few studies on the CPH morphology exist in literature [1–5]. Usually, only small glass vessels (about 4ml) are used. Moreover, they present an horizontal interface, no agitation, the system only consider NaCl and is seeded [1,2]. Therefore, this new effort examines other saline systems, under different concentrations, to study CPH morphology (NaCl, NaCl-$MgCl_2$, NaCl-KCl-$MgCl_2$, and Na_2SO_4). Each time, three different subcoolings

are used. A non-mixing small reactor cell (1.2ml) is used, without agitation, nor seed. Moreover, note that the geometry of the system presents a vertical interface between liquid water and cyclopentane, making the set-up easy to observe under a microscope.

2. Experimental observations

Chemicals utilized (Cyclopentane, NaCl, KCl, $MgCl_2$, and Na_2SO_4) were all provided by Sigma-Aldrich [6,7]. The schematic of reactor system and experimental protocol was well described by Ho-van et al [8]. The microscope is employed to observe and record the CPH crystallization, mainly at the interface between water and CP liquid. Photos of the individual hydrate crystals are taken for classification and comparison.

Effects of electrolytes and initial subcooling on the CPH morphology are illustrated in Figure 1. Three different initial subcoolings are considered in pure water and in presence of six different brine solutions (2.5°C, 3.5°C and 4.3°C). Note that, in presence of salts, the subcooling does not remain the same during the hydrate formation. Indeed, the CPH generation process excludes the salts. Hence the salinity of the brine increases along with the crystallization. Therefore, since the temperature is kept constant, only the initial subcooling is chosen for each experiment.

All pictures of individual crystals have been taken at the end of each experiment (after days), when the crystal growth has ended. In this figure, the grain boundaries are delineated in black. First, individual crystals' size at lower subcooling (2.5°C) is systematically bigger than that at higher subcoolings (3.5°C or 4.3°C). At 4.3°C initial subcooling, the approximate size 0.02–0.3mm, while the size is 0.05–0.5mm at 3.5°C, and 0.1–0.9mm at 2.5°C. This is similar to the observations of Sakemoto et al [1] and Kishimoto *et al.* [2]. Moreover, lower initial subcooling leads to polygons (2.5°C), while at higher subcoolings the smaller crystals take the form of slender polygons (3.5°C), or sword-like shapes (4.3°C). This expected observation can be attributed to the higher crystallization rate at high driving force, leading to a reduction in the crystals size, as described in detail elsewhere [1–4,9].

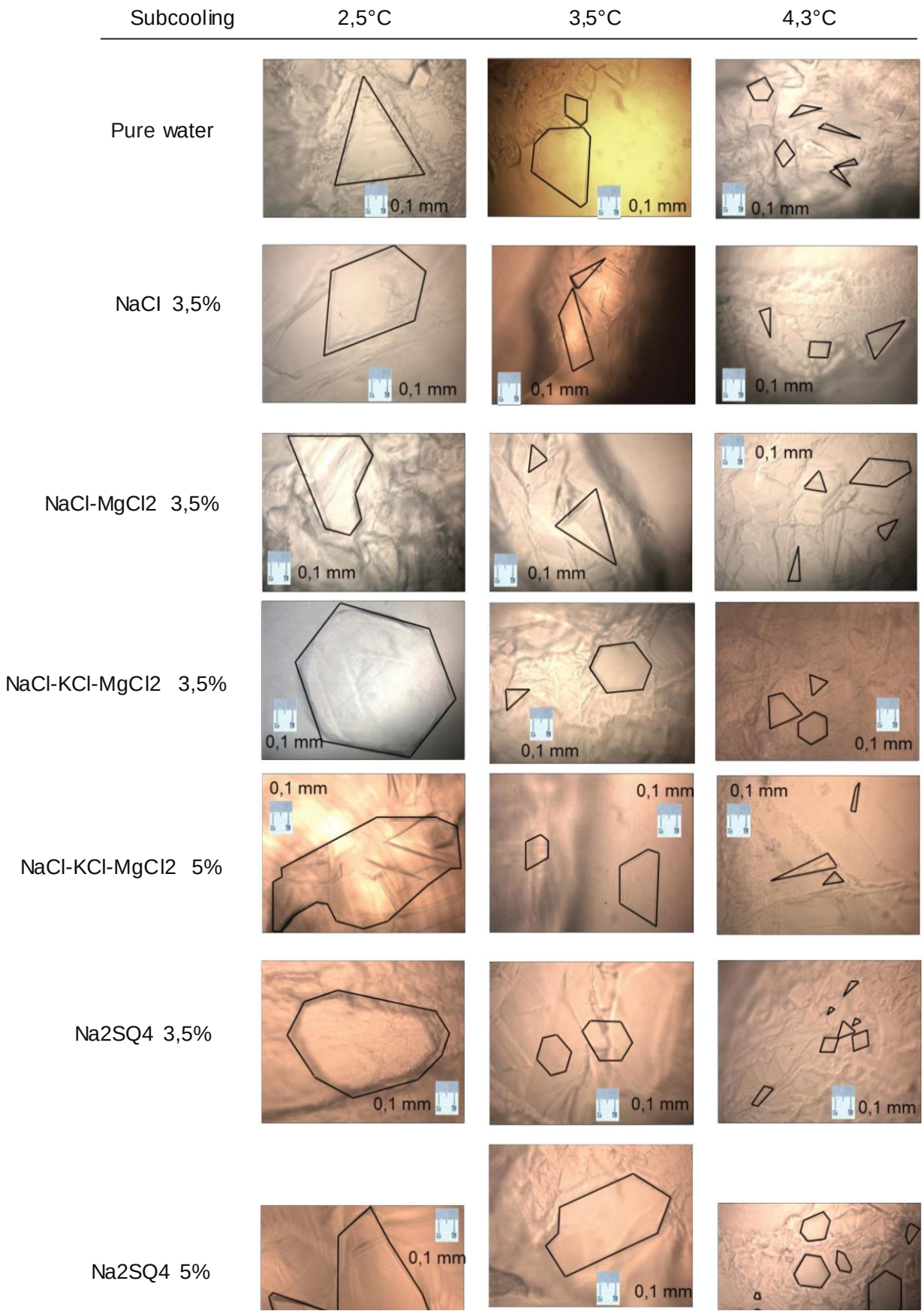

Figure 1. Morphology of individual CPH crystals under different subcoolings in bri ne

However, note that, in these experiments, only 2D pictures are taken. Therefore, all photos are just planar sections of 3D crystals. Hence, sword-like shapes observed can be a slice of bigger cubic CPH crystals. Nevertheless, observations are consistent with literature [1,2], and a better-suited system would be needed to acquire more precise data on CPH morphology.

Second, it is important to notice that the size of CPH crystals is usually the same for all systems at same initial subcooling. Therefore, the kind of salt is not a significant factor to discuss the crystals' shape in the system. Only the effect of subcooling is relevant. Again, this observation agree well with literature [1,2].

Finally, the hydrate crystals in the water phase (right) are likely to forrn with a bigger size compared with those in the CP phase (left), as seen in Figure 2. Indeed, there is a quick growth toward the CP phase and a slower growth rate into the water phase. Ho-Van et al. [8] observed this phenomenon , took videos, and measured the interface growth speed. In the CP phase the individual crystals are more difficult to detect and seemingly stick together as a polycrystalline layer because of their very small size. Many channels and capillaries, which are supposed to be the ways for water and CP migration, can also be seen on the hydrate structure surface.

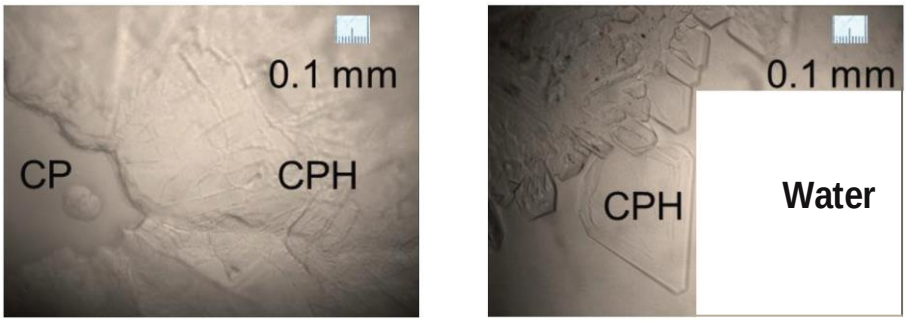

Figure 2. Crystals shape in the CP (left) and water (right) phases at initial subcooling of 3.5°C

3. Conclusion

Results show that the salt concentration does not influence significantly the crystal morphology. However, the subcooling is an essential parameter for all tested systems. Obviously, the size of individual crystals decreases with increasing of subcooling. This points out that subcooling might be used as the only parameter for the morphology classification of individual CPH crystals in such system (no agitation, with salts). Also, bigger crystals have

been found in the water phase rather than in the liquid cyclopentane phase, due to the difference in the transport mechanism.

Literature cited

[1] R. Sakemoto, H. Sakamoto, K. Shiraiwa, R. Ohmura, T. Uchida, Cryst. Growth Des. 2010, 10, 1296–1300

[2] M. Kishimoto, S. Iijima, R. Ohmura, Ind. Eng. Chem. Res. 2012, 51, 5224–5229

[3] M. Mitarai, M. Kishimoto, D. Suh, R. Ohmura, Cryst. Growth Des. 2015, 15, 812–821

[4] M.L. Martinez de Baños, Mechanisms of formation and dissociation of cyclopentane hydrates, Ph.D. thesis, Université de Pau et des Pays de l'Adour, 2015

[5] H. Delroisse, J.-P. Torré, C. Dicharry, Cryst. Growth Des. 2017, 17, 5098–5107

[6] S. Ho-Van, B. Bouillot, J. Douzet, S. Maghsoodloo, J.-M. Herri. AIChE J. 2018, 64 (6)

[7] S. Ho-Van, B. Bouillot, J. Douzet, S. Maghsoodloo Babakhani, J.-M. Herri. Ind. Eng. Chem. Res.2018, 57 (43)

[8] S. Ho-van, B. Bouillot, D. Garcia, J. Douzet, A. Cameirao, S. Maghsoodloo Babakhani, Chem. Eng. Technol. 2019

[9] K. Saito, M. Kishimoto, R. Tanaka, R. Ohmura, Cryst. Growth Des. 2011, 11, 295–301

6.6. Paper VI: Phase equilibrium investigations of mixed cyclopentane and carbon dioxide hydrates in presence of different salt solutions

S. Maghsoodloo Babakhani, S.Ho-Van, B.Bouillot, J.Douzet, J.M.Herri

Submitted to Chemical Engineering Science, 5/2019 (1st revision under process)

CO_2 is responsible for approximately 64% of the enhanced "greenhouse effect"[46]. The disposal of CO_2 is hence urgently required. CO_2 capture by gas hydrate formation in ocean and marine sediments has gained increasing attention [115]. Moreover, the mixed CP + CO_2 hydrates are probably potential for binary desalination and CO_2 capture application [15,46]. Unfortunately, the phase equilibrium data of this hydrates system are still incomplete, especially when electrolytes are considered. Thus, in this effort, in order to improve and develop the techniques of hydrate-based desalination, we explored four-phase equilibrium data (V-L_W-L_{HC}-H) for CP-CO_2 binary hydrates in the presence of NaCl, KCl and a mixture of NaCl-KCl under different salt concentrations. The experiments were carried out in a batch reactor and by an isochoric technique. Moreover, the concentration of salt at final state of crystallization and also during the dissociation process was measured. The experimental results were then discussed and compared to the literature. The van de Waals approach is employed to simulate the equilibrium. Results show that this approach is capable of reproducing the CP-CO_2 binary hydrates dissociation temperature with an average absolute deviation less than 0.4K. Conclusions and some comments on possible future work finish this article.

Phase equilibrium measurements and modelling of mixed cyclopentane and carbon dioxide hydrates in presence of different salt solutions

S.Maghsoodloo-Babakhani[1], S.Ho-Van[1,2], B.Bouillot[1]*, J.Douzet[1], J.M.Herri[1]

[1]*Mines Saint-Etienne, Univ Lyon, CNRS, UMR 5307 LGF, Centre SPIN, F - 42023 Saint-Etienne France;*

[2]*Oil Refinery and Petrochemistry Department, Hanoi University of Mining and Geology,*

Duc Thang, Bac Tu Liem, 100000 Hanoi, Viet Nam

*Corresponding authors: bouillot@emse.fr

Abstract

Interest of Clathrate hydrates for industrial applications is rising. While numerous studies can be found on carbon capture or desalination, this effort investigates thermodynamics of the combined process using cyclopentane (CP) as second guest molecule. This document provides numerous equilibrium data of mixed CO_2/CP hydrates in presence of salt (NaCl, KCl) under differents concentrations. Final dissociation points obtained in a pressurized batch reactor, as well as intermediate dissociation points. Afterward, van der Waals and Platteeuw approach is used to predict equilibrium temperatures. Results show that, in presence of salts, several crystallization events occur in the system. Consequently, different hydrate structures could be formed in the bulk, such as pure CO_2 hydrates and mixed CO_2/CP hydrates. Thermodynamic modeling provides results within 0.4°C uncertainty compared to final dissociation points. In presence of hydrates, uncertainty increases, reinforcing the multi structural hypothesis.

1. Introduction

Clathrate hydrates, sometimes called "Gas Hydrates'', are nonstoichiometric solid compounds of guest and water molecules. Under low temperature and high pressure environments, the water molecules constitute cavities through hydrogen bonding networks. These cavities themselves are thermodynamically unstable and they are stabilized by guest molecules adsorption [1]. The phase equilibria of clathrate hydrates depend on the physical and chemical properties of guest molecules. Moreover, the existence of additives in liquid phase may alter the thermodynamic equilibrium conditions of clathrate hydrates.

Gas hydrate formation is the major cause of blocking pipelines in petroleum industries. Hence, in the history of clathrate hydrates, the focus has always been on how to prevent hydrate formation in gas and oil pipelines. However, clathrate hydrates have received much

attention in over the last two decades due to their potential applications such as gas separation [2,3], gas storage and transportation [4,5], CO_2 capture sequestration [6,7], etc. Furthermore, natural gas hydrates in permafrost regions and oceanic sediments may represent a new source of sustainable energy [8,9].

Seawater desalination or treatment of salty wastewater is a potential application of gas hydrates. The idea is based on salt elimination. When gas hydrate forms in seawater or salty wastewater, the salts remain in the concentrated aqueous solution and they can be removed by a physical process. The next decades is likely to witness a considerable rise in desalination by hydrate formation process since its operational cost and energy consumption could be economical compared to other techniques of desalination [10]. However, developments are still required to increase the efficiency and safety of hydrate-based desalination process.

Using promoters is attracting widespread interest in hydrate-based desalination as they improve hydrate formation rate and moderate the equilibrium pressure. Tetrahydrofuran (THF) and tetra-butyl ammonium bromide (TBAB) are among the most widely discussed types of additives [11–15]. Despite advantages of these promoters on increasing the efficiency of salts removal, their solubility in water is a major issue in hydrate-based desalination process. Cyclopentane (CP) is recognized as being an interesting promoter since it enhances the hydrate formation conditions and is immiscible with water [16]. Cha and Seol [17] investigated upper temperature limit of CO_2 hydrate formation in presence of CP and simulated produced water (8.95 wt% salinity) at isobaric condition (3.1 MPa). They observed that the upper temperature limit for CO_2 hydrate is -2C, whereas for CP-CO_2 hydrate is 16°C. They also reported that CP increases 22 times CO_2 hydrate formation rate. Moreover, salt removal efficiency in the presence of CP was 20% higher than simple hydrate. Zheng et al. [18] measured equilibrium data of CP/CO_2 hydrates including for a 3 wt% NaCl solution. They carried out their experiments with different molar ratios of CP/water using an isochoric procedure. They stated that CP/CO_2 hydrate forms structure II, which is different from structure I pure CO_2 hydrate. In addition, increase in CP concentration led to a major decrease in equilibrium pressure. However, they mentioned the optimal molar ratio of CP is 0.01. Zhang et al. [10] studied on the phase equilibrium of CP/CO_2 and THF-CO_2 binary hydrates in different concentration of sodium chloride solutions based on an isochoric method. They found that both CP and THF decrease the equilibrium pressure and increase the salt removal efficiency. Furthermore, the stability of CP/CO_2 hydrates was more than THF-CO_2 hydrates at low mass fraction of NaCl. Recently, Hong et al [19] provided thermodynamic effects of CP

and its derivatives including cyclopentanone (CP-one) and cyclopentanol (CP-ol) on CO_2 hydrates for seawater desalination application. Some thermodynamic data of CP derivatives + CO_2 hydrates were provided in pure water and in 3.5% NaCl. Besides, the thermodynamic stabilities of these mixed hydrates were found in the following order: CP-CO_2 > CP-one-CO_2> CP-ol-CO_2.

However, there is still a need for more phase equilibrium data of CP/CO_2 hydrates to improve and develop the techniques of hydrate-based desalination. Hence, in the present work, four-phase equilibrium data (V-L_w-L_{HC}-H) for CP/CO_2 binary hydrates in the presence of different salt solutions was investigated. The experiments were carried out in a batch reactor and by an isochoric technique. Moreover, the concentration of salt at final state of crystallization and also during the dissociation process was measured. The experimental results were then discussed and compared to the literature.

In addition, there is a need for modelling tools. Therefore, the use of standard van der Waals and Platteeuw approach has been considered. Kihara parameters for cyclopentane molecule have been optimized, and used for temperature predictions. In the end, conclusions and some comments on possible future work finish this article.

2. Experimental section

2.1. Materials

All materials used in this work are listed by detail in Table 1. Pure water was provided by a "Millipore" purification system. This system is equipped with a cartridge "Milli-Q®-AdvantageA10" and it produce water with conductivity less than 0.055 $\mu S.cm^{-1}$ and TOC (total organic carbon content) less than 5 ppb.

Table 1. Materials

Name	Purity	Supplier
Cyclopentane	98%	Sigma Aldrich
Sodium Chloride	99.5%	Sigma Aldrich
Potassium Chloride	99%	Sigma Aldrich
Carbon dioxide	99.999%	Air Products

2.2. Experimental set-up

A diagram of the experimental set-up is presented in Figure .

The apparatus including two batch reactors was developed in order to study the phase equilibria of clathrate hydrates as well as kinetics. Both reactors have the same features and specifications (except the inner volume, the first is 2.36 liter and the second 2.23 liter). Each reactor is covered by an isolation jacket and the inner temperature is controlled by a cooling bath LAUDA RC6 CS ranging from -15 to 50 C. They are composed of two sapphire windows which allow direct observation. There are vertical stirrers with two sets of blades; the top set of blades is in the gas phase and the bottom set in liquid.

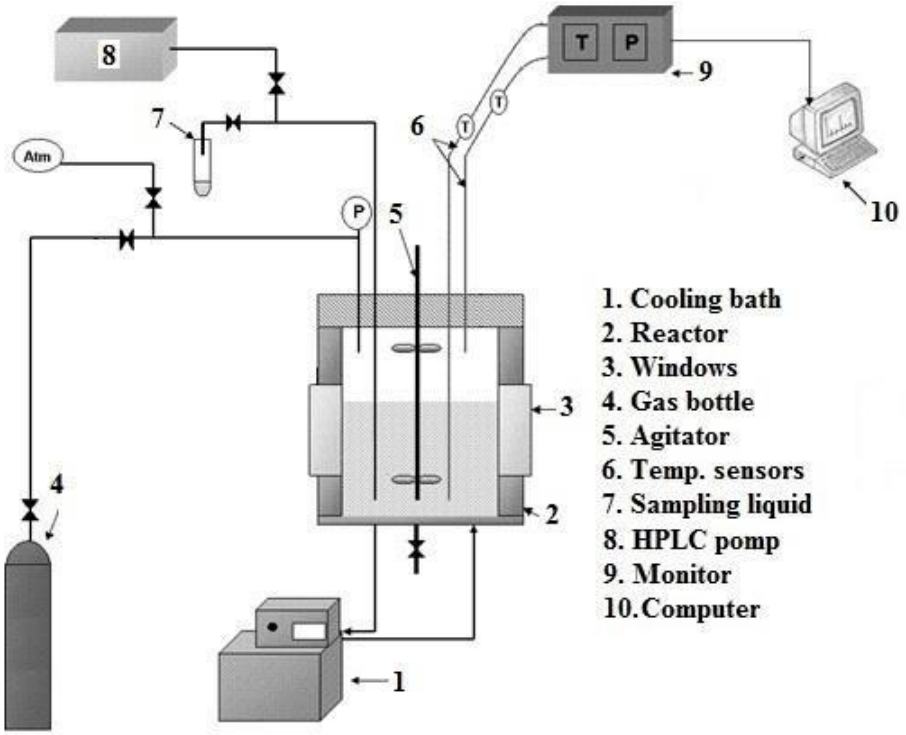

Figure 1. Diagram of experimental set-up

The autoclaves are equipped with two temperature Pt100 temperature sensors at the top and bottom of the cell which measure the temperature in gas and liquid phases, respectively. The accuracy of these probes is ±0.2 C. The pressure is also monitored by a pressure probe in the range 0-10 MPa with accuracy of ±0.01 MPa. This is placed at the top of the cell. The water and CP can be injected in the reactors by a KNAUER P4.1S HPLC pump at high pressure. A mechanical valve is mounted on the reactor which is connected to a capillary tube in the liquid phase to take liquid samples during the course of experiments. Data acquisition is controlled on a personal computer running Labview.

2.3. Experimental method

At first, the autoclave is washed with pure water. The reactor is then filled with nitrogen at 50-60 bars. The pressure is monitored during 24 hours to ensure that there is no gas leak in our experimental set-up. The reactor is then evacuated by the vacuum pump to remove impurities. The reactor is then pressurized by with CO_2 and it is stirred (400 rpm) and maintained at desired initial conditions (several minutes to hours). Thanks to the HPLC pump, about 800 mL of water (containing different concentration of salts or 10 ppm Li^+) and 87.9 mL cyclopentane are introduced to the cell (volumetric ratio between the aqueous solution and cyclopentane is about 9:1). The temperature is then decreased to 1-2°C. After a while (several hours to days), crystallization starts. As hydrate formation is an exothermic process, the temperature slightly increases. From this point, depending on the concentration of aqueous solution as well as pressure, we wait 1-3 days to reach equilibrium. This means that there are no more changes in pressure and temperature. When the equilibrium is reached, a liquid sample about 1-2 mL is taken to measure the salt concentration by ionic chromatography. Then, the dissociation process is started. The temperature is increased stepwise (1 °C/h) and we wait for stability of pressure and temperature. A liquid sample is taken at second equilibrium point. At 2°C below the final equilibrium point, the temperature is augmented 0.5°C/h until the total dissociation. A liquid sample is taken at final equilibrium. The temperature is increased to reach the initial condition. The initial pressure is then changed by purging or inserting CO_2 and the procedure is repeated to obtain further equilibrium points.

3. Results and discussion

3.1. Pressure-Temperature diagrams of CP/CO_2 hydrate with and without salts

A detailed analysis of pressure-temperature variations during the course of experiments is discussed in this section. Five different systems have been studied. First, pure water has been used, in order to certify the quality of the measurements since it is easy to compare the results to literature data. Then, several mixtures involving NaCl and KCl haven been considered: 7%mass NaCl, 3.5%mass KCl, 7%mass KCl, and 1.75%mass NaCl+ 1.75%mass KCl.

Figure 2 illustrates a typical PT diagram of CP/CO_2 hydrate in pure water. Each experiment was started at point A where the CP, pure water and CO_2 were at a condition (pressure and temperature) outside of hydrate forming region. The reactor temperature was then decreased to approximately 1°C. After a while, hydrate formation started (point B on the figure). Since

hydrate formation is an exothermic process, the temperature increased at this point. The hydrate formation was completed at point C and liquid sample was taken if possible. Then hydrate dissociation was initiated by increasing incrementally the system temperature until the dissociation curve meets the cooling line (point D). At this point, the slope of pressure-temperature curve changed sharply and it can be considered as the four-phase equilibrium point of CP/C02 hydrate (V-Lw-LHc-H).

An interesting observation can be made on the heating process. At the beginning, the PT curve remains quite parallel to the cooling curve for a while. Afterward, there is the significant increase in pressure, corresponding to a quick release of gas. Therefore, the first hydrates to dissociate should not contain a huge amount of C02. The filling of hydrates hence is not homogeneous.

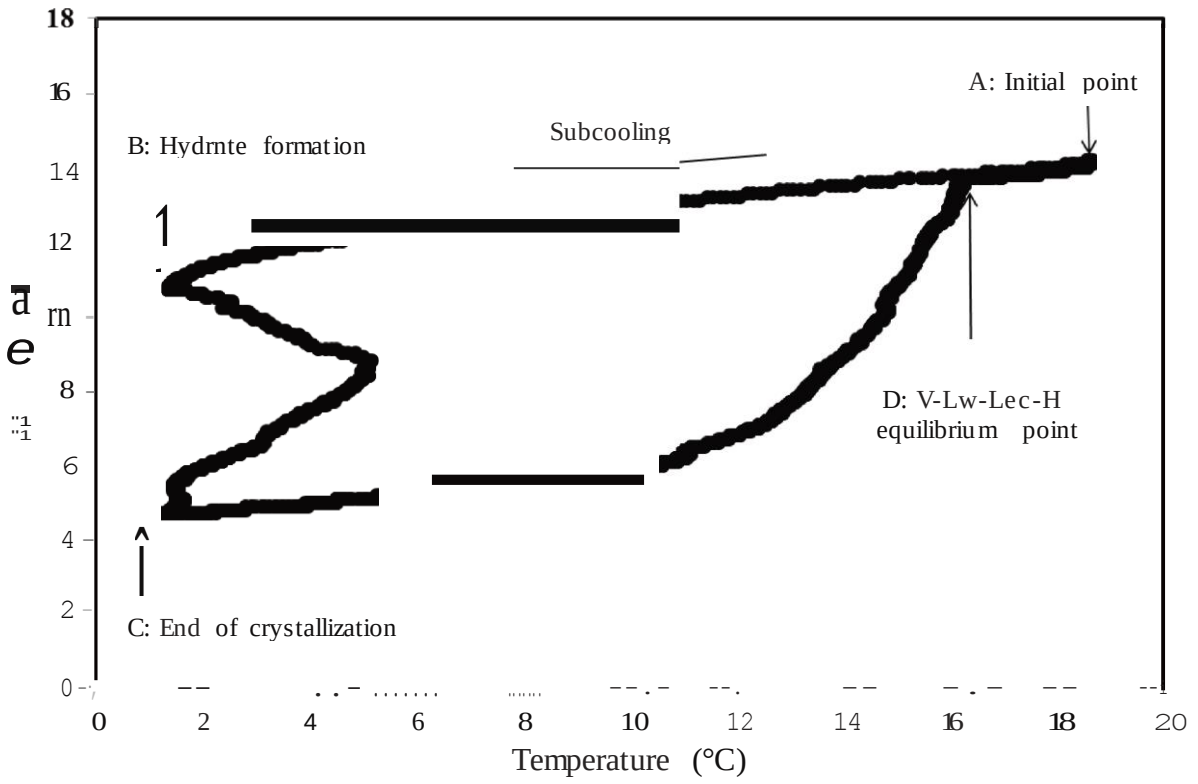

Figure 2. A typical pressure-temperature evolution of CP/$C0_2$ hydrate in pure water

PT diagrams of CP/C02 hydrate in presence of salts may present some interesting phenomena, although sometimes not easy to detect. For instance, results in 7 wt% NaCl were almost the same as CP/C02 hydrate in pure water, but different at the same time. In order to have a better look at this difference, let's discuss results in presence of KCl. Figure presents temperature-pressure evolution of CP/C02 hydrate in presence of 3.5 wt% KCI. As the figure

shows, after cooling the solution at initial condition, the hydrate formation started. Unlike the CP/CO_2 hydrate in pure water, during the crystallization, two increases of temperature were observed due to the exothermic nature of crystallization. That means that several crystallization phenomena occur in the system. Therefore, at least two clathrate phases are expected to be formed in this process. For the sake of this understanding, other equilibrium curves have been drawn on Figure 2: pure CO2 hydrates and CP/CO_2 hydrates, in pure water and KCl solutions.

First of all, let us analyze the crystallization part, from B to C point. Two exothermic peaks are probably related to two crystallization events. Of course, CO_2 and CP can theoretically form different hydrates in the system (pure CO_2, pure CP, and CP/CO_2 hydrates). Note that cyclopentane acts as a promoter of hydrate formation, and therefore lessen the operating condition for mixed hydrate formation. Therefore, CP/CO_2 hydrates are probably the most stable hydrates in the system, and will consume both guest molecules. However, figure 3 also shows that the system is supersaturated regarding CO_2 hydrates (see CO_2 hydrate + 3.5 wt% KCl line) and regarding CP hydrates (below 5.5°C [20]. Consequently, the system can evolve toward CO_2 hydrate or CP hydrate formation. Nonetheless, the significant pressure decrease suggest at least CO_2 consumption, thus probably CO_2 and CP/CO_2 hydrates. Yet, note that CP mostly occupies the large cavities, CO_2 molecules can only fill the small structure II cavities. Hence, less CO_2 are expected to be stored in CP/CO_2 hydrates. Moreover, there is a structural difference between pure CO_2 hydrate (sI), and mixed CP/CO_2 hydrates (sII). On one hand, sI hydrate presents 8 cavities (small + large) able to capture CO_2 molecules, for 42 water molecules, hence an hydration number of 5.25 at best. On the other hand, there are 16 small cavities for 136 water molecules in SII hydrates, hence an hydration number of 8.5 for CO2 molecules at best.

Consequently, assuming that the influence of the volume change, due to cyclopentane enclathration, on pressure is negligeable, the pressure drop in case of CP/CO_2 binary hydrate could be less than pure CO_2 hydrate. As a result, the first temperature increase at the beginning of crystallization could be attributed to the CP/CO_2 binary hydrate formation as the pressure drop is less than the second nucleation event. Therefore, the second nucleation was considered as the formation simple CO_2 hydrate. This could be the first evidence for co-existence of sI simple CO_2 hydrate and sII binary CO_2/CP hydrate in presence of KCl. Of course, this hypothesis still need experimental evidence, maybe from FTIR or Raman spectroscopy.

Secondly, Figure 3 shows that the dissociation behavior (from B to D point) was considerably different from results in pure water. During the dissociation process, two different rates of decomposition were observed. At the beginning of the process, the pressure slightly changed by increasing the temperature, quite similarly to the initial cooling curve, like before (A to B). Therefore, no significant amount of CO_2 seems to be release, thus no serious hydrate dissociation containing carbon dioxide. However, at temperatures higher than 5°C, a small change of temperature led to a significant increase of pressure, hence a considerable release of CO_2. Afterward, the dissociation curve met the cooling line at 6.6°C and 28bar. This could be the V-L_W-H equilibrium point of simple CO_2 hydrate since Deaton and Frost [23] and Fan et al. [24] reported (6.6°C, 27.9bar) and (6.5°C, 27.8bar), respectively, for equilibrium condition of simple CO_2 hydrate.

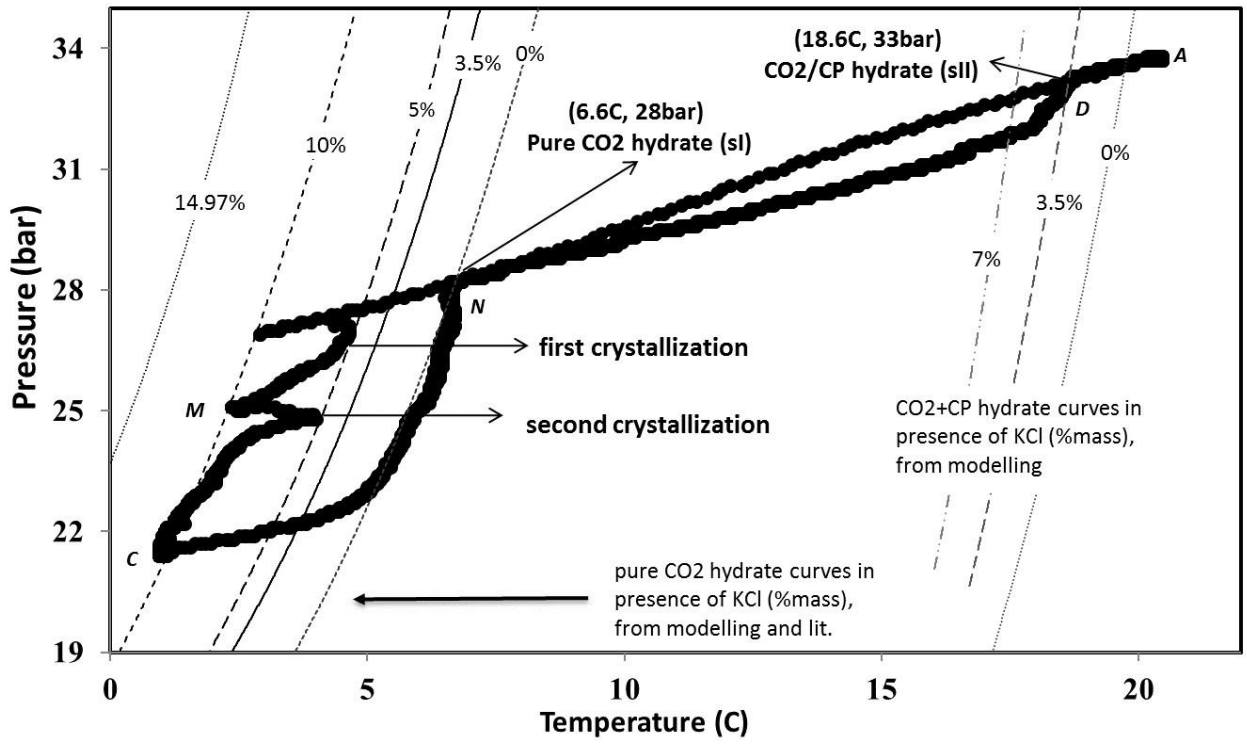

Figure 3. Pressure-temperature evolution of CP/CO_2 hydrate in presence of 3.5 wt% KCl. Curves for pure CO_2 hydrates from Dholabhai et al [21] **and GasHyDyn software from Kwaterski et al** [22]**. Curves for CP/CO_2 hydrates from this work modeling (uncertainty 0.3°C).**

Other results in other systems suggest this could be a coincidence. Anyway, since there were still hydrate crystals inside the reactor, the dissociation process was then continued by increasing temperature. Of course, the junction of curves implies that the amount of CO_2 trapped into the clathrate is small (mostly CP hydrates in the reactor?). However, the slope of

decomposition curve after that is slightly different (lower pressure). This probably illustrates CP/CO_2 hydrate dissociation. Close to the final point (D), at temperatures above 18°C, a sharp increase of pressure was observed. Finally, the curve crossed the cooling line at 18.6°C and 33bar and the last hydrate crystals dissociated. This point is the four-phase equilibrium point of sII binary CP/CO_2 mixed hydrate (V-L_W-L_{HC}-H).

The overall process was verified for all the experiments in presence of KCl. The experimental data for V-L_W-H equilibrium condition of simple CO_2 hydrate and four-phase equilibrium points of CP/CO_2 hydrate (V-L_W-L_{HC}-H) are presented in the following paragraphs and sections.

Before moving to the summary of all results, let's have a look at another mixture in presence of both NaCl and KCl. Again, different formation and dissociation behaviors were observed. Figure 4 presents the pressure-temperature changes during CP/CO_2 hydrate formation and dissociation procedures in presence of NaCl/KCl (1.75% NaCl + 1.75 wt% KCl) mixture in the solution.

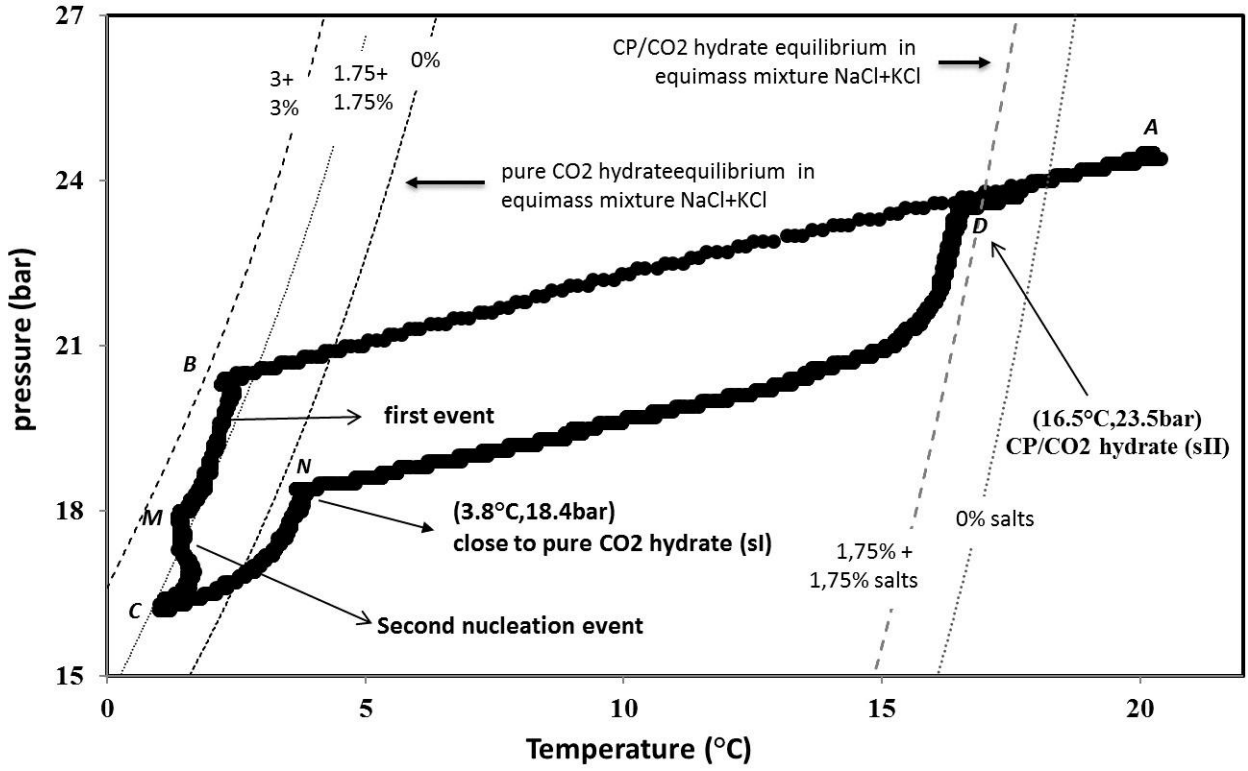

Figure 4. Pressure-temperature evolution of CP/CO_2 hydrate in presence of NaCl/KCl (1.75 wt% NaCl and 1.75 wt% KCl) mixture in the solution. Curves for pure CO_2 hydrates from Dholabhai et al [21] **and GasHyDyn software from Kwaterski et al** [22]**. Curves for CP/CO2 hydrates from this work modeling (uncertainty 0.4°C).**

Once more, the figure provides remarkable observations. During hydrate formation in presence of NaCl/KCl mixture, the second nucleation was again observed. Nonetheless, the temperature change due to exothermic behavior of hydrate formation was less significant than the case of hydrate formation in presence of KCl. The dissociation process could again be divided into two sections. First, the system pressure was noticeably augmented by increasing the temperature. However, the slope of decomposition curve was changed considerably at temperatures above 3.8°C. Unlike the case of hydrate dissociation in presence of KCl, the decomposition curve did not meet the cooling line. This point (3.7°C and 18.4bar) that was previously supposed to be a three-phase equilibrium condition (V-L_W-H) of simple CO_2 hydrate, is a bit different now, although still close to pure CO_2 hydrate equilibrium. When compared to the equilibrium data of CO_2 hydrate in literature the values remain quite similar. For instance, Ohgaki et al. [25] reported (3.76°C and 18.39bar) for V-L_W-H equilibrium condition of simple CO_2 hydrate. This was also verified for the other experiments in presence NaCl-KCl mixtures and will be presented in the following sections.

Repeatedly, the following heating step results in a long curve parallel to initial cooling curve. Therefore, no significant release of CO_2 was observed: CP hydrate dissociation? Low CP/CO_2 hydrates dissociation? The final step encore exhibits a pressure increase, and a final dissociation point corresponding to CP/CO_2 hydrate equilibrium in the brine system.

Up to now, the results of PT diagrams revealed that only sII CP/CO_2 hydrate should be formed in pure water. However, the presence of KCl, and to less extent NaCl (phenomena harder to detect), could lead to the formation of both structures (sI simple CO_2 hydrate and sII binary CP/CO_2 hydrate). In this case, the hydrate dissociation could start with the declathration of simple CO_2 hydrate cavities, and the present a decomposition of binary CP/CO_2 hydrate. This change in the slope of the curve could be attributed to an equilibrium condition, whether V-L_W-H or V-L_W-L_{HC}-H. However, more evidences are needed to support such affirmation.

3.2. Thermodynamic equilibrium results

The new four-phase equilibrium data (V-Lw-L_{HC}-H) for CP/CO_2 binary hydrates in pure water, in presence of NaCl, KCl and a mixture of NaCl-KCl are presented in Table 2.

In order to assess the quality of experimental data, and to evaluate reproducibility of results, experiment in presence of 3.5 wt% KCl has been replicated twice. The four-phase equilibrium

points obtained from both experiments were approximately identical (T=291.75K and P=3.30MPa compared to T=291.80K and 3.32MPa). Thus, it was adequately accurate to ascertain the quality of experimental data produced during the experimentation.

Table 2. Experimental four-phase equilibrium data (V-L_W-L_{HC}-H) of CP/CO_2 binary hydrate in pure water and brine solutions

T (K)	P (MPa)	Salinity (wt%)	
		NaCl	KCl
(±0.2)	(±0.01)	(±0.002%)	(±0.002%)
290.70	1.87	0	0
289.30	1.37	0	0
291.90	2.84	0	0
287.25	1.88	7	0
285.30	1.14	7	0
288.35	2.37	7	0
291.80	3.32	0	3.5
291.75	3.30	0	3.5
290.70	2.44	0	3.5
289.85	1.82	0	3.5
287.60	1.09	0	3.5
284.75	0.66	0	3.5
289.70	3.17	0	7
288.85	2.47	0	7
287.40	1.75	0	7
286.45	1.35	0	7
284.80	0.93	0	7
291.80	3.47	1.75	1.75
290.35	2.79	1.75	1.75
289.65	2.35	1.75	1.75
288.45	1.63	1.75	1.75
286.45	0.99	1.75	1.75
284.55	0.69	1.75	1.75

In addition, the V-L_W-L_{HC}-H experimental results of CP/CO2 hydrate in pure water obtained in this work were compared to literature, see Figure 5.

As the figure shows, by considering the standard instrumental uncertainties, the data obtained in this study adequately agreed with the experimental data in literature [10,26,27].

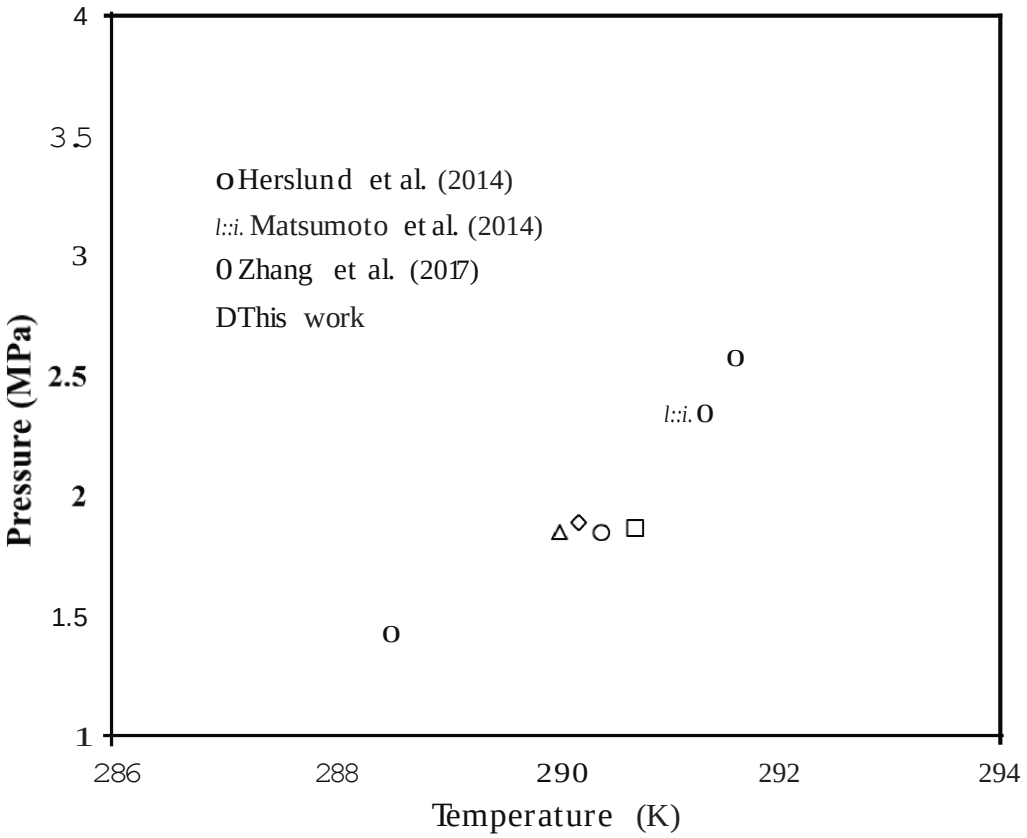

Figure 5.Four-phase equilibrium data of CP/$C0_2$ binary hydrate in pure water, this work compared to literatore

Figure 6 illustrates the four-phase thermodynamic equilibrium data obtained in the present work for CP/C02 hydrate in brine solution. The results of thermodynamic stability boundaries showed that the equilibrium curve of CP/C02 hydrate in presence of salts was located at an upper position than CP/$C0_2$ hydrate in pure water whatever the kinds of salt used. Given the fact that salt molecules can act as inhibitors [1,21,28,29], the thermodynamic equilibrium curve of CP/C02 hydrate in presence of salts was shifted to lower temperatures (or higher pressures) . Furthermore, presence of salt could lead to "salting-out" phenomenon which reduces the solubility of $C0_2$ and cyclopentane in water [30]. Consequently, equilibrium temperature should be changed to lower values.

For instance, the experimental results demonstrate that the presence of 3.5 wt% KCl in aqueous solution changed slightly the position of equilibrium curve compared to the pure water. Moreover, the equilibrium curve of CP/C02 hydrate in presence of 7 wt% KCl shifted considerably to lower temperatures. This highlights the more significant effect of salt on thermodynamic equilibrium of CP/$C0_2$ at higher concentrations.

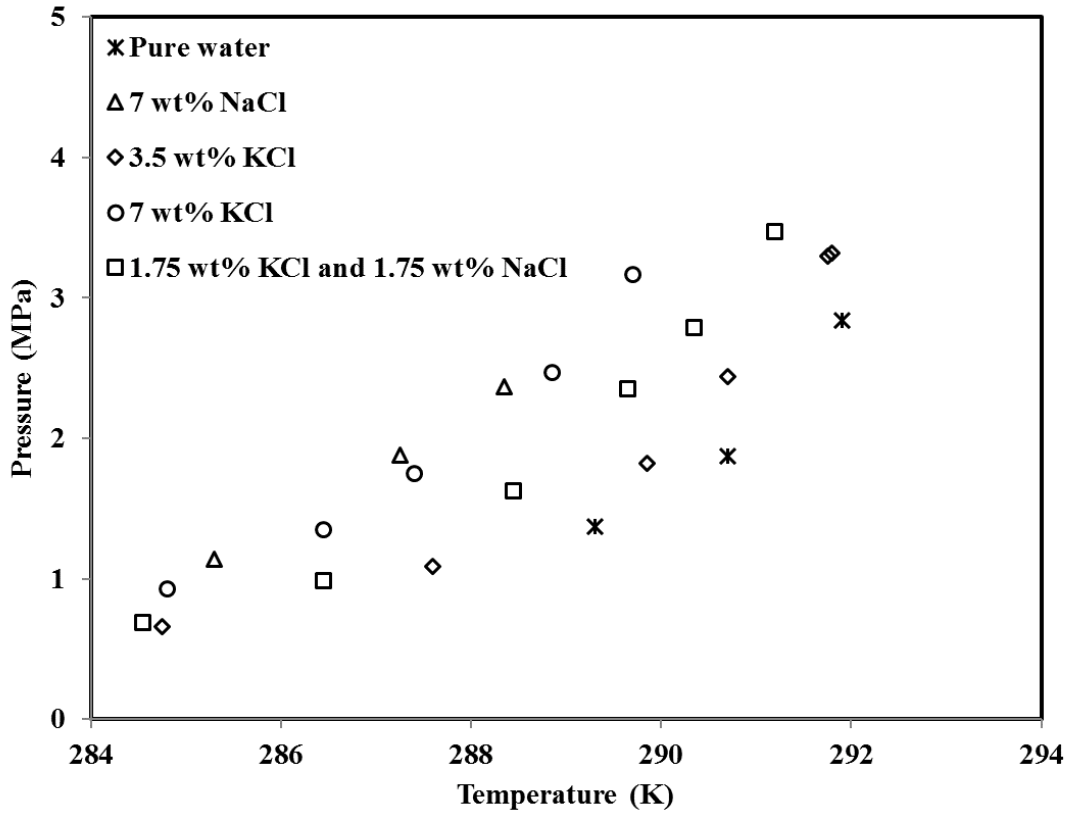

Figure 6. V-L_W-L_{HC}-H equilibrium data of CP/CO_2 hydrate in brine solution obtained in this work

Furthermore, the equilibrium temperature of CP/CO_2 hydrate in presence of 7 wt% KCl was always slightly lower than the equilibrium temperature of 7 wt% NaCl. This means that the inhibitory effect of NaCl is marginally higher than of KCl. This is in good accordance with experimental results of Ho-Van et al. [20,31]. They reported the same observation about the inhibitory effects of NaCl and KCl on thermodynamic equilibrium of simple cyclopentane hydrate. In fact, Sloan and Koh [1] stated that the interaction between the charged ions of salts and dipoles of water molecules is governed by a much stronger Coulombic bond than the van der Waals forces and the hydrogen bond, leading to ion clustering around the solute molecules. Consequently, the water molecules preferentially interact with salt ions rather than water molecules. This prevents hydrate formation. Therefore, it could be supposed that the Coulombic bond in presence of NaCl is stronger than that that in presence of KCl (at the same salt concentration) which causes lower temperature equilibrium.

In this study, the influence of NaCl/KCl mixture (each 1.75 wt%) on the V-Lw-L_{HC}-H equilibrium of CP/CO_2 hydrate was also investigated. The results demonstrate that despite the presence of overall 3.5 wt% salt in aqueous solution, noticeably lower temperatures are

required for hydrate formation compared to that with 3.5 wt% KCl. Nonetheless, this temperature difference is less significant at pressures less than about 1MPa.

3.3. Experimental dissociation data

As aforementioned in the experimental section, some equilibrium data during the intermediate heating stages were also recorded for each experiment. Liquid samples were also taken at these stages in order to determine the salt concentrations by ion chromatography (IC). The results are tabulated in Table 3.

As the table shows, the salt concentration at each dissociation point is greater than its initial concentration. This increase of salt concentration means that the salts remain in the concentrated aqueous solution. Furthermore, it validates and confirms the reliability of our experimental data as well as experimental set-up and procedure.

Table 3. Experimental PT equilibrium condition after crystallization and during dissociation step, including salt concentration at initial and equilibrium conditions

Equilibrium conditions		Initial salt concentration (%)		Equilibrium salt concentration (%)	
T (K)	P (MPa)	NaCl	KCl	NaCl	KCl
(±0.2)	(±0.01)	(±0.002%)	(±0.002%)	(±1.5%)	(±1.5%)
273.95	0.87	0	0	0	0
274.15	0.47	0	0	0	0
283.95	1.98	1.75	1.75	2.07	2.24
286.95	1.44	1.75	1.75	2.07	2.03
284.15	0.78	1.75	1.75	2.28	2.24
274.10	0.45	1.75	1.75	2.21	2.17
288.20	2.96	0	7	0	9.49
287.00	2.22	0	7	0	8.82
274.90	0.94	0	7	0	8.32
282.05	0.72	0	7	0	8.22
286.65	1.69	7	0	7.49	0
274.45	0.56	7	0	8.11	0
284.00	1.73	7	0	9.30	0
289.60	3.08	0	3.5	0	4.43
286.60	2.12	0	3.5	0	4.44
286.85	1.51	0	3.5	0	3.89
284.85	0.62	0	3.5	0	4.34

For the experiments including 3.5 wt% KCl (initial concentration), the results reveal that at a desired temperature (for instance about 286.6K), the salt concentration in aqueous phase at 2.12 MPa is greater than 1.51 (4.44 wt % compared to 3.89 wt%). In other words, the higher initial pressure leads to more salt concentrated solution. Indeed, higher initial pressure means larger driving force. Consequently, water conversion increases and larger quantity of water convert into hydrate structure. This investigation was also observed for 7 wt% KCl (near 288K).

The salt concentration in aqueous solution in presence of a mixture of NaCl/KCl (each initial concentration 1.75 wt%) was also investigated. Given the fact that, the ions of salts do not participate in hydrate formation and hydrate structure do not include them, the change in concentration of both salts should be equal. The results show that, the concentration of NaCl in aqueous phase is almost identical to the concentration of KCl.

4. Modelling thermodynamic equilibrium of mixed CP/CO_2 hydrates

The van der Waals and Plateuw model [32] is employed to describe the clathrate hydrate phase equilibrium. A detailed of this thermodynamic model has been described in details in previous efforts [33][34]. However, some basic information for the liquid/hydrate equilibrium is offered as following:

The equilibrium is calculated based on uniformity of chemical potential of water in the liquid and hydrate phases. A reference phase β is introduced. Accordingly, the equilibrium can be written as follows:

$$\Delta\mu_w^{\beta-H} = \Delta\mu_w^{\beta-L} \quad (1)$$

where $\Delta\mu_w^{\beta-L}$ and $\Delta\mu_w^{\beta-H}$ are the difference between chemical potentials of water in the reference phase β and in the liquid phase or hydrate phase, respectively. The first can be calculated based on the Gibbs-Duhem equation [33], while the second is based on the Waals and Platteeuw model as follows:

$$\Delta\mu_w^{\beta-H} = -RT\sum_i v_i \ln(1-\sum_j \theta_j^i) \quad (2)$$

where R is the universal constant, T the absolute temperature, v_i the number of type i cavities per water molecule in the hydrate and θ_j^i

j

i

the occupancy factor ($\theta^i \in [0, 1]$) of the

cavities of

type i by the guest molecule j. Occupancy factor θ_j can be achieved from integration of

Kihara potential by the Parrish and Prausnitz model [35]. For this calculation, three Kihara parameters (maximum attractive potential ε, distance between the cores and the cavity wall at zero potential energy σ, and the hard-core radius a) are required.

In this work, CO_2 Kihara parameter were taken from Herri et al [33]. CP parameters were obtained by mathematical regression upon data in pure water from Wang et al [36], data from NaCl solution from Zhang et al [10] and our measurements. The geochemical model PHREEQC were used to provide water activity in brine solutions. The others parameters have been taken from literature (Herri *et al.*[33] and Ho-Van *et al.*[20]).

The absolute average deviation (*AAD*) that will be used hereafter is expressed as follows:

$$AAD = \frac{1}{N}\sum_{i=1}^{N}\left|T_{i,\,pred} - T_{i,\exp}\right| \qquad (3)$$

where N is the number of experimental data points, $T_{i,pred}$ (K) is the predicted equilibrium temperature, and $T_{i,exp}$ (K) is the experimental equilibrium temperature.

The Kihara parameters optimization procedure can be read in Herri *et al.* [33]. Finally, note that SRK equation of state was used for the CP/CO_2 vapor liquid equilibrium. Presence of water in vapor and CP phase were neglected. The solubility of CO_2 in water was calculated based on the method described by Galfré et al [37].

5. CP Kihara Parameters

The hard core radius a for CP was determined based on the method described by Tee *el al* [38]. Its value is $a=0.8968nm$. ε and σ were optimized by minimizing the deviation between the predicted and experimental equilibrium data of CP/CO_2 binary hydrates.

Deviation between the measurements and predictions is illustrated in Figures 7 and 8. A numerous values of σ and ε/k were checked for optimization. It is obvious from the figure that the deviation is huge when σ is less than 2.55 or more than 2.74 regardless the value of ε/k_b (k_b being the Boltzmann constant). Therefore, the Kihara parameters for CP can be determined in the valley of Figure 8.

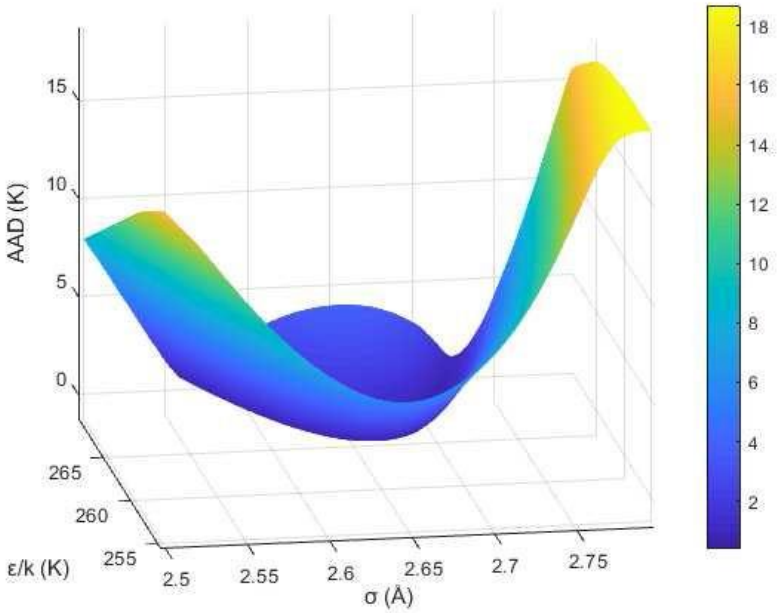

Figure 7. Deviation as a function of the Kihara parameters

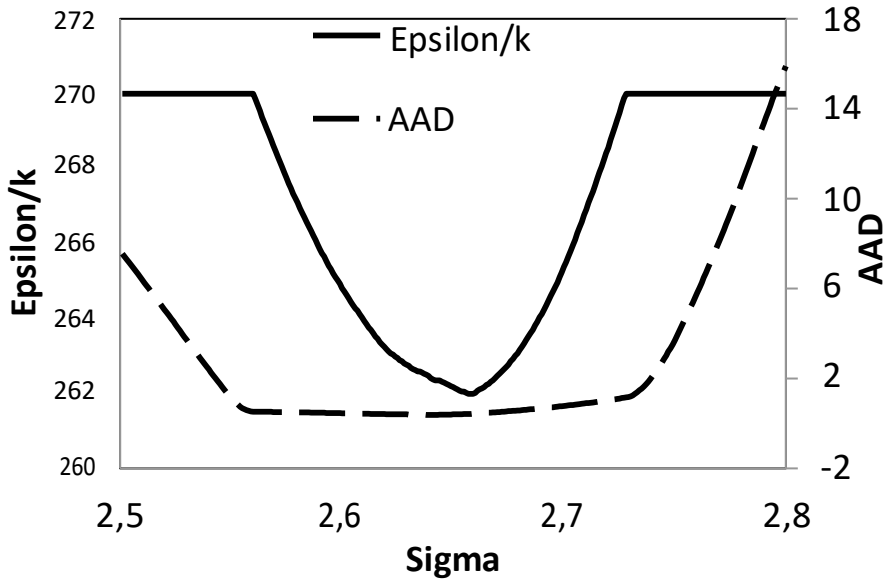

Figure 8. ε/k_b vs. σ at the minimum deviation

The valley of Figure 7 is presented in Figure 8 in only two dimensions. Based on these results, the best set of Kihara parameters was chosen: σ = 2.641 Å, ε/k_b = 262.38 K (with *a=0.8968 nm*).

S. Modelling results

The modelling results are plotted in Figure 9. Simulations present a good agreement with the experimental results. Indeed, the minimum deviation is only 0.2 K in the presence of 7 wt% NaCl, and the maximum average deviation is 0.4 K in presence of 3.5wt% KCl, 7wt% NaCl, or 1.75 wt% KCl – 1.75 wt% NaCl. The total AAD is 0.4 K. This indicates that the equilibrium is well reproduced by using the optimized Kihara parameters for CP.

Moreover, Figure 9 shows that the predicted data in the case of 3.5% wt KCl and equi-weight mixture of 1.75 wt% KCl-1.75 wt% NaCl is very close to each other when considering the same pressure. This can be attributed to the similarity in water activity coefficient of these two brine solutions (0.993 for 3.5% wt KCJ and 0.992 for 1.75 wt% KCJ-1.75 wt% NaCl). As a result, the predicted equilibrium data are nearly identical.

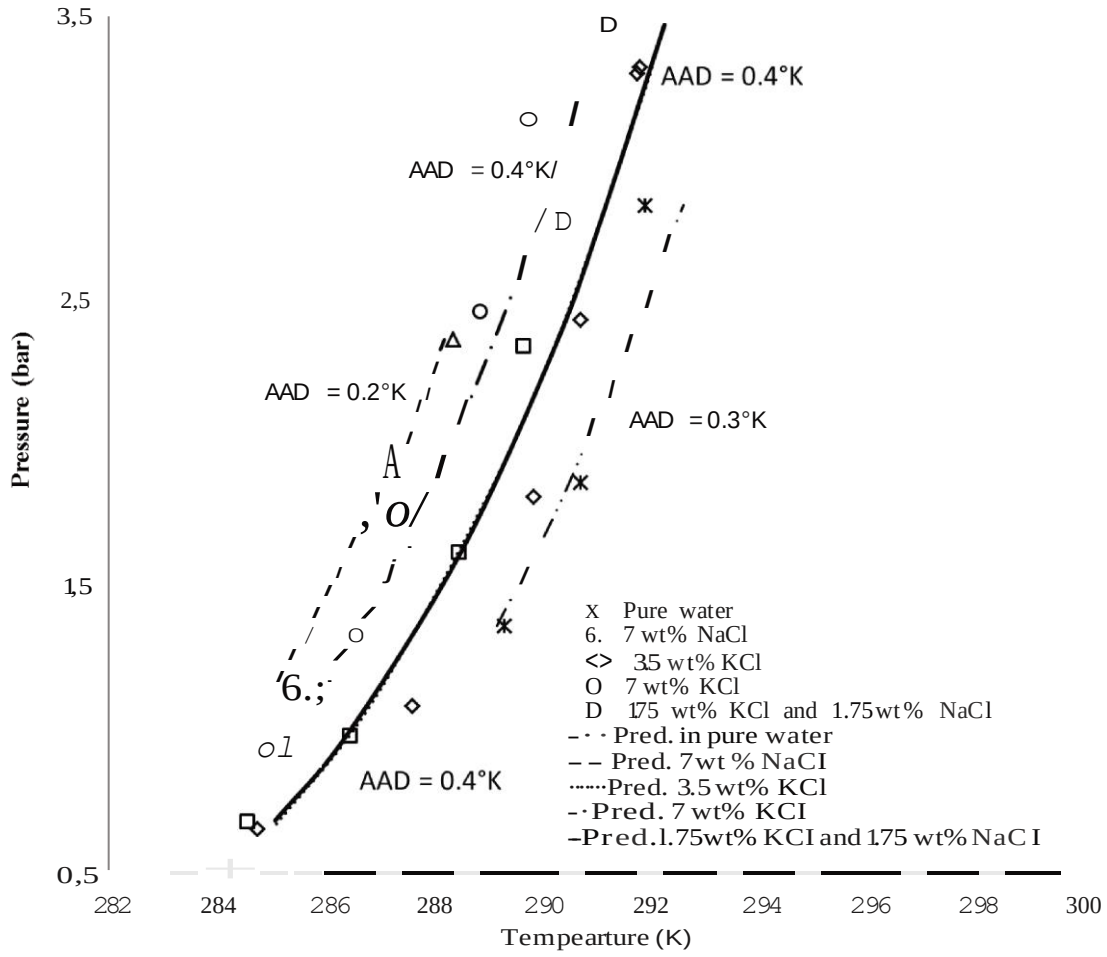

Figure 9. Measured and predicted equilibrium data of binary CP/CO_2 hydrate in pure water and in brine

The numerical data can be found in the Table A1 and Table A2 in the APPENDIX I. Finally, note that the simulated data are close to the experimental measurements at final dissociation. This fact supports again the consistency of the Kihara model as well as the trustworthiness of our experimental data. However, some experimental data from intermediate dissociation points present significant uncertainties compared to simulation results (up to 16.3°C). These data should therefore been carefully considered. One could expect that these point are not at thermodynamic equilibrium, or that the measured ionic concentration is not correct.

6. Conclusion

In the present work, new four-phase equilibrium data (V-L_w-L_{HC}-H) for CP/CO_2 binary hydrates in the presence of NaCl, KCl and a mixture of NaCl-KCl was obtained. Experiments have been conducted in a batch reactor using an isochoric technique in a pressure range of 10-40 bar. A volumetric ratio of 1:9 has been used between cyclopentane and aqueous liquid solution. The results of thermodynamic stability boundaries have shown that the equilibrium temperature of binary CO_2/CP hydrate is significantly higher than simple CO_2 hydrate. Furthermore, at the same concentration of NaCl and KCl, the equilibrium curve of CP/CO_2 hydrate in NaCl aqueous solution are located at an upper position than that in KCl aqueous solution. Concerning the mixture of NaCl-KCl, the influence of NaCl salt on equilibrium temperature is stronger. Indeed, at same overall salt concentration, data are closer to the results in presence of NaCl than in presence of KCl.

Additionally, two crystallization phenomena have been witnessed. Accordingly, at least two dissociation behaviors have been observed during the heating step of the system. Consequently, different crystal structures should have been formed in the reactor. This could be an evidence for co-existence of sI simple CO_2 hydrate and sII binary CP/CO_2 hydrate.

Moreover, simulation results show that the use of van de Waals model is acceptable to describe the equilibrium. The optimized Kihara parameters for CP illustrate a good capability of reproducing the dissociation temperatures of mixed CP/CO_2 hydrate in pure water and in the present of salts. Average deviation is less than 0.4K for all systems tested.

Finally, this research provides valuable thermodynamic data, necessary for the development of hydrate-based CCS/water treatment/desalination applications. Furthermore, it raised new

fundamental questions concerning the co-existence and co-crystallization of different hydrates structures from guest mixtures in presence of thermodynamic inhibitors. Upcoming studies, involving spectroscopic tools, will be used to ascertain the previous observations.

APPENDIX I: SIMULATION ON DISSOCIATION DATA

Table A1. Predicted final dissociation temperatures of mixed CP/CO_2 hydrates.

Final dissociation points					
Equilibrium salt concentration (%) At final dissociation point		Experimental equilibrium conditions		Predicted temperature, K	|Texp-Tpred|, K
NaCl	KCl	Pexp, MPa	Texp, K	Tpred, K	
0	0	1.87	290.7	290.50	0.20
0	0	1.37	289.3	289.17	0.13
0	0	2.84	291.9	292.60	0.70
				AAD	**0.3**
7	0	1.88	287.25	287.16	0.09
7	0	1.14	285.3	284.99	0.31
7	0	2.37	288.35	288.20	0.15
				AAD	**0.2**
0	3.5	3.32	291.8	292.02	0.22
0	3.5	3.30	291.75	292.00	0.25
0	3.5	2.44	290.7	290.42	0.28
0	3.5	1.82	289.85	288.98	0.87
0	3.5	1.09	287.6	286.82	0.78
0	3.5	0.66	284.75	285.02	0.27
				AAD	**0.4**
0	7	3.17	289.7	290.63	0.93
0	7	2.47	288.85	289.32	0.47
0	7	1.75	287.4	287.74	0.34
0	7	1.35	286.45	286.59	0.14
0	7	0.93	284.8	285.08	0.28
				AAD	**0.4**
1.75	1.75	3.47	291.8	292.26	0.46
1.75	1.75	2.79	290.35	291.09	0.74
1.75	1.75	2.35	289.65	290.25	0.60
1.75	1.75	1.63	288.45	288.51	0.06
1.75	1.75	0.99	286.45	286.40	0.05
1.75	1.75	0.69	284.55	285.08	0.53
				AAD	**0.4**

Table A2. Predicted intermediate dissociation temperatures of mixed CP/CO_2 hydrates (*italic* illustrates significant uncertainties with thermodynamic model)

Intermediate dissociation points					
Equilibrium salt concentration (%) (At the time taken samples during dissociation)		Experimental equilibrium conditions		Predicted temperature, K	|Texp-Tpred|, K
NaCl	KCl	Pexp, MPa	Texp, K	Tpred, K	
0	*0*	*0.87*	*273.95*	*290.25*	*16.30*
0	*0*	*0.47*	*274.15*	*287.30*	*13.15*
2.07	*2.24*	*1.98*	*283.95*	*290.18*	*6.23*
2.07	2.03	1.44	286.95	287.90	0.95
2.28	2.24	0.78	284.15	285.26	1.11
2.21	*2.17*	*0.45*	*274.10*	*284.98*	*10.88*
0	9.49	2.96	288.20	289.34	1.14
0	8.82	2.22	287.00	288.34	1.34
0	*8.32*	*0.94*	*274.90*	*286.72*	*11.82*
0	8.22	0.72	282.05	283.96	1.91
7.49	0	1.69	286.65	286.42	0.23
8.11	*0*	*0.56*	*274.45*	*283.23*	*8.78*
9.30	0	1.73	284.00	285.83	1.83
0	4.43	3.08	289.60	291.67	2.07
0	*4.44*	*2.12*	*286.60*	*290.03*	*3.43*
0	3.89	1.51	286.85	288.56	1.71
0	4.34	0.62	284.85	284.32	0.53
				AAD	**4.19**

Acknowledgment

The authors would like to thank French National Research Agency (ANR) for financial support. Especially, this work is part of INNOHYD French ANR-18-CE05-0006 project.

Also, the authors would like to heartily thank Fabien Chauvy for his technical help for all the experiments that are being conducted in the hydrate team at Mines Saint-Etienne.

References

[1] E.D. Sloan, C.A. Koh, Clathrate Hydrates of Natural Gases, Third edit, Taylor & Francis Group, 2007.

[2] H. Hashimoto, T. Yamaguchi, T. Kinoshita, Gas separation of fl ue gas by tetra- n -butylammonium bromide hydrates under moderate pressure conditions, Energy. 129 (2017) 292–298. doi:10.1016/j.energy.2017.04.074.

[3] S. Tomita, S. Akatsu, R. Ohmura, Experiments and thermodynamic simulations for continuous separation of CO 2 from CH 4 + CO 2 gas mixture utilizing hydrate formation, Appl. Energy. 146 (2015) 104–110. doi:10.1016/j.apenergy.2015.01.088.

[4] H. Ganji, J. Aalaie, S.H. Boroojerdi, A.R. Rod, Effect of polymer nanocomposites on methane hydrate stability and storage capacity, J. Pet. Sci. Eng. 112 (2013) 32–35. doi:10.1016/j.petrol.2013.11.026.

[5] S.M. Babakhani, A. Alamdari, Effect of maize starch on methane hydrate formation / dissociation rates and stability, J. Nat. Gas Sci. Eng. 26 (2015) 1–5. doi:10.1016/j.jngse.2015.05.026.

[6] S. Oya, M. Aifaa, R. Ohmura, International Journal of Greenhouse Gas Control Formation , growth and sintering of CO 2 hydrate crystals in liquid water with continuous CO 2 supply : Implication for subsurface CO 2 sequestration, Int. J. Greenh. Gas Control. 63 (2017) 386–391. doi:10.1016/j.ijggc.2017.06.007.

[7] B. Prah, R. Yun, CO2 hydrate slurry transportation in carbon capture and storage, Appl. Therm. Eng. (2017). doi:10.1016/j.applthermaleng.2017.09.053.

[8] Y.F. Makogon, Natural gas hydrates - A promising source of energy, J. Nat. Gas Sci. Eng. 2 (2010) 49–59. doi:10.1016/j.jngse.2009.12.004.

[9] K.A. Kvenvolden, Methane hydrate a major reservoir of carbon in the shallow geosphere?, Chem. Geol. 71 (1988) 41–51. doi:10.1016/0009-2541(88)90104-0

[10] Y. Zhang, S.M. Sheng, X.D. Shen, X.B. Zhou, W.Z. Wu, X.P. Wu, D.Q. Liang, Phase Equilibrium of Cyclopentane + Carbon Dioxide Binary Hydrates in Aqueous Sodium Chloride Solutions, J. Chem. Eng. Data. 62 (2017) 2461–2465. doi:10.1021/acs.jced.7b00404.

[11] M. Karamoddin, F. Varaminian, Water desalination using R141b gas hydrate formation, Desalin. Water Treat. 52 (2014) 2450–2456. doi:10.1080/19443994.2013.798840.

[12] P.J. Herslund, K. Thomsen, J. Abildskov, N. von Solms, A. Galfré, P. Brântuas, M. Kwaterski, J.M. Herri, Thermodynamic promotion of carbon dioxide-clathrate hydrate formation by tetrahydrofuran, cyclopentane and their mixtures, Int. J. Greenh. Gas

Control. 17 (2013) 397–410. doi:10.1016/j.ijggc.2013.05.022.

[13] S. Sun, X. Peng, Y. Zhang, J. Zhao, Y. Kong, Stochastic nature of nucleation and growth kinetics of THF hydrate, J. Chem. Thermodyn. (2016). doi:10.1016/j.jct.2016.12.026.

[14] W. Liu, S. Wang, M. Yang, Y. Song, S. Wang, J. Zhao, Investigation of the induction time for THF hydrate formation in porous media, J. Nat. Gas Sci. Eng. 24 (2015) 357–364. doi:10.1016/j.jngse.2015.03.030.

[15] H. Najibi, K. Momeni, M.T. Sadeghi, Theoretical and experimental study of phase equilibrium of semi-clathrate hydrates of methane + tetra-n-butyl-ammonium bromide aqueous solution, J. Nat. Gas Sci. Eng. (2015). doi:10.1016/j.jngse.2015.11.002.

[16] A. Galfré, M. Kwaterski, P. Braîntuas, A. Cameirao, J.M. Herri, Clathrate hydrate equilibrium data for the gas mixture of carbon dioxide and nitrogen in the presence of an emulsion of cyclopentane in water, J. Chem. Eng. Data. 59 (2014) 592–602. doi:10.1021/je4002587.

[17] J.H. Cha, Y. Seol, Increasing gas hydrate formation temperature for desalination of high salinity produced water with secondary guests, ACS Sustain. Chem. Eng. 1 (2013) 1218–1224. doi:10.1021/sc400160u.

[18] J. nan Zheng, M. jun Yang, Y. Liu, D. yong Wang, Y. chen Song, Effects of cyclopentane on CO2 hydrate formation and dissociation as a co-guest molecule for desalination, J. Chem. Thermodyn. 104 (2017) 9–15. doi:10.1016/j.jct.2016.09.006.

[19] S. Hong, S. Moon, Y. Lee, S. Lee, Y. Park, Investigation of thermodynamic and kinetic effects of cyclopentane derivatives on CO2 hydrates for potential application to seawater desalination, Chem. Eng. J. 363 (2019) 99–106. doi:10.1016/j.cej.2019.01.108.

[20] S. Ho-Van, B. Bouillot, J. Douzet, S. Maghsoodloo, J.-M. Herri, Experimental Measurement and Thermodynamic Modeling of Cyclopentane Hydrates with NaCl, KCl, CaCl2 or NaCl-KCl Present, AIChE. J. 6 (2018) 2207-2218. doi:10.1002/aic.16067.

[21] P.D. Dholabhai, N. Kalogerakis, P.R. Bishnoi, Equilibrium Conditions for Carbon

Dioxide Hydrate Formation in Aqueous Electrolyte Solutions, J. Chem. Eng. Data. 38 (1993) 650–654.

[22] M. Kwaterski, J.M. Herri, Modelling of gas clathrate hydrate equilibria using the electrolyte non-random two-liquid (eNRTL) model, Fluid Phase Equilib. 371 (2014) 22–40. doi:10.1016/j.fluid.2014.02.032.

[23] W.. Deaton, E.. Frost, Gas Hydrates and Their Relation to the Operation of Natural-Gas Pipe Lines, 1946.

[24] S.-S. Fan, G.-J. Chen, Q.-L. Ma, T.-M. Guo, Experimental and modeling studies on the hydrate formation of CO2 and CO2-rich gas mixtures, Chem. Eng. J. 78 (2000) 173–178. doi:10.1016/S1385-8947(00)00157-1.

[25] K. Ohgaki, Y. Makihara, K. Takano, Formation of CO2 Hydrate in Pure and Sea Waters, J. Chem. Eng. Jpn. 26 (1993) 558–564. doi:10.1252/jcej.26.558.

[26] Y. Matsumoto, T. Makino, T. Sugahara, K. Ohgaki, Phase equilibrium relations for binary mixed hydrate systems composed of carbon dioxide and cyclopentane derivatives, Fluid Phase Equilib. 362 (2014) 379–382. doi:10.1016/j.fluid.2013.10.057.

[27] P.J. Herslund, N. Daraboina, K. Thomsen, J. Abildskov, N. von Solms, Measuring and modelling of the combined thermodynamic promoting effect of tetrahydrofuran and cyclopentane on carbon dioxide hydrates, Fluid Phase Equilib. 381 (2014) 20–27. doi:10.1016/j.fluid.2014.08.015.

[28] J. Lee, M. Chun, K. Lee, Y. Kim, H. Lee, Phase Equilibria and Kinetic Behavior of CO2 Hydrate in Electrolyte and Porous Media Solutions: Application to Ocean Sequestration of CO2, Korean J. Chem. Eng. 19 (2002) 673–678. doi:10.1007/BF02699316.

[29] S. Ho-van, B. Bouillot, D. Garcia, J. Douzet, A. Cameirao, S. Maghsoodloo-, Crystallization mechanisms and rates of Cyclopentane Hydrates formation in Brine, Chem. Eng. Technol. (2019) 1–21. doi:10.1002/ceat.201800746.

[30] E.D. Sloan, C.A. Koh, A. Sum, eds., Natural Gas Hydrates in Flow Assurance, 1 edition, Gulf Professional Publishing, Amsterdam ; Boston, 2010.

[31] S. Ho-Van, B. Bouillot, J. Douzet, S. Maghsoodloo Babakhani, J.-M. Herri,

Implementing Cyclopentane Hydrates Phase Equilibrium Data and Simulations in Brine Solutions, Ind. Eng. Chem. Res. 57 (2018) 14774 -14783. doi:10.1021/acs.iecr.8b02796.

[32] J.H. van der Waals, J.C. Platteeuw, Clathrate solutions, Adv. Chem. Phys. 2 (1958) 1–57. doi:10.1002/9780470143483.ch1.

[33] J.-M. Herri, A. Bouchemoua, M. Kwaterski, A. Fezoua, Y. Ouabbas, A. Cameirao, Gas hydrate equilibria for CO2–N2 and CO2–CH4 gas mixtures—Experimental studies and thermodynamic modelling, Fluid Phase Equilib. 301 (2011) 171–190. doi:10.1016/j.fluid.2010.09.041.

[34] D. Le Quang, D. Le Quang, B. Bouillot, J.M. Herri, P. Glenat, P. Duchet-Suchaux, Experimental procedure and results to measure the composition of gas hydrate, during crystallization and at equilibrium, from N2-CO2-CH4-C2H6-C3H8-C4H10 gas mixtures, Fluid Phase Equilib. 413 (2016) 10–21. doi:10.1016/j.fluid.2015.10.022.

[35] W.R. Parrish, J.M. Prausnitz, Dissociation Pressures of Gas Hydrates Formed by Gas Mixtures, Ind. Eng. Chem. Process Des. Dev. 11 (1972) 26–35. doi:10.1021/i260041a006.

[36] M. Wang, Z.G. Sun, C.H. Li, A.J. Zhang, J. Li, C.M. Li, H.F. Huang, Equilibrium Hydrate Dissociation Conditions of CO2+ HCFC141b or Cyclopentane, J. Chem. Eng. Data. 61 (2016) 3250–3253. doi:10.1021/acs.jced.6b00333.

[37] A. Galfré, Captage du dioxyde de carbone par cristallisation de clathrate hydrate en présence de cyclopentane : Etude thermodynamique et cinétique, Ph.D.Thesis, Ecole Nationale Supérieure des Mines de Saint-Etienne, 2014.

[38] L.S. Tee, S. Gotoh, W.E. Stewart, Molecular Parameters for Normal Fluids. Kihara Potential with Spherical Core, Ind. Eng. Chem. Fundam. 5 (1966) 363–367. doi:10.1021/i160019a012.

Chapter VII. General conclusion and perspectives

This work tries to address issues that are crucial to develop water treatment and desalination application *via* CPH or mixed CP/CO_2 hydrates crystallization. They can be formulated as follows:

1) Is CPH a promising possibility for desalination?

2) How to determine CPH and mixed CP/CO_2 hydrates equilibrium?

3) What is the role of salts in influencing CPH or mixed CP/CO_2 hydrates equilibrium?

4) What hydrate is formed in presence of brine, CO_2 and CP?

5) What is the best model to predict CPH and mixed CP/CO_2 hydrates equilibrium?

6) Using CPH hydrate as model system, what can be said about the crystallization mechanism of clathrate hydrates in pure water and in brine?

7) How salts and subcooling affect CPH crystals morphology?

To undertake the first question, all published resources related to CPH in the open literature have been collected and reviewed. Critical analysis on CPH crystallization including thermodynamics, crystallization kinetic, hydrate phase properties has been conducted to provide a basement CPH-based desalination. Moreover, recent advancements on this technology have been updated and clarified. Importantly, a comparison between CPH-based desalting and others traditional methods highlights the potential opportunity of CPH along with some significant challenges yet to overcome, such as: water-hydrate conversion, salt remove efficiency, or purification level of produced water. However, late example has shown that CPH-based desalting is more economy-feasible when it combines with LNG cold energy or CO_2 capture.

Then, in order to determine CPH equilibrium, two poly-thermal methods, at low and high dissociation rates, have been applied in an atmospheric batch reactor. Experimental results illustrated that a temperature shift between the CPH equilibrium temperatures according to two procedures was observed. As the quick procedure tends to miss the right temperature, its results are slightly above the right value. Slow procedure provides results that are very close

to the data reported in the literature. This confirms that slow dissociation method is reliable to determine CPH dissociation temperatures.

Moreover, an isochoric technique was employed in a pressurized batch reactor to investigate mixed CO_2/CP hydrates equilibrium. The experimental results in presence of salts agree well with literature data. The reproducibility of results has also been checked, and confirmed the accuracy method.

The experimental results demonstrate, without surprise, that salts inhibit strongly both CPH and binary CP/CO_2 hydrates equilibrium. This influence is due to both "ion clustering" and "salting-out" phenomena. In addition, each salt affects differently equilibrium. For example, the hydrate inhibiting strength rises in the following order: $MgCl_2$ > NaCl > KCl. Indeed, this influence can be attributed to the difference in salt ion charge density. Small cations with high charge density can lead to powerful electrostatic interaction between the cations and water molecules. This weakens hydrogen bonding interaction between water molecules, inhibiting the hydrate formation. The inhibition of salts on equilibrium reveals that more subcooling is required to form clathrates in brine than that in pure water. Results also shown that CO_2 is a good thermodynamic promoter for cyclopentane hydrate formation, and vice versa, with a temperature shift from +13°C to +15 °C under pressure.

In presence of CP, CO_2 and brine, observations have shown that several hydrate structures could be formed. In theory, since CP form SII clathrates, CP/CO_2 hydrates are expected to present the same polymorph. However, results in presence of KCl or NaCl, suggest the formation of ''two' hydrates: simple SI pure CO_2 hydrate and sII binary CP/CO_2 hydrate. Of course, this observation still needs experimental evidence, maybe from FTIR or Raman spectroscopy.

Based on the experimental data, four approaches have been considered to predict CPH equilibrium: one based on the standard freezing point depression equation for ice, another based on Hu-Lee-Sum correlation, and two others based on van der Waals and Platteeuw model. Among them, the use of van der Waals and Platteeuw aproch combined with a new correlation between the CPH stoichiometry and the water activity (ABOC) furnished the best results (uncertainty < 0.2°C). Concerning CO_2 addition, van der Waals and Platteeuw with Kihara potential approach has been employed. Kihara parameters for CP have been optimized first. The overall results have provided temperature prediction within 0.4°C uncertainty.

Then, penultimate effort has been focused on CPH crystallization mechanisms. A non-mixing small reactor cell under a microscope has been used to observe the crystallization process. Results show that an early nucleation of individual crystal is usually observed near the liquid-liquid (water/CP) interface as a result of impurities like traces of H_2O or CP droplets. The hydrate layer formation starts by a quick crystallization along the water-CP interface, then hydrate layer grows mostly, but not exclusively, toward the CP phase. Accordingly, the CPH crystallization mechanism involves the advection of the water phase through the porous and probably water-wet hydrate layer. Videos on crystallization were made to illustrate the visual mechanisms of CPH in pure water and in brine. Besides, the hydrate layer growth rates have been evaluated with time in different saline solutions and under different initial subcoolings. Results indicate that the growth rate increases with increasing of subcooling and reduces with salt concentration. The hydrate crystal growth also decreases over time due to the increased resistance of hydrate layer, preventing the mass transfer in crystallization process.

At last, our morphology study indicates that the influence of initial subcooling on the size and shape of single hydrate crystals is more significant than the influence of salt and its salinity. The size of hydrate crystals decreases with rising of initial subcooling. This is because of the high crystallization rate at high sucooling. Moreover, lower initial subcooling leads to polygons (2.5°C), while at higher subcoolings the smaller crystals have the geometric shape of slender polygons (3.5°C), or sword-like (4.3°C). These findings demonstrate a possibility of using subcooling as a criterion for CPH morphology classification.

Hopefully, this effort will support the industrial development of CPH based applications. Nevertheless, many studies still need to be conducted to achieve such goal. These are some suggestions of what should happen next:

Since the thermodynamic equilibrium data of CPH and CP/CO_2 hydrates are crucial for desalination application, more comprehensive experimental data in others salt systems like real seawater, NaBr, KBr, NaF, KF, K_2SO_4, Mg_2SO_4, $CaSO_4$ or their mixtures are still required.

The evidence for co-existence of sI simple CO_2 hydrate and sII binary CP/CO_2 hydrate in presence of salts needs to be confirmed by FTIR or Raman spectroscopy

Besides, simulation tools are important to predict equilibrium when experiments are not practical. Our developed thermodynamic models are needed to verify and compare to the new

set of experimental data in order to find and confirm the best consistent model to reproduce equilibrium, whatever the electrolyte included.

Hydrate crystallization mechanism investigation could be continued. Indeed, such experiments and measurements offer valuable data to explain and model mass transfer within hydrate phase. But, first of all, another optical microcopy with higher zoom range and color-tracers that allow tracking the movement of molecules during hydrate crystallization would be highly recommended.

Eventually, more experimental investigations on the effect of subcoolings and others kind of electrolytes on morphology and kinetic of hydrate formation would be needed. This is important to better understand the role of subcooling and salt on hydrate crystallization.

Finally, an upscaling of the separative process is the big next step, with a whole list of new issues, such as the design of the process or the optimization of the operating parameters. An exciting upcoming work!

Scientific production (2015-2019)

Publications published in peer-reviewed journals

- S. Ho-Van, B. Bouillot, J. Douzet, S. Maghsoodloo, J.-M. Herri, Experimental Measurement and Thermodynamic Modeling of Cyclopentane Hydrates with NaCl, KCl, CaCl2 or NaCl-KCl Present, AIChE. J. 6 (2018) 2207-2218. doi:10.1002/aic.16067.

- S. Ho-Van, B. Bouillot, J. Douzet, S. Maghsoodloo Babakhani, J.-M. Herri, Implementing Cyclopentane Hydrates Phase Equilibrium Data and Simulations in Brine Solutions, Ind. Eng. Chem. Res. 57 (2018) 14774 -14783. doi:10.1021/acs.iecr.8b02796.

- S. Ho-van, B. Bouillot, D. Garcia, J. Douzet, A. Cameirao, S. Maghsoodloo-Babakhani, J.M.Herri, Crystallization mechanisms and rates of Cyclopentane Hydrates formation in Brine, Chem. Eng. Technol. (2019) 1–21. doi:10.1002/ceat.201800746.

- S.Ho-Van, B.Bouillot, J.Douzet, S. Maghsoodloo Babakhani, J.M.Herri, Cyclopentane hydrates – a candidate for desalination, Journal of Chemical Engineering Science, (2019). doi:10.1016/j.jece.2019.103359. In Press.

- Maghsoodloo Babakhani, S., Bouillot, B., Douzet, J., Ho-Van, S., Herri, J.M., 2018. PVTx measurements of mixed clathrate hydrates in batch conditions under different crystallization rates: influence on equilibrium. Journal of Chemical Thermodynamics. 122, 73–84.

- Maghsoodloo Babakhani, S., Bouillot, B., Douzet, J., Ho-Van, S., Herri, J.M., 2018. A new approach of studying mixed gas hydrates involving propane at non-equilibrium conditions and final state: An experimental study and modeling. Journal of Chemical Engineering Science. 179, 150–160.

- Maghsoodloo Babakhani, S., Bouillot, B., Ho-Van, S., Douzet, J., Herri, J.-M., 2018. A review on hydrate composition and capability of thermodynamic modeling to predict hydrate pressure and composition. Fluid Phase Equilibria. 472, 22–38.

International Conferences

- Son Ho-Van, Jérome Douzet, Duyen Le-Quang, Baptiste Bouillot, Jean-Michel Herri, Behavior of cyclopentane hydrates formation and dissociation in pure water and in the presence of sodium chloride, INTERNATIONAL CONFERENCES ON EARTH SCIENCES AND SUSTAINABLE GEO-RESOURCES DEVELOPMENT -ESASGD 2016, 150-157, Hanoi, Vietnam, 2016.

- Son Ho Van, Jérome Douzet, Duyen Le-Quang, Baptiste Bouillot, Jean-Michel Herri, Thermodynamic modelling of cyclopentane hydrates in the presence of salts, 2nd International Conference on Integrated Petroleum Engineering for Unconventional Resources IPE, Hanoi, Vietnam, 2017.

- Son Ho-Van, Jérome Douzet, Baptiste Bouillot, Jean-Michel Herri, Experimental Study and Modelling of Cyclopentane Hydrates in the presence of NaCl, KCl and a mixture of NaCl -KCl, The 9th International Conference on Gas Hydrates, Denver, Colorado USA. June 2017.

- Son Ho-Van, Jérome Douzet, Baptiste Bouillot, Jean-Michel Herri,, Experimental determination and modelling of cyclopentane hydrates in the presence of NaCl, KCl, CaCl2, and a mixture of NaCl-KCl, 10th World Congress of Chemical Engineering - WCCE10, 2017. ***Best oral presentation award, Topic GAS HYDRATES***.

- Son Ho-Van, Jérome Douzet, Baptiste Bouillot, Jean-Michel Herri, Experimental study and modelling of cyclopentane hydrates in the presence of salt, 16ème Congrès de la Société Française de Génie des Procédés (SFGP 2017 NANCY), France, 2017.

- Ho-Van, S., Bouillot B., Douzet, J., Maghsoodloo Babakhani, S., Herri, J.M. Phase Equilibrium Data of Cyclopentane Hydrates in Saline Systems of Na_2SO_4-H_2O, $MgCl_2$-H_2O, $MgCl_2$-NaCl-H_2O, and $MgCl_2$-NaCl-KCl-H_2O: Experimental and

Modelling. The 25th international conference on industrial crystallization, Rouen, France. September 2018.

- Ho-Van, S., Bouillot B., Douzet, J., Maghsoodloo Babakhani, S., Herri, J.M. Morphological Study of Cyclopentane Hydrates in Saline Water for Desalination Application. The 25th international conference on industrial crystallization, Rouen, France. September 2018.

- Maghsoodloo Babakhani, S., Ho-Van, S., Bouillot B., Douzet, J., Herri, J.M. Four phase equilibrium conditions of cyclopentane/carbon dioxide binary hydrate in brine solutions: A potential application in water desalination. The 25th international conference on industrial crystallization, Rouen, France. September 2018.

Publication submitted in in peer-reviewed journals

- S. Maghsoodloo Babakhani, S.Ho-Van, B.Bouillot, J.Douzet, J.M.Herri, Phase equilibrium investigations of mixed cyclopentane and carbon dioxide hydrates in presence of different salt solutions. Journal of Chemical Engineering Science, submitted 05/2019.

Article in open access archive without peer-review

- S. Ho-van, B. Bouillot, D. Garcia, J. Douzet, A. Cameirao, S. Maghsoodloo-Babakhani, J.M.Herri, Morphology of Cyclopentane Hydrates in Saline Water, ⟨hal-02197237⟩.